Quantum reversibility, decoherence and transport in dynamical systems

Petitjean, Cyril Jean-Pierre Stéphane

UNIVERSITÉ DE GENÈVE
Département de physique théorique

FACULTÉ DES SCIENCES
Prof. M. Büttiker & Prof. P. Jacquod

Quantum Reversibility, Decoherence and Transport in Dynamical Systems

THÈSE

présentée à la Faculté des sciences de l'Université de Genève
pour obtenir le grade de Docteur ès sciences, mention physique

par

Cyril Jean-Pierre Stéphane Petitjean
de
Belfort, France

Thèse No 3861

GENÈVE
Atelier de reproduction de la Section de physique
2007

UNIVERSITÉ DE GENÈVE

FACULTÉ DES SCIENCES

Doctorat ès sciences
mention physique

Thèse de *Monsieur Cyril PETITJEAN*

intitulée :

"Quantum Reversibility, Decoherence and Transport in Dynamical Systems"

La Faculté des sciences, sur le préavis de Messieurs M. BÜTTIKER, professeur ordinaire et directeur de thèse (Département de physique théorique), Ph. JACQUOD, professeur et codirecteur de thèse (University of Arizona, Physics Department, Tucson, Etats-Unis d'Amérique), J.-P. ECKMANN, professeur ordinaire (Département de physique théorique), A. BUCHLEITNER, docteur (Max-Planck-Institute for Physics of Complex Systems, Nonlinear Dynamics in Quantum Systems, Dresden, Allemagne), D. L. SHEPELYANSKY, docteur (Université Paul Sabatier, Institut de Recherche sur les Systèmes Atomiques et Moléculaires Complexes, Unité Mixte de Recherche 5152 du Centre National de Recherche Scientifique, Laboratoire de physique théorique, Toulouse, France), R. S. WHITNEY, docteur (Institut Laue-Langevin, Theory Group, Grenoble, France), autorise l'impression de la présente thèse, sans exprimer d'opinion sur les propositions qui y sont énoncées.

Genève, le 14 juin 2007

Thèse - 3861 -

Le Doyen, Pierre SPIERER

N.B.- La thèse doit porter la déclaration précédente et remplir les conditions énumérées dans les "Informations relatives aux thèses de doctorat à l'Université de Genève".

Nombre d'exemplaires à livrer par colis séparé à la Faculté : - 7 -

À ma famille avec amour.

Contents

Remerciements

Cette thèse a été réalisée au sein du département de physique théorique de l'université de Genève. Je tiens tout d'abord à remercier Markus Büttiker de m'avoir accueilli dans son groupe de physique mésoscopique. Je lui suis gré de m'avoir soutenu et de m'avoir laissé une grande liberté d'actions.

Mes remerciements s'adressent ensuite à Andreas Buchleitner, Jean-Pierre Eckmann, Dima Shepelyansky et Robert S. Whitney qui ont eu la gentillesse d'accepter le rôle de juré de thèse. Je leur en suis très reconnaissant.

Je tiens à remercier tout particulièrement Philippe Jacquod, qui durant ces quatre années a su me soutenir, m'apporter avec patience et clarté toute l'assistance nécessaire à la mise en oeuvre de mon travail de recherche. J'ai tout particulièrement profité de sa compréhension profonde de la physique et de son sens critique. Il m'a de plus, avec une sincère sympathie, fait partager son enthousiasme, non seulement pour la science mais également pour d'autres sujets annexes comme ses connaissances et ses dégustations de vins valaisans...

Le chapitre 4 est issu d'une collaboration avec Rick Heller, travail très enrichissant qui m'a permis de découvrir Boston et l'université d'Harvard. A ce propos, je tiens à remercier Saijun Wu pour ses discussions pédagogiques et profondes des expériences d'écho de déplacement. De même je remercie Florian Mintert qui m'a fait découvrir les subtilités de l'intrication à plusieurs particules. De plus je me réjouis encore des moments fort agréables que nous avons pu partager soit à Boston, soit à Dresden.

Rob Whitney m'a épaulé dans la compréhension du transport quantique, et cette collaboration a donné naissance à la partie IV de cette thèse. Ce fut un bon moment et j'espère que nous aurons l'occasion de poursuivre ensemble sur ce chemin.

Je suis très reconnaissant à Simon Nigg qui a relu cette thèse afin d'y améliorer l'anglais, tu as fait un travail considérable et je t'en remercie encore.

Je tiens à remercier l'ensemble des secrétaires du département de physique théorique, à savoir Danièle Chevalier , Francine Gennai-Nicole et Cécile Jaggi, sans qui les tâches administratives seraient bien complexes. Une mention parti-

culière à Andreas Malaspinas, sans qui la gestion du réseau informatique, serait un vrai cauchemar.

Il y a aussi toutes les personnes avec qui je n'ai pas vraiment travaillé mais avec qui j'ai beaucoup discuté, tantôt de physique tantôt d'autres choses. je remercie donc, Florian Dubath, Andrew Jordan, Heidi Foerster, Marlies Goorden, Philippe Jacquet, Rosa Lopez, Kirsten Martens, Mikhail Moskalets, Sebastian Pilgram, Mikhail Polianski, David Sanchez, Peter Samuelsson, Janine Splettstoesser, Eugene Sukhorukov, Valentin Rytchkov, Peter Wittwer et Cyrille Zbinden et tous ceux que j'ai pu oublier.

J'adresse une pensée toute particulière à Philippe Jacquod et sa famille : Mireille, Barnabé, Timothée et Lorraine, qui m'ont accueilli lors de mes séjours à Tucson, et j'en garde d'agréables et riches souvenirs.

Enfin je remercie ma famille, sans qui cette thèse n'aurait jamais vu le jour ; et plus particulièrement mes parents, qui ont toujours su me soutenir et m'encourager. Sans eux je ne serais sûrement jamais arrivé jusque là. J'offre aussi de tout mon coeur une pensée des plus tendres à toi, ma femme Gabrielle, qui m'a donné le bonheur et la joie de devenir papa d'une petite Marine, et je te remercie également de continuer à me suivre dans cette voie que d'autres, moins courageux, ont abandonnée.

Cyril Petitjean

Résumé

L'objectif de ce bref résumé est de mettre en valeur un certain nombre de résultats que j'ai obtenu durant mon travail de thèse. Ce dernier n'a pas vocation à être exhaustif, pour plus de détails nous renvoyons le lecteur au chapitre correspondant.

La réversibilité en mécanique quantique

L'émergence de l'irréversibilité dans les systèmes chaotiques classiques est reliée à la propriété dynamique de mélange et à la notion de "coarse-graining" associée aux limitations de la résolution expérimentale. Ce mécanisme est extrêmement réduit dans le cadre d'un traitement quantique. Cette limitation est principalement due à une efficacité plus faible de la propriété de mélange et au principe d'incertitude d'Heisenberg qui diminue le "coarse-graining".

En fait, il a même été montré par Shepelyansky [1], qu'il était possible d'obtenir une dynamique quantique quasiment parfaitement réversible, alors que l'équivalent classique est strictement irréversible. Cette irréversibilité classique est reliée aux erreurs d'arrondi inhérent aux simulations numériques (Voir Figure 1). Cependant il a été réalisé assez rapidement que la connaissance des conditions microscopiques qui gouvernent la dynamique quantique n'est pas accessible avec une précision arbitraire. Par conséquent l'opération de renversion temporelle de l'Hamiltonien ne peut être effectuée de façon exacte. Il y a donc bien un intérêt fondamentale à étudier la sensibilité de la dynamique quantique par rapport à une perturbation de l'Hamiltonien.

Ce constat remonte au travail fondateur de Peres [2]. La quantité fondamentale de cette approche est l'*écho de Loschmidt* également dénommé la *Fidélité*,

$$\mathcal{M}_{\mathrm{L}}(t) = |\langle\psi_0| \exp[iHt] \exp[-iH_0t]|\psi_0\rangle|^2 \tag{1}$$

avec laquelle on reconstruit, à un temps donner, un paquet d'onde étroit $|\psi_0\rangle$ après avoir inverser la dynamique à l'aide d'un Hamiltonien perturbé $H = H_0 + \Sigma$. (on pose $\hbar \equiv 1$). La *Fidélité* quantifie la sensibilité de l'opération de renversement du temps envers l'incertitude relative à l'Hamiltonien. Il s'agit donc bien d'une mesure de l' irréversibilité quantique.

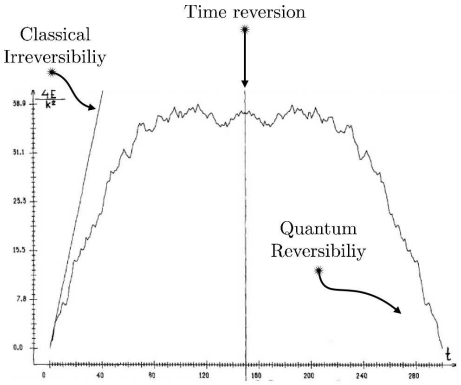

Fig. 1: Dépendance temporelle de l'énergie de l'application standard suite à une inversion temporelle. La ligne droite montre clairement l'irréversibilité de la diffusion classique. Ceci contraste pleinement avec l'évolution complètement réversible de la version quantique Figure adaptée de Shepelyansky [1].

La notion de *Fidélité* apparaît assez naturellement dans le contexte de la *décohérence* [3, 4] de système, possédant peu de degrés de liberté, couplé à un environnement qui possède un grand nombre de degrés de liberté. Brièvement , la présence de la perturbation Σ dans la propagation du retour, permet de tenir compte de l'effet du couplage avec l'environnement. Cette idée initialement développée par Jalabert and Pastawski [5] a suscité un grand intérêt théorique [6–16], pour une revue nous conseillons [17]. La source de cet intérêt était la prédiction dans [5] d'un régime de perturbation où le comportement de la fidélité était principalement gouverné par l'exposant de Lyapunov du système $\mathcal{M}_{\mathrm{L}}(t) \simeq \exp[-\lambda t]$. Les limites de validité de ce régime ont été clarifiées par [6]. Ils démontrèrent que la décroissance de la fidélité en fonction du temps est soit Gaussienne soit exponentielle. Le régime Gaussien domine si la force de la perturbation est suffisamment faible. Lorsque la perturbation devient plus conséquente, la décroissance devient exponentielle. Pour des perturbations pas excessivement élevée le taux est donné par la règle d'or de Fermi, jusqu'à ce que cette dernière dépasse la valeur de l'exposant de Lyapunov du système.

La plupart des recherches précédemment citées sont restreintes à l'étude des propriétés moyennes de la fidélité. La moyenne s'effectue soit sur les conditions initiales soit sur un ensemble d'Hamiltoniens non perturbés ou un ensemble de perturbations. Cependant les fluctuations d'une quantité physique contiennent souvent plus d'informations que leurs moyennes. Pour conséquence, en suivant une procédure similaire à l'approche semiclassique développée dans [5], nous avons déterminé la *variance* de la fidélité $\sigma^2\left[\mathcal{M}_{\mathrm{L}}(t)\right]$ [18]. Nous avons montré que la variance possède un comportement plus riche que sa moyenne. En particulier cette dernière augmente de façon algébrique jusqu'à un temps critique t_c après lequel elle décroît. Cette décroissance est donnée, à l'ordre semiclassique dominant, par la somme d'un terme classique relié à l'exposant de Lyapunov classique λ, un

terme quantique relié à la règle d'or de Fermi Γ et un terme mixte

$$\sigma^2\left[\mathcal{M}_{\mathrm{L}}(t)\right] \simeq \alpha^2(t)e^{-2\lambda t} + \frac{2}{N}e^{-\Gamma t}\,\Theta_{\tau_{\mathrm{E}}}(t) + 2\alpha(t)\mathrm{e}^{-(\lambda+\Gamma)t} \tag{2}$$

La comparaison de ce comportement avec celui de la fidélité moyenne, nous autorise à extraire l'exposant de Lyapunov dans une gamme de paramètres plus large. En effet, de façon similaire à la fidélité moyenne, l'exposant de Lyapunov peut s'obtient si on augmente de façon suffisante la perturbation afin d'atteindre le régime $\Gamma \geq \lambda$. Cependant contrairement à la moyenne, il est encore possible d'obtenir l'exposant de Lyapunov pour le régime $\Gamma \leq \lambda$. En effet pour des temps plus cours que le temps Ehrenfest $\tau_{\mathrm{E}} = \lambda^{-1}\ln\left[N^{-1}\right]$, le comportement de la variance est contrôlée par le terme mixte (Troisième terme de Eq. (1.34))

Nos résultas sont confirmés par des simulations numériques, présentées à la Figure 2. Dans la Figure 2a nous présentons la variance $\sigma^2\left[\mathcal{M}_{\mathrm{L}}\right]$ de la Fidélité en fonction du temps, dans le régime de perturbation faible $\Gamma \ll \lambda$. Cette simulation numérique illustre clairement, l'augmentation initiale de la variance suivie par la décroissance exponentielle prévue par le second terme de Eq. (2). Nous précisons ici qu'aucun paramètre d'ajustement n'a été utilisé, ceci apporte une confirmation numérique importante concernant la validité du préfacteur N^{-1}. La Figure 2b illustre clairement la transition du régime quantique au régime classique de saturation Lyapunov $\lambda \ll \Gamma$.

Ce travail sera discuté en détails au chapitre 2 et est publié dans [114].

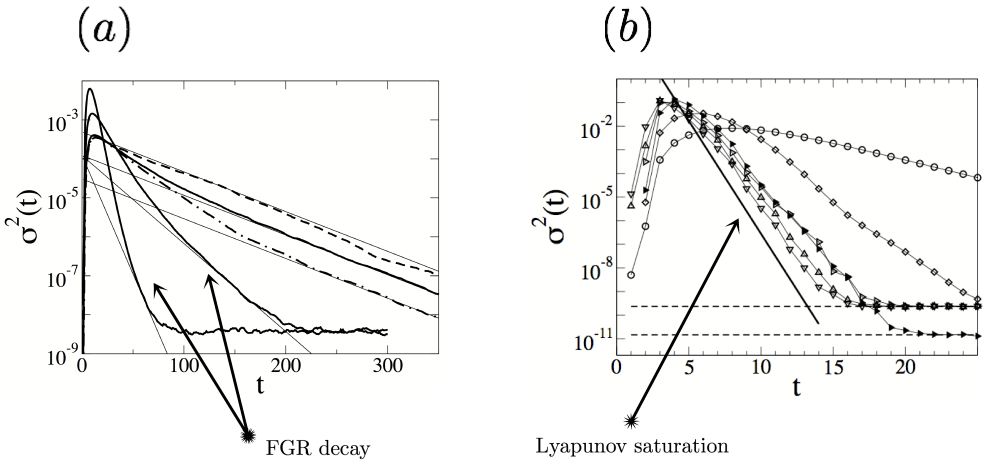

Fig. 2: (a) Variance $\sigma^2\left[\mathcal{M}_{\mathrm{L}}\right]$ de la Fidélité en fonction du temps pour une perturbation faible conduisant au régime FGR ($\Gamma \ll \lambda$). Les lignes fines correspondent aux prédictions théoriques. (b) Variance $\sigma^2\left[\mathcal{M}_{\mathrm{L}}\right]$de la Fidélité en fonction du temps dans le régime Lyapunov ($\lambda \ll \Gamma$). La ligne solide indique la décroissance Lyapunov et fournit ainsi une preuve numérique de l'existence de la saturation Lyapunov. (Pour plus de détails voir chapitre 2)

Le liens entre irréversibilité et décohérence, ne fut pas uniquement réservé aux seuls plaisirs des théoriciens , mais fut également très prolifique au niveau expérimental. En effet les expériences d'écho abondent en résonance magnétique nucléaire (NMR) [19–21] (*Echo de spin*), en optique [22] (*Echo de photon*), dans les réseaux optique [23] (*Echo de paquet d'onde en mouvement*) et en matière condensée [25] (*Echo de charge*). Fondamentalement toutes ces expériences sont basées sur le même principe ; qui consiste à effectuer un changement effectif de la dynamique Hamiltonienne par le jeux de changement d'axes [21]. De manière assez surprenante, il est apparue que l'approche théorique basée sur l'écho de Loschmidt était incapable d'interpréter un certain nombre de résultats expérimentaux. L'exemple le plus frappant est la décroissance gaussienne indépendante de la perturbation trouvée en NMR [26], voir Figure 3. Les résultats reportés ici ont été réalisé dans un cristal de ferrocene. Au sein de ces systèmes, la perturbation peut être contrôlée par les expérimentateurs. La Figure 3 présente l'atténuation de l'écho de polarisation en fonction du temps de refocalisation. Le résultat remarquable qui peut être observé dans cette dernière est que l'atténuation sature pour des perturbations Σ faibles. Ce comportement n'est pas prédit par la théorie de l'écho de Loschmidt, en effet dans cette dernière une décroissance indépendante de la perturbation est uniquement prévue pour une perturbation suffisamment forte.

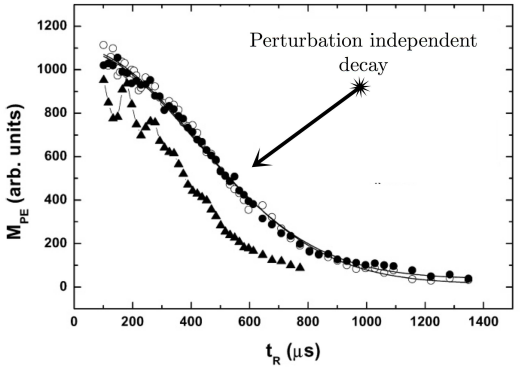

Fig. 3: Atténuation de l'écho de polarisation en fonction du temps de refocalisation dans un système de Ferrocene, pour différentes valeurs de la perturbation. La ligne solide représente la régression gaussienne et montre l' indépendance du taux de décroissance envers la perturbation ; adaptée de H.M. Pastawski et al. [26].

Lorsque nous nous sommes attaqué au problème, nous avons réalisé que l'environnement devait être traité avec précaution. En pratique, dans une expérience d'écho, seulement une inversion temporelle imparfaite est réalisée sur un sous-ensemble restreint de degrés de liberté. Dans le but de capturer l'essentiel de la physique présente dans ce type d'expérience, nous avons développé la notion de *Fidélité partielle*,

$$\mathcal{M}_{\mathrm{B}}(t) = \left\langle \psi_1 \right| \mathrm{Tr}_2 \left[e^{-i\mathcal{H}_{\mathrm{b}}t} e^{-i\mathcal{H}_{\mathrm{f}}t} \rho_0 e^{i\mathcal{H}_{\mathrm{f}}t} e^{i\mathcal{H}_{\mathrm{b}}t} \right] \left| \psi_1 \right\rangle, \tag{3}$$

où seulement une partie des degrés de liberté du système sont renversés par rapport au temps. (L'Hamiltonien lié à la propagation avancée $\mathcal{H}_{\rm f}$ et celui lié a la propagation retardée ne diffèrent que par une renversion temporelle partielle du système) Nous avons dénommé ce dernier "*l'écho de Botzmann*" $\mathcal{M}_{\rm B}(t)$. Le Chapitre 3 est consacré à cet objet et nos résultats sont publiés dans [27].

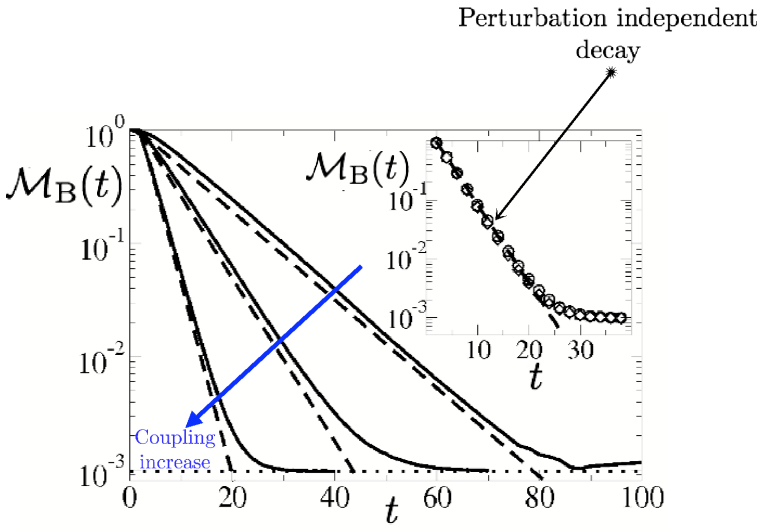

Fig. 4: Graphe principal : Echo de Boltzmann en fonction du temps pour une perturbation fixée mais pour différentes valeurs de la force du couplage avec l'environnement. Les ligne continues correspondent de droite à gauche à une augmentation de l 'intensité du couplage. Les lignes pointillées donnent la décroissance exponentielle théorique, ces derrières sont en bon accord avec les numériques . Encart : $\mathcal{M}_{\rm B}$ pour un couplage donné et différentes petites perturbations. La ligne pointillée indique la prédiction théorique qui est indépendante du couplage. (Pour plus de détails voir chapitre 3)

Nous avons présenté un calcul semiclassique et montré que même si l'opération de renversion temporelle est effectuée aves de plus en plus de précisions, le taux de décroissance sature à une valeur déterminée par le couplage avec l'environnement. Lorsque la perturbation expérimentalement contrôlable est réduite l'écho de Boltzmann est donné par

$$\mathcal{M}_{\rm B}(t) \simeq \exp[-(\Gamma_{\rm f} + \Gamma_{\rm b})t] \tag{4}$$

où $\Gamma_{\rm f,v}$ est la dispersion de la règle d'or de Fermi induite par les couplages avec l'environnement. Nous avons confirmé nos résultas numériques par des simulations (voir Figure 4). Le Graphe principal démontre clairement la décroissance exponentielle de l'écho de Boltzman et sa forte dépendance envers le couplage. De plus, l'encart illustre la situation des faibles perturbations où la décroissance est seulement déterminée par le couplage. Enfin, nous montrons que pour de faibles interactions l'écho de Boltzman atteint un régime Gaussien indépendant de la perturbation

$$\mathcal{M}_{\rm B}(t) \simeq \exp[-(\overline{\mathcal{U}_{\rm f}^2} + \overline{\mathcal{U}_{\rm b}^2})\, t^2/2]. \tag{5}$$

Ceci pourrait bien être l'explication de la décroissance indépendante de la perturbation de l'écho de polarisation observée en NMR [26].

Abandonnant de façon temporaire, la notion de décohérence, nous avons été attiré par l'étude de quantité plus proche des besoins expérimentaux. Nos recherches ont été en grande partie motivées par la diffusion de neutrons [28–30], que nous avons tenté de comprendre de façon plus profonde. Dans ce but , nous avons introduit un nouvel écho que l'on a baptisé "*Echo de déplacement*" [31]. [127].

$$\mathcal{M}_{\mathrm{D}}(t) = \left| \langle\alpha| e^{-i\mathbf{P}\hat{x}} e^{i\hat{H}t} e^{i\mathbf{P}\hat{x}} e^{-i\hat{H}t} |\alpha\rangle \right|^2. \tag{6}$$

Ce dernier est relié aux moyennes d'ensemble des fonctions de corrélation $Y_{jj}(\mathbf{P}, \mathbf{t})$ qui sont présents dans les expériences diffusion de neutron et l'émission/absorption Mössbauer. Physiquement l'écho de déplacement mesure la décroissance de la fidélité, pour laquelle on reconstruit un paquet d'onde, par une inversion temporelle, suite à un déplacement $\mathbf{P}$ dans l'espace de phase. Dans la limite semiclassique, nous montrons que le taux de décroissance est généralement donné par l'exposant de Lyapunov de la dynamique classique. De plus pour des petits déplacements, nous montrons que la décroissance Lyapunov à temps court, est suivie, en raison d'effet quantique, par un givre de la décroissance à une valeur bien supérieure à la valeur ergodique. La moyenne de l'écho de déplacement est,

$$\langle \mathcal{M}_{\mathrm{D}}(t) \rangle \propto \left[\alpha\, e^{-\lambda t} + \frac{g(|\mathbf{P}|L)}{(|\mathbf{P}|L)^2} \right], \tag{7}$$

où $g(|\mathbf{P}|L)$ est une fonction oscillante dont la forme exacte dépend de la dimension du système.

Nos résultats sont corroborés par des simulations numériques. Figure 5a présente l'écho de déplacement en fonction du temps et confirme clairement l'existence de la décroissance Lyapunov. La Figure 1.12b présente la saturation de l'écho dont la dépendance envers le déplacement est conforme à celle prévue par le second terme de Eq. (7).

Ces aspects seront traités avec plus de détails au chapitre 4 et sont publiés dans [127]. Nos résultats sont actuellement testés expérimentalement sur des systèmes de pièges à atomes froids dans le laboratoire du Mara Prentiss de l' université d'Harvard [32].

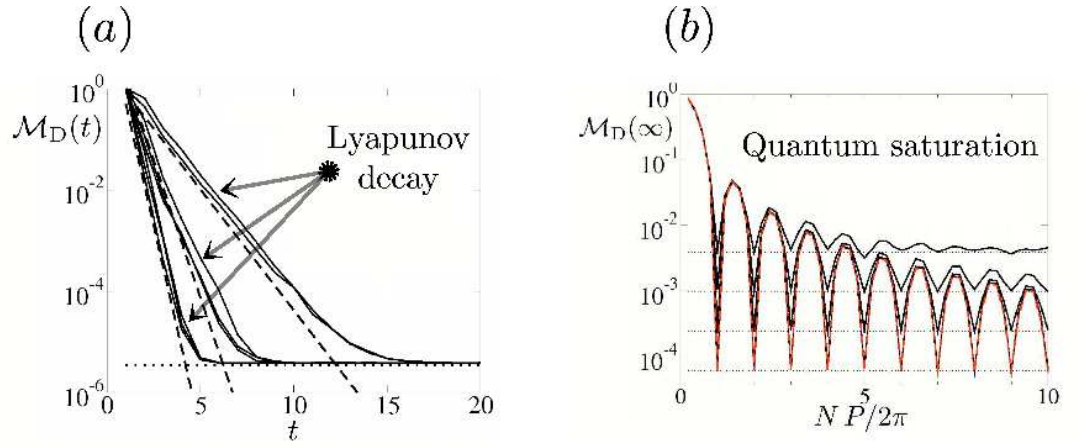

Fig. 5: (a) Echo de déplacement en fonction du temps. Les lignes pointillées correspondent à la décroissance Lyapunov prédite théoriquement . Ces dernières sont en accord avec les simulations numériques. (b) Valeur de la saturation de l'écho de déplacement. La ligne rouge pointillée indique la prédiction théorique. (Pour plus de détails voir chapitre 4)

Intrication et décohérence

Bien que les mesures d'écho quantifient la sensibilité des trajectoires quantiques par rapport à une variation d'un paramètre de contrôle extérieur, un écho n'est pas intrinsèquement une mesure directe de la décohérence. La décohérence est principalement due aux interactions avec l'environnement, aucune opération de renversion par rapport au temps n'est requise. La question fondamentale à laquelle on doit répondre concerne la notion d'interaction entre deux systèmes quantiques. Le traitement de l'interaction au niveau quantique n'est pas une tache facile. Si nous citons E. Schrödinger [33],

> *When two systems (...) enter into temporary interaction (...), and when after a time of mutual influence the systems separate again, then they can no longer be described in the same way as before, viz. by endowing each of them with a representative of its own.* [1]

Ceci définit la notion de corrélations quantiques entre systèmes, habituellement nommée *intrication.*

Dans le cadre de la décohérence, l'analyse des corrélations quantiques entre un système et un environnement est fondamentale. Nous nous sommes donc plongés dans l'étude des propriétés d'intrication d'un système de deux particules en interaction. Ces propriétés sont mesurées par la matrice de densité réduite, obtenue en traçant sur les degrés de liberté d'une des deux particules. Si nous numéro-

[1] Lorsque deux systèmes (...) entrent temporairement en interaction (...), et lorsque après une durée d'influences mutuelles les systèmes se séparent de nouveau, ils ne peuvent plus être décrit de la même manière que précédemment, c.a.d par la simple donnée de leur représentation propre

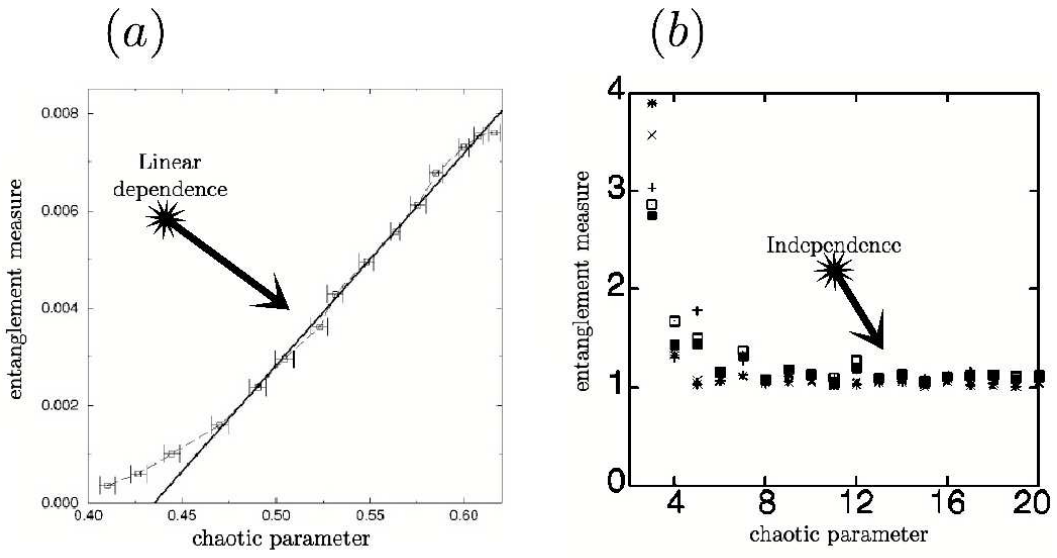

Fig. 6: Deux études numériques sur la génération l'intrication dans un système chaotique. (a) représente le taux d'intrication linéaire d'un "kicked top" couplé en fonction du paramètre de mesure du chaos ; adaptée de Miller and Sarkar [35] ; (b) représente le taux de production d'intrication d'un "kicked top" couplé en fonction du paramètre de mesure du chaos ; adaptée de A. Tanaka et al. [36]. La dépendance linéaire trouvée par [35] semble contredire l' indépendance obtenue par [36]. Cette apparente contradiction est bien expliquée par l'existence de deux régimes d'intrication [37, 38].

tons chaque particule et nommons la matrice densité du système complet $\eta(t)$. La matrice réduite relative à la première particule indexée 0 est donnée par,

$$\eta_0(t) = \mathrm{Tr}_1 \left[\eta(t)\right]. \tag{8}$$

Si cette matrice de densité réduite représente un état mélangé, les particules sont intriquées. Une bonne mesure du degré d'intrication est habituellement fournie par *l'entropie de Von Neumann.*

$$\mathcal{S}\left(\eta_0\right) = -\mathrm{Tr}\left[\eta_0 \ln\left(\eta_0\right)\right]. \tag{9}$$

Néanmoins d'un point de vue technique, il est plus commode de calculer la trace du carré de la matrice densité réduite [4],

$$\mathcal{P}(t) = \mathrm{Tr}_0\left[\eta_0^2(t)\right]. \tag{10}$$

Cette quantité est communément appelée *Pureté* $\mathcal{P}(t)$. La pureté et l'entropie linéaire $\mathcal{S}_{\mathrm{lin}}\left(\eta_1\right) = 1 - \mathcal{P}(t)$ qui lui est associée, ont l'avantage d' être calculable analytiquement et sont reliées à l'écho de Loschmidt [34]. De plus, puisque nous considérons uniquement des états globalement purs, l'entropie linéaire et de Von Neumann se comportent de la même façon.

Dans le cadre restreint du chaos quantique, la question de l'origine de la production de l'intrication au sein d'un système dynamique, fut un sujet assez controversé. En effet les premières tentatives de détermination du taux d'intrication ont été numériques. Dans un premier temps Miller et Sarkar [35] ont fourni des preuves numériques très convaincantes que l'intrication était renforcée par la présence du chaos et même déterminée par l'exposant de Lyapunov (Voir Figure 6). Cependant ces résultats furent remis en question par Tanaka et al. [36] , dont les travaux numériques montrèrent aucune augmentation de l'intrication due à la présence du chaos (Voir Figure 6). La Figure 6a présente le taux moyen d'intrication linéaire, obtenue par Miller et Sarkar pour un système de deux "kick tops quantiques " couplés. La dépendance linéaire du taux d'intrication envers l'exposant de Lyapunov est clairement illustrée. La Figure 6b présente des résultats numériques obtenus par Tanaka et al. sur le même système. Ici pour un chaos suffisamment fort le tau d'intrication sature à une valeur indépendante du paramètre de mesure du chaos. Il est crucial de comprendre que bien que les deux simulations ont été effectuées sur le même système, elle ont été réalisé dans deux régimes différents ; un chaos faible (petit exposant de lyapunov mais encore strictement positif) pour Miller et Sarkar et un chaos fort pour Tanaka et al.. Sur la base de notre expérience du semiclassique [37], nous avons résolu cette apparente contradiction et étudié la transition quantique-classique dans ce type de système [38]. Ceci sera traité au chapitre 5. Nous avons montré comment une interaction, qui s'annule dans la limite classique, génère de l'intrication entre deux particules initialement non intriquées, sans influencer leurs dynamiques classiques. Pour des dynamiques chaotiques, le taux d'intrication sature au niveau de l'exposant de Lyapunov du système lorsque que l'on augmente la force de l'interaction. La décroissance de la pureté est donnée par

$$\mathcal{P}(t) = e^{-2\Gamma_{01}t} + \alpha_0(t)e^{-\lambda_0 t} + \alpha_1(t)e^{-\lambda_1 t} \tag{11}$$

Si on se limite à l'intrication entre particules ($\lambda_0 = \lambda_1$) ou si on considère que la particule 1 joue le rôle de l'environnement ($\lambda_1 \gg 1$), Eq.(11) distingue 2 régimes de décroissance exponentielle pour la pureté :

1. Le régime de la règle d'or de Fermi, $\mathcal{P}(t) \propto e^{-2\Gamma_{01}t}$, si $\Gamma_{01} \leq \lambda_0$. Il correspond à un régime purement quantique généré par le couplage entre les deux particules.
2. La décroissance exponentielle liée à l'exposant de Lyapunov du système, $\mathcal{P}(t) \propto e^{-\lambda_0 t}$, si $\lambda_0 \leq \Gamma_{01}$. Il correspond à un régime purement classique généré par la dynamique classique du système.

Nous avons confirmé numériquement l'existence de ces deux régimes. La Figure 7 présente la Pureté obtenue pour un système de deux "kick rotors" couplé. La Figure 7a présente le régime à fort couplage dans lequel le régime Lyapunov est atteint. Ces numériques correspondent à ceux obtenus par Miller et Sarkar. La Figure 7b considère le régime de faible couplage en comparaison au chaos, et confirme clairement l'existence d'un régime quantique. Ce dernier correspond à celui étudié par Tanaka.

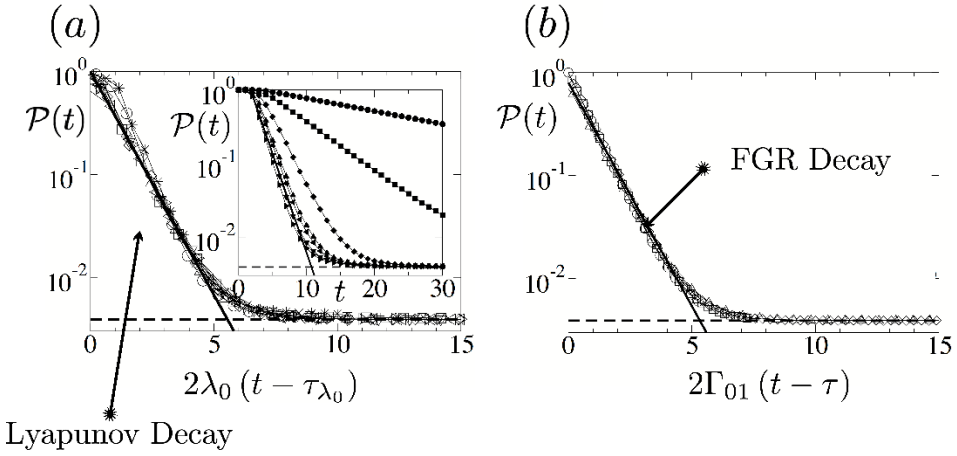

Fig. 7: (a) Graphe principal : La Pureté de la matrice densité réduite dans le régime de Lyapunov de couplage fort, l'axe des temps a ete rééchelonné par l'exposent de lyapunov du système. Encart : La Pureté de la matrice densité réduite en fonction du temps, lorsque l'on augmente la force du couplage. (b) La Pureté de la matrice densité réduite dans le régime FGR ($\Gamma_{01} \leq \lambda_0$)l'axe des temps a ete rééchelonné par la dispersion de la règle d'or de Fermi. (Pour plus de details vois chapitre 5)

Finalement dans le régime de saturation Lyapunov, la fonction de Wigner à une particule suit la dynamique classique de plus de plus précisément dès que l'on rentre de plus en plus profondément dans le régime semiclassique. Ceci démontre que le principe de correspondance quantique-classique ne requière au niveau microscopique aucune limite haute température, ni la présence d'un couplage avec un large nombre de dégrés de liberté extérieur. La Figure. 8 présente l'évolution temporelle d'une distribution classique (en haut à gauche), et trois évolutions dans l'espace de phase de la fonction de Wigner à une particule : (i) (en haut à droite) pour le système libre ; (ii) and (iii) (en bas gauche et droite) pour un système couplé dans le régime Lyapunov. En bas de gauche à droite, on entre de plus en plus profondément dans la limite semiclassique. La distribution classique et la fonction de Wigner se correspondent de mieux en mieux dans cette limite. (On note qu'il ne faut point considérer 4 réplications fantômes due à la procédure numérique utilisée (voir chapitre 5) .

Nous sommes actuellement en train de généralisée cette procédure au cas de l'intrication à plusieurs particules. Cette extension est basée sur la concurrence généralisé développée par Mintert et al. [39].

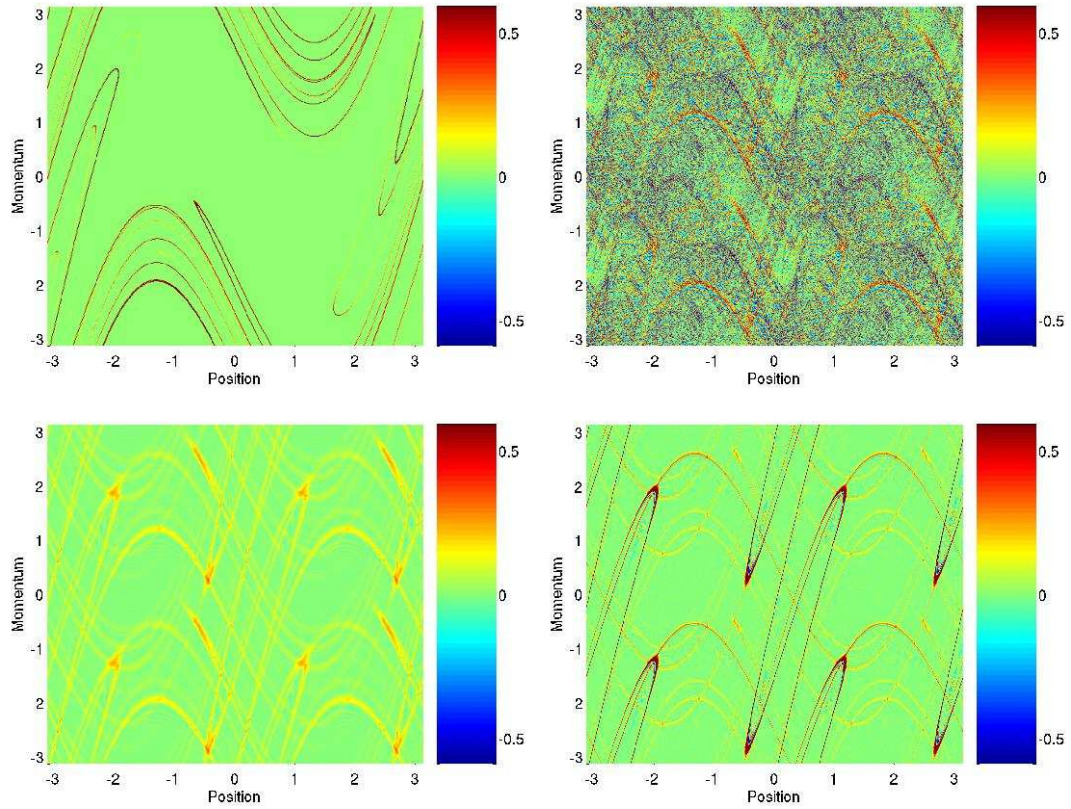

Fig. 8: Representation de l'espace de phase pour une distribution classique (en haut à gauche), la distribution quantique de Wigner non couplée (en haut à droite) et couplée (en bas gauche et droite), avec une augmentation de la limite semiclassique de gauche et droite. (Pour plus de détails voir chapitre 5)

Transport quantique et déphasage

Nous avons appliqué les connaissances acquises lors de nos investigations sur la décohérence, au problème plus pratique du transport quantique dans les systèmes mésoscopiques. En effet ce domaine possède de nombreux phénomènes, comme *la localisation faible* [46, 47] ou *les fluctuations universelles de conductances* (UCF) [48, 49]. Ces dernières représentent une des manifestations les plus spectaculaires de la cohérence quantique. Il reste encore difficile à accéder expérimentalement à l'effet du déphasage sur le transport à travers ce type de systèmes. Cependant le transport mésoscopique a l'avantage de permettre une étude expérimentale de ces phénomènes.

D'un point de vue théorique, les méthodes semiclassique ont été très rapidement employées [41–43] et ont montrées un pouvoir prédictif certains. Effectivement, lorsque le mouvement des électrons est balistique et chaotique, les propriétés de transport sont bien décrites par la théorie des matrices aléatoires (RMT). Cependant suite au travaux fondateurs de Aleiner et Larking [40] une nouvelle échelle de temps doit être considérée, le temps d'Ehrenfest τ_{E}. Le temps d'Ehren-

fest correspond au temps durant lequel un paquet d'onde bien localisé (largeur $\propto \lambda_F$) se disperse jusqu'à atteindre une échelle de longueur macroscopique ($\mathcal{L}$) ; $\tau_E \propto \lambda^{-1} \ln[\mathcal{L}/\lambda_F]$.

Dès que τ_E devient un paramètre essentiel, cette universalité est brisée. Dans ces conditions la théorie des matrices aléatoire cesse de décrire correctement les propriétés de transport. (Voir Figures 9).

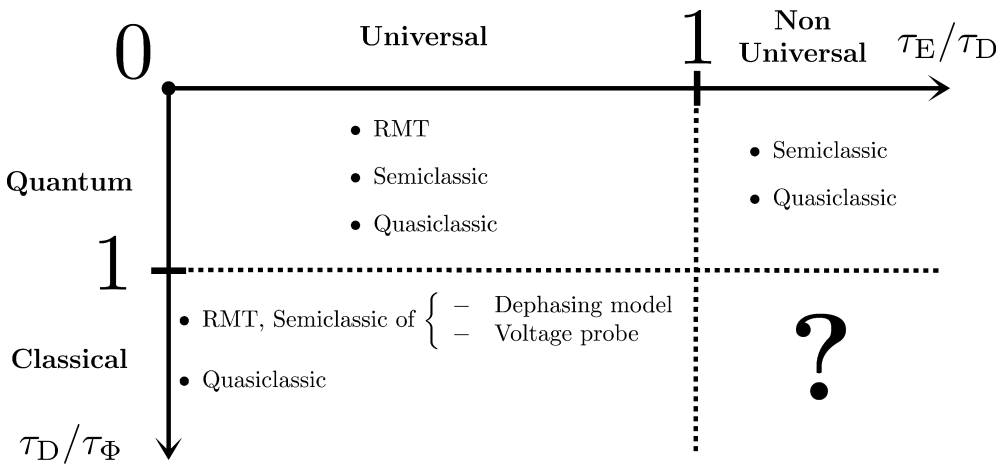

Fig. 9: L'abscisse correspond à l'axe chaotique de retour au domaine classique. Pour un temps d'Ehrenfest τ_E plus grand que le temps de séjours dans la cavité τ_D, des corrections non universelles doivent être pris en compte. L'ordonnée correspond à la transition quantique-classique reliée déphasage. Ce diagramme présente quatre régimes. Le régime purement quantique (secteur en haut à gauche) bien décrit par la RMT et les méthodes semiclassique, le régime non universel quantique (secteur en haut à droite) bien décrit par l'approche semiclassique et quasiclassique [40], le régime de décohérence universelle (secteur en bas à gauche) obtenu via le traitement RMT où semiclassique de modèle plus ou moins phénoménologique, et enfin le domaine non universel classique (secteur en bas à droite) qui constitue l'objet de la Partie V de cette thèse.

Il est important de réaliser que si le temps de déphasage τ_ϕ est l'échelle de temps après laquelle les interférences quantique disparaissent, le temps d'Ehrenfest τ_E est une nouvelle échelle qui gouverne leurs apparitions. Dun coté l'étude de la disparition des effets quantique lié à l'omniprésence du déphasage a été entreprise principalement à l'aide de modèles plus où moins phénoménologiques [50,51]. De l'autre coté l'influence d'un temps d'Ehrenfest fini a été maintenant largement étudiée [42, 43] et à clairement confirmé la brisure de l'universalité quantique.

Cepandant, exception faite du travail de Aleiner et Larking [40], l'étude de la compétition entre le temps d'Ehrenfest et le temps de déphasage n'a pas été très développé. Une telle recherche est fondamentale car chacune de ces échelles de temps détermine une manière particulière d'atteindre le domaine classique.

Le chapitre 6 de cette thèse se concentre sur l'analyse semiclassique du déphasage sur le transport quantique au travers de cavité chaotique avec un temps d'Ehrenfest fini. Ceci nous a permi d'aborder la transition du domaine purement

quantique (secteur en haut à gauche de la Figure 9) au domaine non universel classique (secteur en bas à droitede la Figure 9). Nous avons étudié le déphasage d'un système balistique ouvert dans la limite où la taille du système est large comparée à la longueur d'onde de Fermi [45]. A l'aide de théorie basée sur les trajectoires semiclassique [41–43], nous avons premièrement calculé les corrections de localisation faible pour un point quantique capacitivement couplé à un point quantique externe et fermé. Dans ce but, nous avons étendu le formalisme standard développé par Büttiker [50]. Deuxièmement, en s'inspirant du travail effectué par Whitney [52], nous avons inclus l'effet des barrières tunnel dans la théorie semiclassique de modèle dit de "dephasing voltage probe". (Pour une définition du modèle, voir [50, 51]). Nous avons trouvé, en plu de la suppression algébrique universelle reliée au rapport $\tau_{\rm D}/\tau_\phi$, un facteur de suppression exponentiel de la localisation faible.

$$g^{\rm wl} = \frac{g_0^{\rm wl}}{1+\tau_{\rm D}/\tau_\phi}\,\exp[-\tilde{\tau}/\tau_\phi], \tag{12}$$

Nous avons fait apparaître que l'échelle de temps typique impliquée $\tilde{\tau}$dans cette suppression dépend du système. Dans le cas du modèle de "dephasing voltage probe". il coïncide avec le temps d'Ehrenfest $\tilde{\tau} \propto \tau_{\rm E}$, ce résultat est à comparer avec celui obtenu pour le modèle du point quantique externe, dans ce cas l'échelle de temps dépend de la longueur de corrélation macroscopique du potentiel de couplage$\tilde{\tau} \propto \lambda^{-1}\ln[L/\xi]$.

Nous notons qu'un comportement similaire a été récemment obtenu pour les fluctuations universelles de conductance par Altland, Brouwer and Tian [44].

Bibliographie

[1] D.L. Shepelyansky, Physica **D8**, 208 (1983)

[2] A. Peres, Phys. Rev. A **30**, 1610 (1984).

[3] E. Joos, H.D. Zeh, C. Kiefer, D. Giulini, J. Kupsch, I.-O. Stamatescu, *Decoherence and the Appearance of a Classical World in Quantum Theory*, (Springer, Berlin 2003)

[4] W. H. Zurek, Rev. Mod. Phys. **75**, 715 (2003).

[5] R.A. Jalabert and H.M. Pastawski, Phys. Rev. Lett. **86**, 2490 (2001).

[6] Ph. Jacquod, P.G. Silvestrov, and C.W.J. Beenakker, Phys. Rev. E **64**, 055203(R) (2001).

[7] N.R. Cerruti and S. Tomsovic, Phys. Rev. Lett. **88**, 054103 (2002).

[8] F.M. Cucchietti, C.H. Lewenkopf, E.R. Mucciolo,H.M. Pastawski, and R. O. Vallejos, Phys. Rev. E **65**, 046209 (2002).

[9] Ph. Jacquod, İ. Adagideli, and C.W.J. Beenakker, Phys. Rev. Lett. **89**, 154103 (2002).

[10] Z. P. Karkuszewski, C. Jarzynski, and W.H. Zurek, Phys. Rev. Lett. **89**, 170405 (2002).

[11] J. Vaniček and E.J. Heller, Phys. Rev. E **68**, 056208 (2003).

[12] T. Prosen, T.H. Seligman, and M. Znidaric, Prog. Theor. Phys. Supp. **150**, 200 (2003).

[13] Y. Adamov, I.V. Gornyi, and A.D. Mirlin, Phys. Rev. E **67**, 056217 (2003).

[14] J. Emerson, Y.S. Weinstein, S. Lloyd, and D.G. Cory, Phys. Rev. Lett. **89**, 284102 (2002).

[15] W. Wang, G. Casati, and B. Li, Phys. Rev. E **69**,025201(R) (2004).

[16] A. Iomin, Phys. Rev. E **70**, 026206 (2004).

[17] T. Gorin, T. Prosen, T.H. Seligman, M. Znidaric, Phys. Rep. **435**, 33 (2006).

[18] C. Petitjean, Ph. Jacquod, Phys. Rev. E **71**, 03623 (2005).

[19] E.L. Hahn, Phys. Rev. **80**, 580 (1950).

[20] W.K. Rhim, A. Pines, J.S Waugh, Phys. Rev. Lett. **25**, 218 (1970).

[21] H.M. Pastawski, P. R. Levstein, G. Usaj, Phys. Rev. Lett. **75**, 4310 (1995).

[22] N.A. Kurnit, I.D. Adella, S.R. Hartmann, Phys. Rev. Lett. **13**, 567 (1964)

[23] F.B.J. Buckremer, R. Dumke, H. Levsen, W. Ertmer, Phys. Rev. Lett. **85**, 3121 (2000)

[24] M.F Andersen, A. Kaplan, N. Davidson, Phys. Rev. Lett. **90**, 023001 (2003)

[25] Y. Nakamura, Y.A. Pashkin, T. Yamamoto, J.S. Tsai, Phys. Rev. Lett. **88**, 047901 (2002)

[26] H.M. Pastawski, P.R. Levstein, G. Usaj, J. Raya, and J. Hirschinger, Physica A **283**, 166 (2000)

[27] C. Petitjean, Ph. Jacquod, Phys. Rev. Lett. **97**, 0124103 (2006).

[28] L. Van Hove, Phys. Rev. **95**, 249 (1954).

[29] S.W. Lovesey, *Theory of Neutron Scattering from Condensed Matter*, Vol. 1 (Oxford University Press, New York, 1984).

[30] E.J. Heller, J.R. Reimers and G. Drolshagen, Phys. Rev. A **36**, 2613 (1987).

[31] C. Petitjean, D.V. Bevilaqua, E.J. Heller and Ph. Jacquod, Phys. Rev. Lett. **98** , 164101 (2007).

[32] E.J. Su, S. Wu, M. Prentiss, eprint : physics/0701018.

[33] E. Schrödinger, Proc. Cambridge Phil. Soc. **31**, 555 (1936).

[34] F. M. Cucchietti, D. A. R. Dalvit, J. P. Paz, and W. H. Zurek Phys. Rev. Lett. **91**, 210403 (2003)

[35] P. A. Miller and S. Sarkar, Phys. Rev. E **60**, 1542 (1999)

[36] A. Tanaka, H. Fujisaki, and T. MiyaderaPhys. Rev. E **66**, 04520R (2002)

[37] Ph. Jacquod, Phys. Rev. Lett. **92**, 150403 (2004).

[38] C. Petitjean and Ph. Jacquod, Phys. Rev. Lett. **97**, 194103 (2006).

[39] F. Mintert, A.R.R. Carvalho, M.Kus and A. Buchleitner, Phys. Rep, **415**, 207 (2005).

[40] I.L. Aleiner and A.I. Larkin, Phys. Rev. B **54**, 14423 (1996) ; Phys. Rev. E **55**, R1243 (1997).

[41] K. Richter and M. Sieber, Phys. Rev. Lett. **89**, 206801 (2002).

[42] Ph. Jacquod and R.S. Whitney, Phys. Rev. B **73**, 195115 (2006).

[43] P.W. Brouwer and S. Rahav,Phys. Rev. B **74**, 075322 (2006).

[44] A. Altland, P.W. Brouwer and C. Tian, eprint : cond-mat/0605051.

[45] C. Petitjean, Ph. Jacquod and R.S Whitney, eprint : cond-mat/0612118.

[46] P. W. Anderson, E. Abrahams, and T. V. Ramakrishnan Phys. Rev. Lett. **43**, 718 (1979).

[47] L. P. Gorkov, A. I. Larkin, and D. E. Khmelnitskii, Sov. Phys. JETP **30**, 248 (1979).

[48] B.L. Altshuler, Sov. Phys. JETP **41**, 648 (1985).

[49] P.A. Lee and A.D. Stone, Phys. Rev. Lett. **55** 1622 (1985).

[50] M. Büttiker, Phys. Rev. B **33**, 3020 (1986).

[51] M. J. M de Jong and C. W. J. Beenakker Physica A**A 230**, 219 (1996).

[52] R.S. Whitney, Phys. Rev. B **75**, 235404 (2007).

Part I

Introduction and Summary

CHAPTER 1

Introduction and Summary

Despite decades of investigations, no experiment, nor theoretical calculation has ever invalidated quantum mechanics. Yet, the world surrounding us is made out of quantum mechanical building blocks, which inevitably had people wondering what is the mechanism behind this quantum-classical crossover.

This interpretational quest is as old as quantum theory itself. The source of the problem is the quantum principle of superposition, which, in effect, exponentially expands the set of available states to all of the conceivable superpositions. The first explanation of how a single outcome emerges from this multitude of potentialities was proposed by Bohr with the orthodox Copenhagen interpretation of quantum mechanics. According to the latter, there exists a boundary that preserves a strict distinction between the classical macroscopic world and the microscopic quantum realm. The nature of the boundary between the quantum and the classical was ipso facto only a purely philosophical problem. Moreover the precise location of this boundary is ill defined. Indeed, at first glance we could be tempted to place macroscopic objects on the classical side. This classification, however is immediately invalidated by macroscopic quantum effects. For instance quantum states associated with the currents of superconducting Josephson junctions involve macroscopic numbers of electrons, but still they can tunnel between the minima of the effective potential [2]. Despite the argumentation of Bohr in favor of a mobile boundary, we must admit that this explanation is clearly insufficient.

The correspondence principle states that in certain classical limits, (large quantum numbers), quantum theory should reproduce the predictions of classical theory with vanishing errors. These general arguments can be enriched by invoking the Ehrenfest theorem, according to which a sufficiently narrow quantum wave packet moves along a classical trajectory. However at sufficiently long time the quantum evolution of a system that is chaotic in the classical limit will

not be chaotic. This is due to the discreteness of the quantum spectra. Thus the quantum-classical correspondence is only valid at short times [3–6].

In the 1970's and 1980's the question has been revisited with the work of Zeh and Zurek on *decoherence* [7–9]. The main idea is the realization that macroscopic systems are never isolated from their environments. The evolution of a particular system is thus given by a reduced density matrix obtained after tracing over the environment degrees of freedom. Time evolution of the reduced density matrix is no longer unitary, consequently off diagonal terms vanish and thus with them quantum coherence, as exemplified by the Aharonov-Bohm effect.

In the course of this thesis, my research has been devoted to this quantum to classical transition, with a particular interest in the behavior of systems in which the classical limit is non integrable. This particular class of systems defines a field usually denoted as "*Quantum Chaos*". This thesis treats the interconnection between three fundamental aspects of this field. I started by considering the dynamical properties of chaotic quantum Hamiltonians in the context of *quantum reversibility*. These investigations led me to consider the notions of *entanglement* and *decoherence* for such systems. Finally I have started to work on the issue of dephasing in transport through quantum chaotic systems in the deep semiclassical limit.

The purpose of this chapter is firstly to introduce the fundamental concepts around which this thesis orbits. In section 1.1, we briefly summarize today's knowledge in the field of quantum chaos, and discuss the quantum-to-classical crossover induced by decoherence. Since some of the investigations presented in this thesis pertain to the sub-field of condensed matter physics called "*mesoscopic physics*", we close section 1.1 by a short presentation of the mesoscopic regime. Secondly, in section 1.2 we summarize the main results obtained in this thesis.

1.1 Quantum chaos and decoherence

1.1.1 From classical chaos to quantum chaos

The notion of classical chaos emerged near the end of the 19^{th} century in the study of astronomical problems. The field takes its root in the pioneering works of Poincaré [10], that uncovers the possible unstable behavior of the solar system. Following Poincaré, chaos was mostly investigated by mathematicians, from Birkhoff to Kolmogorov. Only the advent of computers, which facilitated the study of the inherent complexity of such systems, led to a democratization of the subject. From the first numerical investigation by Lorentz [11], chaos has since been found to play a role in physics as well as in other disciplines, and to apply to numerous phenomena from plasma confinement [12] to disease epidemiology [13].

What exactly is chaos ? There exist various references on the subject going from a mathematical treatise [14] to a more physical description [15]. In order to get a panorama of the aspects that are of interest to mathematicians and physicists alike we refer to [16], and for more details to [17] and references therein.

Roughly speaking classical chaos is defined as an exponential sensitivity with respect to initial conditions, see Fig. 1.1. This property can be quantified as

$$|\delta\mathbf{x}(t)| \simeq \exp[\lambda t]\,|\delta\mathbf{x}(0)|, \tag{1.1}$$

where $|\delta\mathbf{x}(0)|$ is the initial separation between two points in phase space and λ, the mean rate of separation of trajectories of the system, is called the *Lyapunov exponent*.

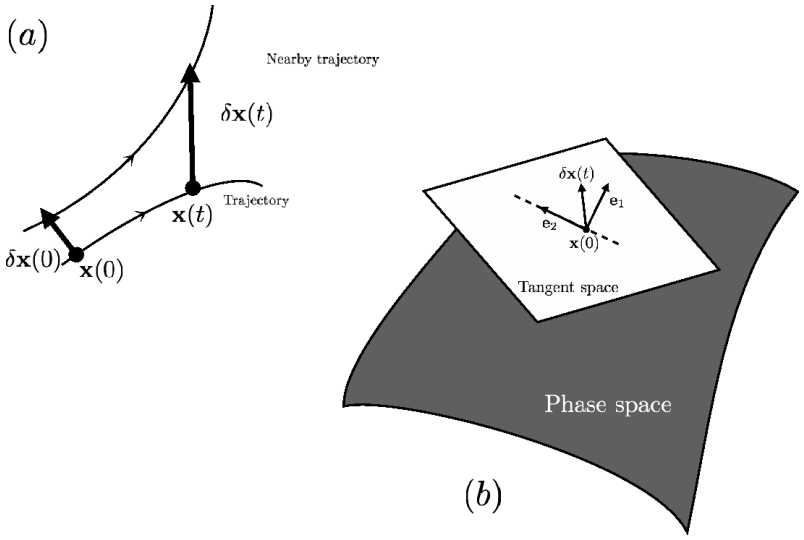

Figure 1.1: Definition of Lyapunov characteristic exponents; $\delta\mathbf{x}(t)$ is a tangent vector. (a) Two nearby initial conditions that separate as time evolves. (b) Tangent space of the Lyapunov exponents λ_1, λ_2 for a two-dimensional flow.

More precisely we need to compute the quantity

$$\mathbf{\Lambda}(\delta\mathbf{x}(0), \delta\mathbf{x}(t)) = \lim_{\substack{t\to\infty \\ |\delta\mathbf{x}(0)|\to 0}} \left(\frac{1}{t}\right) \ln \frac{|\delta\mathbf{x}(t)|}{|\delta\mathbf{x}(0)|}. \tag{1.2}$$

Assuming the existence of a $2d$ dimensional basis $\{\mathbf{e}_i\}$ of $\delta\mathbf{x}(t)$, $\mathbf{\Lambda}$ takes one of the possibly non distinct values $\lambda_i = \mathbf{\Lambda}(\delta\mathbf{x}(0), \mathbf{e}_i)$. (Cf for example Fig. 1.1.) The λ_i can be ordered by size and are independent of the choice of the initial conditions $\delta\mathbf{x}(0)$ [18, 19]. The largest one $\lambda = \max(\lambda_1 \cdots \lambda_i \cdots \lambda_{2d})$ is commonly called the *Lyapunov exponent*.

The opposite extreme to chaos is the integrable regular system, where two points initially close do not diverge exponentially fast. The difference between chaotic and regular relies thus on the rate of divergence. An even more rigorous definition of chaos is provided by the ergodic hierarchy (See [15] for a review).

The latter differentiates between several classes of systems which are :

Ergodic systems : A system is ergodic when its time average and its spatial average can be equated, mathematically this means that the following condition is satisfied

$$\lim_{T\to\infty}\frac{1}{T}\int_0^T \mathrm{d}t\; f\left(x(t)\right) = \int_{\mathcal{M}} \mathrm{d}\mu\; f(x) \tag{1.3}$$

for any observable $f(x)$ in the d-dimensional phase space $\mathcal{M}$, with the invariant measure μ.

Mixing systems : A traditional example of a mixing system considers a shaker containing 20% of orange juice and 80% of vodka. After the liquid has been shaken sufficiently often, every part of it will contain the same initial ratio of orange juice and vodka.

In mathematical terms, if we let A and B be two measurable subsets of phase space $\mathcal{M}$ and assume that the measure $\mu\left[\{y \in B | y = x(t) \,\text{and}\, x(0) \in A\}\right]$ converges to $\mu\left(B\right)$, the mixing property is defined by the following condition

$$\lim_{T\to\infty}\mu\left[A \cap x\left(B(-T)\right)\right] = \mu\left[A\right]\mu\left[B\right], \tag{1.4}$$

where we let $x\left[B(-t)\right] = \{y = x(-t) | x(0) \in B\}$.

We note that mixing presupposes ergodicity.

K-systems : K-systems have a positive KS (Kolmogorov, Krylov, Sinai) entropy [20,21]. This particular entropy is a measure of the degree of chaoticity of the whole system. Intrinsically this is a global property. Following [15,16] we will define the KS entropy. At first if we let $\mathcal{P}$ and $\mathcal{P}'$ be two partitions we define the partition $\mathcal{P} \vee \mathcal{P}'$ as

$$\mathcal{P} \vee \mathcal{P}' = \{A \cap B | A \in \mathcal{P}, B \in \mathcal{P}'\}.$$

Now if one is given a partition $\mathcal{P}(0) = \{A_i(0)\}$ of the phase space $\mathcal{M}$, at time $t = 0$, and if we evolve each element backward in time, after a unit time we get a new partition $\mathcal{P}(-t) = \{A_i(-t)\}$. The elements of $\mathcal{P}(-t) \vee \mathcal{P}(0)$ are typically smaller than any of the $A_i(-t)$. We want to find under which condition the measure of a typical element of $\mathcal{P}(-t+1) \vee \mathcal{P}(-t)$ decrease exponentially as $t \to \infty$. This information is contained in the entropy of the dynamical system. The entropy of a dynamical system with respect to the partition $\mathcal{P}(0)$ and the measure μ is defined by

$$H_\mu\left(f, \mathcal{P}(0)\right) = -\lim_{t\to\infty}\frac{1}{t}\sum_{i=1}^{t}\mu\left[\vee_{j=0}^{t-1}\mathcal{P}(-j)\right]\ln\left[\mu\left[\vee_{j=0}^{t-1}\mathcal{P}(-j)\right]\right]. \tag{1.5}$$

The KS entropy is defined as

$$h_\mu\left(f\right) = \sup_{\mathcal{P}(0)} H_\mu\left(f, \mathcal{P}(0)\right). \tag{1.6}$$

The KS entropy is positive if and only if there is an exponential decrease of the average of the elements of $\vee_{j=0}^{t-1}\mathcal{P}(-j)$. To have positive KS entropy, a system must be mixing.

Let us note that for closed systems, the KS entropy (going backward in time) is naturally related to the Lyapunov exponent (going forward in time) by Pesin theorem [22] :

$$h_\mu(f) = \int_{\mathcal{M}} \left[\sum_{\lambda_i > 0} \mathbf{\Lambda}(\mathbf{x}, \mathbf{e}_i) \right] \mathrm{d}\mu. \tag{1.7}$$

C-systems : C-systems are determined by the structure of their tangent space. The latter decomposes into three parts,

- one component space along the trajectory which has a vanishing Lyapunov exponent,
- one component in which the trajectories diverge exponentially with a exponent locally bounded from below for all times and all initial conditions.
- one space in which the trajectories converge exponentially with a exponent bounded from above for all times and all initial conditions.

Let us note that C-systems have positive KS entropy.

B-systems : Also called Bernoulli systems, in this case at least one observable is discrete and therefore is more easily defined for maps than flows. This class of systems is the strongest in the ergodic hierarchy. Without additional information on where the phase point is or came from, the outcome of the mapping in B-systems, is essentially random, irrespective of the history of the dynamics.

This hierarchy is summarized in Fig. 1.2. Chaos sets in at the level of K-systems, and also includes B and C-systems. All these properties are global and imply that mixed systems (systems that present regular islands) do not fall into this classification.

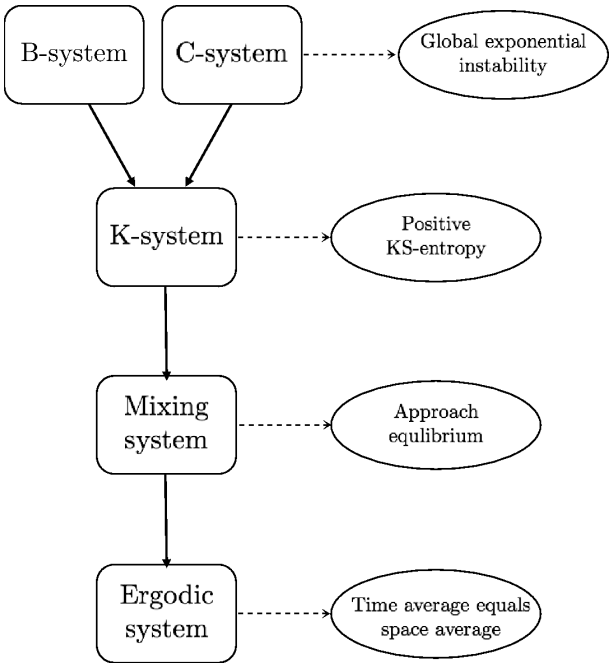

Figure 1.2: Systems exhibiting random behavior and their relationships : The ergodic hierarchy.

The quantum description of systems which are chaotic in their classical limit is the subject of *Quantum Chaos* [17, 23–28].

Attempts to employ classical concepts in quantum mechanics, are as old as quantum theory itself. The Bohr-Sommerfeld quantization rule, a precursor of the modern quantum theory, enters clearly in this category. Integrable systems are characterized by an invariant manifold related to constants of motion, the $2d-$dimensional phase space is then completely stratified into $d-$dimensional sets with the topology of a torus. This means that a phase point is determined by a vector θ consisting of d angles and a $d-$dimensional action vector $\mathbf{I}$. According to that a more refined quantization procedure is known as the Einstein-Brillouin-Keller (EBK) or torus quantization.

$$I_n = \frac{1}{2\pi} \oint_\gamma \mathbf{p}\mathrm{d}\mathbf{q} = \left(n_\gamma + \frac{\mu_\gamma}{4}\right) \hbar, \tag{1.8}$$

where $\mathbf{p}$ and $\mathbf{q}$ are the canonically conjugate monentum and spacial coordinate. I_n is the characteristic actions of the n-torus, μ_γ the corresponding Maslov indices and n_γ is the good quantum number. The contour integral is computed over closed trajectories γ on the n-torus.

According to the laws of classical Hamiltonian dynamics, chaotic systems have more degrees of freedom than the constants of motion. In the simplest case the only constant of motion is the energy. The destruction of constants of motion implies the destruction of tori and as a consequence the path of integration in Eq. (1.8) is ill defined. This fact was already noticed by Einstein, in the early

1917's, when he recognized the non applicability of the EBK method for non integrable system, in the context of the Helium atom [29].

At a dynamical level also, the classical definition of chaos cannot be applied to quantum mechanics, since the Schrödinger equation is linear, the time evolution operator is unitary and the scalar product between two states is constant. The field of *Quantum Chaos* deals with the apparent paradox that despite the presence of the correspondence principle, chaos seems to be absent from quantum mechanics. It addresses fundamental questions, related to the dependance of the quantum properties on the underlying classical dynamics of a physical system.

There are two main approaches to the quantum theory of chaotic systems : The approach through semiclassical quantum mechanics pioneered by Gutzwiller [25] and the approach based on the theory of random matrix (RMT) [30] firstly applied by Bohigas, Giannoni, and Schmit [31], see also Refs [32, 33]. The latter is a statistical approach to quantum chaos. The Bohigas-Giannoni-Schmit conjecture (BGS conjecture) states, on the basis of strong numerical evidence, that statistical properties of quantum systems whose limit is chaotic are well described by RMT. RMT was developed by Wigner and Dyson in the contex of nuclear physics [34, 35], for a review on RMT we refer to [36]. Complex systems, in RMT, are represented by ensemble of Hamiltonians with statistically independent matrix elements only constrained by symmetry. These ensembles can be shown to have maximum statistical entropy. There exist three different symmetry classes characterized by the number $\beta = \{1, 2, 4\}$ of independent components of the Hamiltonian matrix. Systems which present time reversal symmetry and spin rotational symmetry fall in the Gaussian Orthogonal Ensemble (GOE) with $\beta = 1$. Breaking of the time reversal symmetry lead to the Gaussian Unitary Ensemble (GUE) with $\beta = 2$. Finally if we break the spin rotational symmetry but not time reversal symmetry we deal with the Gaussian Symplectic Ensemble (GSE) with $\beta = 4$.

The study of the properties of these ensembles provides us with various quantum signatures of chaos. We refer to [23] for more details and consider here only the example of the level spacing distribution $P(S)$. The spectrum of an Hamiltonian can be partially characterized by $P(S)$, where S is the re-normalized spacing between two consecutive energy levels. For integrable systems it has been shown that levels are uncorrelated thus the level spacing is given by the Poisson distribution [37],

$$P(S) \propto \exp[-S], \tag{1.9}$$

this is clearly different for chaotic systems that present level repulsion characterized by the Wigner-Dyson distribution,

$$P(S) \propto S^{\beta} \exp[-\alpha S^2], \tag{1.10}$$

where α is a numerical factor of order one. Such a signature of chaos has been widely verified in many numerical studies.

In the semiclassical approach, one makes a more direct connection to the classical dynamics. Research in this direction was initiated by Gutzwiller with his

derivation of the *trace formula* [40,41]. Semiclassical trace formulae are sums over Fourier-like components associated with classical paths and establish a connection between quantum object such as the spectral density and pure classical terms such as the action along the orbits and stability amplitudes. Since the action enters as a phase, interference effect are introduced. Gutzwiller's derivation of the quantum density of states, is based on a semiclassical evaluation of the Feynman path integral in terms of a saddle point (stationary phase) approximation. For a review on semiclassical methods we refer to [38,39]. We will here only illustrate the method by a presentation of the semiclassical treatment of the density of state. The latter is related to the trace of the energy dependent Green function $G(\mathbf{r},\mathbf{r}';E)$,

$$d(E) = -\frac{1}{\pi}\,\Im\mathrm{m}\left[\int \mathrm{d}\mathbf{r} G(\mathbf{r},\mathbf{r}E)\right]. \tag{1.11}$$

The semiclassical energy dependent Green function is of the form,

$$G_{\mathrm{sc}}(\mathbf{r},\mathbf{r}';E) = \frac{1}{i\hbar(2\pi i\hbar)^{(d-1)/2}}\sum_{\gamma} D_\gamma(\mathbf{r},\mathbf{r}')\exp\left[\frac{i}{\hbar}S_\gamma(\mathbf{r},\mathbf{r}') - i\mu_\gamma\frac{\pi}{2}\right], \tag{1.12}$$

where the sum is performed over all classical trajectories γ connecting the two fixed points $\mathbf{r}$, $\mathbf{r}'$ at energy E, and

$$S_\gamma(\mathbf{r},\mathbf{r}') = \int_\gamma \mathbf{p}\mathrm{d}\mathbf{q} \tag{1.13}$$

is the accumulated action along the path γ. The classical amplitude D_γ describes the local density in position space and energy of trajectories near γ and can be written as

$$D_\gamma = \left|\begin{array}{cc} \frac{\partial^2 S_\gamma}{\partial\mathbf{r}\partial\mathbf{r}'} & \frac{\partial^2 S_\gamma}{\partial\mathbf{r}\partial E} \\ \\ \frac{\partial^2 S_\gamma}{\partial E\partial\mathbf{r}'} & \frac{\partial^2 S_\gamma}{\partial E^2} \end{array}\right|^{1/2}. \tag{1.14}$$

Finally μ_γ is the Maslov index that counts the number of conjugate points.

This semiclassical treatment leads to a natural representation of the density of state as

$$d(E) = \overline{d}(E) + d^{\mathrm{osc}}(E). \tag{1.15}$$

This decomposition into a smooth part $\overline{d}(E)$ and an oscillating part $d^{\mathrm{osc}}(E)$ has a rigorous meaning only in the semiclassical regime ($E \to \infty$). The smooth part corresponds to the Weyl or Thomas-Fermi part of the density of state. Oscillatory terms arise from contributions to $G(\mathbf{r},\mathbf{r};E)$ of paths of finite length closed in position space. The standard way to obtain $d^{\mathrm{osc}}(E)$ is an evaluation of the integral Eq. (1.12) by stationary phase approximation. This selects the periodic orbits, trajectories closed in configuration space and in phase space. For chaotic systems periodic orbits are isolated and unstable, nevertheless they are dense in the phase space so calculation can be performed. This yields the Gutzwiller trace

formula,

$$d^{\mathrm{osc}}(E) \simeq \sum_{\mathrm{p.o}} \sum_{j=1}^{\infty} \mathcal{A}_{\mathrm{p.o}}(E,j) \cos\left[j\left(S_{\mathrm{po}} - \mu_{\mathrm{p.o}}\frac{\pi}{2}\right)\right], \tag{1.16}$$

where the double sum is taken over contributions from all classical primitive periodic orbits and j denotes their multiple traversal, and the amplitude $\mathcal{A}_{\mathrm{p.o}}(E,j)$ depends on the energy, the time period $T_{\mathrm{p.o}}$ and the stability of the orbits.

Connection between RMT and the semiclassical approach has been recently investigated by Müller et al. [42,43]. The validity of the BGS conjecture has now even been established semiclassically [44].

In this thesis we will use independently RMT and semiclassical methods.

1.1.2 From the quantum to the classical world : Decoherence

In 1932 Erwin Schrödinger proposed a Gedanken experiment in which he superimposed a cat in the two states "alive" and "dead" [45]. This highly strange superposition is allowed by the fundamental superposition principle of quantum mechanics. However, such a state is never encountered in our everyday life. The most important reason for this "disappearance" is *Decoherence*, an effect due to the interaction with the environment. As an illustration we may consider an Aharonov-Bohm interference experiment on a ring, as presented by Stern, Aharonov and Imry [46]. This experiments starts by considering a quantum particle, whose coordinate is x moving around both arms of an Aharonov-Bohm ring threaded by a magnetic flux with an environment (whose coordinate is q) that only interacts with the particle on the right arm. (See Fig. 1.3) The initial wave function that corresponds to the particle having just entered the ring region but not yet interacting with the environment is given by,

$$\Psi(0) = [\psi_{\mathrm{L}}(x;0) + \psi_{\mathrm{R}}(x;0)] \otimes \varphi_0(q), \tag{1.17}$$

where $\psi_{\mathrm{L,R}}(x;0)$ is the initial wave packet of the particle on the Left/Right arm, and $\varphi_0(q)$ is the initial state of the environment assumed to be localized in the right arm.
The interference is examined at time t after each initial wave packet $\psi_{\mathrm{L,R}}(x;0)$ traversed half of the ring. The wave function is then

$$\Psi(t) = [\psi_{\mathrm{L}}(x;t) \otimes \varphi_{\mathrm{L}}(q) + \psi_{\mathrm{R}}(x;t) \otimes \varphi_{\mathrm{R}}(q)], \tag{1.18}$$

where $\varphi_{\mathrm{L,R}}(q)$ is the state the environment was in when the particle passed trough the Left/Right arm. Since the environment is not observed, its coordinate is integrated upon and the interference term is

$$2\Re\mathrm{e}\left[\psi^*_{\mathrm{L}}(x;t)\psi_{\mathrm{R}}(x;t)\int \mathrm{d}q\, \varphi^*_{\mathrm{L}}(q)\varphi_{\mathrm{R}}(q)\right]. \tag{1.19}$$

The latter must be compared to the interference term $2\Re\mathrm{e}\left[\psi_{\mathrm{L}}^{*}(x;t)\psi_{\mathrm{R}}(x;t)\right]$ obtained in the absence of the environment. The effect of the environment can be thus interpreted as a loss of coherence effect. In the language of the reduced density matrix,

$$\eta(t) = \sum_{i,j\in\{\mathrm{L,R}\}} |\psi_i\rangle\langle\psi_j| \int \mathrm{d}q\, \varphi_i^{*}(q)\varphi_j(q), \tag{1.20}$$

this corresponds to a destruction of the off diagonal terms $\eta_{\mathrm{LR}}(t)$, $\eta_{\mathrm{RL}}(t)$ due to the decoherence. Indeed the integral $\int \mathrm{d}q\, \varphi_i^{*}(q)\varphi_j(q)$, vanishes in the limit of orthogonal environment states and thus interference is lost.

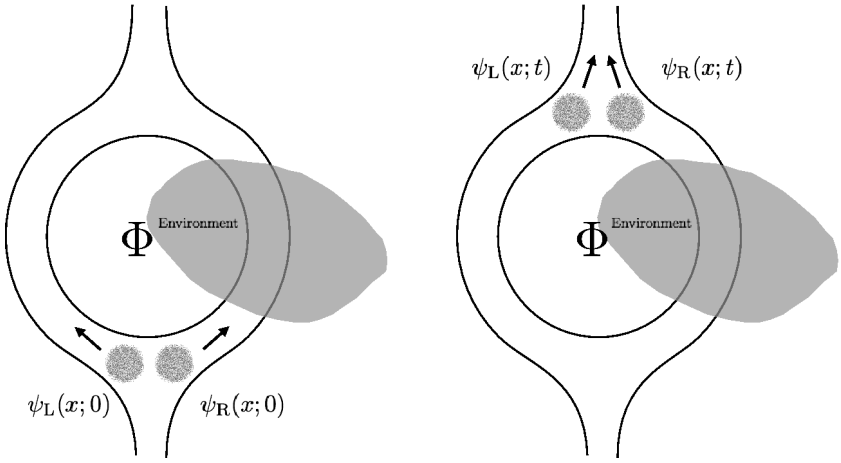

Figure 1.3: Intuitive schema of the decoherence process. A wavepacket which represent the system is split coherently between two arms, one of which interact with an environment. The two partial wavepacket recombine on the other side, decoherence due to the system-environment interaction affect the interference between the two arms.

Historically, the study of decoherence was initiated in the 1970's and 1980's with the work of Zeh [47] and Zurek [48] on the emergence of classicality in the quantum framework [7–9]. They pointed out that the problem of the classical limit of quantum mechanics is based on the incorrect assumption of a closed macroscopic system ruled by the Schrödinger equation. This is not justified in our present world, indeed macroscopic objects are interacting with their natural environment and thus can never be considered as isolated. What exactly is decoherence ? It is the process, due to the coupling of a system to an environment, that induce the loss of quantum mechanical interferences . Consequently the relevant theoretical framework for the study of decoherence is the theory of open quantum systems [54]. The interaction of an open quantum system with its surrounding environment creates quantum correlations i.e entanglement between the state of the system and the state of environment. There exist numerous tractable models of environment, the most popular one is made of a collection of harmonic oscillators [49–52], or equivalently a quantum field [53].

The description of open quantum systems is based on the concept of the density matrix, and standard treatment of decoherence consist in deriving a quan-

tum master equation after tracing out the environment degrees of freedom. In the particular case of a particle interacting with a scalar field ϕ (i.e a collection of harmonic oscillators), the master equation can be exactly derived, in the limit of high temperature. The density matrix of the particle $\eta(x, x')$ in position representation evolves like [9],

$$\underbrace{\frac{\mathrm{d}\eta}{\mathrm{d}t} = -\frac{i}{\hbar}[H, \eta]}_{\substack{\text{Von Neumann}\\ \text{Equation}}} \quad \underbrace{-\gamma(x-x')\left(\frac{\partial}{\partial x} - \frac{\partial}{\partial x'}\right)\eta}_{\text{Relaxation}} \quad \underbrace{-\frac{\gamma}{\lambda_T^2}(x-x')^2\,\eta}_{\text{Decoherence}}. \tag{1.21}$$

The first term of the Eq. (1.21) corresponds to the Von Neumann equation and delivers the reversible classical evolution of the expectation value of any observable. The second term causes dissipation, the relaxation rate γ is proportional to the viscosity due to the interaction with the scalar field. That interaction induces a loss of energy and a decrease of the average momentum. The last term is of diffusive nature and induces fluctuation. The latter term has no effect on the diagonal (classical) elements but induces a strong decay of the coherent off diagonal terms. In the semiclassical limit $\hbar \mapsto 0$ this term dominates the second one and it follows that,

$$\eta(x, x', t) = \eta(x, x', 0)\, e^{-\gamma t\left(\frac{x-x'}{\lambda_T}\right)^2} \tag{1.22}$$

with $\lambda_T = \hbar/\sqrt{2mk_{\mathrm{B}}T}$ the thermal De Broglie wavelength. It follows that quantum coherence between two points separated by a length $x - x'$ will disappear on a time scale

$$\tau_\phi = \gamma^{-1}\left(\frac{\lambda_T}{x-x'}\right)^2. \tag{1.23}$$

It is important to realize that this decoherence time scale is actually extremely short for a macroscopic objet. As an example the order of magnitude is approximately 10^{-23} seconds for a relaxation time γ^{-1} of the order of the age of the universe and a system of size 1 cm at 300 K. This result must be taken with care because such extrapolations on such simplistic systems are not justified, nevertheless it clearly indicates the fragility of coherent superpositions for macroscopic objects. On the contrary, in the limit of more microscopic objects at low temperature, the decoherence time can be much larger than many other time scales, this will be illustrated in the next section on mesoscopic systems.

Decoherence is a very effective process to restore the principle of correspondence, and thus extremely relevant in the particular context of quantum chaos. Indeed for chaotic systems we have a competition between two effects. The Lyapunov exponential spreading and the unavoidable folding of a typical wave packet, will induce quantum interference, that are dynamically destroyed by the localization effect of the decoherence. Part III of this thesis is devoted to this quantum-classical transition.

Since 1990, the investigation of decoherence raised a lot of new interest. This is due to the advent of quantum information theory, where decoherence must

be, at first glance, fought in order to preserve the superposition of states (key ingredient of a quantum computer), but is also essential for the final read out, which is actually a measurement.

1.1.3 Chaos and mesoscopic physics

The mesoscopic regime is reached in small condensed matter systems at sufficiently low temperatures for the electrons to propagate coherently across the sample [55–59]. In this regime electronic transport presents various interesting features due to the interference between the electronic wave function. They depend on fundamental lenght scales that we will list now :

- The shortest length is the Fermi wave length λ_{F}. It varies from a few Angstrom in metals to one hundred Angstrom in semiconductors.
- Disorder in the systems is characterized by the elastic mean free path l. l is the typical distance between two successive collisions with impurities
- The phase coherence length L_Φ is the characteristic length for the interferences of the electronic wave function. L_Φ increases with decreasing temperature.

These latter length scales must be compared to the typical size of the sample L involved in the measurement. In the particular case of the mesoscopic regime where $L \ll L_\Phi$, one can distinguish the ballistic regime $L \ll l$ regime and the diffusive $l \ll L$ one (See Fig. 1.4). In most cases the phase breaking length L_ϕ is related to inelastic events like electron-electron interaction, electron-phonon interaction or coupling to an external environment. However it is important to understand that coherence loss is not controlled by a single parameter, indeed L_ϕ will depend on the temperature, the applied voltage, the external circuit or other more subtle parameters.

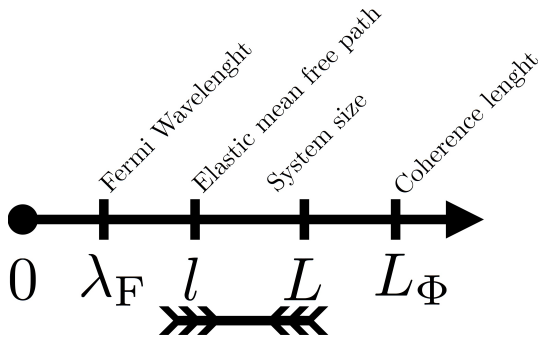

Figure 1.4: Characteristic length scales in a mesoscopic system at low temperature. The limit $L \ll L_\Phi$ implies that a quantum mechanical treatment must be used. The limit $\lambda_{\mathrm{F}} \ll L$ justifies a semiclassical treatment. Ballistic systems are defined by $L \ll l$ in contrast to diffusive (disordered) ones for which $l \ll L$.

What happens in the mesoscopic regime ? In macroscopic theory, electronic transport is described by Ohm's law. The electrical conductivity σ is defined by $\mathbf{j} = \sigma\mathbf{E}$ describing the linear relation between the electric current density $\mathbf{j}$ and the applied electric field $\mathbf{E}$. In the quasiclassical description of diffusion, the electron is assumed to lose phase coherence after each collision with an impurity ($L_\Phi \approx l$), the conductivity can thus be introduced as a local intensive quantity. However the quantity that is measured directly is the conductance G defined as the ratio between the current and the applied voltage. In mesoscopic systems $L_\Phi \geq l$ and the local description of the conductivity breaks down. Some novel transport properties of mesoscopic conductors may be roughly listed as follows :

Sample specificity : Mesoscopic conductors of the same material fabricated with the same process will have different measured transport coefficient. This is due to different microscopic conditions, like different impurity potential configurations [60, 61].

Non locality : For sufficiently large phase coherence lengths, the region of the sample outside the current path will strongly influence the measured quantities [62].

Violation of macroscopic symmetries : Most macroscopic symmetry properties do not follow immediately from microscopic ones but also depend on further conditions, as for example the symmetry of the averaged scattering potential. Consequently a number of these symmetry properties are violated in mesoscopic conductors [62–64].

Dependence on the measurement Set-Up : In mesoscopic physics, it is not only what is measured which matters, but how it is measured. The reason for that is, as we learn in basic quantum mechanic, that the measurement apparatus has an influence on the system. The probe-configuration dependence of the dephasing rate in certain mesoscopic interferometers [65] is clearly an illustration of the Set-Up sensitivity.

These facts taken together demonstrate that the concept of conductivity as an intensive quantity clearly breaks down at the mesoscopic scale. It is thus meaningful to discuss only measurable quantities like the conductance.

The conductance of a metallic sample betweenr_0 and r_1 is related to the transmission probability distribution $P(r_0, r_1)$ for an electron to reach the point r_1 when it initially started at r_0. In quantum mechanics probabilities are obtained from complex amplitudes $A_n = |A_n|e^{i\phi_n}$ where n is a possible realization of a path. The classical value corresponds to the approximation of incoherent scattering, $P_{\rm cl}(r_0, r_1) = \sum_n A_n A_n^*$, the quantum corrections are generated by the interference term,

$$P_{\rm quant}(r_0, r_1) = P_{\rm cl}(r_0, r_1) + \sum_{n \neq m} A_n A_m^* \tag{1.24}$$

Generally the contribution of the interference term disappears after averaging over disorder or small energy interval, except for the interference between A_n

and its time reversed path A_{-n} which both have have identical phase $\phi_n = \phi_{-n}$ in the absence of a magnetic field. This has as a consequence for example an enhancement of the average return probability. $\langle P_{\text{quant}}(r_0, r_0)\rangle = 2\langle P_{\text{cl}}(r_0, r_0)\rangle$, which gives a negative correction to the classical conductance. This is one of the most studied quantum effects in mesoscopic systems and is called *the weak localization correction* [75, 76]. This effect is illustrated in Fig. 1.5b. where a measurement of the magnetoresistance has been performed for two cavities with different shapes. An enhancement of the resistance at zero magnetic field is clearly identified. Indeed in the presence of a magnetic field, each time reversed pair of trajectories $(n, -n)$ acquires one extra phase. The coherence is thus destroyed and the weak localization disappears.

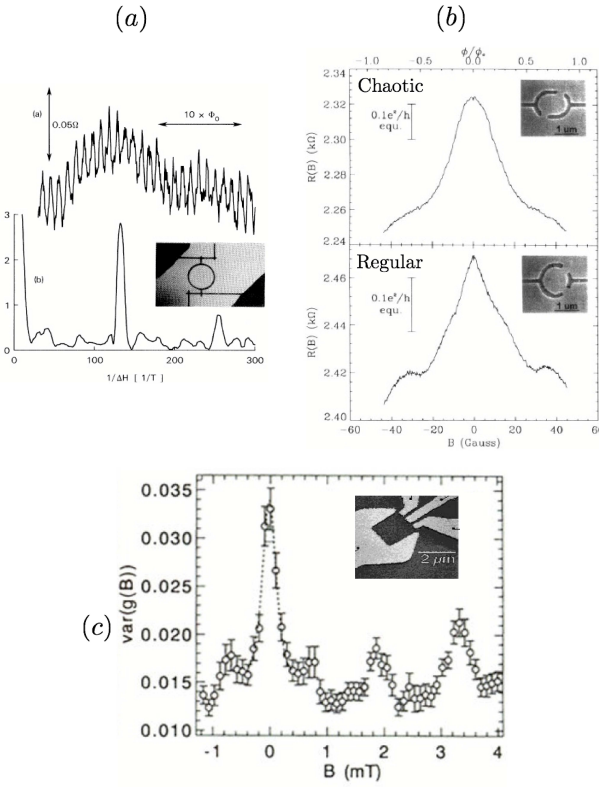

Figure 1.5: Some experimental data that illustrate the most investigated mesoscopic quantum effects. (a) Magnetoresistance of a ring measured at low temperature ($0.01K$) together with the Fourier power spectrum in arbitrary units containing peaks at h/e and $h/2e$; adapted from R. A. Webb et al. [71]; (b) Magnetoresistance for stadium cavities (Chaotic) and circular cavities (Regular) ; adapted from Chang et al. [72]; (c) Variance of shape-distortion magnetoconductance fluctuations in unit of $(e^2/h)^2$; adapted from Chan et al. [68].

Another quantum effect, strongly investigated is *the Aharanov-Bohm oscillations* [73, 74] of the conductance in multiply connected geometries like a ring pierced by a magnetic flux. In this case the phase difference between the two arms is mostly due to the presence of a vector potential. The extra phase will be

proportional to the ratio between the external magnetic flux and the quantum flux $\Phi_0 = h/e$. Consequently the conductance will oscillate in function of the magnetic flux with a period Φ_0 and higher harmonics. These Aharanov-Bohm oscillations are illustrated in Fig. 1.5a.

The last effect we would like to mention is *the universal conductance fluctuations* [60, 77]; the reproducible fluctuations in the conductance versus magnetic field or Fermi energy with a variance of the order e^2/h, independent of the average conductance. A typical measurement of conductance variance as a function of the magnetic field is presented in Fig. 1.5c.

As previously mentioned there exist two distinct mesoscopic regimes : The diffusive $l \ll L$ regime and the ballistic $l \geq L$ regime. Mesoscopic physics was initially focused on the diffusive one. In the latter the randomness is due to the presence of disorder; the classical motion of electrons is a random walk between the impurities. From a theoretical point of view, these systems have been investigated by various techniques like the diagrammatic technic based on the impurity Green functions or supersymmetry [78, 79]. Due to the technological advances, a

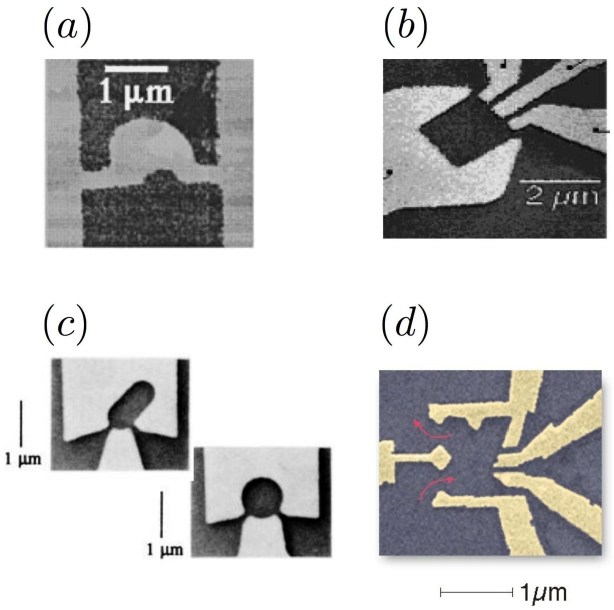

Figure 1.6: Some ballistic quantum dots. (a) adapted from Keller et al. [67]; (b) adapted from Chan et al. [68]; (c) adapted from Marcus et al. [69]; (d) adapted from Marcus et al. [70].

new generation of mesoscopic systems has been generated. Clean electronic devices with an elastic mean free path l larger than the typical size of the system L but still larger than the Fermi wavelength were built (for a review see [66]). The electronic motion is thus ballistic and solely determined by the boundary conditions of the sample. Consequently the choice of the imposed external potential confinement leads to various shapes of cavities/quantum dots from integrable to chaotic ones (See example in Fig. 1.6). This gives us a clear connection with

quantum chaos. As illustrated in Fig. 1.5b the underlying classical dynamics affects the transport properties. The weak localization peak line shape shows a Lorentzian behavior for chaotic cavities, in contrast to the linearly decreasing shape of regular one.This particular behavior is explained in [86].

As in closed systems, ballistic chaotic quantum open systems can be treated by RMT [80] or a semiclassical approach [81].

Starting from the scattering theory of transport [64, 90] RMT provides a statistical description and allows us to calculate the transport quantities (average conductance, shot noise) and their universal quantum corrections (weak localization, UCF). The hypothesis behind RMT is a well developed wave chaos. In the disorder regime, the diffractive scattering serves this requirement well. For the ballistic case the process is more subtle and essentially provided by the underlying classical chaos. Applicability of RMT is limited to a particular regime. Indeed the classical ergodicity must be established on a time scale much shorter than the life time of an electron in the system. Moreover the number of non ergodic trajectories (direct or few bouncing trajectories) must be reduced. This requires that the inverse Lyapunov exponent λ^{-1} and the typical time between bounces τ_{B} must be smaller than the dwell time τ_{D} of the cavities $\tau_{\mathrm{B}}, \lambda^{-1} \ll \tau_{\mathrm{D}}$. The last requirement to reach the RMT universality is that all times scale involved are smaller than the Heisenberg time $\tau_{\mathrm{H}} = \hbar/\Delta$, where Δ is the mean level spacing. In particular if we fulfilled the condition $\tau_{\mathrm{D}} \ll \tau_{\mathrm{H}}$, we can neglect the details of the opening contacts. Before considering the semiclassical methods, we want to emphasize the notion of ensemble averaging, involved in the RMT procedure. For diffusive systems, the averaging is related to different realizations of the disorder, in contrast to ballistic systems in which small variations of the shape will be used.

Semiclassical approaches are proven to be helpful for understanding chaotic mesoscopic systems and provide generally a simple physical picture of numerous phenomena. A first quasiclassical approach to transport in disordered systems has been proposed by Chakravarty and Schmid [82], who studied interference between diffusive electron paths in random $\delta-$potentials. More sophisticated methods based on the semiclassical evaluation of the Kubo conductivity have been developed by Argaman [83, 84]. The semiclassical approach of the scattering theory of transport [64], has been pioneered by Baranger, Jalabert and Stone [85, 86]. In this latter work the main step consists in replacing the Green function involved in the scattering matrix by its semiclassical expression and then evaluating the obtained integrals in the stationary phase approximation. Recently this approach has been completed by Brouwer and Rahav [88], and Jacquod and Whitney [87] on the basis of the work developed by Richter and Sieber [89].

Due to its importance in the semiclassical approach used in this thesis, we present now the basic concept of the scattering approach. The scattering matrix represents the solution of the Schrödinger equation for a sample that is connected to semi-infinite leads. The connection between the conductance and a scattering problem goes back to Landauer [90]. This idea has been developed by Büttiker [64]. For a review with more applications we refer to [91, 92].

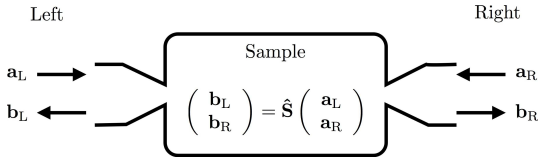

Figure 1.7: Example of a two terminal geometry scattering problem. Outgoing and incoming operators are related by the scattering matrix $\hat{\mathbf{s}}$ of Eq. (1.26).

The main idea of the scattering theory of transport is to relate the conductance with the quantum probability of transmission of carriers. In order to illustrate this, we consider a conductor connected to M leads (See Fig.1.7 for an illustration of the two leads geometry (Left and Right)).

Far from the sample, due to the translational invariance in the leads, the transversal and the longitudinal electronic motions are separable. This permits us to quantize the transverse motion and define the notion of quantum channels. We then introduce two sets of second quantized operators $\mathbf{a}_\alpha$ and $\mathbf{b}_\alpha$ see Fig.1.7. Here $\mathbf{a}_\alpha^\dagger$ is a vector of the operators $a_{\alpha;n}^\dagger$, $(n \in \{1, \cdots, N_\alpha\})$ which create a carrier in the incoming channel n in lead α. Similarly $\mathbf{b}_\alpha$ is a vector of the operators $b_{\alpha;n}$, $(n \in \{1, \cdots, N_\alpha\})$ which annihilate a carrier in the outgoing channel n in lead α. Outgoing and incoming operators are related by the scattering matrix relation,

$$\mathbf{b}_{\alpha;n} = \sum_\beta \sum_{m=1}^{N_\beta} \mathbf{s}_{\alpha\beta;nm} \mathbf{a}_{\beta;m}, \tag{1.25}$$

For a two lead geometry, the scattering matrix reduces to,

$$\hat{\mathbf{s}} = \begin{pmatrix} \mathbf{s}_{\mathrm{LL}} & \mathbf{s}_{\mathrm{RL}} \\ \mathbf{s}_{\mathrm{LR}} & \mathbf{s}_{\mathrm{RR}} \end{pmatrix} \tag{1.26}$$

The average current $\langle I_\alpha \rangle$ (in unit of e/h) at a cross-section on the lead α is given by,

$$\langle I_\alpha(t) \rangle = \left\langle \sum_{n=1}^{N_\alpha} \int \mathrm{d}E \mathrm{d}E' \exp\left[\frac{it}{\hbar}(E - E')\right] \left[\mathbf{a}_{\alpha;n}^\dagger(E)\mathbf{a}_{\alpha;n}(E') - \mathbf{b}_{\alpha;n}^\dagger(E)\mathbf{b}_{\alpha;n}(E')\right] \right\rangle \tag{1.27}$$

Flux conservation requires that the scattering matrix is unitary, $\hat{\mathbf{s}}\hat{\mathbf{s}}^\dagger = \mathbb{I}$. Using Eq. (1.25), the quantum statistical average

$$\left\langle \mathbf{a}_{\alpha;n}^\dagger(E)\mathbf{a}_{\beta;m}(E') \right\rangle = \delta_{\alpha\beta}\delta_{nm}\delta(E - E')f_\alpha(E), \tag{1.28}$$

with $f_\alpha(E)$ the Fermi distribution in the lead α, we obtain, from Eq. (1.27), the average current,

$$\langle I_\alpha(t) \rangle = \sum_\beta eV_\beta \int \mathrm{d}E \left(-\frac{\partial f_\beta}{\partial E}\right) \left(N_\alpha \delta_{\alpha\beta} - \mathrm{Tr}\left[\mathbf{s}_{\alpha\beta}^\dagger \mathbf{s}_{\alpha\beta}\right]\right). \tag{1.29}$$

The conductance for a small applied voltage $g_{\alpha\beta} = \frac{\mathrm{d}I_\alpha}{\mathrm{d}V_\beta}$, is thus given in unit of e^2/h by,

$$g_{\alpha\beta} = \int \mathrm{d}E \left(-\frac{\partial f_\beta}{\partial E}\right) \left(N_\alpha \delta_{\alpha\beta} - \mathrm{Tr}\left[\mathbf{s}^\dagger_{\alpha\beta}\mathbf{s}_{\alpha\beta}\right]\right) \tag{1.30}$$

Now we limit ourselves to a two lead geometry in a steady state (i.e, at zero frequency). In the zero temperature limit we get the Landauer-Buttiker formula

$$g = \mathrm{Tr}\left[\mathbf{s}^\dagger_{\mathrm{RL}}\mathbf{s}_{\mathrm{RL}}\right] \tag{1.31}$$

where each element of the scattering matrix is evaluated at the Fermi energy.

The above formulae are constrained to a purely coherent picture. However there exist some more or less phenomenological extension of the scattering formalism, to investigate the disappearance of quantum effects on the conductance [93–98]. Voltage [93] and dephasing probe [94] models are certainly the most popular ones.

In these latter, an additional fictitious lead is connected to the system via a point contact of transparency ρ. A voltage is applied to this lead to ensure that no current flows through it on average. Voltage and dephasing probes are used to introduce respectively inelastic and elastic incoherent scattering, into a fully quantum coherent system. The origin of the success, of this approach is clearly the possibility to use the formalism developed in the purely coherent limit.

Part IV of this thesis is devoted to an extension of this standard scattering formalism that allows one to include the dephasing due to external sources.

1.2 Summary of obtained results

The purpose of this brief summary is to emphasize some particular result, that I obtained during my PhD thesis. This outline is only a short introductory guide, for more details see the corresponding chapters.

1.2.1 Reversibility in quantum mechanics

In classical chaotic systems, irreversibility results from dynamical phase-space mixing together with the coarse-graining associated with the finite experimental resolution. In quantum mechanics, this mechanism is strongly inhibited by a less efficient mixing and a coarse-graining limited by the Heisenberg uncertainty principle.

In fact, it was shown by Shepelyansky [99], that we can even obtain an almost perfectly reversible quantum dynamics when the corresponding classical one is irreversible. (See Fig. 1.8). The classical irreversibility is due to rounding-off errors inherent to numerical computation. However it was quite rapidly realized that the microscopic conditions that govern the quantum dynamics can not be resolved with an arbitrary precision. Consequently the exact time reversal operation of the Hamiltonian can not be achieved. It is thus of fundamental interest to investigate the sensitivity of the quantum dynamics to a perturbation of the Hamiltonian.

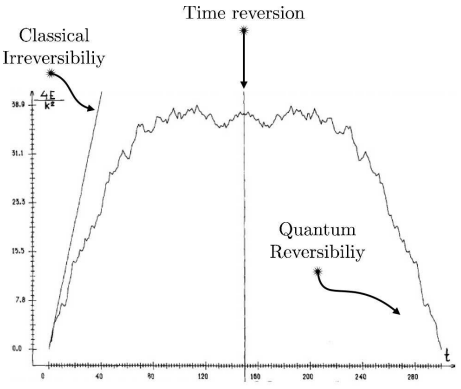

Figure 1.8: Time dependence of the standard map energy, after a time reversion. The straight line shows clearly the classical irreversible diffusion, in contrast with the completely reversible quantum evolution; adapted from Shepelyansky [99].

This approach goes back to the seminal work of Peres [100]. The central quantity of this approach is the so called *Loschmidt echo* (or the *Fidelity*),

$$\mathcal{M}_{\mathrm{L}}(t) = |\langle\psi_0| \exp[iHt] \exp[-iH_0t]|\psi_0\rangle|^2 \tag{1.32}$$

with which a narrow wave packet $|\psi_0\rangle$ can be reconstructed by inverting the dynamics after a given time with a perturbed Hamiltonian $H = H_0 + \Sigma$ (we set

$\hbar \equiv 1$). The *Fidelity* quantifies the sensitivity of the time inversion operation due to the uncertainty in the Hamiltonian and in this sense, it is a measure of quantum irreversibility.

The notion of *Fidelity* appears quite naturally in the context of *Decoherence* [8] of systems with few degrees of freedom coupled to an environment with many more degrees of freedom. Roughly speaking the presence of a Hamiltonian perturbation Σ in the backward propagation, expresses the effect of the coupling with the environment. This idea initially developed by Jalabert and Pastawski [101] raised a lot of theoretical interest [102–112], for a review see [113]. The source of this interest was the prediction in [101] of a regime of perturbation where the behavior of the fidelity is essentially governed by the Lyapunov exponent of the system $\mathcal{M}_{\mathrm{L}}(t) \simeq \exp[-\lambda t]$. The range of validity of this regime was clarified in Ref. [102]. The authors show that the decay of the Fidelity with time is either Gaussian or exponential. The Gaussian regime prevails when the strength of the perturbation is weak enough. As the perturbation is further increased, the decay of the fidelity becomes exponential. For not too strong perturbation, the decay is given by the perturbation induced Fermi golden rule rate, until the latter exceeds the system's Lyapunov exponent,

$$\mathcal{M}_{\mathrm{L}}(t) = \exp\left[-\min\left(\Gamma,\, \lambda\right)\right]. \tag{1.33}$$

Most of the following investigations considered only the *average* properties of the *Fidelity* $\langle \mathcal{M}_{\mathrm{L}} \rangle$, where the average is performed either over different initial states, or different elements of an ensemble of unperturbed Hamiltonians and/or perturbation. However the fluctuations of a physical quantity often contain more information than its average. Consequently we investigated the time-dependent *variance* of the *Fidelity* $\sigma^2\left[\mathcal{M}_{\mathrm{L}}(t)\right]$ [114], by following the semiclassical approach developed in Ref. [101]. We showed that the variance has a much richer behavior than its average. We have shown that the variance first increases algebraically up to a critical time t_c, after which it decays. To leading semiclassical order, this decay is given by the sum of a classical term related to the classical Lyapunov exponent λ, a quantum term related to the Fermi Golden rule Γ and a mixed term, as

$$\sigma^2\left[\mathcal{M}_{\mathrm{L}}(t)\right] \;\simeq\; \alpha^2(t) e^{-2\lambda t} + \frac{2}{N} e^{-\Gamma t}\, \Theta_{\tau_{\mathrm{E}}}(t) + 2\alpha(t) \mathrm{e}^{-(\lambda+\Gamma)t} \tag{1.34}$$

The comparison with the behavior of the average fidelity allowed the extraction of the classical Lyapunov exponent in a larger parameter range. Indeed the Lyapunov exponent can be accessed, like in the average fidelity, if we increase the perturbation to reach the regime $\Gamma \geq \lambda$. However in contrast to the average value, it is still possible to extract the Lyapunov exponent in the regime $\Gamma \leq \lambda$. Indeed for times shorter than the Ehrenfest time $\tau_{\mathrm{E}} = \lambda^{-1} \ln\left[N^{-1}\right]$ the behavior of the variance is ruled by the mixed terms (third term of Eq. (1.34))

Our results are corroborated by numerical simulations, as presented in Fig. 1.9. In Fig. 1.9a we present the variance $\sigma^2\left[\mathcal{M}_{\mathrm{L}}\right]$ of the Fidelity as a function of time,

in the regime of weak perturbation $\Gamma \ll \lambda$. This numerical simulation clearly illustrates the initial increase of the variance followed by the predicted exponential FGR decay indicated by the second term of Eq. (1.34). We emphasize that there is no adjustable free parameter, and this carries a strong numerical evidence of the validity of the prefactor N^{-1}. Fig. 1.9b clearly illustrate transition from the quantum regime to the classical Lyapunov saturation $\lambda \ll \Gamma$.

This work will be discussed in more detail in chapter 2 and has been published in Ref. [114].

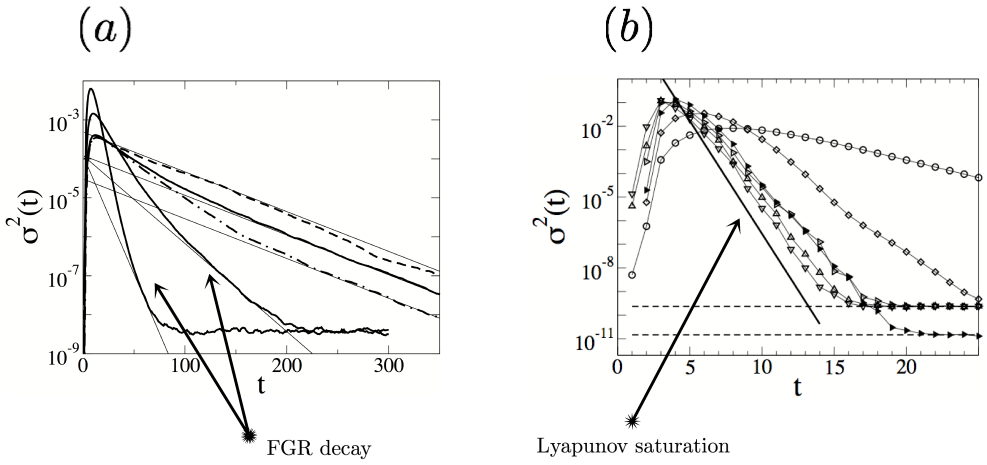

Figure 1.9: (a) Variance $\sigma^2[\mathcal{M}_{\mathrm{L}}]$ of the Fidelity versus time for weak perturbation leading to the FGR regime ($\Gamma \ll \lambda$).Thin solid lines correspond to theoretical prediction. (b) Variance $\sigma^2[\mathcal{M}_{\mathrm{L}}]$ of the Fidelity versus time in the Lyapunov regime ($\lambda \ll \Gamma$). The solid line indicates the Lyapunov decay. (For more details see chapter 2)

The connection between irreversibility and decoherence was not only a theoretical game but was also quite fertile at the experimental level. Indeed echo experiments abound in nuclear magnetic resonance (*Spin echo*) [115–117], optics (*Photon echo*) [118], cold atomic systems (*Motional wave packet echo*) [119], microwave cavites (*Echo Spectroscopy*) [120] and condensed matter systems (*Charge echo*) [121]. Fundamentally all these experiments are based on the same principle, that the sign of the Hamiltonian can be changed by means of an effective change of coordinate axes [117].

The theoretical approach based on the *Loschmidt echo* was unable to provide a satisfactory explanation of some particular experimental results, such as for example the gaussian, perturbation independent decay, found in NMR [122], see Fig. 1.10. The measurements reported here were performed in a single crystal of ferrocene. In such system, the perturbation Σ can be tuned. In Fig. 1.10 we present the attenuation of the polarization echo as a function of the refocusing time. The remarkable result that can be observed in figure Fig. 1.10 is that attenuation saturates with a decreasing perturbation Σ. This behavior is not predicted by the Loschmidt echo theory, indeed in the latter a perturbation independent decay is predicted for strong enough perturbation. We provided a first step to

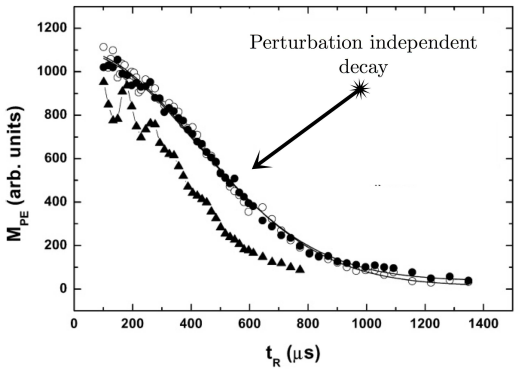

Figure 1.10: Attenuation of the polarization echo as a function of the refocusing time in a ferrocene system, for different values of perturbation. The solid line represents a gaussian fitting that shows the perturbation independent decay; adapted from Pastawski et al. [122].

solve this puzzling result in Ref [123]. In real echo experiments, only imperfect time-reversal operations are performed on a subset of the total number of degrees of freedom. To capture the physics of these experiments, we developed the notion of the *partial Fidelity*,

$$\mathcal{M}_{\rm B}(t) = \left\langle \psi_{\rm sys} \right| {\rm Tr}_{\rm env} \left[e^{-i\mathcal{H}_{\rm b}t} e^{-i\mathcal{H}_{\rm f}t} \rho_0 e^{i\mathcal{H}_{\rm f}t} e^{i\mathcal{H}_{\rm b}t} \right] \left| \psi_{\rm sys} \right\rangle, \tag{1.35}$$

where only a part of the system's degrees of freedom can be time-reversed. (Forward $\mathcal{H}_{\rm f} = H_{\rm sys} + H_{\rm env} + \mathcal{U}_{\rm f}$ and backward $\mathcal{H}_{\rm b} = -(H_{\rm sys} + \Sigma_{\rm sys}) + H'_{\rm env} + \mathcal{U}_{\rm b}$ Hamiltonians differs only by a partial time-inversion over the system). We named it the *Boltzmann echo* $\mathcal{M}_{\rm B}(t)$. Chapter 3 is devoted to this new object and our results are published in Ref. [123]. We presented a semiclassical calculation and showed that even when the time-reversal operation is performed more and more accurately, the decay rate of the *Boltzmann echo* saturates at a value given by the decoherence rate due to the coupling with the surrounding environment. As the experimentally controllable perturbation is reduced, the Boltzmann echo is given by

$$\mathcal{M}_{\rm B}(t) \simeq \exp[-(\Gamma_{\rm f} + \Gamma_{\rm b})t] \tag{1.36}$$

where $\Gamma_{\rm f,v}$ is the Fermi Golden rule spreading due to the forward/ backward coupling with the environment. We confirmed our analytical results by numerical simulations (See Fig.1.11). The main panel in Fig. 1.11 demonstrates clearly the exponential decay of the Boltzmann echo and its strong dependence on the coupling. Additionally, the inset illustrates that when the perturbation is sufficiently weak a perturbation independent decay solely ruled by the coupling is reached.

Finally at weak interaction, we show that the Boltzmann echo reaches a gaussian regime independent of the perturbation

$$\mathcal{M}_{\rm B}(t) \simeq \exp[-(\overline{\mathcal{U}_{\rm f}^2} + \overline{\mathcal{U}_{\rm b}^2})\, t^2/2]. \tag{1.37}$$

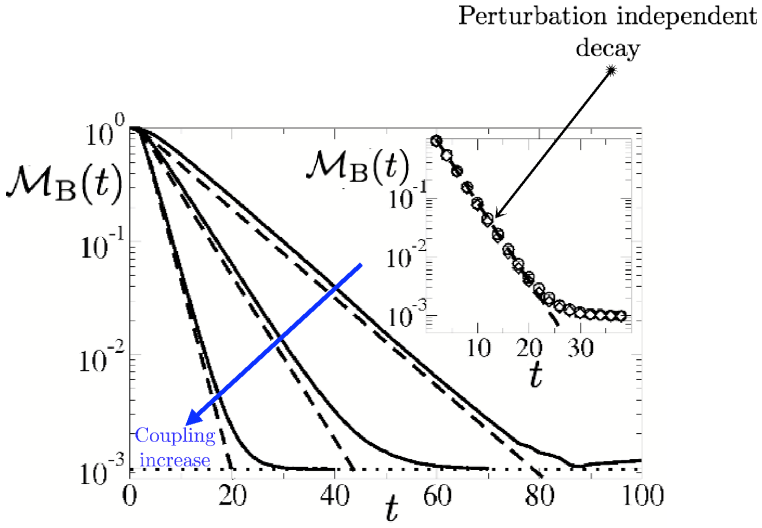

Figure 1.11: Main plot: Boltzmann echo versus time at fixed perturbation but for different value of the environment coupling strenght. The full lines correspond from right to left to a increase of the coupling strength. The dashed lines give the predicted exponential decay. Inset : $\mathcal{M}_B$ for a fixed coupling strength, and different small perturbations. The dashed line indicates the theoretical prediction which is independent of the perturbation. (For more details see chapter 3)

This might well be the explanation for the experimentally observed NMR-independent decay of polarization echoes [122].

Leaving temporarily aside the notion of *Decoherence*, we were attracted by the study of quantities closer to the experimental interest. Our investigation was most notably motivated by neutron scattering [124–126], which we tried to understand better. To that end, we introduced a new echo which we dubbed "*Displacement echo*" [127].

$$\mathcal{M}_D(t) = \left| \langle\alpha| e^{-i\mathbf{P}\hat{x}} e^{i\hat{H}t} e^{i\mathbf{P}\hat{x}} e^{-i\hat{H}t} |\alpha\rangle \right|^2. \tag{1.38}$$

The latter is related to the ensemble average of the correlation function $Y_{jj}(\mathbf{P}, \mathbf{t})$ in incoherent neutron scattering and Mössbauer emission/absorption. Physically $\mathcal{M}_D$ measures the decay of the fidelity with which a wave packet is reconstructed by a perfect time-reversal operation performed after a phase space displacement $\mathbf{P}$. In the semiclassical limit, we showed that the decay rate is generically given by the Lyapunov exponent of the classical dynamics. For small displacements, we additionally showed that, following a short-time Lyapunov decay, the decay freezes well above the ergodic value because of quantum effects. The average displacement echo is given by,

$$\langle \mathcal{M}_D(t) \rangle \propto \left[\alpha\, e^{-\lambda t} + \frac{g(|\mathbf{P}|L)}{(|\mathbf{P}|L)^2} \right], \tag{1.39}$$

where $g(|\mathbf{P}|L)$ is an oscillatory function, which depends on the system's spatial dimension.

Our analytical results are corroborated by numerical simulations. Fig. 1.12a presents the displacement echo as a function of time and clearly confirms the existence of Lyapunov decay. Fig. 1.12b delivers the saturation value of the echo, and shows the quantum freeze at a displacement-dependent value as predicted by the last term of Eq. (1.39).

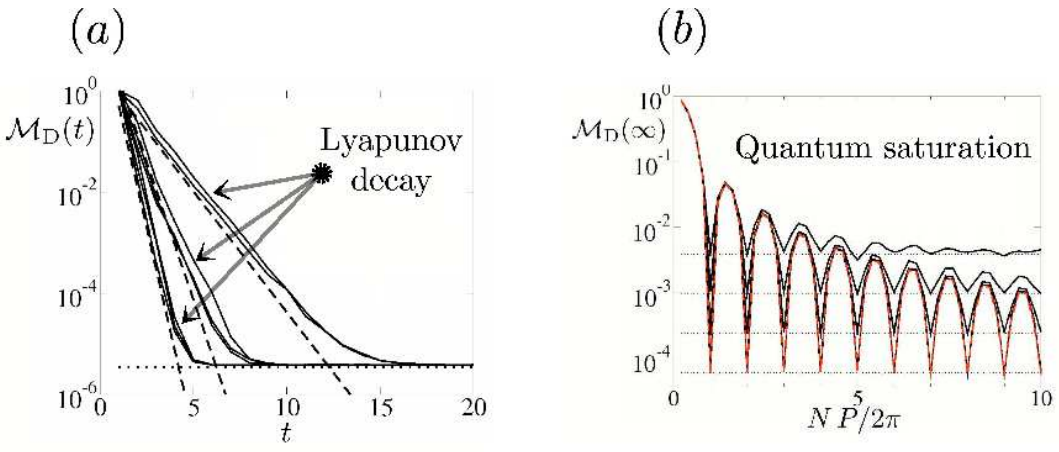

Figure 1.12: (a) Displacement echo versus time. The dashed lines correspond to the theoretical Lyapunov decay prediction. (b) Saturation value of the displacement echo. The red dashed line indicates the theoretical prediction. (For more details see chapter 4)

These aspects will be discussed in more detail in chapter 4 and are published in [127]. Our results are currently being tested experimentally on trapped cold atoms systems in the laboratory of Mara Prentiss at Harvard university [128].

1.2.2 Entanglement and decoherence

Although the echo approach quantifies the sensitivity of quantum trajectories to the change of an external/control parameter, an echo is not intrinsically a direct measure of decoherence. Decoherence is mainly due to the interaction with an environment and no time reversion is involved. The fundamental question we must address is thus the notion of interaction between two quantum systems. Investigate interaction between quantum systems is not a trivial task. If we quote Schrödinger [129],

> *When two systems (...) enter into temporary interaction (...), and when after a time of mutual influence the systems separate again, then they can no longer be described in the same way as before, viz. by endowing each of them with a representative of its own.*

This defines the notion of quantum correlations between systems, commonly named *Entanglement*.

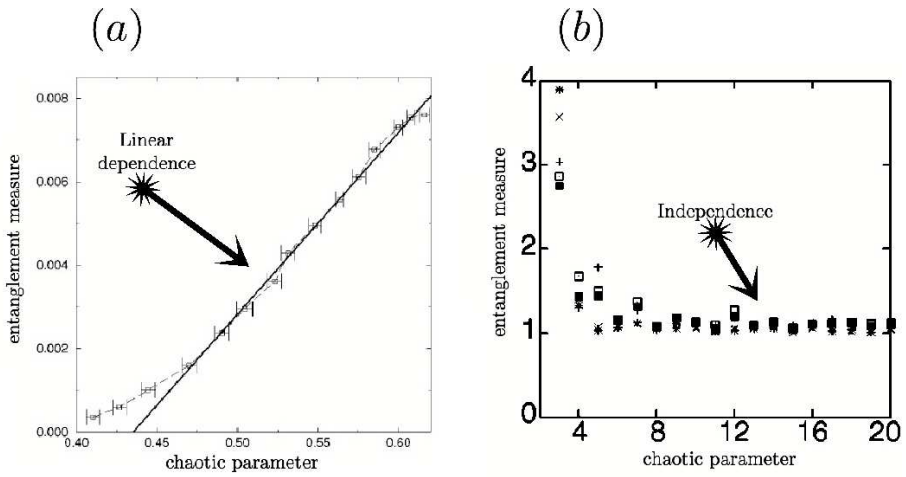

Figure 1.13: Two numerical investigations on the entanglement generation in chaotic systems. (a) presents the linear entanglement rate of a coupled kicked top as a function of the chaoticity parameter; adapted from Miller and . Sarkar [131] ; (b) presents the entanglement rate of production of a coupled kicked top as a function of the chaoticity parameter; from Tanaka et al. [132]. The linear dependence found on the left seems to contradict the independence obtained on the right. This apparent contradiction is well explained by the existence of two regimes of entanglement [133, 134].

In the context of decoherence, the investigations of quantum correlations between system and environment are thus of fundamental interest. We then turned to study *entanglement* properties of two interacting particles. These properties are quantified by the reduced density matrix, obtained by tracing out the degrees of freedom of one of the particles. If we enumerate the particles, and let $\eta(t)$ be the density matrix of the full system, the reduced density matrix related to the first particle, labeled 0 is given by,

$$\eta_0(t) = \mathrm{Tr}_1 \left[\eta(t)\right]. \tag{1.40}$$

If this reduced density matrix represents a mixed state, particles are entangled. A good measure of the degree of mixture is usually given by the *Von Neumann entropy*

$$\mathcal{S}\left(\eta_0\right) = -\mathrm{Tr}_0 \left[\eta_0 \ln\left(\eta_0\right)\right]. \tag{1.41}$$

However, at a technical level, it is more convenient to calculate the trace of the squared reduced density matrix [9],

$$\mathcal{P}(t) = \mathrm{Tr}_0 \left[\eta_0^2(t)\right]. \tag{1.42}$$

This quantity is referred to as the *Purity* $\mathcal{P}(t)$. The purity and the associated linear entropy $\mathcal{S}_{\mathrm{lin}}\left(\eta_0\right) = 1 - \mathcal{P}(t)$ are analytically tractable quantities that relate to the Loschmidt echo [130]. Moreover, as we consider global pure states, the linear entropy and the Von Neumann entropy behaved in the same way.

In the particular context of chaos, the question on the origin of entanglement production in a dynamical system was a hot topic. The first attempt to determine the rate of entanglement was numerical. Detailed numerical investigation performed by Miller and Sarkar [131] (see Fig.1.13) showed that entanglement is favored by chaos and even given by the classical Lyapunov exponent of the system. However this result was challenged by Tanaka et al. [132] whose numeric showed no increase at all (see Fig.1.13). Fig.1.13a presents the linear entanglement rate versus the average Lyapunov exponent performed by Miller and Sarkar based on two coupled quantum kick tops. The linear dependence of the entanglement rate with the Lyapunov exponent is clearly presented. Fig.1.13b presents similar numerics performed by Tanaka et al. on the same system. Here for strong enough chaos, the entanglement rate saturates at a value independent of the chaotic parameter. However it is crucial to realize that although the two models are the same, the numerical investigations have been performed in two different regimes; weak chaos (small but positive Lyapunov exponent) regime for Miller and Sarkar and strong (large Lyapunov exponent) chaos for Tanaka.

Based on our semiclassical expertise [133], we solved this apparent contradiction and investigated the quantum-classical correspondence in such bipartite systems [134]. This will be treated in chapter 5. We showed how a classically vanishing interaction generates entanglement between two initially non entangled particles, without affecting their classical dynamics [134]. We showed that for chaotic dynamics, the rate of entanglement is shown to saturate at the Lyapunov exponent of the classical dynamics as the interaction strength increases. The decay of the purity is given by,

$$\mathcal{P}(t) = e^{-2\Gamma_{01}t} + \alpha_0(t)e^{-\lambda_0 t} + \alpha_1(t)e^{-\lambda_1 t}. \tag{1.43}$$

If we focus on entanglement of identical particles $\lambda_0 = \lambda_1$ or if we consider that the particle 1 plays the role of an environement $\lambda_1 \gg 1$, Eq.(1.43) distinguishes 2 regimes for the exponential decay of the purity :

1. The Golden rule exponential decay, $\mathcal{P}(t) \propto e^{-2\Gamma_{01}t}$, if $\Gamma_{01} \leq \lambda_0$. It corresponds to a purely quantum regime generated by the coupling between the two particles

2. The System's Lyapunov exponential decay, $\mathcal{P}(t) \propto e^{-\lambda_0 t}$, if $\lambda_0 \leq \Gamma_{01}$. It corresponds to a purely classical regime generated by the system's classical dynamics

We numerically confirmed the existence of theses two regimes. In Fig. 1.14 we present the purity obtained for a system of two coupled kicked rotators. Fig. 1.14a present the regime of strong coupling in which the Lyapunov regime is reached. This numeric corresponds to the one obtains by Miller and Sarkar. Fig. 1.14b considers the regime of a weak coupling regime as compared to the chaos, and confirms clearly the existence of the quantum regime. This quantum regime corresponds to the one investigated by Tanaka.

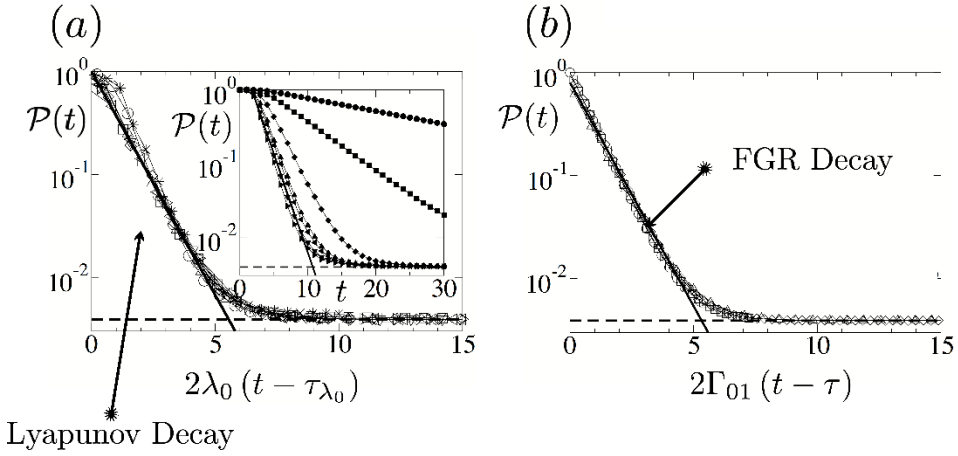

Figure 1.14: (a) Main plot: Purity of the reduced density matrix in the Lyapunov regime of strong coupling, the time axis has been rescaled with the system' s Lyapunov exponent. Inset : Purity of the reduced density matrix versus time, when we increase the coupling strength. (b) Purity of the reduced density matrix in the FGR regime ($\Gamma_{01} \leq \lambda_0$) the time axis has been rescaled with the Fermi golden rule spreading. (For more details see chapter 5)

Finally in the Lyapunov saturation regime, the one-particle Wigner function follows classical dynamics better and better as one goes deeper and deeper into the semiclassical limit. This demonstrates that quantum-classical correspondence at the microscopic level requires neither high temperatures, nor coupling to a large number of external degrees of freedom. Fig. 1.15 present the time-evolution of a classical distribution (top left), and three quantum phase-space evolution of the one-particle Wigner function : (i) (top right) for a free system; (ii) and (iii) (bottom left and right) for a coupled system in the Lyapunov regime. From the bottom left panel to the bottom right panel, one goes deeper into the semiclassical limit. If we avoid the 4 ghost replications due to the numerical procedure (see chapter 5), this figure illustrates that correspondence with the classical panel becomes better as we move deeper into the semiclassical limit.

We are currently working on a generalization of this bipartite model to the case of multipartite entanglement based on the generalized concurrence developed by F. Mintert et al. [135].

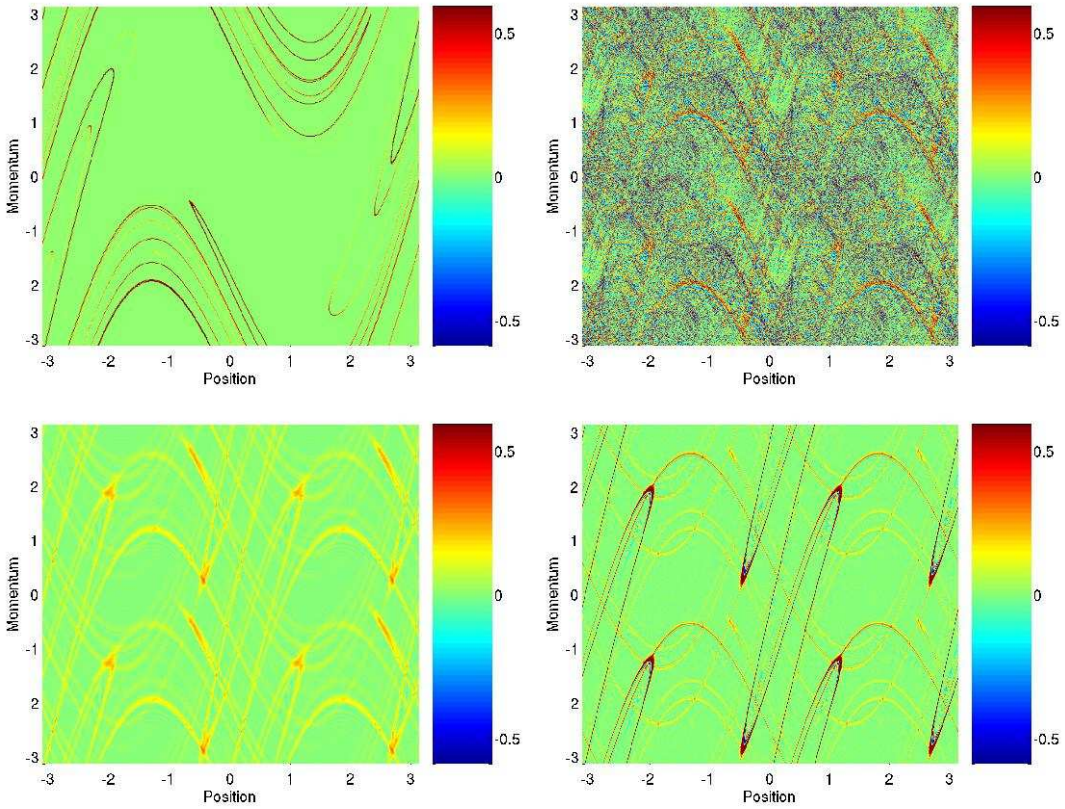

Figure 1.15: Phase-space plots for a classical distribution (top left), uncoupled (top right) and coupled (bottom left and right) quantum Wigner distributions, with an increase of the semiclassical limit from left to right.

1.2.3 Quantum transport and dephasing

We applied the knowledge, gained from the conceptual investigations of decoherence, to the problem of quantum transport in mesoscopic systems. In this field various well established phenomena like the *weak localization correction* [75,76] or the *Universal Conductance Fluctuations* (UCF) [60, 77] represent most spectacular manifestations of quantum coherence. The effect of dephasing on transport through such systems is still difficult to access experimentally, nevertheless mesoscopic transport has the advantage of permitting some experimental investigation.

From a theoretical point of view, semiclassical methods have been quickly involved [87–89] and have shown a clear predictive power. Indeed when the ballistic motion of the electron is chaotic, the transport properties are universal and well captured by RMT. However following the seminal work of Aleiner and Larking [136] a new semiclassical time scale the *Ehrenfest time* τ_{E} affects the coherent propagation of transport. The Ehrenfest time corresponds to the time during it takes for an initally well localized wavepacket (width $\propto \lambda_{\mathrm{F}}$) spreads to a macroscopical length scale ($\mathcal{L}$); $\tau_{\mathrm{E}} \propto \lambda^{-1} \ln[\mathcal{L}/\lambda_{\mathrm{F}}]$.

Once τ_{E} becomes a relevant parameter, universality is broken and RMT ceases

to describe correctly the transport properties. (See Fig. 1.16).

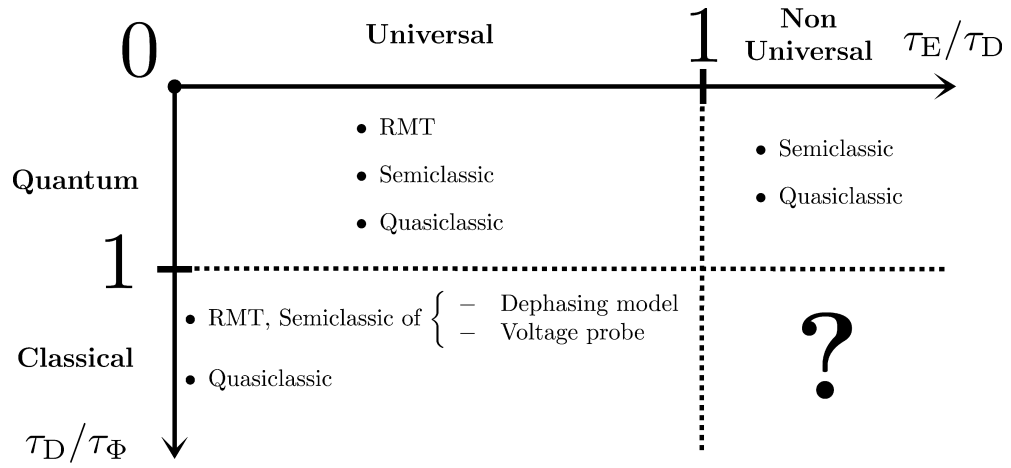

Figure 1.16: The abscissa corresponds to the chaotic axe to reach the classicality. For an Ehrenfest time τ_E greater that the dwell time of the cavity, non universal corrections to RMT must be considered. The verticla axis corresponds to the quantum to classical transition due to the dephasing. There are four distinct regimes. The purely universal quantum regime (top left quarter) well characterized by RMT and semiclassical method, the non universal quantum regime (top right quarter) well described by the semiclassical approach and quasiclassical one [136], the universal decoherence regime (bottom left quarter) obtained by the RMT/ semiclassical treatment of some more or les phenomenological mode. Finally the non universal classical domains (bottom right quarter) constitute the central framework of the Part V of the thesis.

It is important to realize that whereas the dephasing time τ_ϕ is the long time cut-off for quantum interference. The Ehrenfest time τ_E is the time scale that controls the appearance of such interferences. On one side the disappearance of quantum effects on conductance due to the unavoidable dephasing has been studied, mostly with the help of phenomenological models [93, 94]. On the other side the influence of a finite τ_E has now been widely analyzed theoretically [87,88], and clearly confirms, the breakdown of the universal quantum result.

However, except for the work of Aleiner and Larkin [136], the investigations on the competition between the Ehrenfest time and the dephasing time was not much developed. This question is of fundamental interest and has been recently reviewed [137, 138]. Indeed each time scale indicates a way to reach the classical domain. The dephasing time leads to the quantum to classical transition that can be described at a universal level (See Fig. 1.16.). The Ehrenfest time τ_E indicates a non universal way to reach classicality.

Chapter 6 of this thesis is devoted to a semiclassical analysis of dephasing on quantum transport through chaotic systems at finite Ehrenfest time. This leads us to consider the transition from a universal quantum regime (top left quarter of Fig. 1.16) to a non universal classical domains (bottom right quarter of Fig. 1.16) and leads us to address the notion of universality of the dephas-

ing. We investigated dephasing in open ballistic chaotic systems in the limit of a large system size to Fermi wavelength ratio [137]. Using the trajectory-based semiclassical theory [87–89], we firstly calculate the weak localization correction to the conductance for a quantum dot capacitively coupled to an external closed quantum dot. To this end, we performed an extension of the standard scattering formalism developed by Büttiker [93]. Secondly, following the method of Whitney [139], we included the tunneling in the trajectory-based semiclassical theory of a dephasing voltage probe (For the model definition, see [93, 94]).

We found, in addition to the universal algebraic suppression with the ration of dwell time τ_{D} through the cavity and the dephasing time τ_ϕ, an exponential suppression of the weak localization factor,

$$g^{\mathrm{wl}} = \frac{g_0^{\mathrm{wl}}}{1+\tau_{\mathrm{D}}/\tau_\phi}\,\exp[-\tilde{\tau}/\tau_\phi]. \tag{1.44}$$

We pointed out that the typical time scale $\tilde{\tau}$ involved in this suppression is system dependent. In the dephasing probe model, it coincides with the Ehrenfest time $\tilde{\tau} \propto \tau_{\mathrm{E}}$, in contrast, when dephasing occurs due to the coupling to an external dot, this time scale depends on the macroscopic correlation length of the coupling potential, $\tilde{\tau} \propto \lambda^{-1}\ln[L/\xi]$. We noted that a similar behavior has been found recently for the universal conductance fluctuations by Altland, Brouwer and Tian [138].

Bibliography

[1] N. Bohr, Nature **121**, 580, (1928).

[2] A. J. Leggett, S. Chakravarty, A. T. Dorsey, M. P. A. Fisher, A. Garg and W. Zwerger, Rev. Mod. Phys. **59**, 1 (1987).

[3] G.P. Berman and G.M. Zaslavsky, Physica **91** A, 450 (1978).

[4] M.V. Berry and N.L. Balasz, J. Phys. A **12**, 625 (1979).

[5] G.M. Zaslavsky, Phys. Rep. **80**, 157 (1981).

[6] B.V. Chirikov, F.M. Izrailev, and D.L. Shepelyansky, Sov. Sci. Rev. **26**, 209 (1981).

[7] J. A., Wheeler and W. H. Zurek, *Quantum Theory and Measurement*, (Princeton University Press, 1983).

[8] E. Joos, H.D. Zeh, C. Kiefer, D. Giulini, J. Kupsch, I.-O. Stamatescu, *Decoherence and the Appearance of a Classical World in Quantum Theory*, (Springer, Berlin 2003)

[9] W. H. Zurek, Rev. Mod. Phys. **75**, 715 (2003).

[10] H. Poincaré, *Les Méthodes Nouvelles de la mécanique Céleste*, (Gauthier-Villars, Paris 1882).

[11] E.N. Lorenz, J. Atmos. Sci. **20**, 130 (1963).

[12] R. D. Hazeltine and J. D.Meiss, *Plasma confinement*, (Addison-Wesley, Redwood City, 1992).

[13] W. M. Schaffer and M. Kot, *Differential systems in ecology and epidemiology in Chaos*, Arun V. Holden, Ed. (Princeton University Press, Princeton, 1986).

[14] A. Katok and B. Hasselblatt, *Introduction to the modern theory of dynamical systems*, (Cambridge University Press, Cambridge 1995).

[15] A. J. Lichtenberg and M. A. Lieberman, *Regular and Chaotic Dynamics*, 2 Ed. (Springer-Verlag, New York, 1992).

[16] P. Collet and J-P. Eckmann, *Concepts and Results in Chaotic Dynamics, A short course*, (Springer-Verlag, Berlin Heidelberg 2006).

[17] P. Cvitanović, R. Artuso, R. Mainieri, G. Tanner and G. Vattay, *Chaos: Classical and Quantum*, `ChaosBook.org` (Niels Bohr Institute, Copenhagen 2005)

[18] H. Furstenberg, Trans. Am. Math. Soc. **108**, 377 (1963).

[19] V.I. Oseledets, Trans. Mosc. Math. Soc. **19**, 197 (1968).

[20] A.N. Kolmogorov, Dokl. Akad. Nauk. SSSR 124, 754 (1959)

[21] Ya.G. Sinai, Proc. Int. Cong. Math. (1962); Izv. Akad. Nauk. SSSR, Mt. **30**, 15 (1966).

[22] Ya. B. Pesin, Russian Math. Surveys **32**, 55 (1977).

[23] F. Haake, *Quantum Signatures of Chaos*, 2. Ed. (Springer-Verlag, New York 2001).

[24] A.M. Ozorio de Almeida, *Hamiltonian Systems: Chaos and Quantization*, (Cambridge University Press, 1988).

[25] M.C. Gutzwiller, *Chaos in Classical and Quantum Mechanics*, (Springer-Verlag, Berlin, 1990).

[26] Proceedings of the 1989 Les Houches Summer School on *Chaos and Quantum Physics*, edited by M.-J. Giannoni, A. Voros, and J. Zinn-Justin (North-Holland, Amsterdam, 1991).

[27] L.E. Reichl, *The Transition to Chaos in Conservative Classical Systems: Quantum Manifestations*, (Springer-Verlag, New York 1992).

[28] Proceedings of the 1991 Enrico Fermi International School of Physics on *Quantum Chaos*, edited by G. Casati, I. Guarneri and U. Smilansky (North-Holland, Amsterdam, 1993).

[29] A. Einstein, Verh. Dtsch. Phys. Ges. **19**, 82 (1917).

[30] M.L. Mehta, *Random Matrices* (Academic, New York, 1991).

[31] O. Bohigas, M. J. Giannoni, and C. Schmit. Phys. Rev. Lett. **52**, 1 (1984).

[32] G. Casati, F. Valz-Gris, and I. Guarneri, Lett. Nuovo Cim. **28**, 279 (1980).

[33] M.V. Berry, Ann. Phys. **131**, 163 (1981)

[34] E.P. Wigner, Proc. Cambridge Phil. Soc., **47**, 790 (1951).

[35] F.J. Dyson, J. Math. Phys., **3**, 140 (1962).

[36] T. Guhr, A. Müller-Groeling, and H. A. Weidenmüller, Phys.Rept. **299** 189(1998).

[37] M. V. Berry and M. Tabor, Proc. R. Soc. London A **356**, 375 (1977).

[38] M. Brack and R.K. Bhaduri, *Semiclassical Physics*, (Addison-Wesley, New York 1997).

[39] K. Richter, *Semiclassical Theory of Mesoscopic Quantum Systems*, Springer Tracts in Modern Physics (Springer-Verlag, 2000).

[40] M.C. Gutzwiller, J. Math. Phys. **11**, 1791 (1970).

[41] M.C. Gutzwiller, J. Math. Phys. **12**, 343 (1971).

[42] S.Müller, S. Heusler, P. Braun, F. Haake and A. Altland, Phys. Rev. Lett. **93**, 014103 (2004).

[43] S. Müller, S. Heusler, P. Braun, F. Haake and A. Altland, Phys. Rev. E 72, 046207 (2005).

[44] S. Heusler, S. Müller, A. Altland, P. Braun, and F. Haake, Phys. Rev. Lett. **98**, 044103 (2007).

[45] E. Schrödinger, Die Naturwissenshaften **48** , 52 (1932).

[46] A. Stern, Y. Aharonov, and Y. Imry, Phys. Rev. A **41**, 3436 (1990).

[47] H. D. Zeh, Found. Phys. **1**, 69 (1970).

[48] W. H. Zurek, Phys. Rev. D **24**, 1516 (1981).

[49] R. P. Feynman and F. L.Vernon, Ann. Phys. **24**, 118 (1963).

[50] A. O. Caldeira, and A. J. Leggett, Physica A **121**, 587 (1983).

[51] A. O. Caldeira, and A. J. Leggett, Ann. Phys. **149**, 374 (1983).

[52] A. O. Caldeira, and A. J. Leggett, , Phys. Rev. A **31**, 1059 (1985).

[53] W. G. Unruh and W. H. Zurek, Phys. Rev. D **40**, 1071 (1989).

[54] H.-P. Breuer and F. Petruccione, *The Theory of Open Quantum Systems*, (Oxford University Press, Oxford, 2002).

[55] *Mesoscopic Phenomena in Solids*, edited by B.L. Altshuler, P.A. Lee, and R.A. Webb, (North-Holland, Amsterdam, 1991).

[56] Proceedings of the 1994 Les Houches Summer School on *Mesoscopic Quantum Physics*, edited by E. Akkermans, G. Montambaux, J.-L. Pichard, and J. Zinn-Justin (North-Holland, Amsterdam, 1995).

[57] S. Datta, *Electronic Transport in Mesoscopic Systems*, (Cambridge University Press, Cambridge, 1995).

[58] Y. Imry, *Introduction to Mesoscopic Physics*, (Oxford University Press, Oxford, 1997).

[59] Proceedings of the 1999 Enrico Fermi International School of Physics on *New Directions in Quantum Chaos*, edited by G. Casati, I. Guarneri and U. Smilansky (North-Holland, Amsterdam, 2000)

[60] B.L. Altshuler, Sov. Phys. JETP **41**, 648 (1985).

[61] P.A. Lee. A.D. Stone, H. Fukuyama, Phys. Rev. B **35**, 1039 (1987).

[62] S. Washburn and R. A. Webb, Adv. Phys. **35**, 375 (1986).

[63] B. L. Altshuler and D. E. Khmelnitskii, JETP Lett. **42**, 359 (1985).

[64] M. Büttiker, IBM J. Res. Develop. **32**, 317 (1988).

[65] G. Seelig, S. Pilgram, A. N. Jordan, and M. Büttiker Phys. Rev. B **68**, 161310 (2003).

[66] L.P. Kouwenhoven, C.M. Marcus, P.L. McEuen, S. Tarucha, R.M. Westervelt, and N.S. Wingreen, *Electron Transport in Quantum Dots*, NATO ASI Conference Proceedings, ed. by L. P. Kouwenhoven, G. Schon, L.L. Sohn (Klewer, 1997).

[67] M. W. Keller, O. Millo, A. Mittal, and D. E. Prober, Surf. Sci. **305**, 501 (1994).

[68] I. H. Chan, R. M. Clarke, C. M. Marcus, K. Campman, and A. C. Gossard Phys. Rev. Lett. **74**, 3876 (1995)

[69] C. M. Marcus, A. J. Rimberg, R. M. Westervelt, P. F. Hopkins, and A. C. Gossard, Phys. Rev. Lett. **69**, 506 (1992)

[70] Figure take from http://marcuslab.harvard.edu.

[71] R. A. Webb, S. Washburn, C. P. Umbach, and R. B. Laibowitz, Phys. Rev. Lett. **54**, 2696 (1985).

[72] A. M. Chang, H. U. Baranger, L. N. Pfeiffer, and K. W. West, Phys. Rev. Lett. **73**, 2111 (1994).

[73] Y. Gefen, Y. Imry, and M. Ya. Azbel', Surf. Sci. **142**, 203 (1984)

[74] M. Büttiker, Y. Imry, and M. Ya. Azbel', Phys. Rev. A **30**, 1982 (1984)

[75] P. W. Anderson, E. Abrahams, and T. V. Ramakrishnan Phys. Rev. Lett. **43**, 718 (1979).

[76] L. P. Gorkov, A. I. Larkin, and D. E. Khmelnitskii, Sov. Phys. JETP **30**, 248 (1979).

[77] P.A. Lee and A.D. Stone, Phys. Rev. Lett. **55** 1622 (1985).

[78] A. D. Mirlin in: Ref [59]

[79] K.B. Efetov *Supersymmetry in Disorder and Chaos* (Cambridge University Press, Cambridge, 1999).

[80] C. W. J. Beenakker Rev. Mod. Phys. **69**, 731 (1997).

[81] R. A. Jalabert in: Ref [59]

[82] S. Chakravarty and A. Schmid, Phys. Rep. **140**, 193 (1986)

[83] N. Argaman, Phys. Rev. Lett. **75**, 2750 (1995).

[84] N. Argaman, Phys. Rev. B **53**, 7035 (1996).

[85] R. A. Jalabert, H. U. Baranger and A. D. Stone, Phys. Rev. Lett. **65**, 2442(1990).

[86] H. U. Baranger, R. A. Jalabert and A. D. Stone, Phys. Rev. Lett. **70**, 3876 (1993)

[87] Ph. Jacquod and R.S. Whitney, Phys. Rev. B **73**, 195115 (2006).

[88] P.W. Brouwer and S. Rahav, Phys. Rev. B **74**, 075322 (2006).

[89] K. Richter and M. Sieber, Phys. Rev. Lett. **89**, 206801 (2002).

[90] R. Landauer, IBM J. Res. Develop. **1**, 223 (1957).

[91] A.D. Stone, A. Szafer. IBM J. Res. Develop. **32**, 384 (1988)

[92] C. W. J. Beenakker and H. van Houten, Solid State Phys. **44**, 1 (1991).

[93] M. Büttiker, Phys. Rev. B **33**, 3020 (1986).

[94] M. J. M de Jong and C. W. J. Beenakker Physica A **230**, 219 (1996).

[95] M.G. Vavilov and I.L. Aleiner, Phys. Rev. B **60**, R16311 (1999).

[96] G. Seelig and M. Büttiker, Phys. Rev. B **64**, 245313 (2001).

[97] P. W. Brouwer and C. W. J. Beenakker Phys. Rev. B **55**, 4695 (1997)

[98] M.L. Polianski and P.W. Brouwer, J. Phys. A: Math Gen. **36**, 3215 (2003).

[99] D.L. Shepelyansky, Physica **D8**, 208 (1983)

[100] A. Peres, Phys. Rev. A **30**, 1610 (1984).

[101] R.A. Jalabert and H.M. Pastawski, Phys. Rev. Lett. **86**, 2490 (2001).

[102] Ph. Jacquod, P.G. Silvestrov, and C.W.J. Beenakker, Phys. Rev. E **64**, 055203(R) (2001).

[103] N.R. Cerruti and S. Tomsovic, Phys. Rev. Lett. **88**, 054103 (2002).

[104] F.M. Cucchietti, C.H. Lewenkopf, E.R. Mucciolo, H.M. Pastawski, and R. O. Vallejos, Phys. Rev. E **65**, 046209 (2002).

[105] Ph. Jacquod, İ. Adagideli, and C.W.J. Beenakker, Phys. Rev. Lett. **89**, 154103 (2002).

[106] Z. P. Karkuszewski, C. Jarzynski, and W.H. Zurek, Phys. Rev. Lett. **89**, 170405 (2002).

[107] J. Vaniček and E.J. Heller, Phys. Rev. E **68**, 056208 (2003).

[108] T. Prosen, T.H. Seligman, and M. Znidaric, Prog. Theor. Phys. Supp. **150**, 200 (2003).

[109] Y. Adamov, I.V. Gornyi, and A.D. Mirlin, Phys. Rev. E **67**, 056217 (2003).

[110] J. Emerson, Y.S. Weinstein, S. Lloyd, and D.G. Cory, Phys. Rev. Lett. **89**, 284102 (2002).

[111] W. Wang, G. Casati, and B. Li, Phys. Rev. E **69**, 025201(R) (2004).

[112] A. Iomin, Phys. Rev. E **70**, 026206 (2004).

[113] T. Gorin, T. Prosen, T.H. Seligman, M. Znidaric, Phys. Rep. **435**, 33 (2006).

[114] C. Petitjean, Ph. Jacquod, Phys. Rev. E **71**, 03623 (2005).

[115] E.L. Hahn, Phys. Rev. **80**, 580 (1950).

[116] W.K. Rhim, A. Pines, J.S Waugh, Phys. Rev. Lett. **25**, 218 (1970).

[117] H.M. Pastawski, P. R. Levstein, G. Usaj, Phys. Rev. Lett. **75**, 4310 (1995).

[118] N.A. Kurnit, I.D. Adella, S.R. Hartmann, Phys. Rev. Lett. **13**, 567 (1964)

[119] F.B.J. Buckremer, R. Dumke, H. Levsen, W. Ertmer, Phys. Rev. Lett. **85**, 3121 (2000)

[120] M.F Andersen, A. Kaplan, N. Davidson, Phys. Rev. Lett. **90**, 023001 (2003)

[121] Y. Nakamura, Y.A. Pashkin, T. Yamamoto, J.S. Tsai, Phys. Rev. Lett. **88**, 047901 (2002)

[122] H.M. Pastawski, P.R. Levstein, G. Usaj, J. Raya, and J. Hirschinger, Physica A **283**, 166 (2000)

[123] C. Petitjean, Ph. Jacquod, Phys. Rev. Lett. **97**, 0124103 (2006).

[124] L. Van Hove, Phys. Rev. **95**, 249 (1954).

[125] S.W. Lovesey, *Theory of Neutron Scattering from Condensed Matter*, Vol. 1 (Oxford University Press, New York, 1984).

[126] E.J. Heller, J.R. Reimers and G. Drolshagen, Phys. Rev. A **36**, 2613 (1987).

[127] C. Petitjean, D.V. Bevilaqua, E.J. Heller and Ph. Jacquod, Phys. Rev. Lett. **98** , 164101 (2007).

[128] E.J. Su, S. Wu, M. Prentiss, eprint: physics/0701018.

[129] E. Schrödinger, Proc. Cambridge Phil. Soc. **31**, 555 (1936).

[130] F. M. Cucchietti, D. A. R. Dalvit, J. P. Paz, and W. H. Zurek Phys. Rev. Lett. **91**, 210403 (2003)

[131] P. A. Miller and S. Sarkar, Phys. Rev. E **60**, 1542 (1999)

[132] A. Tanaka, H. Fujisaki, and T. MiyaderaPhys. Rev. E **66**, 04520R (2002)

[133] Ph. Jacquod, Phys. Rev. Lett. **92**, 150403 (2004).

[134] C. Petitjean and Ph. Jacquod, Phys. Rev. Lett. **97**, 194103 (2006).

[135] F. Mintert, A.R.R. Carvalho, M.Kus and A. Buchleitner, Phys. Rep, **415**, 207 (2005).

[136] I.L. Aleiner and A.I. Larkin, Phys. Rev. B **54**, 14423 (1996); Phys. Rev. E **55**, R1243 (1997).

[137] C. Petitjean, Ph. Jacquod and R.S Whitney, eprint: cond-mat/0612118.

[138] A. Altland, P.W. Brouwer and C. Tian, eprint: cond-mat/0605051.

[139] R.S. Whitney, Phys. Rev. B **75**, 235404 (2007).

Part II

Reversibility in Quantum Mechanics : An Echo Approach

CHAPTER 2

Mesoscopic fluctuations of the Loschmidt echo

2.1 Introduction

Fluctuations of a physical quantity often contain more information than its average. For example, quantum signatures of classical chaos are absent in the average density of states, but strongly affect spectral fluctuations [1]. In the search for such signatures, a powerful approach has been to investigate the sensitivity to an external perturbation that is exhibited by the quantum dynamics [2]. Going back to Ref. [3], the central quantity in this approach is the Loschmidt Echo [4], i.e. the fidelity

$$\mathcal{M}_{\rm L}(t) = |\langle\psi_0| \exp[iHt] \exp[-iH_0t]|\psi_0\rangle|^2 \tag{2.1}$$

with which an initial quantum state ψ_0 is reconstructed after the dynamics is time-reversed using a perturbed Hamiltonian, $H = H_0 + \epsilon V$ (we set $\hbar \equiv 1$). Most investigations of $\mathcal{M}_{\rm L}(t)$ (which we will briefly summarize below, see [5] for a review) considered the properties of the *average* fidelity $\overline{\mathcal{M}_{\rm L}(t)}$, either over different ψ_0, or different elements of an ensemble of unperturbed Hamiltonians H_0 (having for instance the same classical Lyapunov exponent λ) and/or perturbation V. Curiously enough, the variance $\sigma^2(\mathcal{M}_{\rm L})$ of the fidelity has been largely neglected so far. The purpose of this chapter is to fill this gap. We will see that the variance $\sigma^2(\mathcal{M}_{\rm L})$ has a much richer behavior than $\overline{\mathcal{M}_{\rm L}(t)}$, allowing for the extraction of λ in a larger parameter range, and exhibiting a nonmonotonous behavior with a non-self-averaging maximal value $\sigma(t_c)/\overline{\mathcal{M}_{\rm L}(t_c)} \simeq 1$.

We first summarize what is known about the average fidelity $\overline{\mathcal{M}_{\rm L}(t)}$ in quantum chaotic systems. One usually distinguishes between three regimes of perturbation strength, which are characterized by three different energy scales [6]:

the energy bandwidth B of H_0, the golden rule spreading $\Gamma = 2\pi\epsilon^2\overline{|\langle a|V|b\rangle|^2}/\Delta$ of an eigenstate $|a\rangle$ of H_0 over the eigenbasis $\{|\alpha\rangle\}$ of H, and the level spacing $\Delta = BN^{-1}$ ($N^{-1} = \nu^d/\Omega$ is the effective Planck's constant, given by the ratio of the wavelength volume to the system's volume).
These three regimes are ;

(i) the weak perturbation regime $\Gamma < \Delta$, with a typical Gaussian decay

$$\overline{\mathcal{M}_{\rm L}(t)} \simeq \exp(-\overline{\Sigma^2}t^2),$$

$\Sigma^2 \equiv \epsilon^2(\langle\psi_0|V^2|\psi_0\rangle - \langle\psi_0|V|\psi_0\rangle^2)$, $\overline{\Sigma^2} \simeq \Gamma\Delta N$ [3, 7] (corrections to this Gaussian decay have been discussed in Ref. [8]),

(ii) the semiclassical golden rule regime $\Delta < \Gamma < B$, where the decay is exponential with a rate set by the smallest of Γ and λ [4, 6, 9],

$$\overline{\mathcal{M}_{\rm L}(t)} \simeq \exp[-\min(\Gamma, \lambda)t],$$

(iii) the strong perturbation regime $\Gamma > B$ with another Gaussian decay [6]

$$\overline{\mathcal{M}_{\rm L}(t)} \simeq \exp(-B^2t^2).$$

This classification is based on the scheme of Ref. [6] which relates the behavior of $\overline{\mathcal{M}_{\rm L}(t)}$ to the local spectral density of eigenstates of H_0 over the eigenbasis of H [6, 10]. Accordingly, regime **(ii)** corresponds to the range of validity of Fermi's golden rule, where the local spectral density has a Lorentzian shape [6, 10, 11]. Quantum disordered systems with diffractive impurities, on the other hand, have been predicted to exhibit golden rule decay $\propto \exp[-\Gamma t]$ and Lyapunov decay $\propto \exp[-\lambda t]$ in different time intervals for a single set of parameters [13]. It is also worth mentioning that regular systems exhibit a very different behavior, where in the semiclassical regime **(ii)**, $\overline{\mathcal{M}_{\rm L}(t)}$ decays as a power-law [14] (see also Ref. [15]). Finally, while in chaotic systems the averaging procedure has been found to be ergodic, i.e. considering different states ψ_0 is equivalent to considering different realizations of H_0 or V, the Lyapunov decay exists only for specific choices where ψ_0 has a well defined classical meaning, like a coherent or a position state [4, 12, 16, 17].

Investigations beyond this qualitative picture have focused on crossover regions between the regimes **(i)** and **(ii)** [8] and deviations from the behavior **(ii)** $\simeq \exp[-\min(\Gamma, \lambda)t]$ due to action correlations in weakly chaotic systems [18]. Ref. [19] provides the only analytical investigation of fluctuations of $\mathcal{M}_{\rm L}(t)$ to date. It shows that, for classically large perturbations, $\Gamma \gg B$, $\overline{\mathcal{M}_{\rm L}(t)}$ is dominated by very few exceptional events, so that a typical ψ_0's fidelity is better described by $\exp[\overline{\ln(\mathcal{M}_{\rm L})}]$, and that $\mathcal{M}_{\rm L}(t)$ does not fluctuate after the Ehrenfest time $\tau_{\rm E} = \lambda^{-1}|\ln[N^{-1}]|$. We will see that these conclusions do not apply to the regime **(ii)** of present interest. While some numerical data for the distribution of $\mathcal{M}_{\rm L}(t)$ in the weak perturbation regime **(i)** were presented in Ref. [20], we focus here on chaotic systems and investigate the behavior of $\sigma^2(\mathcal{M}_{\rm L})$ in the semiclassical regime **(ii)**.

2.2 Semiclassical regime

We first follow a semiclassical approach along the lines of Ref. [4]. We consider an initial Gaussian wavepacket $\psi_0(\mathbf{x}) = (\pi\nu^2)^{-d/4} \exp[i\mathbf{p}_0 \cdot (\mathbf{x}-\mathbf{r}_0) - |\mathbf{x}-\mathbf{r}_0|^2/2\nu^2]$, and approximate its time-evolution by

$$\langle \mathbf{r}| \exp(-iH_0 t)|\psi_0\rangle = \int d\mathbf{x} \sum_s K_s^{H_0}(\mathbf{r},\mathbf{x};t)\psi_0(\mathbf{x}), \tag{2.2a}$$

$$K_s^{H_0}(\mathbf{r},\mathbf{x};t) = \frac{C_s^{1/2}}{(2\pi i)^{d/2}} \exp[iS_s^{H_0}(\mathbf{r},\mathbf{x};t)]. \tag{2.2b}$$

The semiclassical propagator is expressed as a sum over classical trajectories (labelled s) connecting $\mathbf{r}$ and $\mathbf{x}$ in the time t. For each s, the partial propagator contains the action integral $S_s^H(\mathbf{r},\mathbf{x};t)$ along s (where we included a Maslov index), and the determinant C_s of the stability matrix [21]. We recall that this approach allows to calculate the time evolution of smooth, localized wavepackets up to algebraically long times $\propto \mathcal{O}(N^a) \gg \tau_{\rm E}$ (with $a > 0$) [22].

The fidelity then reads,

$$\mathcal{M}_{\rm L}(t) = \left| \int d\mathbf{r}_1 \prod_{i=1}^{2} \int d\mathbf{x}_i \; \psi_0(\mathbf{x}_1)\psi_0^*(\mathbf{x}_2) \sum_{s_1,l_1} K_{s_1}^{H_0}(\mathbf{x}_1,\mathbf{r}_1;t) \; [K_{l_1}^{H}(\mathbf{x}_2,\mathbf{r}_1;t)]^* \right|^2 \tag{2.3}$$

We want to calculate $\mathcal{M}_{\rm L}^2(t)$. Squaring Eq. (2.3), we see that $\mathcal{M}_{\rm L}^2(t)$ is given by eight sums over classical paths and twelve spatial integrations. Noting that ψ_0 is a narrow Gaussian wavepacket, we first linearize all eight action integrals around $\mathbf{r}_0$,

$$S_s(\mathbf{x},\mathbf{r};t) \simeq S_s(\mathbf{r}_0,\mathbf{r};t) - (\mathbf{x}-\mathbf{r}_0)\cdot\mathbf{p}_s. \tag{2.4}$$

We can then perform the Gaussian integrations over the eight initial positions $\mathbf{x}_i$, and so forth. In this way $\mathcal{M}_{\rm L}^2(t)$ is expressed as a sum over eight trajectories connecting $\mathbf{r}_0$ to four independent final points $\mathbf{r}_j$ over which one integrates,

$$\mathcal{M}_{\rm L}^2(t) = \int \prod_{j=1}^{4} d\mathbf{r}_j \sum_{s_i,l_i;i=1}^{4} e^{i(\Phi^{H_0}-\Phi^H)} \left(\prod_i (C_{s_i}C_{l_i})^{1/2} \left(\frac{\nu^2}{\pi}\right)^{d/2} e^{-\frac{\nu^2}{2}(\delta\mathbf{p}_{s_i}^2+\delta\mathbf{p}_{l_i}^2)} \right), \tag{2.5}$$

where we introduced $\delta\mathbf{p}_s = \mathbf{p}_s - \mathbf{p}_0$.

The expression of Eq.(2.5) is schematically described in Fig. 2.1. Classical trajectories are represented by a full line if they correspond to H_0 and a dashed line for H, with an arrow indicating the direction of propagation. In the semiclassical limit $S_s \gg 1$ (we recall that actions are expressed in units of $\hbar$), Eq. (2.5) is dominated by terms which satisfy a stationary phase condition, i.e. where the variation of the difference of the two action phases

$$\Phi^{H_0} = S_{s_1}^{H_0}(\mathbf{r}_0,\mathbf{r}_1;t) - S_{s_2}^{H_0}(\mathbf{r}_0,\mathbf{r}_2;t) - S_{s_3}^{H_0}(\mathbf{r}_0,\mathbf{r}_3;t) + S_{s_4}^{H_0}(\mathbf{r}_0,\mathbf{r}_4;t), \tag{2.6a}$$

$$\Phi^{H} = S_{l_1}^{H}(\mathbf{r}_0,\mathbf{r}_1;t) - S_{l_2}^{H}(\mathbf{r}_0,\mathbf{r}_2;t) - S_{l_3}^{H}(\mathbf{r}_0,\mathbf{r}_3;t) + S_{l_4}^{H}(\mathbf{r}_0,\mathbf{r}_4;t), \tag{2.6b}$$

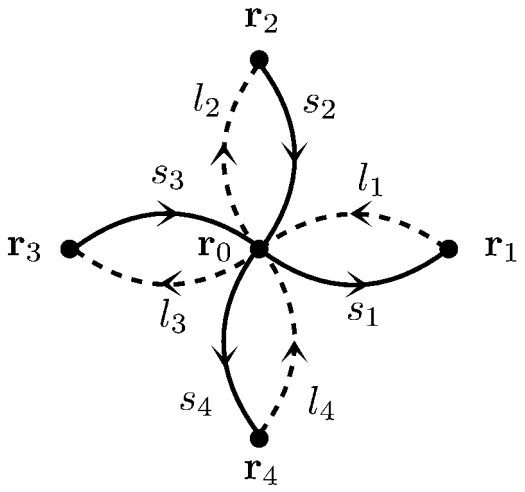

Figure 2.1: Diagrammatic representation of the squared fidelity $\mathcal{M}_{\mathrm{L}}^2(t)$.

has to be minimized. These stationary phase terms are easily identified from the diagrammatic representation as those where two classical trajectories s and l of opposite direction of propagation are *contracted*, i.e. $s = l$, up to a quantum resolution given by the wavelength ν. Setting $s = l$ for two trajectories generated by two different Hamiltonians $H = H_0 + \epsilon V$, is justified by the structural stability of hyperbolic systems for not too large ϵ [24]. This is represented in Fig. 2.2 by bringing two lines together in parallel. Contracting either two dashed or two full lines allows for an almost exact cancellation of the actions, hence an almost perturbation-independent contribution, up to a contribution arising from the finite resolution ν with which the two paths overlap. However when a full line is contracted with a dashed line, the resulting contribution still depends on the action $\delta S_s = -\epsilon \int_s dt\, V(\mathbf{q}(t), t)$ accumulated by the perturbation along the classical path s, spatially parametrized as $\mathbf{q}(t)$. Since we are interested in the variance $\sigma^2(\mathcal{M}_{\mathrm{L}}) = \overline{\mathcal{M}_{\mathrm{L}}^2} - \overline{\mathcal{M}_{\mathrm{L}}}^2$ (this is indicated by brackets in Fig. 2.2) we must subtract the terms contained in $\overline{\mathcal{M}_{\mathrm{L}}}^2$ corresponding to independent contractions in each of the two subsets (s_1, l_1, s_2, l_2) and (s_3, l_3, s_4, l_4). Consequently, all contributions to $\sigma^2(\mathcal{M}_{\mathrm{L}})$ require pairing of spatial coordinates, $|\mathbf{r}_i - \mathbf{r}_j| \leq \nu$, for at least one pair of indices $i, j = 1, 2, 3, 4$. With these considerations, the four dominant contributions to $\sigma^2(\mathcal{M}_{\mathrm{L}})$ are depicted on the right-hand side of Fig. 2.2, and will be computed in the following subsections.

2.2.1 Classical contribution : Lyapunov regime

The first contribution, depicted on the right-hand side of Fig. 2.2, corresponds to $s_1 = l_1 \simeq s_3 = l_3$ and $s_2 = l_2 \simeq s_4 = l_4$, which requires $\mathbf{r}_1 \simeq \mathbf{r}_3$, $\mathbf{r}_2 \simeq \mathbf{r}_4$. This

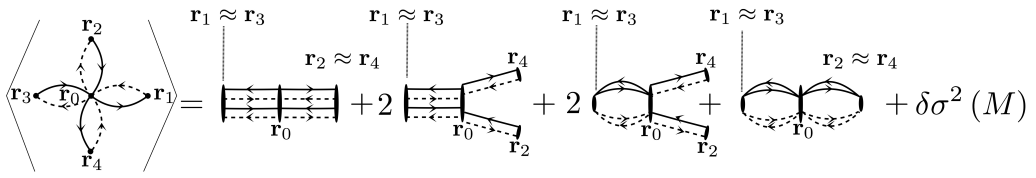

$$\sigma^2\,(M) \quad = \alpha^2(t)\,e^{-2\lambda t} + 2\,\alpha(t) e^{-(\lambda+\Gamma)t} + \frac{2}{N}\,\Theta_{\tau_{\rm E}}(t) e^{-\Gamma t} + \frac{1}{N^2}\,\Theta_{\tau_{\rm E}}(t) + \delta\sigma^2\,(M)$$

Figure 2.2: Diagrammatic representation of the averaged fidelity variance $\sigma^2(\mathcal{M}_{\rm L})$ and the three time-dependent contributions that dominate semiclassically, together with the contribution giving the long-time saturation of $\sigma^2(\mathcal{M}_{\rm L})$. Semiclassical subdominants contributions are denoted by $\delta\sigma^2$. (For a quick tutorial on diagrams see Appendix 2.6.)

gives a contribution

$$\sigma_1^2 = \left(\frac{\nu^2}{\pi}\right)^{2d} \left\langle \int d\mathbf{r}_1 d\mathbf{r}_3 \sum C_{s_1}^2 \exp[-2\nu^2 \delta\mathbf{p}_{s_1}^2 + i\delta\Phi_{s_1}] \delta_\nu(|\mathbf{r}_1 - \mathbf{r}_3|) \right\rangle^2, \quad (2.7)$$

where

$$\delta\Phi_{s_1} = \epsilon \int_0^t dt' \nabla V[\mathbf{q}(t')][\mathbf{q}_{s_1}(t') - \mathbf{q}_{s_3}(t')] \quad (2.8)$$

arises from the linearization of V on $s = s_1, l_1 \simeq l = s_3, l_3$ [4, 12], and $\mathbf{q}_{s_1}(t')$ lies on s_1 with $\mathbf{q}(0) = \mathbf{r}_0$ and $\mathbf{q}(t) = \mathbf{r}_1$. In Eq. (2.7) the integrations are restricted by $|\mathbf{r}_1 - \mathbf{r}_3| \leq \nu$ because of the finite resolution with which two paths can be equated, this is also enforced by the presence of $\delta\Phi_s$ as we will see momentarily. For long enough times, $t \gg t^*$, the phases $\delta\Phi_s$ fluctuate randomly and exhibit no correlation between different trajectories. This time t^* is defined by $|\epsilon \int_0^{t^*} dt\, V(\mathbf{q}_s(t), t)| = 1$ for a typical trajectory s. One thus applies the Central Limit Theorem (CLT)

$$\langle \exp\left[i\delta\Phi_s\right] \rangle = \exp\left[-\langle \delta\Phi_s^2 \rangle / 2\right] \simeq \exp\left[-\epsilon^2 \int dt \langle \nabla V(0) \cdot \nabla V(t) \rangle |\mathbf{r}_1 - \mathbf{r}_3|^2 / 2\lambda\right].$$

After performing a change of integration variable $\int d\mathbf{r} \sum_s C_s = \int d\mathbf{p}$ and using the asymptotic expression $C_s \simeq (m/t)^d \exp[-\lambda t]$ [21], one gets

$$\sigma_1^2 \;\; = \;\; \alpha^2(t) e^{-2\lambda t}, \quad (2.9)$$

with $\alpha(t) = \alpha_0 t^{-d}\,\Theta_{\tau_\lambda}(t)$, and $\Theta_{\tau_\lambda}(t)$ the Heaviside step function centered in τ_λ, see appendix 2.7 for more details.

2.2.2 Mixed contribution

The second dominant term is obtained from $s_1 = l_1 \simeq s_3 = l_3$, $s_2 = l_2$ and $s_4 = l_4$, with $\mathbf{r}_1 \simeq \mathbf{r}_3$, or equivalently $s_1 = l_1$, $s_3 = l_3$ and $s_2 = l_2 \simeq s_4 = l_4$ with $\mathbf{r}_2 \simeq \mathbf{r}_4$. Therefore this term comes with a multiplicity of two, and one obtains

$$\begin{aligned}\sigma_2^2 &= 2\left(\frac{\nu^2}{\pi}\right)^{2d}\left\langle \int d\mathbf{r}_1 d\mathbf{r}_3 \sum C_{s_1}^2 \exp[-2\nu^2\delta\mathbf{p}_{s_1}^2 + i\delta\Phi_{s_1}]\delta_\nu(|\mathbf{r}_1-\mathbf{r}_3|)\right\rangle \\ &\quad\times\left\langle \int d\mathbf{r}_2 \sum C_{s_2}\exp[-\nu^2\delta\mathbf{p}_{s_2}^2 + i\delta S_{s_2}]\right\rangle^2, \end{aligned} \tag{2.10}$$

again with the restriction $|\mathbf{r}_1 - \mathbf{r}_3| \leq \nu$. To calculate the first bracket on the right-hand side of Eq. (2.10), we first average the complex exponential, assuming again that enough time has elapsed so that actions are randomized. The CLT gives $\langle\exp[i\delta S_{s_2}]\rangle = \exp(-\frac{1}{2}\langle\delta S_{s_2}^2\rangle)$ with

$$\langle\delta S_{s_2}^2\rangle = \epsilon^2\int_0^t d\tilde{t}\int_0^t d\tilde{t}'\langle V[\mathbf{q}(t')]V[\mathbf{q}(t')]\rangle. \tag{2.11}$$

Here $\mathbf{q}(t')$ lies on s_2 with $\mathbf{q}(0) = \mathbf{r}_0$ and $\mathbf{q}(t) = \mathbf{r}_2$. In hyperbolic systems, correlators typically decay exponentially fast,

$$\langle V[\mathbf{q}(t')]V[\mathbf{q}(t')]\rangle \propto \exp[-\eta|t-t'|], \tag{2.12}$$

with an upper bound on η set by the smallest positive Lyapunov exponent [25]. One thus obtains $\langle\delta S_{s_2}^2\rangle = \Gamma t$. Usually $\Gamma \propto \epsilon^2$ is identified with the golden rule spreading of eigenstates of H over those of H_0 [6, 8]. It is dominated by the short-time behavior of $\langle V[\mathbf{q}(t')]V[\mathbf{q}(0)]\rangle$. We stress however that for long enough times, $\langle\delta S_{s_2}^2\rangle \propto t$ still holds to leading order even with a power-law decay of the correlator $\langle V[\mathbf{q}(t')]V[\mathbf{q}(t')]\rangle \propto |t-t'|^{-\eta}$, provided η is sufficiently large, $\eta \geq 1$. We note that similar expressions as Eq. (2.11) relating the decay of $\overline{\mathcal{M}_{\mathrm{L}}}$ to time integrations over the perturbation correlator have been derived in Refs. [7, 20] using a different approach than the semiclassical method of Ref. [4] used here. Further using the sum rule

$$(\nu^2/\pi)^d\left(\int d\mathbf{r}\sum C_s\exp[-\nu^2\delta\mathbf{p}_s^2]\right)^2 = 1, \tag{2.13}$$

one finally obtains

$$\sigma_2^2 = 2\alpha(t)e^{-\lambda t}e^{-\Gamma t}. \tag{2.14}$$

2.2.3 Quantum contribution : FGR regime

The third and last dominant time-dependent term arises from either $s_1 = s_3$, $l_1 = l_3$, $s_2 = l_2$, $s_4 = l_4$ and $\mathbf{r}_1 \simeq \mathbf{r}_3$, or $s_1 = l_1$, $s_2 = s_4$, $l_2 = l_4$, $s_3 = l_3$ and $\mathbf{r}_2 \simeq \mathbf{r}_4$. It thus also has a multiplicity of two and reads

$$\sigma_3^2 = 2\left(\frac{\nu^2}{\pi}\right)^{2d} \left\langle \int d\mathbf{r}_1 d\mathbf{r}_2 d\mathbf{r}_3 d\mathbf{r}_4 \sum C_{s_1} C_{l_1} C_{s_2} C_{s_4} \delta_\nu(|\mathbf{r}_1 - \mathbf{r}_3|) \times \exp[-\nu^2(\delta\mathbf{p}_{s_1}^2 + \delta\mathbf{p}_{l_1}^2 + \delta\mathbf{p}_{s_2}^2 + \delta\mathbf{p}_{s_4}^2)] \exp[i(\delta S_{s_2} - \delta S_{s_4})] \right\rangle. \quad (2.15)$$

The integrations, again, have to be performed with $|\mathbf{r}_1 - \mathbf{r}_3| \leq \nu$. We incorporate this restriction in the calculation by making the ergodicity assumption, setting

$$\left\langle \int d\mathbf{r}_1 d\mathbf{r}_2 d\mathbf{r}_3 d\mathbf{r}_4 \ldots \delta_\nu(|\mathbf{r}_1 - \mathbf{r}_3|) \right\rangle = \frac{1}{N} \left\langle \int d\mathbf{r}_1 d\mathbf{r}_2 d\mathbf{r}_3 d\mathbf{r}_4 \ldots \right\rangle \Theta_{\tau_\mathrm{E}}(t), \quad (2.16)$$

which is valid for times larger than the Ehrenfest time [26]; for shorter times, $t < \tau_\mathrm{E}$, the third diagram on the right-hand side of Fig. 2.2 goes into the second one. One then averages the phases using the CLT to get

$$\sigma_3^2 = \frac{2}{N} e^{-\Gamma t} \Theta_{\tau_\mathrm{E}}(t). \quad (2.17)$$

2.2.4 Long-time saturation

Subdominant terms $\delta\sigma^2$ are obtained by higher-order contractions (e.g. setting $\mathbf{r}_2 \simeq \mathbf{r}_4$ in the second and third graphs on the right hand-side of Fig. 2.2). They either decay faster, or are of higher order in N^{-1}, or both. We only discuss here the term which gives the long-time saturation at the ergodic value $\sigma^2(\mathcal{M}_\mathrm{L}) \simeq N^{-2}$, the others will be detailed in the appendix 2.8. For $t > \tau_\mathrm{E}$, there is a phase-free (and hence time-independent) contribution with four different paths, resulting from the contraction $s_1 = s_3$, $l_1 = l_3$, $s_2 = s_4$, $l_2 = l_4$, and $\mathbf{r}_1 \simeq \mathbf{r}_3$, $\mathbf{r}_2 \simeq \mathbf{r}_4$. Its contribution is sketched as the fourth diagram on the right-hand side of Fig. 2.2. It gives

$$\sigma_4^2 = \left(\frac{\nu^2}{\pi}\right)^{2d} \left\langle \int d\mathbf{r}_1 d\mathbf{r}_3 \sum C_{s_1} C_{l_1} \exp[-\nu^2(\delta\mathbf{p}_{s_1}^2 + \delta\mathbf{p}_{l_1}^2)] \delta_\nu(|\mathbf{r}_1 - \mathbf{r}_3|) \right\rangle^2.$$

From the sum rule of Eq. (2.13), and again invoking the long-time ergodicity of the semiclassical dynamics, Eq. (2.16), one obtains the long-time saturation of $\sigma^2(M)$,

$$\sigma_4^2 = \frac{1}{N^2} \Theta_{\tau_\mathrm{E}}(t). \quad (2.18)$$

Note that for $t < \tau_\mathrm{E}$, this contribution does not exist by itself and is included in σ_1^2, Eq. (2.9).

2.2.5 Semiclassical results

According to our semiclassical approach, the fidelity has a variance given to leading order by the sum of the four terms of Eqs. (2.9, 2.14, 2.17) and (2.18).

$$\sigma^2_{\rm sc}(t) \;=\; \alpha^2(t)e^{-2\lambda t} + 2\alpha(t)\mathrm{e}^{-(\lambda+\Gamma)t} + \frac{2}{N}e^{-\Gamma t}\,\Theta_{\tau_{\rm E}}(t) + \frac{1}{N^2}\,\Theta_{\tau_{\rm E}}(t). \quad (2.19)$$

Eq. (2.19) is the central result of this chapter. We see that for short enough times, i.e. before ergodicity and the saturation of $\mathcal{M}_{\rm L}(t) \simeq N^{-1}$ and $\sigma^2(\mathcal{M}_{\rm L}) \simeq N^{-2}$ is reached, the first term on the right-hand side of Eq. (2.19) will dominate as long as $\lambda < \Gamma$. For $\lambda > \Gamma$ on the other hand, $\sigma^2(\mathcal{M}_{\rm L})$ exhibits a behavior $\propto \exp[-(\lambda+\Gamma)t]$ for $t < \tau_{\rm E}$, turning into $\propto N^{-1}\exp[-\Gamma t]$ for $t > \tau_{\rm E}$. Thus, contrary to $\overline{\mathcal{M}_{\rm L}}$, $\sigma^2(\mathcal{M}_{\rm L})$ allows to extract the Lyapunov exponent from the second term on the right-hand side of Eq. (2.19) even when $\lambda > \Gamma$. Also one sees that, unlike the strong perturbation regime $\Gamma \gg B$ [19], $\mathcal{M}_{\rm L}(t)$ continues to fluctuate above the residual variance $\simeq N^{-2}$ up to a time $\simeq \Gamma^{-1}|\ln N^{-1}|$ in the semiclassical regime $B > \Gamma > \Delta$. For $\Gamma \ll \lambda$, $\Gamma^{-1}|\ln N^{-1}| \gg \tau_{\rm E}$ and $\mathcal{M}_{\rm L}(t)$ fluctuates beyond $\tau_{\rm E}$.

We conclude this section by mentioning that applying the Random Matrix Theory (RMT) approach [27] to longer times reproduces Eq. (2.19) with $\lambda \to \infty$. This reflects the fact that RMT is strictly recovered for $\tau_{\rm E} = 0$ only. The derivation of these result is oultined in appendix 2.9

2.3 Short time behavior

The previous semiclassical approach breaks down at short times for which not enough phase is accumulated to motivate a stationary phase approximation. This time is very short, of the order of the inverse energy of the particle, i.e. $O(N^{-a})$, where $a \geq 0$ depends on the system dimension and the energy-momentum relation. (For $E \propto p^2$ and in two dimensions, one has $a = 1$.)

To get the short-time behavior of $\sigma^2(\mathcal{M}_{\rm L})$, we instead Taylor expand the time-evolution exponentials $\exp[\pm iH_{(0)}t] = 1 \pm iH_{(0)}t - H^2_{(0)}t^2/2 + ... + O(H^5_{(0)}t^5)$. The resulting expression for $\sigma^2(\mathcal{M}_{\rm L})$ contains matrix elements such as $\langle\psi_0|H^a_{(0)}|\psi_0\rangle$, $a = 1, 2, 3, 4$, which one then calculates using a RMT approach [27] for the chaotic quantized Hamiltonian $H_{(0)}$ [6, 9, 20]. Keeping non-vanishing terms of lowest order in t, one has a quartic onset

$$\sigma^2(\mathcal{M}_{\rm L}) \simeq (\overline{\Sigma^4} - \overline{\Sigma^2}^2)t^4$$

for $t \ll \Sigma^{-1}$, with $\Sigma^a \equiv [\epsilon^2(\langle\psi_0|V^2|\psi_0\rangle - \langle\psi_0|V|\psi_0\rangle^2)]^{a/2}$. Random matrix theory gives $(\overline{\Sigma^4} - \overline{\Sigma^2}^2) \propto (\Gamma B)^2$, with a system-dependent prefactor of order one. From this and Eq. (2.19) one concludes that $\sigma^2(\mathcal{M}_{\rm L})$ has a nonmonotonous behavior,

i.e. it first rises at short times, until it decays after a time t_c which one can evaluate by solving $\sigma^2_{\rm sc}(t_c) = (\Gamma B)^2 t_c^4$. In the regime $B > \Gamma > \lambda$ one gets

$$t_c = \left(\frac{\alpha_0}{\Gamma B}\right)^{\frac{1}{2}+d} \left[1 - \lambda \left(\frac{\alpha_0}{\Gamma B}\right)^{\frac{1}{2}+d} \frac{1}{2+d} + \mathcal{O}\left(\lambda^2 \left\{\frac{\alpha_0}{\Gamma B}\right\}^{\frac{1}{2+d}}\right)\right], \tag{2.20}$$

and thus

$$\sigma^2(t_c) \simeq (\Gamma B)^2 \left(\frac{\alpha_0}{\Gamma B}\right)^{\frac{4}{2+d}} \left[1 - \frac{4\lambda}{2+d} \left(\frac{\alpha_0}{\Gamma B}\right)^{\frac{1}{2+d}} + \mathcal{O}\left(\lambda^2 \left\{\frac{\alpha_0}{\Gamma B}\right\}^{\frac{2}{2+d}}\right)\right]. \tag{2.21}$$

We explicitely took the t-dependence $\alpha(t) = \alpha_0 t^{-d}$ into account. We estimate that $\alpha_0 \propto (\Gamma\lambda)^{-d/2}$ (See appendix 2.7) to get $\sigma^2(t_c) \propto (B/\lambda)^{2d/2+d} \gg 1$. Because $0 \leq \mathcal{M}_{\rm L}(t) \leq 1$, this value is however bounded by $\overline{\mathcal{M}_{\rm L}}^2(t_c)$.

Since in the other regime $\Gamma \ll \lambda$, one has

$$t_c = \left(\frac{\sqrt{2N^{-1}}}{\Gamma B}\right)^{\frac{1}{2}} \left[1 - \frac{(2N^{-1})^{\frac{1}{4}}}{4} \left(\frac{\Gamma}{B}\right)^{\frac{1}{2}} + \mathcal{O}\left(N^{-\frac{3}{4}} \left\{\frac{\Gamma}{B}\right\}^{\frac{3}{4}}\right)\right], \tag{2.22}$$

and thus

$$\sigma^2(t_c) \simeq 2N^{-1} \left[1 - (2N^{-1})^{1/4} \sqrt{\frac{\Gamma}{B}}\right] \tag{2.23}$$

we predict that $\sigma^2(t_c)$ grows during the crossover from $\Gamma \ll \lambda$ to $\Gamma > \lambda$, until it saturates at a non-self-averaging value, $\sigma(t_c)/\overline{\mathcal{M}_{\rm L}}(t_c) \simeq 1$, independently on N^{-1} and B, with possibly a weak dependence on Γ and λ.

2.4 Numerical simulations

To illustrate our results, we present some numerical data. We based our simulations on the kicked rotator model with Hamiltonian [28]

$$H_0 = \frac{\hat{p}^2}{2} + K_0 \cos\hat{x} \sum_n \delta(t-n). \tag{2.24}$$

We concentrate on the regime $K > 7$, for which the dynamics is fully chaotic with a Lyapunov exponent $\lambda = \ln[K/2]$. We quantize this Hamiltonian on a torus, which requires considering discrete values $p_l = 2\pi l/N$ and $x_l = 2\pi l/N$, $l = 1, ...N$, hence N^{-1} is the effective Planck's constant. The fidelity Eq. (2.1) is computed for discrete times $t = n$, as

$$M(n) \;=\; |\langle\psi_0| \left(U^*_{\delta K}\right)^n (U_0)^n |\psi_0\rangle|^2 \tag{2.25}$$

using the unitary Floquet operators $U_0 = \exp[-i\hat{p}^2/2N^{-1}]\exp[-iK_0\cos\hat{x}/N^{-1}]$ and $U_{\delta K}$ having a perturbed Hamiltonian H with $K = K_0 + \delta K$. The quantization procedure results in a matrix form of the Floquet operators, whose matrix elements in $x-$representation are given by

$$(U_0)_{l,l'} = \frac{1}{\sqrt{N}} \exp\left[i\frac{\pi(l-l')^2}{N}\right] \exp\left[-i\frac{NK_0}{2\pi}\cos\frac{2\pi l'}{N}\right].$$

The local spectral density of eigenstates of $U_{\delta K}$ over those of U_0 has a Lorentzian shape with a width $\Gamma \propto (\delta K N)^2$ (there is a weak dependence of Γ in K_0) in the range $B = 2\pi \gtrsim \Gamma > \Delta = 2\pi/N$). This is illustrated in the inset to Fig. 2.6.

Numerically, the time-evolution of ψ_0 in the fidelity, Eq. (2.25), is calculated by recursive calls to a fast-Fourier transform routine. Thanks to this algorithm, the matrix-vector multiplication $U_{0,\delta K}\psi_0$ requires $O(N \ln N)$ operations instead of $O(N^2)$, and thus allows to deal with very large system sizes. Our data to be presented below correspond to system sizes of up to $N \leq 262144 = 2^{18}$ which allowed us to collect enough statistics for the calculation of $\sigma^2(\mathcal{M}_\mathrm{L})$.

We now present our numerical results. Fig. 2.3 shows the distribution $P(\mathcal{M}_\mathrm{L})$ of $\mathcal{M}_\mathrm{L}(t)$ in the regime $\Gamma < \lambda$ for different times. It is seen that even though $P(\mathcal{M}_\mathrm{L})$ is not normally distributed, it is still well characterized by its variance. A calculation of $\sigma^2(\mathcal{M}_\mathrm{L})$ is thus meaningful.

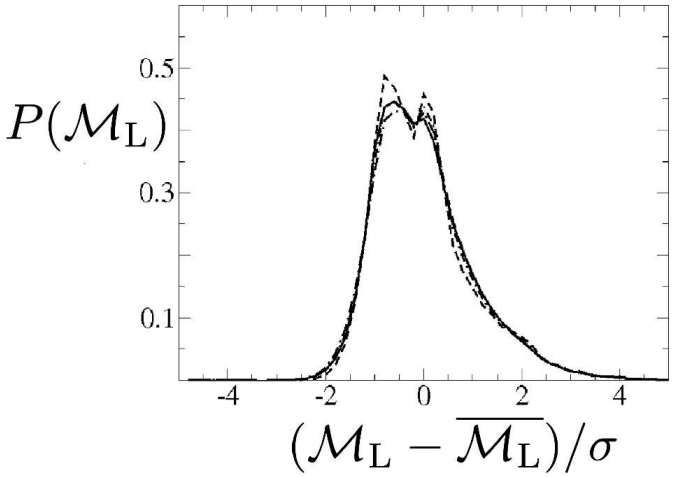

Figure 2.3: Distribution $P(\mathcal{M}_\mathrm{L})$ of the fidelity computed for 10^4 different ψ_0 for $N = 32768$, $\delta K = 5.75 \cdot 10^{-5}$ (i.e. $\Gamma \simeq 0.09$), at times $t = 25, 50, 75$ and 100 kicks.

We next focus on σ^2 in the golden rule regime with $\Gamma \ll \lambda$. Data are shown in Fig. 2.4. One sees that $\sigma^2(\mathcal{M}_{\rm L})$ first rises up to a time t_c, after which it decays. The maximal value $\sigma^2(t_c)$ in that regime increases with increasing perturbation, i.e. increasing Γ. Beyond t_c, the decay of σ^2 is very well captured by Eq. (2.17), once enough time has elapsed. This is due to the increase of $\sigma^2(t_c)$ above the self-averaging value $\propto N^{-1}$ as Γ increases. Once the influence of the peak disappears, the decay of $\sigma^2(\mathcal{M}_{\rm L})$ is very well captured by σ_3^2 given in Eq. (2.17), without any adjustable free parameter. Finally, at large times, $\sigma^2(\mathcal{M}_{\rm L})$ saturates at the value given in Eq. (2.18).

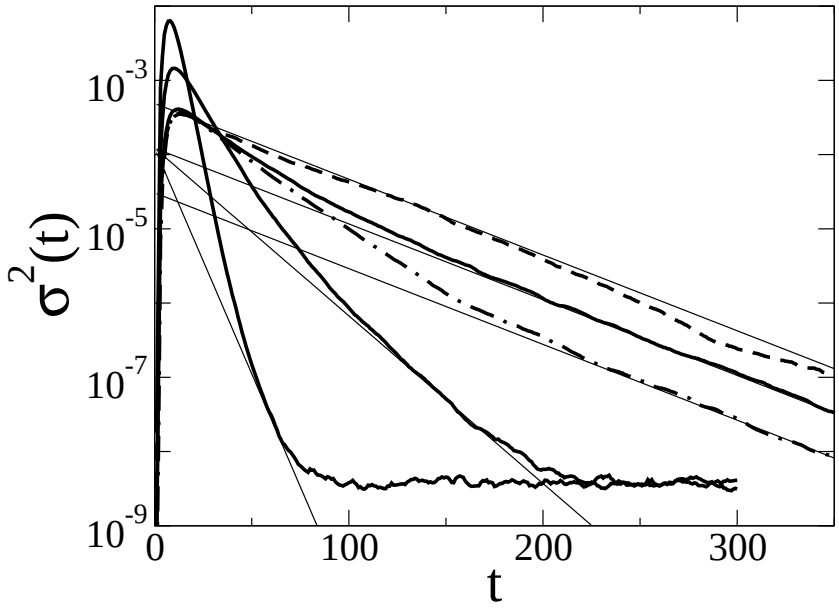

Figure 2.4: Variance $\sigma^2(\mathcal{M}_{\rm L})$ of the fidelity versus. t for weak $\Gamma \ll \lambda$, $N = 16384$ and $10^5 \cdot \delta K = 5.9$, 8.9 and 14.7 (thick solid lines), $N = 4096$ and $\delta K = 2.4 \cdot 10^{-4}$ (dashed line) and $N = 65536$ and $\delta K = 1.48 \cdot 10^{-5}$ (dotted-dashed line). All data have $K_0 = 9.95$. The thin solid lines indicate the decays $= 2N^{-1} \exp[-\Gamma t]$, with $\Gamma = 0.024(\delta K \cdot N)^2$ (there is no adjustable free parameter). The variance has been calculated from 10^3 different initial states ψ_0.

As δK increases, so does Γ and $\sigma^2(\mathcal{M}_{\rm L})$ decays faster and faster to its saturation value until $\Gamma \gtrsim \lambda$. Once Γ starts to exceed λ, the decay saturates at $\exp(-2\lambda t)$. This is shown in Fig. 2.5, which corroborates the Lyapunov decay of $\sigma^2(\mathcal{M}_{\rm L})$ predicted by Eqs. (2.9). Note that in Fig. 2.5, the decay exponent differs from the Lyapunov exponent $\lambda = \ln[K/2]$ due to the fact that the fidelity averages $\langle C_s \rangle \propto \langle \exp[-\lambda t] \rangle \neq \exp[-\langle \lambda \rangle t]$ over finite-time fluctuations of the Lyapunov exponent [19]. At long times, $\sigma^2(\mathcal{M}_{\rm L})$ saturates at the ergodic value $\sigma^2(\mathcal{M}_{\rm L}, t \to \infty) = N^{-2}$, as predicted. Finally, it is seen in both Figs. 2.4 and 2.5 that t_c decreases as the perturbation is cranked up. Moreover, there is no

N-dependence of $\sigma^2(t_c)$ at fixed Γ. These two facts are at least in qualitative, if not quantitative, agreement with Eq. (2.20). The behavior of $\sigma^2(t_c)$ as a function

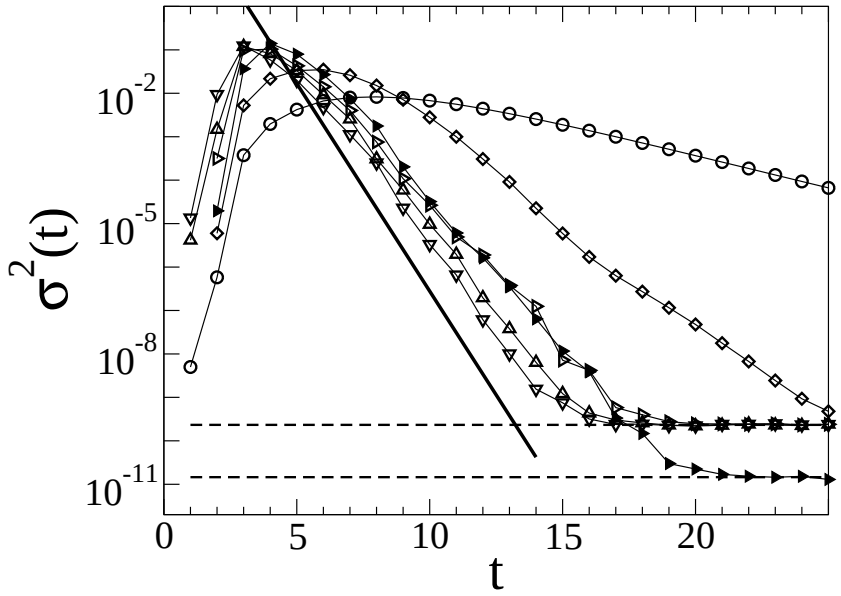

Figure 2.5: Variance $\sigma^2(\mathcal{M}_{\rm L})$ of the fidelity versus t in the lyapunav regime with $\Gamma \gtrsim \lambda$ for $N = 65536$, $K_0 = 9.95$ and $\delta K \in [3.9 \cdot 10^{-5}, 1.1 \cdot 10^{-3}]$ (open symbols), and $N = 262144$, $K_0 = 9.95$, $\delta K = 5.9 \cdot 10^{-5}$ (full triangles). The solid line is $\propto \exp[-2\lambda_1 t]$, with an exponent $\lambda_1 = 1.1$, smaller than the Lyapunov exponent $\lambda = 1.6$, because the fidelity averages $\langle \exp[-\lambda t] \rangle$ (see text). The two dashed lines give the long time saturation N^{-2}. In all cases, the variance has been calculated from 10^3 different initial states ψ_0.

of Γ is finally shown in Fig. 2.6. First we show in the inset the behavior of the local spectral density

$$\rho(\epsilon) \;=\; \sum_{\alpha} |\langle a|\alpha\rangle|^2 \delta(\epsilon - \epsilon_\alpha + \epsilon_a), \tag{2.26}$$

of eigenstates $\{|a\rangle\}$ (with quasienergy eigenvalues ϵ_a) of U_0 over the eigenstates $\{|\alpha\rangle\}$ (with quasienergy eigenvalues ϵ_α) of $U_{\delta K}$ (Latin (Greek) letter is reserved for the unperturbed (pertutrbed) dynamics). As mentioned above, $\rho(\epsilon)$ has a Lorentzian shape with a width given by $\Gamma \simeq 0.024(\delta K \cdot N)^2$. Having extracted the $N-$ and $\delta K-$dependence of Γ, we next plot in the main part of Fig. 2.6 the maximum $\sigma^2(t_c)$ of the fidelity variance as a function of the rescaled width Γ/B of $\rho(\epsilon)$. As anticipated, $\sigma^2(t_c)$ first increases with Γ until it saturates at a value $\gtrsim 0.1$, independently on N^{-1}, Γ or λ, once $\Gamma \simeq B$. These data confirm Eq. (2.21) and the accompanying reasoning. Note that once Γ exceeds the bandwidth B, $\rho(\epsilon)$ is no longer Lorentzian, and the decay of both $\mathcal{M}_{\rm L}(t)$ and $\sigma^2(\mathcal{M}_{\rm L})$ is no longer exponential [6].

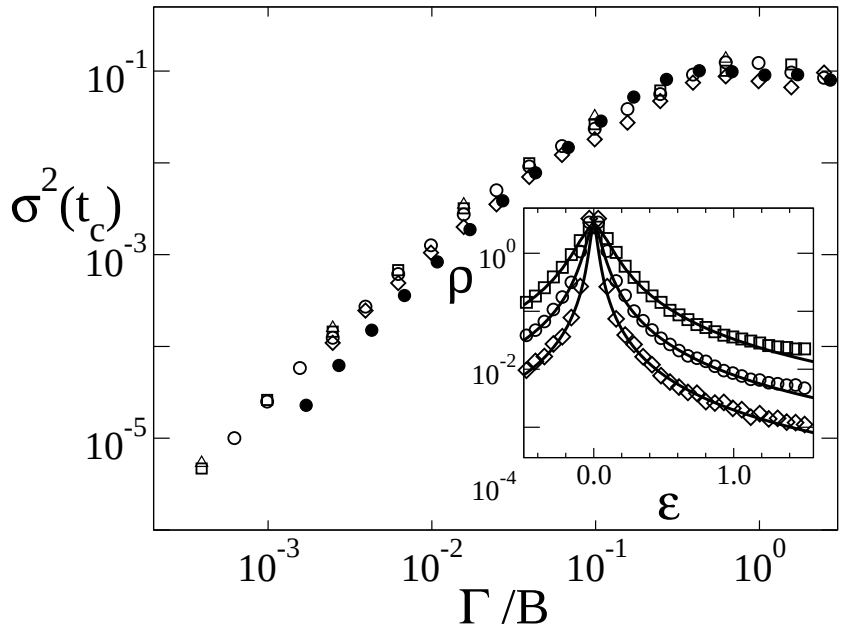

Figure 2.6: Maximal variance $\sigma^2(t_c)$ as a function of Γ/B, for $K_0 = 10.45$, $N = 4096$, 16384, 65536 and 262144 (empty symbols) and $K_0 = 50.45$, $N = 16384$ (full circles). The variance has been calculated from 10^3 different initial states ψ_0. Inset: local spectral density of states $\rho(\epsilon)$ of eigenstates of an unperturbed kicked rotator with $K_0 = 12.56$ over the eigenstates of a perturbed kicked rotator with $K = K_0 + \delta K$, $\delta K = 5 \cdot 10^{-3}$. System sizes are $N = 250$ (diamonds), $N = 500$ (circles) and $N = 1000$ (squares). The solid lines are Lorentzian with widths $\Gamma \simeq 0.0125$, 0.05 and 0.0124 in agreement with the formula $\Gamma = 0.024\ (\delta K \cdot N)^2$.

2.5 Conclusions

In conclusion we have applied both a semiclassical and a RMT approach to calculate the time-dependent variance $\sigma^2(\mathcal{M}_\mathrm{L})$ of the fidelity $\mathcal{M}_\mathrm{L}(t)$ of Eq. (2.1). We found that $\sigma^2(\mathcal{M}_\mathrm{L})$ exhibits a nonmonotonous behavior with time, first rises algebraically up to a critical time t_c, before decaying exponentially at larger times. To leading order in the effective Planck's constant N^{-1}, this decay is given by the sum of a classical term $\simeq \exp[-2\lambda t]$, a quantum term $\simeq 2N^{-1}\exp[-\Gamma t]$ and a mixed term $\simeq 2\exp[-(\Gamma+\lambda)t]$. Compared to the behavior of the average fidelity, this allows for the extraction of the classical Lyapunov exponent λ in a larger parameter range. Finally the maximum value of $\sigma^2(\mathcal{M}_\mathrm{L})$ is characterized by a non-self-averaging behavior when the perturbation becomes sizable against the system's Lyapunov exponent.

2.6 Appendix A: Tutorial on diagrams

The schematic description used in this chapter has the advantage of facilitating the reading and the determination of the semiclassical contribution involved in the variance. All dominant and subdominant contributions obtained are built with the help of the six fundamentals diagrams listed in Fig. 2.7.

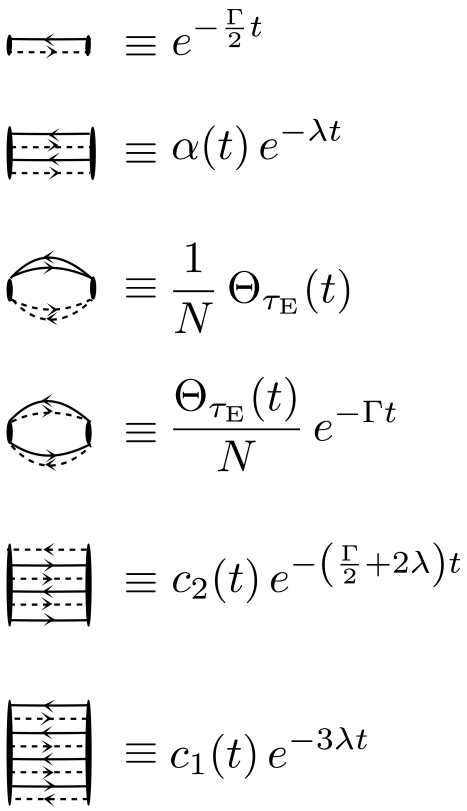

Figure 2.7: The fundamental semiclassical diagrams .

The rule to construct more sophisticated diagrams is very simple, we can form any combination of theses fundamental diagrams, the only requirement is to preserve the symmetry between forward and backward propagation path and fix the total number of path to eight for the variance. We note here that the semiclassical averaged Loschmidt echo can be obtained in the same way if we fix the total number of paths to four, like in Fig. 2.8. The analytical evaluation of the composite diagrams is straightforward, it is given by the product of the analytical value of the fundamental diagram components involved.

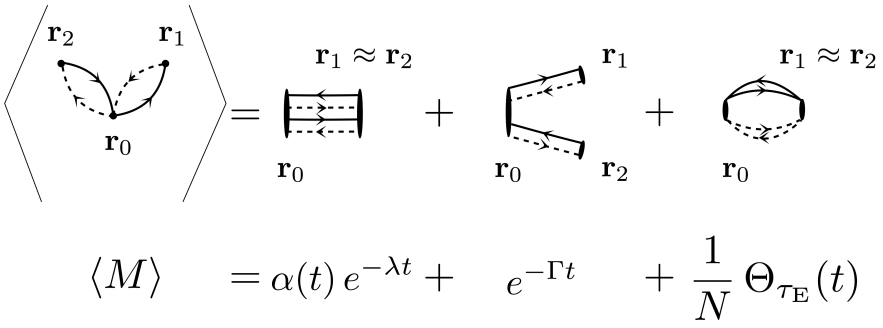

Figure 2.8: Diagrammatic representation of the averaged $\langle \mathcal{M}_{\rm L} \rangle$ fidelity, and the two time-dependent contributions (Lyapunov term $\alpha(t)e^{-\lambda t}$and Fermi Golden rule term $e^{-\Gamma t}$), together with the contribution giving the long-time saturation of $\langle \mathcal{M}_{\rm L} \rangle$.

2.7 Appendix B : Lyapunov prefactor α

The exact formal expression of the Lyapunov prefactor $\alpha(t)$ depends on the force correlator like,

$$\alpha(t) = \left(\frac{\lambda \nu^2 m^2}{t^2 \epsilon^2 \int_0^t d\tau \, \langle \nabla V(0) \nabla V(\tau) \rangle} \right)^{\frac{d}{2}}. \tag{2.27}$$

Setting the Lyapunov time equal to a few times the time of flight through a correlation length of the perturbation potential, as is the case for billiards or maps, we can express the force correlator as a function of the perturbation correlator, this yields,

$$\epsilon^2 \int d\tau \, \langle \nabla V[\mathbf{q}(0)] \nabla V[\mathbf{q}(\tau)] \rangle \;\; \propto \;\; \frac{\Gamma}{\left(V_F \lambda^{-1}\right)^2}.$$

Consequently the prefactor $\alpha(t)$, after the use of the Heisenberg uncertainty relation $\nu p_F = 2\pi N^{-1}$, becomes,

$$\alpha(t) \propto \left(\frac{\lambda \Gamma}{t^2} \right)^{\frac{d}{2}} = \alpha_0 t^{-d}, \tag{2.28}$$

We note that the presence of the divergence at short time is essential. It is related to the assymptotic form of the C_s that delivers the correct short time behavior of the quantum propagator $\lim_{t \mapsto 0} K(\mathbf{r}_0, \mathbf{r}, t) = \delta(\mathbf{r}_0 - \mathbf{r})$. Although the divergence of the prefactor is not a real problem in the semiclassical regime, we

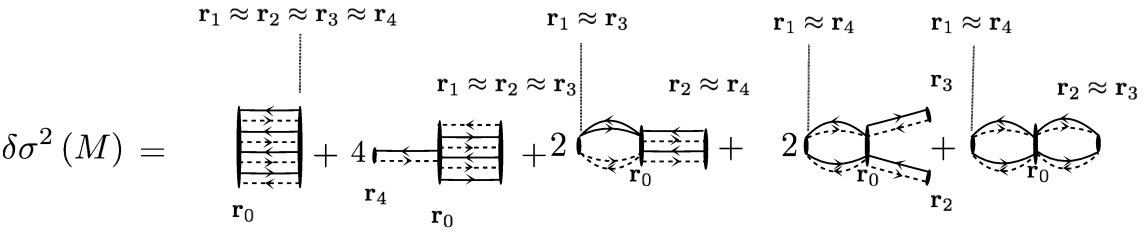

$$\delta\sigma^2(M) = c_1(t)e^{-3\lambda t} + 4c_2(t)e^{-(\Gamma+2\lambda)t} + \frac{2\alpha(t)}{N}e^{-\lambda t} + \frac{2\Theta_{\tau_E}(t)}{N}e^{-2\Gamma t} + \frac{\Theta_{\tau_E}(t)}{N^2}e^{-2\Gamma t}$$

Figure 2.9: Diagrammatic representation of the subdominants contribution of the averaged fidelity variance $\sigma^2(\mathcal{M}_L)$. (For a quick tutorial on diagrams see Appendix B.)

will determine a cutoff time. Since the Lyapunov contribution results of a stationary approximation, this approximation is valid only if we accumulated enough phase, typically the inequality $\langle \delta\Phi_{s_1}^2 \rangle \geq 1$ must be fulfilled. If we substitute $\delta^2\mathbf{r}(t) = \exp[2\lambda t]\nu^2$ in the residual action $\delta\Phi_{s_1}^2$, we can define the minimum time after which we can get the Lyapunov regime as,

$$\tau_\lambda = \frac{1}{\lambda}\ln\left[\frac{\lambda}{\nu G}\right]. \tag{2.29}$$

where $G = \int_0^t d\tau \langle \nabla V(0)\nabla V(\tau)\rangle$ is the average value of the force correlator.

2.8 Appendix C : Subdominant semiclassical contributions

For the sake of completeness we present here the five main subdominant semiclassical contributions to the averaged fidelity variance. These terms are obtained by additional path contractions and/ or require a supplementary ergodic assumption. As more restriction must be fulfilled this terms can be firstly neglected in almost investigation. These contributions denoted $\delta\sigma^2$ in the Fig. 2.2 are depicted on the right-hand side of Fig. 2.9.

2.8.1 Full contraction contribution.

The first diagram on Fig. 2.9 corresponds to a full contraction of all paths, $s_1 = l_1 \simeq s_2 = l_2 \simeq s_3 = l_3 \simeq s_4 = l_4$ which requires $\mathbf{r}_1 \simeq \mathbf{r}_2 \simeq \mathbf{r}_3 \simeq \mathbf{r}_4$.This gives a contribution,

$$\delta\sigma_1^2 = \left(\frac{\nu^2}{\pi}\right)^{2d}\left\langle \int d\mathbf{r}_1 d\mathbf{r}_2 d\mathbf{r}_3 d\mathbf{r}_4 \sum C_{s_1}^4 \prod_{j=2}^{4}\delta_\nu(\mathbf{r}_1 - \mathbf{r}_j)\exp[-4\nu^2\delta\mathbf{p}_{s_1}^2 + i\delta\Lambda_{s_1}]\right\rangle, \tag{2.30}$$

where

$$\delta\Lambda_s = \int_0^t \mathrm{d}t' \epsilon \nabla V\left[\mathbf{q}(t')\right] \left\{\left[\mathbf{q}_s(t') - \mathbf{q}_l(t')\right] + \left[\mathbf{q}_s(t') - \mathbf{q}_{l'}(t')\right] - \left[\mathbf{q}_s(t') - \mathbf{q}_{l''}(t')\right]\right\} \tag{2.31}$$

is the extra phase arissing from the linearization of the perturbation V on $s = s_1, l_1 \simeq l = s_2, l_2 \simeq l' = s_3, l_3 \simeq l'' = s_4, l_4$, and $\mathbf{q}_{s_1}(t')$ lies on s_1 with $\mathbf{q}_{s_1}(0) = \mathbf{r}_0$ and $\mathbf{q}_{s_1}(t) = \mathbf{r}_1$. In Eq. (2.30) the integrations are restricted by $|\mathbf{r}_1 - \mathbf{r}_{2,3,4}| \leq \nu$. Then we apply the CLT, and note that cross terms can be neglected

$$\langle \exp[i\delta\Lambda_{s_1}] \rangle = \exp^{-\frac{1}{2}\langle \delta^2 \Lambda_{s_1} \rangle} \simeq \exp\left[-\frac{\epsilon^2}{2\lambda} \int d\tau \, \langle \nabla V(0) \nabla V(\tau) \rangle \left(\sum_{j=2}^{4} |\mathbf{r}_1 - \mathbf{r}_j|^2 \right) \right].$$

After performing a change of integration variable $\int d\mathbf{r} \sum_s C_s = \int d\mathbf{p}$ and replacing the remaining C_s by their asymptotic expression one gets,

$$\delta\sigma_1^2 \;\; = \;\; c_1(t) e^{-3\lambda t}, \tag{2.32}$$

with $c_1(t) = 2^{\frac{d}{2}} \alpha^3(t)$.

2.8.2 Triple contractions contributions

Now we consider a triple contraction of pairs of paths. Theses kind of terms are depicted by the second diagram on Fig. 2.9. The contraction $s_1 = l_1 \simeq s_2 = l_2 \simeq s_3 = l_3$ and $s_4 = l_4$ which requires $\mathbf{r}_1 \simeq \mathbf{r}_2 \simeq \mathbf{r}_3$ is one of these triple contractions. Since we have a freedom in choosing the non contracted pair of path, this diagram comes with a multiplicity of four. This gives a contribution,

$$\begin{aligned} \delta\sigma_2^2 \;\; &= \;\; 4 \left(\frac{\nu^2}{\pi} \right)^{2d} \left\langle \int d\mathbf{r}_1 d\mathbf{r}_2 d\mathbf{r}_3 \sum C_{s_1}^3 \prod_{j=2}^{3} \delta_\nu(\mathbf{r}_1 - \mathbf{r}_j) \exp[-3\nu^2 \delta\mathbf{p}_{s_1}^2 + i\delta\Xi_{s_1}] \right\rangle \\ &\quad \times \left\langle \int d\mathbf{r}_4 \sum C_{s_4} \exp[-\nu^2 \delta\mathbf{p}_{s_4}^2 + i\delta S_{s_4}] \right\rangle, \end{aligned} \tag{2.33}$$

where $\delta\Xi_{s_1}$ is the extra phase given by the linearization of the perturbation V on $s = s_1, l_1 \simeq l = s_2, l_2 \simeq l' = s_3, l_3$,

$$\delta\Xi_s = \int_0^t \mathrm{d}t' \, \epsilon V\left[\mathbf{q}_s(t')\right] + \epsilon \nabla V\left[\mathbf{q}_s(t')\right] \left\{\left[\mathbf{q}_s(t') - \mathbf{q}_l(t')\right] + \left[\mathbf{q}_s(t') - \mathbf{q}_{l'}(t')\right]\right\}, \tag{2.34}$$

$\mathbf{q}_{s_1}(t')$ lies again on s_1 with $\mathbf{q}_{s_1}(0) = \mathbf{r}_0$ and $\mathbf{q}_{s_1}(t) = \mathbf{r}_1$. In Eq. (2.30) the integration are restricted by $|\mathbf{r}_1 - \mathbf{r}_{2,3}| \leq \nu$. Then we apply the CLT and note that cross terms can again be neglected,

$$\begin{aligned} \left\langle e^{i\delta\Xi_{s_1}} \right\rangle = e^{-\frac{1}{2}\left\langle \delta\Xi_{s_1}^2 \right\rangle} \;\; &\simeq \;\; \exp\left[-\frac{\left\langle \delta S_{s_1}^2 \right\rangle}{2} - \frac{\epsilon^2}{2\lambda} \int d\tau \, \langle \nabla V(0) \nabla V(\tau) \rangle \left(\sum_{j=2}^{3} |\mathbf{r}_1 - \mathbf{r}_j|^2 \right) \right. \\ &\left. - \frac{\epsilon^2}{\lambda} \int d\tau \, \langle V(0) \nabla V(\tau) \rangle \cdot \left(\sum_{j=2}^{3} (\mathbf{r}_1 - \mathbf{r}_j) \right) \right]. \end{aligned}$$

After the change of variable and the replacement of C_s by their asymptotic expressions, one finally obtains

$$\delta\sigma_2^2 \;=\; 4c_2(t)\, e^{-(2\lambda+\Gamma)t}, \tag{2.35}$$

with $c_2(t) = c_2\alpha^2(t)$,

$$c_2 = \left(\frac{4}{3}\right)^{\frac{d}{2}} \exp\left[d\frac{\epsilon^2}{\lambda}\frac{\left(\int d\tau |\,\langle V(0)\nabla V(\tau)\rangle\,|\right)^2}{\int d\tau\,\langle \nabla V(0)\nabla V(\tau)\rangle}\right],$$

which reduces to, $c_2 = \left(\frac{4}{3}\right)^{\frac{d}{2}} \exp\left[\frac{d}{2}\frac{\Gamma}{\lambda}\right]$ under the same assumption as in appendix 2.7.

2.8.3 Subdominant classical contribution

The third diagram depicted on Fig. 2.9 is related to the quantum contribution σ_3. Only one additional contraction is added. However this last one kills the quantum part of the diagrams and replaces it by a Lyapunov contribution. This term is obtained form $s_1 = s_3$, $l_1 = l_3$, $s_2 = l_2 \simeq s_4 = l_4$ or equivalently $s_1 = l_1 \simeq s_3 = l_3$, $l_2 = l_4$ and $s_2 = s_4$, both set of contractions require $\mathbf{r}_1 \simeq \mathbf{r}_3$ and $\mathbf{r}_2 \simeq \mathbf{r}_4$. This gives the contributions,

$$\begin{aligned}\delta\sigma_3^2 \;=\; & 2\left(\frac{\nu^2}{\pi}\right)^{2d}\left\langle \int d\mathbf{r}_1 d\mathbf{r}_3 \sum C_{s_1}C_{l_1}\exp[-\nu^2(\delta\mathbf{p}_{s_1}^2+\delta\mathbf{p}_{l_1}^2)]\delta_\nu(|\mathbf{r}_1-\mathbf{r}_3|)\right\rangle \\ & \times\left\langle \int d\mathbf{r}_2 d\mathbf{r}_4 \sum C_{s_4}^2\exp[-\nu^2\delta\mathbf{p}_{s_4}^2 + i\delta\Phi_{s_4}]\delta_\nu(|\mathbf{r}_2-\mathbf{r}_4|)\right\rangle,\end{aligned} \tag{2.36}$$

We recognize that Eq. (2.36) is the product of the long time saturation contribution and the Lyapunov contribution of the averaged Loschmidt echo thus,

$$\delta\sigma_3^2 \;=\; \frac{2\alpha(t)}{N}e^{-\lambda t}\,\Theta_{\tau_{\mathrm{E}}}(t) \tag{2.37}$$

Since only one λ is present in the exponent, this term seems to be dominant compared to $\sigma_1^2 = \alpha^2(t)\exp[-2\lambda t]$. However this interpretation is incorrect, indeed $\delta\sigma_3^2$ supersedes σ_1^2 only after the Ehrenfest time (this is enforced by the presence of the Heaviside function) and after the Ehrenfest time $\delta\sigma_3^2$ reduced to the saturation value and thus has no influence on the variance.

2.8.4 Subdominant quantum contributions

The two last diagrams correspond to a purely subdominant quantum contribution. Theses contributions are obtained equivalently by the RMT calculus (see appendix 2.9).

The former corresponds to a cross contraction of one unperturbed (perturbed) path of the set (s_1, l_1, s_2, l_2) with one perturbed (unperturbed) path of the set (s_3, l_3, s_4, l_4). These correspond to the contraction $s_1 = l_4$, $l_1 = s_4$, $s_2 = l_2$ and $s_3 = l_3$ with $\mathbf{r}_1 \simeq \mathbf{r}_4$ or $s_1 = l_1$, $s_2 = l_3$, $l_2 = s_3$ and $s_4 = l_4$ with $\mathbf{r}_2 \simeq \mathbf{r}_3$. We get,

$$\begin{aligned} \delta\sigma_4^2 &= 2\left(\frac{\nu^2}{\pi}\right)^{2d}\left\langle \int d\mathbf{r}_2 \sum C_{s_2} \exp[-\nu^2\delta\mathbf{p}_{s_2}^2 + i\delta S_{s_2}]\right\rangle^2 \\ &\times \left\langle \int d\mathbf{r}_1 d\mathbf{r}_4 \sum C_{s_1}^2 \exp\left[-\nu^2\delta\mathbf{p}_{s_1}^2 + i\left(\delta S_{s_1} + \delta S_{s_4}\right)\right] \delta_\nu(|\mathbf{r}_1 - \mathbf{r}_4|)\right\rangle, \end{aligned} \tag{2.38}$$

We recognized the first integral as the FGR contribution and the second integral has to be performed with the restriction $|\mathbf{r}_1 - \mathbf{r}_4| \leq \nu$, with the use of the ergodic assumption

$$\left\langle \int d\mathbf{r}_1 d\mathbf{r}_4 \cdots \delta_\nu(|\mathbf{r}_1 - \mathbf{r}_4|)\right\rangle = \frac{1}{N}\left\langle \int d\mathbf{r}_1 d\mathbf{r}_4 \cdots \right\rangle.$$

We finally get,

$$\delta\sigma_4^2 = \frac{2}{N} e^{-2\Gamma t}\,\Theta_{\tau_{\rm E}}(t) \tag{2.39}$$

The last diagram corresponds to the full cross contraction between perturbed and unperturbed paths taken in the sets (s_1, l_1, s_2, l_2) (s_3, l_3, s_4, l_4). We have only one possibility namely $s_1 = l_4$, $l_1 = s_4$, $s_2 = l_3$ and $l_2 = s_3$, we have thus

$$\delta\sigma_5^2 = \left(\frac{\nu^2}{\pi}\right)^{2d}\left\langle \int d\mathbf{r}_1 d\mathbf{r}_4 \sum C_{s_1}^2 \exp[-\nu^2\delta\mathbf{p}_{s_1}^2 + i\left(\delta S_{s_1} + \delta S_{s_4}\right)]\delta_\nu(|\mathbf{r}_1 - \mathbf{r}_4|)\right\rangle^2 \tag{2.40}$$

which leads to,

$$\delta\sigma_5^2 = \frac{1}{N^2} e^{-2\Gamma t}\,\Theta_{\tau_{\rm E}}(t) \tag{2.41}$$

2.8.5 Summary of subdominant contributions

The semiclassical subdominant contributions are given by the sum of five terms of the Eqs. (2.32, 2.35, 2.37, 2.39) and (2.41)

$$\delta\sigma^2 = c_1(t)e^{-3\lambda t} + 4c_2 e^{-(\Gamma+2\lambda)t} + \frac{2\alpha(t)}{N}e^{-\lambda t} + \frac{2}{N}e^{-2\Gamma t}\,\Theta_{\tau_{\rm E}}(t) + \frac{1}{N^2}e^{-2\Gamma t}\,\Theta_{\tau_{\rm E}}(t) \tag{2.42}$$

2.9 Appendix D : Random matrix derivation

Here we present the random matrix derivation of the fluctuation of the Loschmidt echo. At first we denote the set of eigenstates of the unperturbed hamiltonian

H_0 by $\{|a\rangle\}$ (with the quasienergy eigenvalues ϵ_a) and the eigenstates of the perturbed hamiltonian H by $\{|\alpha\rangle\}$ (with quasienergy eigenvalues ϵ_α). Latin (Greek) letters are thus reserved for the unperturbed (perturbed) dynamics. We note that under the sole assumption that the two hamiltonians are classically chaotic, RMT assume that both sets of eigenstates are rotationally invariant [27]

In the traditional RMT treatement [7, 29], the derivation is based on a expansion of the initial state $|\psi_0\rangle$ over either the eigenbasis of the unperturbed hamiltonian or over the eigenbasis of the perturbed hamiltonian. Here we use an mixed basis, this will permit us to clearly illustrate the equivalence between the random matrix and the semiclassical derivations.

We thus let ,

$$|\psi_0\rangle\langle\psi_0| = \sum_{\alpha,a} \eta_{\alpha a}\, |a\rangle\langle\alpha| \tag{2.43}$$

Since we will perform an ensemble average, we recall that RMT implies that the averages are independent of the initial state ψ_0. Consequently we note the averaging rules verified by the complex number $\eta_{\alpha_i a_i}$ according to a broken time symmetry (GUE ensemble).

$$\overline{\eta_{\alpha_1 a_1}} = N^{-1}\,\delta_{\alpha_1 a_1} \tag{2.44a}$$

$$\overline{\eta_{\alpha_1 a_1}\eta^*_{\alpha_2 a_2}} = N^{-2}\,(\delta_{\alpha_1 a_1}\,\delta_{\alpha_2 a_2} + \delta_{\alpha_1 \alpha_2}\,\delta_{a_1 a_2}) \tag{2.44b}$$

$$\overline{\eta_{\alpha_1 a_1}\eta^*_{\alpha_2 a_2}\eta_{\alpha_3 a_3}\eta^*_{\alpha_4 a_4}} = N^{-4}\left(\sum_{i\neq j\neq k\neq l} \delta_{M_{1i}}\,\delta_{M_{2j}}\,\delta_{M_{3k}}\,\delta_{M_{4l}}\right), \tag{2.44c}$$

where δ is the Kronecker delta and for the last line,

$$M = \begin{pmatrix} \alpha_1 \\ a_2 \\ \alpha_3 \\ a_4 \end{pmatrix} \cdot \begin{pmatrix} a_1 & \alpha_2 & a_3 & \alpha_4 \end{pmatrix} = \begin{pmatrix} \alpha_1 a_1 & \alpha_1\alpha_2 & \alpha_1 a_3 & \alpha_1\alpha_4 \\ a_1 a_2 & \alpha_2 a_2 & a_2 a_3 & \alpha_4 a_2 \\ \alpha_3 a_1 & \alpha_2\alpha_3 & \alpha_3 a_3 & \alpha_3\alpha_4 \\ a_1 a_4 & \alpha_2 a_4 & a_3 a_4 & \alpha_4 a_4 \end{pmatrix}$$

is the 4×4 matrix of all permitted indices contractions.

Now we note that the averaged squared fidelity is given by,

$$\begin{aligned} \overline{\mathcal{M}^2_{\mathrm{L}}}(t) = & \sum_{\{\alpha\},\{\beta\},\{a\},\{b\}} \overline{\eta_{\alpha_1 a_1}\eta^*_{\alpha_2 a_2}\exp\left[-i\sum_{j=1}^{4}(-1)^j \Delta_{\beta_j b_j}\right]} \\ & \times \overline{\prod_{i=1}^{2}\langle\alpha_{2i-1}|\beta_{2i-1}\rangle\langle\beta_{2i-1}|b_{2i-1}\rangle\langle b_{2i-1}|\alpha_{2i-1}\rangle\,\langle\alpha_{2i}|\beta_{2i}\rangle\langle\beta_{2i}|b_{2i}\rangle\langle b_{2i}|\alpha_{2i}\rangle}, \end{aligned} \tag{2.45}$$

where we let $\Delta_{\beta_j b_j} = E_{\beta_j} - E_{b_j}$. According to Eq. (2.44c), we can perform 24 contractions, as we are interested in the variance $\sigma^2(\mathcal{M}_{\mathrm{L}})$ we must subtract the four terms contained in $\overline{\mathcal{M}_{\mathrm{L}}}^2$ corresponding to independent contractions in each

of the two subsets (α_1, a_1, α_2, a_2) and (α_3, a_3, α_4, a_4). We thus end with 20 contractions, that split into 6 kinds of contributions. Consequently the variance can be rewritten as,

$$\begin{aligned}
\sigma^2_{\rm RMT}(t) &= \sum_{\{\alpha\},\{\beta\},\{a\},\{b\}} \overline{\exp\left[-i\sum_{j=1}^{4}(-1)^j\Delta_{\beta_j b_j}\right]} \\
&\times \Big(2\,\delta\alpha_1\alpha_4\,\delta a_1 a_4\,\delta\alpha_2 a_2\,\delta\alpha_3 a_3 \;+\; \delta\alpha_1\alpha_4\,\delta\alpha_2\alpha_3\,\delta a_1 a_4\,\delta a_2 a_3 \\
&\quad + 8\,\delta\alpha_1 a_3\,\delta\alpha_2\alpha_3\,\delta a_1 a_2\,\delta\alpha_4 a_4 + 6\,\delta\alpha_1 a_3\,\delta\alpha_2 a_4\delta a_1 a_2\delta\alpha_3\alpha_4 \\
&\quad + 2\,\delta\alpha_1 a_1\,\delta\alpha_2 a_4\,\delta\alpha_3 a_3\,\delta\alpha_4 a_2 \;+\; \delta_{\alpha_1 a_3}\,\delta_{\alpha_2 a_4}\,\delta_{\alpha_3 a_1}\,\delta_{\alpha_4 a_2}\Big) \\
&\times \overline{\prod_{i=1}^{2}\langle\alpha_{2i-1}|\beta_{2i-1}\rangle\langle\beta_{2i-1}|b_{2i-1}\rangle\langle b_{2i-1}|\alpha_{2i-1}\rangle\,\langle\alpha_{2i}|\beta_{2i}\rangle\langle\beta_{2i}|b_{2i}\rangle\langle b_{2i}|\alpha_{2i}\rangle},
\end{aligned} \tag{2.46}$$

Using that at large perturbation strength, $|\langle\alpha|a\rangle|^2$ becomes Lorentzian,

$$|\langle\alpha|a\rangle|^2 = \frac{\Gamma/2\pi}{(E_\alpha - E_a)^2 + \Gamma^2/4}, \tag{2.47}$$

with a width $\Gamma \simeq \overline{|\langle\alpha_0|\Sigma|\beta\rangle|^2}/\Delta$ given by the golden rule. This leads to

$$\sigma^2_{\rm RMT} = \frac{2}{N}e^{-\Gamma t} + \frac{1}{N^2} + \frac{8}{N^2}e^{-\Gamma t} + \frac{6}{N^3} + \frac{2}{N}e^{-2\Gamma t} + \frac{1}{N^2}e^{-2\Gamma t} \tag{2.48}$$

This establishes a one to one correspondence between the semiclassical treatment and the RMT one in the limit of a zero Ehrenfest time. Indeed we identified the first term of Eq. (2.48) as the quantum contribution, the second as the saturation. All The other terms correspond to the main subdominant contributions. The two last terms correspond exactly to the set of the subdominant quantum contributions. Finally the third term corresponds to the triple contraction contribution, the fourth gives the fully contracted contributions at their ergodic values, where we replaced $\exp[-\lambda t]$ by N^{-1}.

We emphasize that this perfect mapping is enforced by the exact correspondence between the RMT contraction and the semi-classical path contraction.

Bibliography

[1] F. Haake, *Quantum Signatures of Chaos* (Springer, Berlin, 2000).

[2] R. Schack and C.M. Caves, Phys. Rev. Lett. **71**, 525 (1993).

[3] A. Peres, Phys. Rev. A **30**, 1610 (1984).

[4] R.A. Jalabert and H.M. Pastawski, Phys. Rev. Lett. **86**, 2490 (2001).

[5] T. Gorin, T. Prosen, T.H. Seligman, M. Znidaric, Phys. Rep. **435**, 33 (2006).

[6] Ph. Jacquod, P.G. Silvestrov, and C.W.J. Beenakker, Phys. Rev. E **64**, 055203(R) (2001).

[7] T. Prosen, T.H. Seligman, and M. Znidaric, Prog. Theor. Phys. Supp. **150**, 200 (2003).

[8] N.R. Cerruti and S. Tomsovic, Phys. Rev. Lett. **88**, 054103 (2002).

[9] F.M. Cucchietti, C.H. Lewenkopf, E.R. Mucciolo, H.M. Pastawski, and R. O. Vallejos, Phys. Rev. E **65**, 046209 (2002).

[10] D.A. Wisniacki and D. Cohen, Phys. Rev. E **66**, 046209 (2002).

[11] Ph. Jacquod and D. L. Shepelyansky, Phys. Rev. Lett. **75**, 3501 (1995).

[12] J. Vanicek and E.J. Heller, Phys. Rev. E **68**, 056208 (2003).

[13] Y. Adamov, I.V. Gornyi, and A.D. Mirlin, Phys. Rev. E **67**, 056217 (2003).

[14] Ph. Jacquod, İ. Adagideli, and C.W.J. Beenakker, Europhys. Lett. **61**, 729 (2003).

[15] J. Emerson, Y.S. Weinstein, S. Lloyd, and D.G. Cory, Phys. Rev. Lett. **89**, 284102 (2002).

[16] Ph. Jacquod, İ. Adagideli, and C.W.J. Beenakker, Phys. Rev. Lett. **89**, 154103 (2002).

[17] A. Iomin, Phys. Rev. E **70**, 026206 (2004).

[18] W. Wang, G. Casati, and B. Li, Phys. Rev. E **69**, 025201(R) (2004).

[19] P.G. Silvestrov, J. Tworzydło, and C.W.J. Beenakker, Phys. Rev. E **67**, 025204(R) (2003).

[20] T. Gorin, T. Prosen, and T.H. Seligman, New J. Phys. **6**, 20 (2004).

[21] P. Cvitanović, R. Artuso, R. Mainieri, G. Tanner, and G. Vattay, *Chaos: Classical and Quantum*, `ChaosBook.org` (Niels Bohr Institute, Copenhagen 2003).

[22] See e.g.: E.J. Heller and S. Tomsovic, Phys. Today **46**(7), 38 (1993).

[23] J. Vaniček, Phys. Rev. E **70**, 055201(R) (2004).

[24] see e.g.: A.B. Katok and B. Hasselblatt, *Introduction to the Modern Theory of Dynamical Systems* (Cambridge University Press, 1996). In the context of the fidelity, this point was first mentioned in Ref. [12]. See Chapter 4 for more detail one the structural stability in the echo context and Ref. [23].

[25] P. Collet and J.-P. Eckmann, J. Stat. Phys. **115**, 217 (2004).

[26] G.P. Berman and G.M. Zaslavsky, Physica A **91**, 450 (1978); M.V. Berry and N.L. Balasz, J. Phys. A **12**, 625 (1979).

[27] M.L. Mehta, *Random Matrices* (Academic, New York, 1991).

[28] F. M. Izrailev, Phys. Rep. **196**, 299 (1990).

[29] Ph. Jacquod, I. Adagideli, C.W.J. Beenakker Phys.Rev.Lett. **89** , 154103 (2002).

CHAPTER 3

Echoes in interacting systems : The Boltzmann echo

3.1 From Loschmidt echo to Boltzmann echo

One of the central problems faced by the founders of statistical physics in the last decades of the nineteenth century was to reconcile the time-asymmetric evolution of macroscopic systems with time-symmetric microscopic dynamics [1]. They came up with a probabilistic solution to this *irreversibility paradox*. Macroscopic states, they argued, are superpositions of an enormous amount of microscopic states, the majority of them evolving in accordance with the second law of thermodynamics. The likelihood that a macroscopic state violates the second law of thermodynamics is thus minute, typically exponentially small in the number of atoms it contains. Irreversibility at the macroscopic level follows "by assuming a very improbable (i.e. with a very low entropy) initial state of the entire universe" [2, 3]. This mechanism works equally well in either quantum or classical systems.

Simple mechanisms of irreversibility already exist at the microscopic level in chaotic (in particular mixing) classical systems with few degrees of freedom. As a matter of fact, mixing ensures that, after a sufficiently long evolution time, two initially well separated phase-space distributions will evenly fill phase-space cells of any given size. Since phase-space points can never be located with infinite precision, irreversibility sets in after mixing has occurred on a scale smaller than the phase-space resolution scale. This mechanism cannot be carried over to quantum systems, however, mostly because the Schrödinger time-evolution is unitary, in either real- or momentum-space. Microscopic quantum systems are generically stable under time-reversal, even when their classical counterpart is

irreversible [4]. Peres instead suggested to investigate quantum irreversibility at the microscopic level through the fidelity

$$\mathcal{M}_{\mathrm{L}}(t) = \left|\langle\psi_0 \left|\exp[iHt]\exp[-iH_0t]\right|\psi_0\rangle\right|^2, \tag{3.1}$$

with which a quantum state ψ_0 can be reconstructed by inverting the dynamics after a time t with a perturbed Hamiltonian $H = H_0 + \Sigma$ [5]. Because of its connection with the gedanken time-reversal experiment proposed by Loschmidt in his argument against Boltzman's H-theorem [1], $\mathcal{M}_{\mathrm{L}}(t)$ has been dubbed the *Loschmidt Echo* by Jalabert and Pastawski [6].

Echo experiments abound in nuclear magnetic resonance [7, 8], optics [9], atomic [10], and condensed matter physics [11]. Fundamentally, they are all based on the same principle of a sequence of electromagnetic pulses whose purpose it is to reverse the sign of the Hamiltonian, $H_0 \to -H_0$, by means of effective changes of coordinate axes [7]. Imperfections in the pulse sequence result instead in $H_0 \to -H_0 - \Sigma$, and one therefore expects the Loschmidt Echo to capture the physics of the experiments. This line of reasoning however neglects the fact that the time-reversal operation affects at best only part of the system, for instance because the system is composed of so many degrees of freedom, that the time arrow can be inverted only for a fraction of them. This is generically the case, as any system is coupled to an external, uncontrolled environment. To capture the physics of echo experiments one thus has to take into account that,

(i) the system decomposes into two interacting subsystems 1 and 2;

(ii) the initial state of the controlled subsystem 1 is prepared, i.e. well defined, and its final state is measured and compared to the initial one;

(iii) both the initial and final states of the uncontrolled subsystem 2 are unknown;

(iv) the Hamiltonian of system 1 is time-reversed with some tunable accuracy, however both the Hamiltonian of system 2 and the interaction between the two subsystems are uncontrolled.

We therefore propose to investigate the physics of echo experiments by means of the following partial fidelity (we set $\hbar \equiv 1$)

$$\mathcal{M}_{\mathrm{B}}(t) = \Big\langle \big\langle\psi_1\big|\mathrm{Tr}_2\left[e^{-i\mathcal{H}_{\mathrm{b}}t}e^{-i\mathcal{H}_{\mathrm{f}}t}\eta_0 e^{i\mathcal{H}_{\mathrm{f}}t}e^{i\mathcal{H}_{\mathrm{b}}t}\right]\big|\psi_1\big\rangle\Big\rangle, \tag{3.2}$$

where the forward and backward (partially time-reversed) Hamiltonians read

$$\mathcal{H}_{\mathrm{f}} = H_1 \otimes \mathbb{I}_2 + \mathbb{I}_1 \otimes H_2 + \mathcal{U}_{\mathrm{f}}, \tag{3.3a}$$

$$\mathcal{H}_{\mathrm{b}} = -[H_1 + \Sigma_1] \otimes \mathbb{I}_2 + \mathbb{I}_1 \otimes [H_2 + \Sigma_2] + \mathcal{U}_{\mathrm{b}}. \tag{3.3b}$$

The experiment starts with an initial density matrix $\eta_0 = |\psi_1\rangle\langle\psi_1| \otimes \eta_{\mathrm{env}}$, which is propagated forward in time with $\mathcal{H}_{\mathrm{f}}$. After a time t, we invert the dynamics

of system 1. The imperfection in that time-reversal operation is modelled by Σ_1, while Σ_2 allows for system 2 to be affected by this operation (we will see below that tracing over the degrees of freedom of system 2 makes $\mathcal{M}_{\rm B}(t)$ independent of either H_2 or Σ_2). We leave open the possibility that the interaction between the two systems is affected by the time-reversal operation, i.e. $\mathcal{U}_{\rm f}$ may or may not be equal to $\mathcal{U}_{\rm b}$. Because one has no control over system 2, the corresponding degrees of freedom are traced out. For the same reason, the outmost brackets in Eq. (3.2) indicate an average over $\eta_{\rm env}$. We name $\mathcal{M}_{\rm B}(t)$ the *Boltzmann Echo* to stress its connection to Boltzmann's counterargument to Loschmidt that time cannot be inverted for all components of a system with many degrees of freedom.

3.2 Semiclassical approach

We now present our calculation, and define the regime of validity. We let Γ_{Σ_1} and $\Gamma_{\rm f,b}$ the classical correlators for Σ_1 and $\mathcal{U}_{\rm f,b}$ respectively (see below). Together with the one- and two-particle level spacings $\delta_{1,2}$ and bandwidths $B_{1,2}$, they define the range of validity of the semiclassical approach as $\delta_1 < \Gamma_{\Sigma_1} < B_1$, $\delta_2 < \Gamma_{\rm f,b} < B_2$ [12, 13]. Equivalently, they can be regarded as the golden rule width of the Lorentzian broadening of the levels of H_1 induced by Σ_1 and $\mathcal{U}_{\rm f,b}$ respectively [12].

As a starting point, we take chaotic one-particle Hamiltonians $H_{1,2}$, and a smooth interaction potential $\mathcal{U}$ which depends only on the distance between the particles. We assume that it is characterized by a typical classical length scale, which in particular is larger than the de Broglie wavelength ν of particle 1. For pedagogical reasons, we take narrow Gaussian wavepackets for the initial state of both particles, $\psi_i(\mathbf{q}) = \langle \mathbf{q}|\psi_i\rangle = (\pi\nu^2)^{-d_i/4}\exp[i\mathbf{p}_i\cdot(\mathbf{q}-\mathbf{r}_i) - |\mathbf{q}-\mathbf{r}_i|^2/2\nu^2]$. We note however that within our semiclassical approach, more general states can be taken for the environment, such as random pure states $\eta_{\rm env} = \sum_{\alpha\beta} a_\alpha a_\beta^* |\phi_\alpha\rangle\langle\phi_\beta|$, random mixtures $\eta_{\rm env} = \sum_\alpha |a_\alpha|^2 |\phi_\alpha\rangle\langle\phi_\alpha|$ or thermal mixtures $\eta_{\rm env} = \sum_n \exp\left[-\beta E_n\right] |n\rangle\langle n|$. Arbitrary initial states for both subsystems can be considered within the RMT approach.

From Eqs. (3.2) and (3.3) we can rewrite $\mathcal{M}_{\rm B}(t)$ as

$$\begin{aligned}\mathcal{M}_{\rm B}(t) \;=\; \int \mathrm{d}\mathbf{z}_2 \Bigg| \int \prod_{i=1}^{2} \mathrm{d}\mathbf{x}_i \prod_{j=1}^{3} \mathrm{d}\mathbf{q}_j \psi_1(\mathbf{q}_1)\psi_2(\mathbf{q}_2)\psi_1^\dagger(\mathbf{q}_3) \\ \times \left\langle \mathbf{q}_3, \mathbf{z}_2 \left| e^{-i\mathcal{H}_{\rm b}t} \right| \mathbf{x}_1, \mathbf{x}_2 \right\rangle \left\langle \mathbf{x}_1, \mathbf{x}_2 \left| e^{-i\mathcal{H}_{\rm f}t} \right| \mathbf{q}_1, \mathbf{q}_2 \right\rangle \Bigg|^2 . \end{aligned} \tag{3.4}$$

We next introduce the semiclassical propagators ($a = \mathrm{f}, \mathrm{b}$ labels forward or backward evolution; $\epsilon^{(f)} = -\epsilon^{(b)} = 1$),

$$\left\langle \mathbf{x}_1, \mathbf{x}_2 \left| e^{-i\mathcal{H}_a t} \right| \mathbf{q}_1, \mathbf{q}_2 \right\rangle \;=\; \sum_{s_1,\, s_2} \mathcal{C}^{1/2}_{s_1,s_2} e^{i\left\{\epsilon^{(a)} S^{(a)}_{s_1}(\mathbf{q}_1,\mathbf{x}_1;t) + S^{(a)}_{s_2}(\mathbf{q}_2,\mathbf{x}_2;t) + \mathcal{S}^{(a)}_{s_1,s_2}(\mathbf{q}_1,\mathbf{x}_1;\mathbf{q}_2,\mathbf{x}_2;t)\right\}}, \tag{3.5}$$

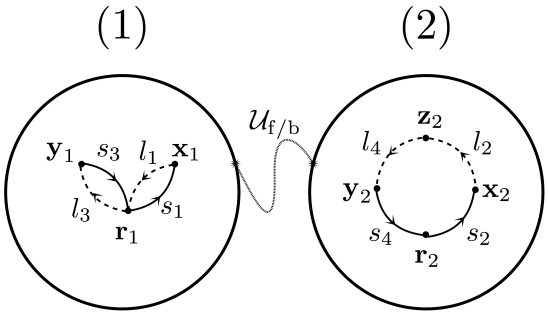

Figure 3.1: Schematic description of the Boltzmann echo $M_{\mathrm{B}}(t)$. Each system is characterized by a disk. Classical trajectories are represented by a full line if they correspond to an unperturbed propagation $H_{1,2}$ and a dashed line for an perturbed propagation $H_{1,2} + \Sigma_{1,2}$, with an arrow indicating the direction of propagation.

which are expressed as sums over pairs of classical trajectories, labeled s_i (l_i) for particle i connecting $\mathbf{q}_i$ to $\mathbf{x}_i$ in the time t with dynamics determined by H_i or $H_i + \Sigma_i$. Under our assumption of a classically weak coupling, classical trajectories are only determined by the one-particle Hamiltonians. Each pair of paths gives a contribution containing one-particle action integrals denoted by S_{s_i} (where we included the Maslov indices) and two-particle action integrals $\mathcal{S}^{(\mathrm{f,b})}_{s_1,s_2} = \int_0^t \mathrm{d}\tau \mathcal{U}_{\mathrm{f,b}}[\mathbf{q}_{s_1}(\tau), \mathbf{q}_{s_2}(\tau)]$ accumulated along s_1 and s_2 and the determinant $\mathcal{C}_{s_1,s_2} = C_{s_1} C_{s_2}$ of the stability matrix corresponding to the two-particle dynamics in the $(d_1 + d_2)-$dimensional space [15].

Our choice of initial Gaussian wave packets allows us to linearize the one-particle action integrals in $\mathbf{q}_j - \mathbf{r}_i$. We furthermore set $\mathcal{S}^{(a)}_{s_1,s_2}(\mathbf{q}_1, \mathbf{x}_1; \mathbf{q}_2, \mathbf{x}_2; t) \simeq \mathcal{S}^{(a)}_{s_1,s_2}(\mathbf{r}_1, \mathbf{x}_1; \mathbf{r}_2, \mathbf{x}_2; t)$, keeping in mind that $\mathbf{r}_1$ and $\mathbf{r}_2$, taken as arguments of the two-particle action integrals, have an uncertainty $\mathcal{O}(\nu)$. We then perform six Gaussian integrations to get

$$\begin{aligned} \mathcal{M}_{\mathrm{B}}(t) &= (4\pi\nu^2)^{\frac{2d_1+d_2}{2}} \int \prod_{i,j=1}^{2} \mathrm{d}\mathbf{x}_i \mathrm{d}\mathbf{y}_j \mathrm{d}\mathbf{z}_2 \\ &\times \sum_{\text{paths}} \mathcal{A}_{s_1} \mathcal{A}_{s_2} \mathcal{A}^{\dagger}_{s_3} \mathcal{A}^{\dagger}_{s_4} \mathcal{A}^{\dagger}_{l_1} \mathcal{A}_{l_3} C^{\frac{1}{2}}_{l_2} C^{\frac{1}{2}\dagger}_{l_4} e^{i\{\Phi_1+\Phi_2+\Phi_{12}\}}, \end{aligned} \tag{3.6}$$

where we wrote $\mathcal{A}_{s_i} = C^{\frac{1}{2}}_{s_i} \exp[-\frac{\nu^2}{2}(\mathbf{p}_{s_i} - \mathbf{p}_i)^2]$. Paths with odd (even) indices correspond to system 1 (2). A schematic representation of the semiclassical Boltzmann echo is given in Fig. 3.1.

The semiclassical expression for $\mathcal{M}_{\mathrm{B}}(t)$ is obtained by enforcing a stationary phase condition on Eq. (3.6), i.e. keeping only terms which minimize the variation

of the three action phases

$$\Phi_1 = S^{(\mathrm{f})}_{s_1}(\mathbf{r}_1,\mathbf{x}_1;t) - S^{(\mathrm{b})}_{l_1}(\mathbf{r}_1,\mathbf{x}_1;t) - S^{(\mathrm{f})}_{s_3}(\mathbf{r}_1,\mathbf{y}_1,t) + S^{(\mathrm{b})}_{l_3}(\mathbf{r}_1,\mathbf{y}_1;t), \quad (3.7a)$$

$$\Phi_2 = S^{(\mathrm{f})}_{s_2}(\mathbf{r}_2,\mathbf{x}_2;t) + S^{(\mathrm{b})}_{l_2}(\mathbf{x}_2,\mathbf{z}_2;t) - S^{(\mathrm{f})}_{s_4}(\mathbf{r}_2,\mathbf{y}_2;t) - S^{(\mathrm{b})}_{l_4}(\mathbf{y}_2,\mathbf{z}_2;t), \quad (3.7b)$$

$$\Phi_{12} = \mathcal{S}^{(\mathrm{f})}_{s_1,s_2} + \mathcal{S}^{(\mathrm{b})}_{l_1,l_2} - \mathcal{S}^{(\mathrm{f})}_{s_3,s_4} - \mathcal{S}^{(\mathrm{b})}_{l_3,l_4}. \quad (3.7c)$$

The semiclassically relevant terms are identified by path contractions. The first stationary phase approximation over Φ_1 corresponds to contracting unperturbed paths with perturbed ones, $s_1 \simeq l_1$ and $s_3 \simeq l_3$. This pairing is allowed by our assumption of a classically weak Σ_1 [16]. The phase Φ_1 is then given by the difference of action integrals of the perturbation Σ_1 on paths s_1 and s_3, $\Phi_1 = \delta S_{s_1}(\mathbf{r}_1,\mathbf{x}_1;t) - \delta S_{s_3}(\mathbf{r}_1,\mathbf{y}_1,t)$, with $\delta S_{s_i} = \int_0^t \mathrm{d}\tau \Sigma_1[\mathbf{q}_{s_i}(\tau)]$. Here, $\mathbf{q}_{s_i}(\tau)$ lies on s_i with $\mathbf{q}_{s_i}(0) = \mathbf{r}_1$ and $\mathbf{q}_{s_1}(t) = \mathbf{x}_1$, $\mathbf{q}_{s_3}(t) = \mathbf{y}_1$. A similar procedure for Φ_2 requires $s_2 \simeq s_4$ and $l_2 \simeq l_4$, and thus $\mathbf{x}_2 \simeq \mathbf{y}_2$. These contractions lead to an exact cancellation $\Phi_2 = 0$, and one gets

$$\begin{aligned}\mathcal{M}_{\mathrm{B}}(t) &= (4\pi\nu^2)^{\frac{2d_1+d_2}{2}} \int \prod_{i,j=1}^{2} \mathrm{d}\mathbf{x}_i \mathrm{d}\mathbf{y}_j \mathrm{d}\mathbf{z}_2 \; \delta_\nu(\mathbf{x}_2-\mathbf{y}_2) \\ &\times \sum |\mathcal{A}_{s_1}|^2 |\mathcal{A}_{s_2}|^2 |\mathcal{A}_{s_3}|^2 |C_{l_2}| e^{i\left[\delta S_{s_1} - \delta S_{s_3} + \Phi_{12}.\right]}. \end{aligned} \quad (3.8)$$

Here, $\delta_\nu(\mathbf{x}_2-\mathbf{y}_2)$ restricts the spatial integrations to $|\mathbf{x}_2-\mathbf{y}_2| \leq \nu$ because of the finite resolution with which two paths can be equated.

The semiclassical Boltzmann Echo (3.8) is dominated by two contributions. The first contribution is non diagonal in that all paths are uncorrelated. Applying the central limit theorem one has

$$\langle \exp\left[i\left\{\delta S_{s_1} - \delta S_{s_3} + \Phi_{12}\right\}\right]\rangle = \exp\left[-\left\langle \delta S^2_{s_1}\right\rangle - \left\langle (\mathcal{S}^{(\mathrm{f})}_{s_1,s_2})^2\right\rangle - \left\langle (\mathcal{S}^{(\mathrm{b})}_{s_1,s_2})^2\right\rangle\right],$$

where

$$\left\langle \delta S^2_{s_1}\right\rangle = \int_0^t \mathrm{d}\tau \mathrm{d}\tau' \langle \Sigma_1[\mathbf{q}_{s_1}(\tau)]\Sigma_1[\mathbf{q}_{s_1}(\tau')]\rangle$$

and

$$\left\langle (\mathcal{S}^{(\mathrm{f,b})}_{s_1,s_2})^2\right\rangle = \int_0^t \mathrm{d}\tau \; \mathrm{d}\tau' \langle \mathcal{U}_{\mathrm{f,b}}[\mathbf{q}_{s_1}(\tau),\mathbf{q}_{s_2}(\tau)]\mathcal{U}_{\mathrm{f,b}}[\mathbf{q}_{s_1}(\tau'),\mathbf{q}_{s_2}(\tau')]\rangle.$$

In chaotic systems, correlators typically decay exponentially fast, thus $\left\langle \delta S^2_{s_1}\right\rangle \simeq \Gamma_{\Sigma_1} t$ and $\left\langle (\mathcal{S}^{(\mathrm{f,b})}_{s_1,s_2})^2\right\rangle \simeq \Gamma_{\mathrm{f,b}} t$. Finally using the two sum rules

$$(4\pi\nu^2)^{\frac{\mathrm{d}_i}{2}} \int \mathrm{d}\mathbf{x}_i \sum_{s_i} |\mathcal{A}_{s_i}|^2 = 1, \quad (3.9a)$$

$$\int \mathrm{d}\mathbf{x}_i \int \mathrm{d}\mathbf{y}_i \delta_\nu(\mathbf{y}_i - \mathbf{x}_i) \sum_{l_i} |C_{l_i}| = 1, \quad (3.9b)$$

one obtains the nondiagonal contribution

$$\mathcal{M}_{\mathrm{B}}^{(\mathrm{nd})}(t) \;=\; \exp\left[-\left(\Gamma_{\Sigma_1}+\Gamma_{\mathrm{f}}+\Gamma_{\mathrm{b}}\right)t\right]. \tag{3.10}$$

The second contribution is diagonal, with $s_1 \simeq s_3$ and $\mathbf{x}_1 \simeq \mathbf{y}_1$. From Eq. (3.8) it reads

$$\begin{aligned}\mathcal{M}_{\mathrm{B}}^{(\mathrm{d})}(t) \;&=\; (4\pi\nu^2)^{\frac{2d_1+d_2}{2}} \int \prod_{i=1}^{2} \mathrm{d}\mathbf{x}_i \mathrm{d}\mathbf{y}_i d\mathbf{z}_2 \; \delta_\nu(\mathbf{x}_i-\mathbf{y}_i) \\ &\times \;\sum |\mathcal{A}_{s_1}|^4 |\mathcal{A}_{s_2}|^2 |C_{l_2}| e^{i\left[\Delta S_{s_1}+\Delta\mathcal{S}^{(\mathrm{f})}_{s_1,s_2}+\Delta\mathcal{S}^{(\mathrm{b})}_{s_1,l_2}\right]},\end{aligned} \tag{3.11}$$

where

$$\Delta S_{s_1} = \int_0^t \mathrm{d}\tau \nabla_1 \Sigma_1[\mathbf{q}_{s_1}(\tau)] \cdot [\mathbf{q}_{s_3}(\tau) - \mathbf{q}_{s_1}(\tau)],$$

and

$$\Delta\mathcal{S}^{(\mathrm{f,b})}_{s_1,s_2} = \int_0^t \mathrm{d}\tau \nabla_1 \mathcal{U}_{\mathrm{f,b}}[\mathbf{q}_{s_1}(\tau), \mathbf{q}_{s_2}(\tau)] \cdot [\mathbf{q}_{s_3}(\tau) - \mathbf{q}_{s_1}(\tau)].$$

We perform a change of coordinates $\int d\mathbf{x}_1 \sum |C_{s_1}| = \int d\mathbf{p_1}$, and use both the asymptotics $|C_{s_1}| \propto \exp\left[-\lambda_1 t\right]$ valid for chaotic systems [15] and the sum rules of Eqs. (3.9) to get

$$\mathcal{M}_{\mathrm{B}}^{(\mathrm{d})}(t) \;=\; \alpha_1 \exp\left[-\lambda_1 t\right]. \tag{3.12}$$

Here, α_1 is only algebraically time-dependent with $\alpha_1(t=0) = \mathcal{O}(1)$ [17]. Together, diagonal (3.12) and nondiagonal (3.10) contributions sum up to our main result, Eq. (3.13). We finally note that the long-time saturation at the inverse Hilbert space size of system 1, $\mathcal{M}_{\mathrm{B}}(\infty) = N_1^{-1}$, is obtained from Eq. (3.6) with the contractions $s_1 \simeq s_3$, $s_2 \simeq s_4$, $l_1 \simeq l_3$ and $l_2 \simeq l_4$.

3.3 Results

According to our semiclassical approach, the averaged Boltzmann echo is given to leading order by the sum of the two terms of Eq. (3.10) and Eq. (3.12).

$$\mathcal{M}_{\mathrm{B}}(t) \simeq \exp\left[-\left(\Gamma_{\Sigma_1}+\Gamma_{\mathrm{f}}+\Gamma_{\mathrm{b}}\right)t\right] + \alpha_1 \exp\left[-\lambda_1 t\right]. \tag{3.13}$$

The second term on the right-hand side of Eq. (3.13) exists exclusively for a classically meaningful initial state ψ_1 such as a Gaussian wavepacket or a position state, but the first term is much more generic. It emerges from both a semiclassical or a RMT treatment and does not depend on the initial preparation ψ_1 of system 1. Analyzing Eq. (3.13), we first note that $\mathcal{M}_{\mathrm{B}}(t)$ depends neither on H_2 nor on Σ_2. This is so because one traces over the uncontrolled degrees of freedom. We stress that this holds even for classically strong Σ_2. Most importantly, besides

strong similarities with the Loschmidt Echo, such as competing golden rule and Lyapunov decays [6,12], the Boltzmann Echo can exhibit a Σ_1-independent decay given by the decoherence rates $\Gamma_{\rm f,b}$ in the limit $\Gamma_{\Sigma_1} \ll \Gamma_{\rm f,b}$.

Extending our analysis to the regime $\Gamma_{\Sigma_1} \ll \delta_1$, $\Gamma_{\rm f,b} \ll \delta_2$ by means of quantum perturbation theory, we find a gaussian decay of $\mathcal{M}_{\rm B}(t)$,

$$\mathcal{M}_{\rm B}(t) = \exp\left[-\left(\overline{\Sigma_1^2}/4 + \overline{\mathcal{U}_{\rm f}^2}/2 + \overline{\mathcal{U}_{\rm b}^2}/2\right) t^2\right], \tag{3.14}$$

in terms of the typical squared matrix elements of Σ_1 and $\mathcal{U}_{\rm f,b}$. Also, at short times a parabolic decay of $\mathcal{M}_{\rm B}(t)$ prevails for any coupling strength. Also in that regime we have a competition between a Σ_1-dependent decay and a $\mathcal{U}$-dependent decay. It is thus possible to reach either a Gaussian or an exponential, Σ_1-independent decay, depending on the balance between the accuracy Σ_1 with which the time-reversal operation is performed and the coupling between controlled and uncontrolled degrees of freedom. This might explain the experimentally observed saturation of the polarization echo as Σ_1 is reduced [14], though a more precise analysis of these experiments in the light of the results presented here is necessary. Finally for the sake of completeness we note that at short times a parabolic decay of $\mathcal{M}_{\rm B}(t)$ prevails for any coupling strength. Moreover, if system 1 is integrable, the decay of $\mathcal{M}_{\rm B}(t)$ is power-law in time [18].

3.4 Numerical simulations

We numerically illustrate our findings. We consider two coupled kicked rotators with Hamiltonian

$$H_i = p_i^2/2 + K_i \cos(x_i) \sum_n \delta(t - nT), \tag{3.15a}$$

$$\mathcal{U} = \epsilon \sin(x_1 - x_2 - 0.33) \sum_n \delta(t - nT). \tag{3.15b}$$

We concentrate on the regime $K_i > 7$, for which the dynamics is fully chaotic with Lyapunov exponent $\lambda_i \approx \ln[K_i/2]$. The time-reversed one-particle Hamiltonians are obtained through $K_i \to K_i + \sigma_i$. We here restrict ourselves to the case $\mathcal{U} = \mathcal{U}_{\rm f} = \mathcal{U}_{\rm b}$. Both rotators are quantized on the torus with discrete momenta $p_n = 2\pi n/N$, $n = 1, 2, ...N$. The one- and two-particle bandwidths and level spacings are given by $B_1 = 2\pi$, $\delta_1 = 2\pi/N$ and $B_2 = 4\pi$, $\delta_2 = 4\pi/N^2$. For more details on the numerical procedure, we refer the reader to Ref. [19].

We first checked that $\mathcal{M}_{\rm B}(t)$ is independent of K_2 (as long as system 2 remains chaotic) and σ_2, and therefore set $K_2 = K_1$, $\sigma_2 = 0$ from now on. The main panel in Fig. 3.2 shows that for $B_1 > \Gamma_{\Sigma_1} > \delta_1$, $B_2 > \Gamma_{\mathcal{U}} > \delta_2$, Eq. (3.13) is satisfied. Additionally, the inset of Fig. 3.2 illustrates that when $\Gamma_{\Sigma_1} \ll 2\Gamma_{\mathcal{U}}$, the decay depends mostly on $\mathcal{U}$, and one effectively obtains a perturbation (Σ_1) independent decay. All our numerical results thus confirm the validity of Eq. (3.13).

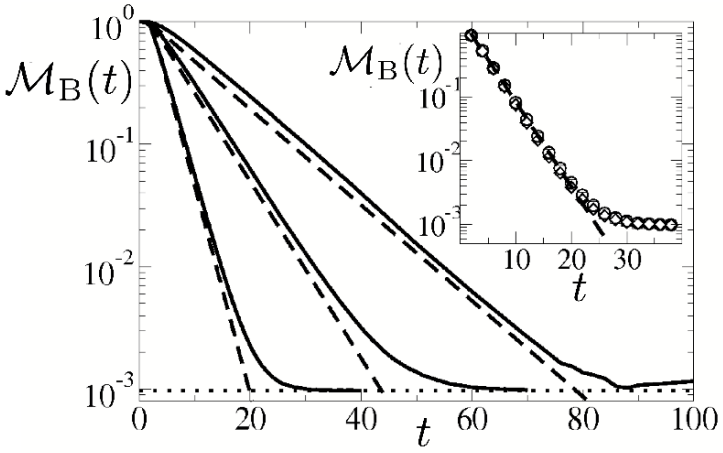

Figure 3.2: Main plot: Boltzmann echo for $N = 1024$, $K_1 = K_2 = 10.09$, and $\sigma_1 = 0.0018$ ($\Gamma_{\Sigma_1} \simeq 0.09$). Data have been calculated from 50 different initial states. The full lines correspond to $\epsilon = 0$, 0.0018 and 0.0037 (from right to left) and the dashed lines give the predicted exponential decay given by the first term on the right-hand side of Eq. (3.13), with $\Gamma_{\mathcal{U}} = 1.2\,10^4\epsilon^2, \Gamma_{\Sigma_1} = 2.6\,10^4\sigma_1^2$ (dashed lines have been slightly shifted for clarity). The dotted line gives the saturation N^{-1}. Inset : $\mathcal{M}_{\rm B}$ for $\epsilon = 0.0037$, and $\sigma_1 = 0.0003$ (circles; $\Gamma_{\Sigma_1} \simeq 2.\,10^{-3}$), $\sigma_1 = 0.0006$ (squares; $\Gamma_{\Sigma_1} \simeq 9.\,10^3$), and 0.0009 (diamonds; $\Gamma_{\Sigma_1} \simeq 0.02$). The dashed line indicates the theoretical prediction $\mathcal{M}_{\rm B}(t) = \exp[-0.3t]$.

3.5 Conclusions

In this chapter, we presented a semiclassical calculation of the Boltzmann echo for two classically chaotic subsystems and compared our results with those obtained from a Random Matrix Theory (RMT) treatment of the problem. Our main result is that, in the regime of classically weak but quantum mechanically strong imperfection Σ_1 and coupling $\mathcal{U}_{\rm f,b}$, $\mathcal{M}_{\rm B}(t)$ is the sum of two exponentials Cf. Eq. (3.13). Other regimes of decay exist. For quantum mechanically weak $\Gamma_{\Sigma_1} \ll \delta_1$ and $\Gamma_{\rm f,b} \ll \delta_2$, one has a Gaussian decay Eq. (3.14).

The equivalence between Boltzmann and Loschmidt echoes is broken by $\Gamma_{\rm f,b}$, the decoherence rate of system 1 induced by the coupling to system 2 (or by $\overline{\mathcal{U}^2_{\rm f,b}}$ at weak interaction). Skillfull experimentalists can thus investigate decoherence in echo experiments with weak time-reversal imperfection Σ_1 for which $\Gamma_{\Sigma_1} \ll \Gamma_{\rm f,b}$, and thus

$$\mathcal{M}_{\rm B}(t) \simeq \exp[-(\Gamma_{\rm f} + \Gamma_{\rm b})t]$$

or at weak interaction,

$$\mathcal{M}_{\rm B}(t) \simeq \exp[-(\overline{\mathcal{U}^2_{\rm f}} + \overline{\mathcal{U}^2_{\rm b}})\, t^2/2],$$

as Σ_1 is reduced. This might well be the explanation for the experimentally observed Σ_1-independent decay of polarization echoes [14].

In conclusion we proposed to analyze echo experiments in the light of the *Boltzmann echo* of Eq. (3.2). Our semiclassical and RMT analysis showed that the decay of $\mathcal{M}_B(t)$ saturates at a finite value even when the time-reversal operation is performed with infinite accuracy. Further work should attempt to quantitatively connect these results with echo experiments [8–11, 14]. This object has been recently used by W.H. Zurek et al. [20] in order to investigate the decoherence from a many-body independent spin environment. Their conclusions corroborate ours.

Bibliography

[1] J. Loschmidt, J. Sitzungsber. der kais. Akad. d. W. Math. Naturw. II **73**, 128 (1876).

[2] For references on Maxwell's, Gibbs' and Boltzmann's probabilistic interpretation of the second law and a discussion of the microscopic origin of macroscopic irreversibility see e.g.: J.L. Lebowitz, Physica A **263**, 516 (1999).

[3] L. Boltzmann, Ann. der Phys. **57**, 773 (1896).

[4] D.L. Shepelyansky, Physica D **8**, 208 (1983).

[5] A. Peres, Phys. Rev. A **30**, 1610 (1984).

[6] R.A. Jalabert and H.M. Pastawski, Phys. Rev. Lett. **86**, 2490 (2001).

[7] E.L. Hahn, Phys. Rev. **80**, 580 (1950).

[8] A.Z. Zhang, B.H. Meier, and R.R. Ernst, Phys. Rev. Lett. **69**, 2149 (1992); H.M. Pastawski, P. R. Levstein, G. Usaj, Phys. Rev. Lett. **75**, 4310 (1995).

[9] N.A. Kurnit, I.D. Abella, and S.R. Hartmann, Phys. Rev. Lett. **13**, 567 (1964).

[10] F.B.J. Buckremer, R. Dumke, H. Levsen, and W. Ertmer, Phys. Rev. Lett. **85**, 3121 (2000); M.F Andersen, A. Kaplan, and N. Davidson, Phys. Rev. Lett. **90**, 023001 (2003).

[11] Y. Nakamura, Yu.A. Pashkin, T. Yamamoto, and J.S. Tsai, Phys. Rev. Lett. **88**, 047901 (2002).

[12] Ph. Jacquod, P.G. Silvestrov, and C.W.J. Beenakker, Phys. Rev. E **64**, 055203(R) (2001).

[13] Ph. Jacquod, Phys. Rev. Lett. **92**, 150403 (2004); *ibid* **93**, 219903 (2004).

[14] H.M. Pastawski, P.R. Levstein, G. Usaj, J. Raya, and J. Hirschinger, Physica A **283**, 166 (2000).

[15] P. Cvitanović, R. Artuso, R. Mainieri, G. Tanner, and G. Vattay, *Chaos: Classical and Quantum*, `ChaosBook.org` (Niels Bohr Institute, Copenhagen 2003).

[16] This is rigorously justified by the structural stability of hyperbolic systems considered here; see e.g. J. Vanicek and E.J. Heller, Phys. Rev. E **68**, 056208 (2003) and Chapter 4.

[17] Detailed expression of α is given in Appendix 2.7 of Chapter 2.

[18] Calculation for regular system is straight forward, if we use the asymptotic $|C_{s_1}| \propto t^{-d}$ valid for regular system. See Ph. Jacquod, İ. Adagideli, and C.W.J. Beenakker, Europhys. Lett. **61**, 729 (2003).

[19] F.M. Izrailev, Phys. Rep. **196**, 334 (1979).

[20] W. H. Zurek, F. M. Cucchietti and J. P. Paz , Acta Physica Polonica B, **38**,1685. (2007),

CHAPTER 4

The Displacement echo

4.1 Introduction

The fidelity with which a wavefunction is reconstructed after an imperfect time-reversal operation was originally introduced as a measure of reversibility in quantum mechanics [1]. Dubbed the Loschmidt Echo, it has received much attention in recent years in the context of decoherence and the quantum classical correspondence [2–7]. For a generic perturbation of the Hamiltonian, four different decay regimes were found: the Gaussian perturbative regime, the Fermi Golden Rule (FGR) regime, the Lyapunov regime, and the regime of classically large perturbations. Of special interest is the Lyapunov regime where the purely quantum mechanical fidelity decays with the Lyapunov exponent of the classical dynamics. It suggests the existence of a universal regime of environment-independent decoherence rate [2, 8, 9].

In this chapter we analyze the decay of the Loschmidt echo under a new, non-generic perturbation, namely an instantaneous phase space displacement. Our investigation is partly inspired by spectroscopies such as neutron scattering, Mössbauer γ-ray, and certain electronic transitions in molecules and solids [10–12]. In these spectroscopies phase space displacement (momentum boost or position shift) takes place with little or no change in the potential. Under this non-generic perturbation, we find that the decay rate of the average fidelity is always set by the Lyapunov exponent. Moreover, for small displacements, the initial Lyapunov decay is followed at larger times by a quantum freeze of the fidelity at a displacement-dependent saturation value. Both semiclassics and random matrix theory predict that the freeze persists up to infinitely large times.

4.2 Differential cross section and displacement echo

As our starting point, we recall that , following Lovesey [13], the differential cross section for incoherent neutron scattering and Mössbauer emission/absorption is (from now on we set $\hbar \equiv 1$)

$$\frac{d^2\sigma}{d\Omega dE} = \mathcal{N}\frac{P_{\text{out}}}{P_{\text{in}}}\frac{\sigma_i}{4\pi}\mathcal{S}_i(\mathbf{P},\omega), \tag{4.1}$$

where Ω is the solid scattering angle, $\mathcal{N}$ is the number of scatterers, σ_i is the total incoherent cross section, P_{in} and P_{out} are the initial and final magnitudes of the neutron, $\mathbf{P}$ is the momentum transfer and $\mathcal{S}_i(\mathbf{P},\omega)$ is the response function for the considered scattering.

The response function is expressed in terms of the Fourier transform of a correlation function,

$$\mathcal{S}_i(\mathbf{P},\omega) = \frac{1}{2\pi\mathcal{N}}\int \mathrm{d}t\, e^{-i\omega t}\sum_j Y_{jj}\left(\mathbf{P},\mathbf{t}\right), \tag{4.2}$$

where the correlation function $Y_{jj}\left(\mathbf{P},\mathbf{t}\right)$ may be expressed as [13, 14]

$$Y_{jj}\left(\mathbf{P},\mathbf{t}\right) = \left\langle e^{-i\mathbf{P}\cdot\hat{\mathbf{r}}_\mathbf{j}} e^{i\hat{H}t} e^{i\mathbf{P}\cdot\hat{\mathbf{r}}_\mathbf{j}} e^{-i\hat{H}t}\right\rangle. \tag{4.3}$$

Here, the brackets represent an ensemble average, $\hat{\mathbf{r}}_\mathbf{j}$ are the position operators of the nuclei and $\hat{H}$ is the typical Hamiltonian of the target system. The ensemble average of the correlation function can be written [10]:

$$Y_{jj}\left(\mathbf{P},\mathbf{t}\right) \approx \frac{1}{Q}\int\left(\frac{d^{2N}\alpha}{\pi^N}\right)\Phi\left(\alpha\right)\left\langle\alpha\right| e^{-i\mathbf{P}\cdot\hat{\mathbf{r}}_\mathbf{j}} e^{i\hat{H}t} e^{i\mathbf{P}\cdot\hat{\mathbf{r}}_\mathbf{j}} e^{-i\hat{H}t}\left|\alpha\right\rangle, \tag{4.4}$$

where $|\alpha\rangle$ are coherent states with N degrees of freedom, $Q = \mathrm{Tr}\left[e^{-\beta\hat{H}}\right]$, and $\Phi\left(\alpha\right)$ is a thermal weight, which tends to $e^{-\beta H_{cl}(\alpha)}$ at high temperatures. The notation $e^{i\hat{H}_\mathbf{P}t} = e^{-i\mathbf{P}\cdot\hat{\mathbf{r}}_\mathbf{j}} e^{i\hat{H}t} e^{i\mathbf{P}\cdot\hat{\mathbf{r}}_\mathbf{j}}$ suggests that we identify the kernel of the integral $I\left(t\right) = \left\langle\alpha\right| e^{-i\mathbf{P}\cdot\hat{\mathbf{r}}_\mathbf{j}} e^{i\hat{H}t} e^{i\mathbf{P}\cdot\hat{\mathbf{r}}_\mathbf{j}} e^{-i\hat{H}t}\left|\alpha\right\rangle$ with the kernel of a Loschmidt echo problem, we thus introduce the momentum *displacement echo*

$$\mathcal{M}_\mathrm{D}\left(t\right) = \left|I(t)\right|^2 = \left|\left\langle\alpha\right| e^{i\hat{H}_\mathbf{P}t} e^{-i\hat{H}t}\left|\alpha\right\rangle\right|^2. \tag{4.5}$$

The physical process described by $I(t)$ is the following. The state $|\alpha\rangle$ is propagated under the hamiltonian $\hat{H}$ for a time t. At this time, we applied the backward Hamiltonian $\hat{H}_\mathbf{P}$. This corresponds to a first increase of the momentum of the jth particle, due to the boost, followed by a backward propagation under the hamiltonian $\hat{H}$ for a time t and finally a decrease of the momentum of the jth particle. $I(t)$ involves the overlap between this final state and the initial one. Fig. 4.1 shows a phase-space picture of these processes.

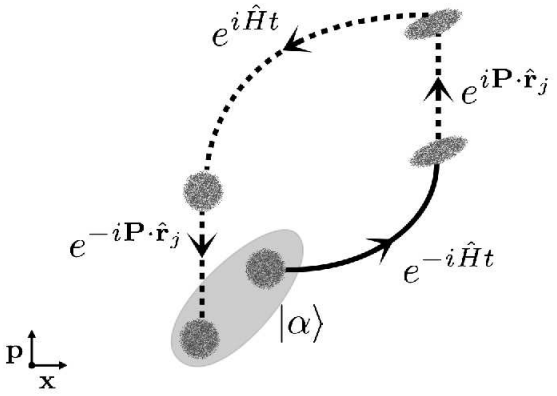

Figure 4.1: Phase-space illustration of the physical process involved in the displacement echo. Momentum is the vertical coordinate, position the horizontal one. Dashed lines correspond of the process related to $\hat{H}_{\mathbf{P}}$. The coherent state is represented by the cloud marked "$|\alpha\rangle$". The overlap is represented by the shaded area.

4.3 Structural stability

As an introduction to our semiclassical calculation of the displacement echo $\mathcal{M}_{\mathrm{D}}(t)$, we first discuss the validity of the diagonal approximation used in Ref. [2] for the semiclassical approach to the Loschmidt echo and point out why this approximation is even better for the displacement echo. The diagonal approximation for the Loschmidt echo equates each classical trajectory γ generated by an unperturbed Hamiltonian H with a classical trajectory γ_V generated by a perturbed Hamiltonian $H_V = H + V$. This procedure is not justified a priori in chaotic systems where one expects that an infinitesimally small perturbation generates trajectories diverging exponentially fast away from their unperturbed counterpart. It was however pointed out by Cerruti and Tomsovic [4], and later by Vaníček and Heller [6], that structural stability theorems [15, 16] justify this approximation. Roughly speaking one can show that, given a uniformly hyperbolic Hamiltonian system H, and a generic perturbation V, each classical trajectory γ'_V generated by the (still hyperbolic) perturbed Hamiltonian $H+V$ is almost always arbitrarily close to one unperturbed trajectory γ. In general the two trajectories do not share common endpoints, however these endpoints are close enough that they are not resolved quantum-mechanically. This is illustrated in the left panel of Fig. 1. The semiclassical expression for the kernel of the Loschmidt echo involves a double sum over both the perturbed and the unperturbed classical trajectories, so that both γ'_V and γ are included. After a stationary phase condition, this double sum is reduced to a single sum where γ'_V and γ are equated. In other words, a semiclassical particle follows γ in the forward direction, and γ'_V in the backward direction because this is the best way to minimize the action. The action difference is simply given by the integral of the perturbation along the backward trajectory, and it is in general time-dependent. In the case of a uniform phase-space displacement, the diagonal approximation becomes even better. This

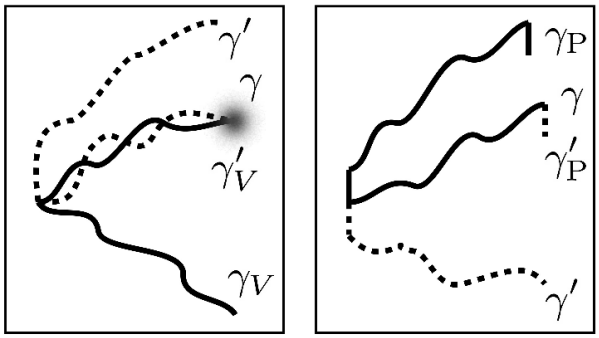

Figure 4.2: Illustrative view of structural stability. Left panel: generic perturbation. γ and γ' are two orbits of the unperturbed Hamiltonian, γ_V is the orbit of the perturbed Hamiltonian with the same initial condition as γ, while γ'_V is the orbit of the perturbed Hamiltonian with the same initial condition as γ'. The endpoints of γ and γ'_V are separated by less than a quantum-mechanical resolution scale (shaded area). Right panel: phase space displacement. Labels are the same as in the left panel, with $\mathbf{P}$ replacing V as subscript for perturbed trajectories. Note that $\gamma'_{\mathbf{P}}$ and γ lie on top of each other.

is so because any classical trajectory of the unperturbed Hamiltonian is also a trajectory of the perturbed Hamiltonian, up to displacements at the trajectory's ends. This is illustrated in the right panel of Fig. 4.2. The fact that the action difference is here time-independent has the important consequence that the FGR decay is replaced by a time-independent saturation term. The Lyapunov decay term is left almost unaffected, as it depends on the classical measure of nearby trajectories with perturbed initial conditions and does not depend on quantum action phases. We also note that for displacement echoes there is no Gaussian perturbative decay, since phase space displacements do not change the spectrum of the system aside from some possible but irrelevant global shift.

4.4 Semiclassical approach

For a quantitative approach to the problem, we semiclassically evaluate $\mathcal{M}_{\mathrm{D}}(t)$ for the case of an initial Gaussian wavepacket,

$$\langle \mathbf{r} \mid \alpha\left(\mathbf{r}_0, \mathbf{p}_0\right)\rangle = \left(\pi\nu^2\right)^{-\frac{d}{4}} \exp[i\mathbf{p}_0 \cdot (\mathbf{r}-\mathbf{r}_0) - (\mathbf{r}-\mathbf{r}_0)^2 / 2\nu^2].$$

Following Ref. [17], we semiclassically propagate $|\alpha\rangle$ with the help of the van Vleck propagator, linearly expanding around $\mathbf{r_0}$:

$$\langle \mathbf{r}' | \, e^{-i\hat{H}t} \, |\alpha\rangle_{\mathrm{sc}} \simeq \left(-\frac{i\nu}{\sqrt{\pi}}\right)^{\frac{d}{2}} \sum_{\gamma} C_{\gamma}^{\frac{1}{2}} \exp\left[iS_{\gamma} - i\frac{\pi}{2}\mu_{\gamma} - \frac{\nu^2}{2}\left(\mathbf{p}_{\gamma} - \mathbf{p}_0\right)\right] \quad (4.6)$$

Here, the sum runs over all possible classical trajectories γ connecting $\mathbf{r}_0$ and $\mathbf{r}'$ in the time t, $\mathbf{p}_{\gamma} = -\partial S_{\gamma}/\partial \mathbf{r}|_{\mathbf{r}=\mathbf{r}_0}$ is the initial momentum on γ, S_{γ} is the classical action accumulated on γ, μ_{γ} is the Maslov index and $C_{\gamma} = \left|-\partial^2 S_j\left(\mathbf{r}, \mathbf{r}'; t\right) / \partial r_i \partial r'_{\gamma}\right|_{\mathbf{r}=\mathbf{r}_0}$.

The kernel $I(t)$ of $\mathcal{M}_{\rm D}(t)$ involves a double sum over classical trajectories, γ and γ', and can be interpreted as the overlap between a wavepacket that is boosted and subsequently propagated with a wavepacket that is first propagated and subsequently boosted [10]. Enforcing a stationary phase condition kills all but the contributions with the smallest actions. They correspond to $\gamma = \gamma'$ and one has

$$I\left(t\right) = \left(\frac{\nu^2}{\pi}\right)^{\frac{d}{2}} \int {\rm d}\mathbf{r}' \sum_{\gamma} e^{i\mathbf{P}\cdot(\mathbf{r}'+\mathbf{r}_0)}\, C_\gamma \exp -\frac{\nu^2}{2}\left[\left(\mathbf{p}_\gamma - \mathbf{p}_0\right)^2 + \left(\mathbf{p}_\gamma - \mathbf{p}_0 - \mathbf{P}\right)^2\right]. \quad (4.7)$$

Taking the squared amplitude $|I(t)|^2$ one obtains the semiclassical expression for the displacement echo

$$\begin{aligned} \mathcal{M}_{\rm D}(t) &= \left(\frac{\nu^2}{\pi}\right)^{d} \int {\rm d}\mathbf{r}\, {\rm d}\mathbf{r}' \sum_{\gamma,\gamma'} e^{i\mathbf{P}\cdot(\mathbf{r}-\mathbf{r}')}\, C_\gamma\, C_{\gamma'} \\ &\times \exp -\frac{\nu^2}{2}\Big[\left(\mathbf{p}_\gamma - \mathbf{p}_0\right)^2 + \left(\mathbf{p}_\gamma - \mathbf{p}_0 - \mathbf{P}\right)^2\Big] \\ &\times \exp -\frac{\nu^2}{2}\left[\left(\mathbf{p}_{\gamma'} - \mathbf{p}_0\right)^2 + \left(\mathbf{p}_{\gamma'} - \mathbf{p}_0 - \mathbf{P}\right)^2\right]. \end{aligned} \quad (4.8)$$

We calculate $\langle \mathcal{M}_{\rm D}(t)\rangle$, the ensemble-averaged displacement echo over a set of initial Gaussian wavepackets with varying center of mass $\mathbf{r}_0$. There are two qualitatively different contributions to $\langle \mathcal{M}_{\rm D}(t)\rangle$. The first contribution $\langle \mathcal{M}_{\rm D}(t)\rangle_{\rm c}$ comes from pairs $\gamma \approx \gamma'$ of correlated trajectories that remain within a distance $\lesssim \nu$ of each other for the whole duration t of the experiment, while the second contribution $\langle \mathcal{M}_{\rm D}(t)\rangle_{\rm u}$ arises from pairs of uncorrelated trajectories (γ, γ'). For the first contribution, we write $\exp[i\mathbf{P}(\mathbf{r}-\mathbf{r}')] \approx 1$, which is true in the semiclassical limit where $\nu \to 0$, and set $\gamma = \gamma'$. One then has

$$\langle \mathcal{M}_{\rm D}(t)\rangle_{\rm c} = \left(\frac{\nu^2}{\pi}\right)^{d} \int {\rm d}\mathbf{r}{\rm d}\mathbf{r}'\, \delta_\nu(\mathbf{r}-\mathbf{r}')\Big\langle \sum_{\gamma} C_\gamma^2\, e^{-\nu^2\left[(\mathbf{p}_\gamma-\mathbf{p}_0)^2+(\mathbf{p}_\gamma-\mathbf{p}_0-\mathbf{P})^2\right]}\Big\rangle, \quad (4.9)$$

where $\delta_\nu(\mathbf{r}-\mathbf{r}')$ restricts the integrals to $|\mathbf{r}-\mathbf{r}'| \leq \nu$. The calculation of (4.9) is straightforward. The integral over $\mathbf{r}'$ gives a factor ν^d. One then replaces one C_γ by its asymptotic value, $C_\gamma \propto \exp[-\lambda t]$, and uses the second C_γ to perform a change of integration variable $\int {\rm d}\mathbf{r} \sum_\gamma C_\gamma = \int {\rm d}\mathbf{p}$. After a Gaussian integration, one finally gets the correlated contribution to $\langle \mathcal{M}_{\rm D}(t)\rangle$ as

$$\langle \mathcal{M}_{\rm D}(t)\rangle_{\rm c} = \alpha\, e^{-\frac{(\mathbf{P}\nu)^2}{2}}\, e^{-\lambda t}. \quad (4.10)$$

Here, α is a weakly time-dependent number of order one [2].

For the uncorrelated part, an ergodicity assumption is justified at sufficiently

large times, under which one gets

$$\langle \mathcal{M}_{\mathrm{D}}(t)\rangle_{\mathrm{u}} = f(\mathbf{P})\,\langle \tilde{M}_{\mathrm{D}}(t)\rangle_{\mathrm{u}}, \tag{4.11a}$$

$$f(\mathbf{P}) = \frac{1}{\Omega^2}\int \mathrm{d}\mathbf{r}\mathrm{d}\mathbf{r}' e^{i\mathbf{P}\cdot(\mathbf{r}-\mathbf{r}')}, \tag{4.11b}$$

$$\langle \tilde{M}_{\mathrm{D}}(t)\rangle_{\mathrm{u}} = \left(\frac{\nu^2}{\pi}\right)^d \left(\int \mathrm{d}\mathbf{x} \sum_\gamma C_\gamma e^{-\frac{\nu^2}{2}\left[(\mathbf{p}_\gamma-\mathbf{p}_0)^2+(\mathbf{p}_\gamma-\mathbf{p}_0-\mathbf{P})^2\right]}\right)^2, \tag{4.11c}$$

with the system's volume $\Omega \propto L^d$. It is straightforwardly seen that

$$\langle \tilde{M}_{\mathrm{D}}(t)\rangle_{\mathrm{u}} = \exp[-(\mathbf{P}\nu)^2/2],$$

and

$$f(\mathbf{P}) = \frac{g(|\mathbf{P}|L)}{(|\mathbf{P}|L)^2},$$

in term of an oscillatory function $g(|\mathbf{P}|L) = 4\sin^2(|\mathbf{P}|L/2)$ for $d = 1$ and $g(|\mathbf{P}|L) = 4J_1^2(|\mathbf{P}|L)$ for $d = 2$. For $d = 3$, g is given by Bessel and Struve functions. The uncorrelated contribution to the displacement echo reads

$$\langle \mathcal{M}_{\mathrm{D}}(t)\rangle_{\mathrm{u}} = e^{-\frac{\mathbf{P}\nu)^2}{2}}\ \frac{g(|\mathbf{P}|L)}{(|\mathbf{P}|L)^2}, \tag{4.12}$$

which, together with Eq. (4.10) gives the average displacement echo as

$$\langle \mathcal{M}_{\mathrm{D}}(t)\rangle = e^{-\frac{(\mathbf{P}\nu)^2}{2}}\ \left[\alpha\, e^{-\lambda t} + \frac{g(|\mathbf{P}|L)}{(|\mathbf{P}|L)^2}\right]. \tag{4.13}$$

In addition, as is the case for Loschmidt echoes, $\langle \mathcal{M}_{\mathrm{D}}(t)\rangle \geq N^{-1}$ where N is the size of the Hilbert space.

Eq. (4.13) is the main result of this chapter. It states that $\mathcal{M}_{\mathrm{D}}(t)$ is the sum of a time-dependent decaying term of classical origin and a time-independent term of quantum origin. The latter can also be obtained within random matrix theory. The prefactor $\exp[-(\mathbf{P}\nu)^2/2] \to 1$ in the semiclassical limit and is thus of little importance. We see that generically, $\mathcal{M}_{\mathrm{D}}(t)$ follows a classical exponential decay, possibly interrupted by a quantum freeze as long as the displacement is not too large, $g(|\mathbf{P}|L)\Big/(|\mathbf{P}|L)^2 > N^{-1}$ [18]. We note that in the semiclassical limit, $\mathcal{M}_{\mathrm{D}}(t \to 0) \to 1$, because of the saturation of $\alpha(t \to 0) \to 1$ and the disappearance of uncorrelated contributions at short times. Most importantly, there is no displacement-dependent decay, i.e. no counterpart to the FGR decay nor the perturbative Gaussian decay for $\mathcal{M}_{\mathrm{D}}(t)$, because phase-space displacements leave the spectrum unchanged, up to a possible homogeneous shift. The situation bears similarities with spectral and wavefunction variations in perturbed billiards. When the perturbation is an homogeneous spatial displacement, the spectrum is left unchanged [19].

What does the "freeze" correspond to physically? It is the elastic component in any of the mentioned spectroscopies: Mössbauer, neutron, and molecular electronic, and was first identified by van Hove in connection with neutron scattering [14]. There is a finite probability, above the $1/N$ statistical limit, of not changing quantum state in spite of being "hit"; this is the source for example of the recoilless peak in Mössbauer spectroscopy.

4.5 Numerical simulations

We now check our predictions numerically . We specialize to the kicked rotator model with Hamiltonian

$$H_0 = \frac{\hat{p}^2}{2} + K \cos \hat{x} \sum_n \delta(t-n). \tag{4.14}$$

We focus on the regime $K > 7$, for which the dynamics is fully chaotic with Lyapunov exponent $\lambda = \ln[K/2]$. We quantize this Hamiltonian on a torus, which requires to consider discrete values $p_l = 2\pi l/N$ and $x_l = 2\pi l/N$, $l = 1, ...N$. In these units, one has $L = N$. The displacement echo of Eq. (4.5) is computed for discrete times $t = n$, as

$$\mathcal{M}_{\rm D}(n) = \left| \langle \psi_0 | e^{-iP\hat{x}} \left(\mathcal{U}^\dagger\right)^n e^{iP\hat{x}} \left(\mathcal{U}\right)^n |\psi_0\rangle \right|^2, \tag{4.15}$$

with $P = |\mathbf{P}|$. Here, we used the unitary Floquet time-evolution operator $\mathcal{U}$ whose matrix elements in $x-$representation are given by

$$\mathcal{U}_{l,l'} = \frac{1}{\sqrt{N}} \exp\left[i \frac{\pi (l-l')^2}{N} \right] \exp\left[-i \frac{NK}{2\pi} \cos \frac{2\pi l'}{N} \right].$$

The time-evolution of ψ_0 in Eq. (4.15), is calculated by recursive calls to a fast-Fourier transform routine.

Fig. 4.5 shows the behavior of the echo for displacements in the range $P \gg 2\pi/N$ for which $\langle \mathcal{M}_{\rm D}(t) \rangle_{\rm u} \ll N^{-1}$ and thus plays no role. It is seen that the decay rate of the displacement echo strongly depends on the kicking strength K, but is largely independent of the displacement P. We quantitatively found that in that regime, $\mathcal{M}_{\rm D}(t) \approx \exp[-\lambda_0 t]$, in terms of the reduced Lyapunov exponent λ_0 [20]. The inset shows moreover, that lowering the displacement to the regime $P = m2\pi/N$ with $m \leq 5$ does not affect the decay rate of $\mathcal{M}_{\rm D}(t)$, i.e. there is no FGR decay for the displacement echo.

We focus in Fig. 4.5 on smaller displacements $P \leq 2\pi/N$. The behavior of $\langle \mathcal{M}_{\rm D}(t) \rangle$ clearly satisfies Eq. (4.13), with a quantum freeze at a displacement-dependent value following a decay with a slope given by the Lyapunov exponent. We show in the main panel the P-dependence of the value at which $\mathcal{M}_{\rm D}(t)$ freezes. The data unambiguously confirm the algebraically damped oscillations predicted in Eq. (4.13).

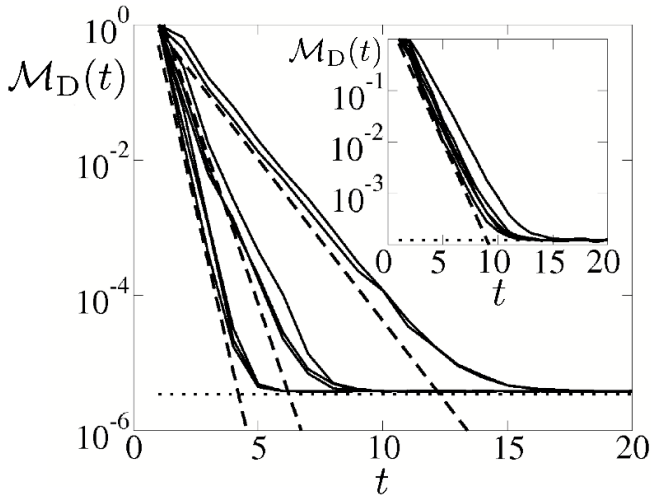

Figure 4.3: Main plot : Displacement echo $\mathcal{M}_{\rm D}(t)$ for the kicked rotator model with $N = 262144$, and displacements $P = m \times 2\pi/N$, $m = 10$, 20, 30. Averages have been performed over a set of 10000 different initial coherent states. The full lines correspond to kicking strengths $K = 10.09$, 50.09 and 200.09 (from right to left) and the dashed lines (slightly shifted for clarity) give the predicted exponential decay given by the reduced Lyapunov exponent $\lambda_0 = 1.1$, 2.5, 3.7. The dotted line gives the saturation at N^{-1}. Inset : Displacement echo for $N = 8192$, $K = 10.09$, and displacements $P = 2\pi/N$, $4\pi/N, \ldots 10\pi/N$. Data are obtained from 1000 different initial coherent states. The dashed line gives the predicted exponential decay given by the reduced lyapunov exponent $\lambda_0 = 1.1$. The dotted line gives the minimal saturation value at N^{-1}.

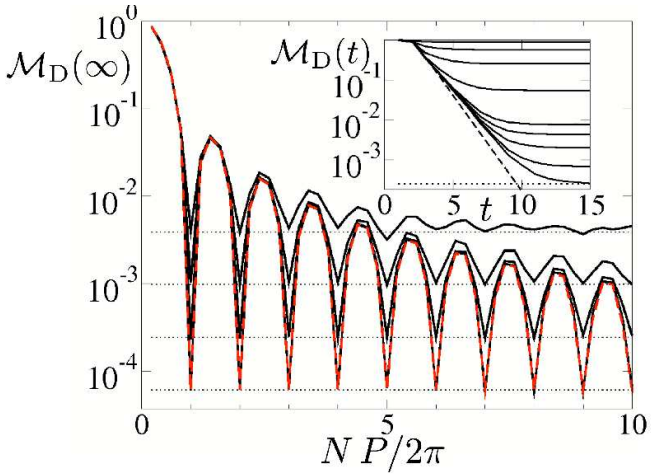

Figure 4.4: Main plot: Saturation value $\mathcal{M}_{\rm D}(\infty)$ of the displacement echo as a function of the rescaled displacement $NP/2\pi$ for the kicked rotator model with $N = 256$, 1024, 4096, 16384 (full lines, from top to bottom). Data are obtained from 1000 different initial coherent states. The dotted lines give the saturation at N^{-1}. The red dashed line gives the theoretical prediction $\mathcal{M}_{\rm D}(\infty) = {\rm Max}(4\exp[-(\nu P)^2/2]\sin^2(PL/2)\Big/(PL)^2, N^{-1})$ for $N = 16384$. Inset: Quantum freeze of the displacement echo for kicking strength $K = 10.09$, $N = 4096$, and $P \in [0, 2\pi/N]$. The dashed line gives the decay with the reduced Lyapunov exponent $\lambda_0 = 1.1$ (see text).

4.6 Conclusions.

In summary, we have presented a semiclassical calculation of phase-space displacement echoes. We showed that they are generically given by the sum of a classical decay and a quantum freeze term (4.13). Because phase-space displacements do not generate time-dependent action differences, and because they vanish in first order perturbation theory, there is no other time-dependent decay, in contrast to Loschmidt echoes [1–4, 6].

To conclude, we note that neutron scattering correlation functions are given by the average $\langle I(t)\rangle$ of the kernel of $\mathcal{M}_{\rm D}(t)$. Starting back from Eq. (4.7), one gets

$$|Y_{jj}\,(\mathbf{P},\mathbf{t})\,| \simeq \exp[-(\mathbf{P}\nu)^2/4]\,\frac{g^{1/2}(|\mathbf{P}|L)}{|\mathbf{P}|L}, \tag{4.16}$$

i.e. $|Y_{jj}|$ is given by the quantum freeze term only.

This is so, since the correlations between pairs of trajectories that are necessary for the existence of the Lyapunov term appear only once $I(t)$ is squared. The Lyapunov decay is in this sense similar to diffuson and cooperon correlators in disordered electronic systems, which appear in averages over *products* of Green's functions, but cannot be traced back to the impurity-averaged Greens function.

Bibliography

[1] A. Peres, Phys. Rev. A **30**, 1610 (1984).

[2] R.A. Jalabert and H.M. Pastawski, Phys. Rev. Lett. **86**, 2490 (2001).

[3] Ph. Jacquod, P.G. Silvestrov, and C.W.J. Beenakker, Phys. Rev. E **64**, 055203(R) (2001).

[4] N.R. Cerruti and S. Tomsovic, Phys. Rev. Lett. **88**, 054103 (2002).

[5] Z. P. Karkuszewski, C. Jarzynski, and W.H. Zurek, Phys. Rev. Lett. **89**, 170405 (2002).

[6] J. Vaniček and E.J. Heller, Phys. Rev. E **68**, 056208 (2003).

[7] T. Gorin et al., Phys. Rep. **435**, 33 (2006)

[8] W.H. Zurek and J.P. Paz, Physica D **83**, 300 (1995).

[9] Ph. Jacquod, Phys. Rev. Lett. **94**, 150403 (2004).

[10] E.J. Heller, J.R. Reimers and G. Drolshagen, Phys. Rev. A **36**, 2613 (1987).

[11] M. Lax, *Symmetry Principles in Solid State and Molecular Physics* (Wiley, New York, 1974).

[12] More generally, any measurement of momentum or position time correlators (or combinations of the two) can be viewed as a fidelity experiment under certain phase space displacement.

[13] S.W. Lovesey, *Theory of Neutron Scattering from Condensed Matter*, Vol. 1 (Oxford University Press, New York, 1984).

[14] L. Van Hove, Phys. Rev. **95**, 249 (1954).

[15] M.W. Hirsch and S. Smale, *Differential Equations, Dynamical Systems, and Linear Algebra* (Academic Press, New York, 1974)

[16] J. Vaníček, Phys. Rev. E **70**, 055201(R) (2004);

[17] S. Tomsovic and E.J. Heller, Phys. Rev. Lett. **67**, 664 (1991).

[18] The fidelity freeze reported here differs from the one found by T. Prosen and M. Žnidarič, Phys. Rev. Lett. **94**, 044101 (2005). In particular, because the spectrum is left unchanged by phase-space displacements, the freeze of $\mathcal{M}_{\mathrm{D}}(t)$ found here persists up to $t \to \infty$.

[19] D. Cohen, A. Barnett and E.J. Heller, Phys. Rev. E **63**, 046207 (2001).

[20] The reduced Lyapunov exponent is somehow smaller than $\lambda = \ln[K/2]$. This is due to the fact that $\langle C_\gamma \rangle \propto \langle \exp[-\lambda t] \rangle \neq \exp[-\langle \lambda \rangle t]$, thus finite-time fluctuations reduce the observed effective Lyapunov exponent λ_0. See: P.G. Silvestrov, J. Tworzydło, and C.W.J. Beenakker, Phys. Rev. E **67**, 025204(R) (2003).

Part III

Entanglement and Decoherence : A Dynamical Approach

CHAPTER 5

Toward a semiclassical approach to decoherence

5.1 Introduction

In the decades since its inception, no observed phenomenon, or experimental result ever contradicted quantum theory. Yet, the world surrounding us, despite being made out of quantum mechanical building blocks, behaves classically most of the time. This suggests that, one way or another, classical physics emerges from quantum mechanics. Today's common understanding of this quantum-classical correspondence is based on the realization that no finite-sized system is ever fully isolated. It is then hoped that a large regime of parameters exists where the coupling of the system to external degrees of freedom destroys quantum interferences without modifying the system's classical dynamics. Indeed, such a coupling usually induces loss of coherence on a time scale much shorter than it relaxes the system [1, 2].

The standard approach to decoherence starts from a master equation valid in the regime of weak system-environment coupling [1, 2]. The master equation determines the time-evolution of the system's Wigner function $W(\mathbf{p},\mathbf{q}) = (2\pi\hbar)^{-d}\int \mathrm{d}\mathbf{x}\exp[i\mathbf{p}\mathbf{x}]\eta(\mathbf{q}+\mathbf{x}/2,\mathbf{q}-\mathbf{x}/2)$ (η is the system's density matrix) as

$$\begin{aligned}\partial_t W &= \Big\{H,W\Big\} + \sum_{n\geq 1}\frac{(i\hbar)^{2n}}{2^{2n}(2n+1)!}\partial_q^{2n+1}V\partial_p^{2n+1}W \\ &\quad +2\gamma\partial_p(pW) + D\partial_{pp}^2 W. \end{aligned} \tag{5.1}$$

The first term on the right-hand side of Eq. (5.1) is the classical Poisson bracket. The second term, written here for a spatially dependent potential $V(\mathbf{q})$ only,

already exists in closed systems and generates quantum corrections to the dynamical evolution of W. This term starts to become comparable to the Poisson bracket at the Ehrenfest time $\tau_{\rm E} = \lambda^{-1} \ln N$, where λ is the Lyapunov exponent of the classical dynamics, and N the size of the system's Hilbert space. The two terms on the second line of Eq. 5.1 are induced by the coupling to the environment. In the limit of weak coupling, $\gamma \to 0$, but finite diffusion constant, $D \propto \gamma T = \text{Cst}$, the friction term vanishes, leaving the classical dynamics unaffected. This requires to consider the high temperature limit. Simultaneously, for large enough D, the momentum diffusion term induces enough noise so as to kill the quantum corrections before they become important. The time-evolution of W is then governed by the classical Poisson bracket, that is to say, classical dynamics emerges out of quantum mechanics. Refs. [3,4] illustrated this scenario numerically.

Our motivation in the present chapter is multiple. First, it is unclear how generic this scenario is, since it is based on a master equation derived under restrictive assumptions, for instance on the environment, the dimensionality of the system or the strength of the coupling between system and environment [1, 2]. Moreover, it formally requires to consider infinite temperatures. Last but not least, and with the specific exception of the kicked harmonic oscillator investigated in Ref. [4], there is not much analytical understanding of the decoherence process in generic dynamical systems, i.e. except for the regular case, master equations are usually integrated numerically. Second, for coupled systems, claims have been made of an entropy production governed by the system's Lyapunov exponent λ [2, 5], based on appealing but incomplete analytical arguments, and without strong numerical evidence [6]. A Lyapunov decay of the fidelity has recently been analytically predicted [7] and numerically observed [8], however, decoherence and fidelity are two different things, especially in the generic situation where the system and environment Hamiltonians do not commute with the coupling Hamiltonian [9, 11].

We revisit these issues and consider at first the simple situation of two interacting quantized dynamical systems. Entanglement generation between two identical particles has already been considered in Refs. [11–15]. All results to date are consistent with the scenario proposed in Ref. [11], according to which bipartite entanglement, results from two contributions:

(i) a quantum-mechanical one, which depends on the coupling strength between the two systems,

(ii) a dynamical one, which, in chaotic systems, is determined by the total system's spectrum of Lyapunov exponents.

The entanglement generation rate is given by the weakest of the coupling strength and the Lyapunov exponent. This picture holds in the regime of classically weak but quantum-mechanically strong coupling (this will be made quantitative below). For regular systems, entanglement generation is slower than for chaotic

ones, typically power-law in time [11, 15].

The purpose of this chapter is fourfold. First, we address the problem of decoherence and bipartite entanglement from a microscopic point of view, i.e. without relying on effective differential equations. This allows for a clear identification of the regime of validity of our theory. Second, we provide strong numerical evidences for the existence of a regime of Lyapunov rate of entanglement generation in bipartite systems (the numerical evidences presented in Ref. [13] were challenged in Ref. [14]). Third, we discuss our results from the point of view of the quantum-classical correspondence, and present numerical phase-space dynamics results showing that this correspondence is fully achieved in the regime of Lyapunov entanglement generation. This is, we believe, the first clear microscopic demonstration of the quantum-classical correspondence. Fourth we extended our bipartite model of the decoherence to a multipartite case. The latter extension reveals an interesting problem, yet unsolved.

5.2 Bipartite model

In order to capture the physics of decoherence, on the basis of our understanding of the entanglement generation, we consider firstly a bipartite toy model. The total universe is decomposed into a *system*, a particle labeled 0, in interaction with an *environment*, a particle labeled 1. We consider thus the Hamiltonian,

$$\mathcal{H} = H_0 \otimes \mathbb{I}_1 + \mathbb{I}_0 \otimes H_1 + \mathcal{U}_{01}. \tag{5.2}$$

in which the one-particle Hamiltonian $H_{0,1}$ dynamics is chaotic and $\mathbb{I}_{0,1}$ is the identity over the Hilbbert space of the corresponding particle. Here we only specify that the interaction potential $\mathcal{U}_{01}$ is smooth, varying over a distance much larger than the particles' de Broglie wavelength ν, and that it depends only on the distance between the particles.

We start with an initial separable density matrix $\eta(0) = |\psi_0\rangle \langle\psi_0| \otimes \eta_{env}$.

The initial state of the system is a single narrow Gaussian wave packet centred on r_0, $\psi_0(\mathbf{q}) = (\pi\nu^2)^{-d_0/4} \exp[i\mathbf{p}_0 \cdot (\mathbf{q} - \mathbf{r}_0) - |\mathbf{q} - \mathbf{r}_0|^2/2\nu^2]$. If we were only interested by the entanglement properties of our bipartite system, we would consider a similar initial state for particle 1. True environments, however, differ from single particles in that they have much shorter time scales and a much bigger Hilbert space, and they cannot be initially prepared in a pure Gaussian wavepacket. Consequently for the environment, we consider, a random mixed state $\eta_{env} = \sum_{\alpha,\beta} a_\alpha a^*_\beta |\Phi_\alpha\rangle \langle\Phi_\beta|$, with $\Phi_\alpha(\mathbf{q}) = (\pi\nu^2)^{-d_1/4} \exp[i\mathbf{p}_\alpha \cdot (\mathbf{q} - \mathbf{r}_\alpha) - |\mathbf{q} - \mathbf{r}_\alpha|^2/2\nu^2]$. This choice is used for pedagogical reasons but we are not limited by this assumption, more general states as the thermal states $\eta_{env} = \sum_n \exp[-\beta E_n] |n\rangle \langle n|$ can be used.

5.2.1 Reduced density matrix

Setting $\hbar = 1$ the two-particle density matrix evolves according to $\eta(t) = \exp[-i\mathcal{H}t]\,\eta(0)\,\exp[i\mathcal{H}t]$. The elements $\eta_0(\mathbf{x}_0, \mathbf{y}_0; t) = \int d\mathbf{x}_1 \langle \mathbf{x}_0, \mathbf{x}_1 |\, \eta(t)\, | \mathbf{y}_0, \mathbf{x}_1 \rangle$ of the reduced density matrix read,

$$\eta_0(\mathbf{x}_0, \mathbf{y}_0; t) = (\pi\nu^2)^{-\frac{d}{2}} \int \mathrm{d}\mathbf{x}_1 \prod_{i=0}^{3} \int \mathrm{d}\mathbf{q}_i \; \psi_0(\mathbf{q}_0)\psi_0^\dagger(\mathbf{q}_2) \, \langle \mathbf{q}_1 | \eta_{env} | \mathbf{q}_3 \rangle \\ \times \left\langle \mathbf{x}_0, \mathbf{x}_1 \left| e^{-i\mathcal{H}t} \right| \mathbf{q}_0, \mathbf{q}_1 \right\rangle \left\langle \mathbf{q}_2, \mathbf{q}_3 \left| e^{i\mathcal{H}t} \right| \mathbf{y}_0, \mathbf{x}_1 \right\rangle , \quad (5.3)$$

where we let $d = d_0 + d_1$.

We next introduce the two-particle semiclassical propagator

$$\left\langle \mathbf{x}_0, \mathbf{x}_1 \left| e^{-i\mathcal{H}t} \right| \mathbf{q}_0, \mathbf{q}_1 \right\rangle = (-i)^{\frac{d}{2}} \sum_{s_0, s_1} \mathcal{C}_{s_0,s_1}^{1/2} \, e^{i\left\{ S_{s_0}(\mathbf{q}_0, \mathbf{x}_0; t) + S_{s_1}(\mathbf{q}_1, \mathbf{x}_1; t) + \mathcal{S}_{s_0,s_1}(\mathbf{q}_0, \mathbf{x}_0; \mathbf{q}_1, \mathbf{x}_1; t) \right\}}, \quad (5.4)$$

which is expressed as sums over pairs of classical trajectories, labeled s_i for particle i connecting $\mathbf{q}_i$ to $\mathbf{x}_i$ in the time t with dynamics determined by H_i. Under our assumption of a classically weak coupling, classical trajectories are only determined by the one-particle Hamiltonians. Each pair of paths gives a contribution containing one-particle action integrals denoted by S_{s_i} (where we included the Maslov indices) and two-particle action integrals $\mathcal{S}_{s_0,s_1} = \int_0^t \mathrm{d}\tau \, \mathcal{U}_{01}[\mathbf{q}_{s_0}(\tau), \mathbf{q}_{s_1}(\tau)]$ accumulated along s_0 and s_1 and the real, positive determinant $\mathcal{C}_{s_0,s_1} = C_{s_0} C_{s_1}$ of the stability matrix corresponding to the two-particle dynamics in the $(d_0 + d_1)-$dimensional space [19]. We note that if $\mathcal{U}_{01}$ factorize as $\mathcal{U}_{01} = V_0 \otimes \mathbb{I}_1 + \mathbb{I}_0 \otimes V_1$, $\mathcal{S}_{s_0,s_1}(\mathbf{q}_0, \mathbf{x}_0; \mathbf{q}_1, \mathbf{x}_1; t) = S_{s_0}^{V_0}(\mathbf{q}_0, \mathbf{x}_0; t) + S_{s_1}^{V_1}(\mathbf{q}_1, \mathbf{x}_1; t)$, the two-particle action thus vanishes and no entanglement or decoherence is generated, as it should be.

Our choice of an initial Gaussian wave packet for the systems allows us to linearize the one-particle system action integrals in $\mathbf{q}_{0,2} - \mathbf{r}_0$. Since the environment is itself a superposition of Gaussian wave packets $\Phi_\alpha(\mathbf{q})$, a linearization of the one-particle environmental action integrals in $\mathbf{q}_{1,3} - \mathbf{r}_{a,b}$ can also be performed. We furthermore set $\mathcal{S}_{s_0,s_1}(\mathbf{q}_0, \mathbf{x}_0; \mathbf{q}_1, \mathbf{x}_1; t) \simeq \mathcal{S}_{s_0,s_\alpha}(\mathbf{r}_0, \mathbf{x}_0; \mathbf{r}_\alpha, \mathbf{x}_1; t)$, keeping in mind that $\mathbf{r}_0$ and $\mathbf{r}_\alpha$, taken as arguments of the two-particle action integrals, have an uncertainty $\mathcal{O}(\nu)$.

We then perform four Gaussian integrations in $\mathbf{q}_i$ to get

$$\eta_0(\mathbf{x}_0, \mathbf{y}_0; t) \;=\; (4\pi\nu^2)^{\frac{d_0}{2}} \sum_{s_0, l_0} \mathcal{F}_{s_0,l_0}(t) \, \mathcal{A}_{s_0} \mathcal{A}_{l_0}^\dagger \exp[i\varphi_0], \quad (5.5)$$

with

$$\mathcal{F}_{s_0,l_0}(t) \;=\; (4\pi\nu^2)^{\frac{d_1}{2}} \int d\mathbf{x}_1 \sum_{\alpha,\beta} a_\alpha a_\beta^* \sum_{s_\alpha, l_\beta} \mathcal{A}_{s_\alpha} \mathcal{A}_{l_\beta}^\dagger \exp[i(\varphi_1 + \varphi_{01})], \quad (5.6)$$

where we wrote $\mathcal{A}_{s_i} = C_{s_i}^{\frac{1}{2}} \exp\left[-\frac{\nu^2}{2} (\mathbf{p}_{s_i} - \mathbf{p}_i)^2 \right]$ and note that environment's paths are labeled with greek letters, the indice 0 being reserved for the system.

The functional $\mathcal{F}_{s_0,l_0}(t)$ in Eq. (5.6) is the semiclassical Feynman-Vernon influence functional [16]. Similar semiclassical expression of the Feynman-Vernon influence functional have been previously obtained by Möhring and Smilansky [17] for the special case when the system's motion is constrained to be classical.

The semiclassical expression of $\eta_0(\mathbf{x}_0, \mathbf{y}_0; t)$ is obtained by enforcing a stationary phase condition on Eq. (5.5) and Eq. (5.6), i.e keeping only terms which minimize the variation of the following three action phases,

$$\varphi_0 = S_{s_0}(\mathbf{r}_0, \mathbf{x}_0; t) - S_{l_0}(\mathbf{r}_0, \mathbf{y}_0; t) \tag{5.7a}$$
$$\varphi_1 = S_{s_\alpha}(\mathbf{r}_\alpha, \mathbf{x}_1; t) - S_{l_\beta}(\mathbf{r}_\beta, \mathbf{x}_1; t) \tag{5.7b}$$
$$\varphi_{01} = \mathcal{S}_{s_0,s_\alpha}(\mathbf{r}_0, \mathbf{r}_\alpha; \mathbf{x}_0, \mathbf{x}_1; t) - \mathcal{S}_{l_0,l_\beta}(\mathbf{r}_0, \mathbf{r}_\beta; \mathbf{y}_0, \mathbf{x}_1; t) \tag{5.7c}$$

Semiclassically, a stationary phase approximation corresponds to a path contraction. The first stationary phase approximation over φ_1 yield $s_\alpha = l_\beta$ which requires $\mathbf{r}_\alpha = \mathbf{r}_\beta$ and thus $\alpha = \beta$. Consequently $\mathcal{F}_{s_0,l_0}$ reduces to,

$$\mathcal{F}_{s_0,l_0}(t) = (4\pi\nu^2)^{\frac{d_1}{2}} \sum_{\alpha,\, s_\alpha} |a_\alpha|^2 \int \mathrm{d}\mathbf{x}_1 \, |\mathcal{A}_{s_\alpha}|^2 \, e^{i(\mathcal{S}_{s_0,s_\alpha} - \mathcal{S}_{l_0,s_\alpha})} \tag{5.8}$$

Now if we use the sum rule [7],

$$(4\pi\nu^2)^{\frac{d_i}{2}} \int \mathrm{d}\mathbf{x}_i \sum_s |\mathcal{A}_s|^2 = 1, \tag{5.9}$$

and note that on average $\sum_\alpha \langle |a_\alpha|^2 \rangle = 1$, it is straightforward to see that

$$\mathrm{Tr}_0[\eta_0(t)] = 1, \tag{5.10}$$

and

$$\eta_0(\mathbf{x}_0, \mathbf{y}_0; t) = [\eta_0(\mathbf{y}_0, \mathbf{x}_0; t)]^*, \tag{5.11}$$

as required. Enforcing a further stationary phase condition on phase φ_0 amounts to performing an average over different initial conditions,
$\langle \cdots \rangle \equiv (\Omega_0\Omega_1)^{-1} \int \mathrm{d}\mathbf{r}_0 \mathrm{d}\mathbf{r}_1 \cdots$. This results in $s_0 = l_0$, which requires $\mathbf{x}_0 \simeq \mathbf{y}_0$, and thus

$$\langle \eta_0(\mathbf{x}_0, \mathbf{y}_0; t) \rangle = \frac{\delta_{\mathbf{x}_0,\mathbf{y}_0}}{\Omega_0}, \tag{5.12}$$

with Ω_0 the spacial volume of the system. Consequently only diagonal elements of the reduced density matrix have a non vanishing average and the ergodicity is due to the average over the initial conditions.

Alltogether, these results demonstrate that the semiclassical method used preserves the main properties of the reduced density matrix, such as the unitarity and the hermicity.

5.2.2 Purity

Although only diagonal elements of the reduced density matrix have a non vanishing average, η_0 has, for each initial condition, a non vanishing off-diagonal matrix element, with a zero-centered distribution whose variance is given by $\langle \eta_0(\mathbf{x}_0, \mathbf{y}_0; t)\eta_0(\mathbf{y}_0, \mathbf{x}_0; t)\rangle$. This variance was derived in [11] in order to obtain the semiclassical purity $\mathcal{P}(t) = \mathrm{Tr}_0\,[\eta_0^2]$. The treatment presented in [11] is however not totally correct, as some contributions were missed due to an improper averaging procedure. Here we directly calculate the semiclassical purity, which is a good measure of entanglement in the case of a unitary two-particle evolution. It varies between 0 (maximally entangled states) and 1 (product states). The calculation proceeds along the lines of Ref. [11]. With the help of the bipartite semiclassical propagator Eq. (5.4), the semiclassical purity reads

$$\mathcal{P}(t) = (4\pi\nu^2)^{-d} \int \prod_{i=\{0,1\}} \mathrm{d}\mathbf{x}_i \mathrm{d}\mathbf{y}_i \sum_{\substack{s_0,k_0\\ l_0,m_0}} \mathcal{A}_{s_0}\mathcal{A}^\dagger_{l_0}\mathcal{A}_{k_0}\mathcal{A}^\dagger_{m_0} \times \sum_{\substack{\alpha,\beta,\\ \gamma,\delta}} \sum_{\substack{s_\alpha,k_\gamma\\ l_\beta,m_\delta}} a_\alpha a^*_\beta a_\gamma a^*_\delta \mathcal{A}_{s_\alpha}\mathcal{A}^\dagger_{l_\beta}\mathcal{A}_{k_\gamma}\mathcal{A}^\dagger_{m_\delta} e^{i\{\Phi_0+\Phi_1+\Phi_{01}\}} \quad (5.13)$$

with the phases,

$$\Phi_0 = S_{s_0}(\mathbf{r}_0, \mathbf{x}_0; t) - S_{l_0}(\mathbf{r}_0, \mathbf{y}_0; t) + S_{k_0}(\mathbf{r}_0, \mathbf{y}_0; t) - S_{m_0}(\mathbf{r}_0, \mathbf{x}_0; t) \quad (5.14a)$$

$$\Phi_1 = S_{s_\alpha}(\mathbf{r}_\alpha, \mathbf{x}_1; t) - S_{l_\beta}(\mathbf{r}_\beta, \mathbf{x}_1; t) + S_{k_\gamma}(\mathbf{r}_\gamma, \mathbf{y}_1; t) - S_{m_\delta}(\mathbf{r}_\delta, \mathbf{y}_1; t) \quad (5.14b)$$

$$\Phi_{01} = \mathcal{S}_{s_0,s_\alpha} - \mathcal{S}_{l_0,l_\beta} + \mathcal{S}_{k_0,k_\gamma} - \mathcal{S}_{m_0,m_\delta} \quad (5.14c)$$

The expression of Eq. (5.13) is depicted in Fig. 5.1. Classical trajectories are represented by a full line, with an arrow indicating the direction of propagation. Each particle is delimited by a disk.

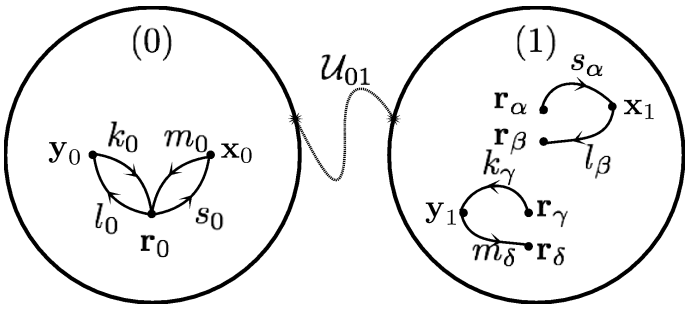

Figure 5.1: Diagrammatic representation of the purity.

In the semiclassical limit Eq. (5.13) is again dominated by terms which satisfy a stationary phase condition, i.e. where the variation of the action phase differences Φ_0, Φ_1, Φ_{01} has to be minimized. These stationary phase terms can be

easily identified from the diagrammatic representation as those where two classical trajectories s and l of opposite direction of propagation are *contracted*, i.e. $s = l$, up to a quantum resolution given by the wavelength ν.

As we consider the weak coupling regime, where the one-particle actions vary faster than their two-particle counterparts. We thus perform a stationary phase approximation on the one-particle actions. Firstly stationary phase approximation over Φ_0 corresponds to setting $s_0 = m_0$ and $k_0 = l_0$, which leads to an exact cancellation of $\Phi_0 = 0$. A similar procedure for Φ_1 corresponds to setting $s_\alpha = l_\beta$ and $k_\gamma = m_\delta$, which requires $\mathbf{r}_\alpha = \mathbf{r}_\beta$ and $\mathbf{r}_\gamma = \mathbf{r}_\delta$. It follows that only diagonal contributions are preserved, and $\Phi_1 = 0$. The semiclassical purity $\mathcal{P}(t)$ can be expressed over only four sets of classical trajectories s_0, k_0, s_α, k_γ and the two-particle phase Φ_{01} reduces to,

$$\delta\Phi_{01} = \mathcal{S}_{s_0,s_\alpha} - \mathcal{S}_{k_0,s_\alpha} + \mathcal{S}_{k_0,k_\delta} - \mathcal{S}_{s_0,k_\delta} \tag{5.15}$$

and the semiclassical purity is given by,

$$\mathcal{P}_{\rm sc}(t) = \Bigg\langle (4\pi\nu^2)^d \int \prod_{i=\{0,1\}} d\mathbf{x}_i d\mathbf{y}_i \sum_{s_0,k_0} |\mathcal{A}_{s_0}|^2 |\mathcal{A}_{k_0}|^2 \times \sum_{\alpha,\gamma} \sum_{s_\alpha,k_\gamma} |a_\alpha|^2 |a_\gamma|^2 \, |\mathcal{A}_{s_\alpha}|^2 \left|\mathcal{A}_{k_\gamma}\right|^2 \exp[i\delta\Phi_{01}] \Bigg\rangle \tag{5.16}$$

The analysis of Eq. (5.16) delivers three time-dependent contributions that dominate semiclassically; the *quantum contribution*, the *classical contribution* from the system and from the environment. The *long-time saturation* is also obtained and decomposed into a system contribution and environment contribution.

Quantum contribution

The quantum contribution corresponds to the non-diagonal terms, in which all paths are uncorrelated. For long enough times $\tau \geq \tau_*$, the phases $\delta\Phi_{01}$ fluctuate randomly and exhibit no correlation between different trajectories. This time τ_* is defined by

$$\left| \int_0^{\tau_*} \mathrm{d}\tau \, \mathcal{U}_{01}[\mathbf{q}_s(\tau), \mathbf{q}_l(\tau)] \right| = 1 \tag{5.17}$$

for a typical trajectories s, l. Eq. (5.17) corresponds to a sufficient accumulation of phase $\mathcal{S}_{s,l}$. One then applies a separation of the phase and amplitude average in Eq. (5.16) and uses the Central Limit Theorem (CLT) to find $\left\langle e^{i\delta\Phi_{01}} \right\rangle = e^{-2\left\langle \mathcal{S}^2_{s_0,s_\alpha} \right\rangle}$, where

$$\left\langle \mathcal{S}^2_{s_0,s_\alpha} \right\rangle = \int_0^t \mathrm{d}\tau \mathrm{d}\tau' \left\langle \mathcal{U}_{01}\left[\mathbf{q}_{s_0}(\tau), \mathbf{q}_{s_\alpha}(\tau)\right] \mathcal{U}_{01}\left[\mathbf{q}_{s_0}(\tau'), \mathbf{q}_{s_\alpha}(\tau')\right] \right\rangle , \tag{5.18}$$

is the interaction correlator. In hyperbolic systems, correlators typically decay exponentially $\propto e^{\eta|\tau-\tau'|}$ with an upper bound on η set by the smallest positive Lyapunov exponent [18], thus $\left\langle \mathcal{S}^2_{s_0,s_\alpha} \right\rangle \simeq \Gamma_{01} t$. An RMT calculation can identify this decay with the golden rule spreading of eigenstates of the total two-particle Hamiltonian $\mathcal{H}$ over those of the non-interacting one $H_0 + H_1$. Finally using the two sum rules

$$\left\langle (4\pi\nu^2)^{\frac{d_i}{2}} \int \mathrm{d}\mathbf{x}_i \sum_{s_0} |\mathcal{A}_{s_0}|^2 \right\rangle = 1, \tag{5.19a}$$

$$\left\langle (4\pi\nu^2)^{\frac{d_i}{2}} \int \mathrm{d}\mathbf{x}_i \sum_{\alpha} \sum_{s_\alpha} |a_\alpha|^2 |\mathcal{A}_{s_\alpha}|^2 \right\rangle = 1, \tag{5.19b}$$

one obtains the nondiagonal quantum contribution to the semiclassical purity,

$$\mathcal{P}_{\mathrm{sc}_1}(t) \;=\; \exp\left[-2\Gamma_{01} t\right]. \tag{5.20}$$

Classical contribution from the system

The system's diagonal contribution corresponds to $s_0 \simeq k_0$ which requires $\mathbf{x}_0 \simeq \mathbf{y}_0$. From Eq. (5.16) it reads

$$\mathcal{P}_{\mathrm{sc}_2}(t) = \left\langle (4\pi\nu^2)^d \int \prod_{i=\{0,1\}} \mathrm{d}\mathbf{x}_i \mathrm{d}\mathbf{y}_i \, \delta_\nu \left(|\mathbf{x}_0 - \mathbf{y}_0|\right) \sum_{s_0} |\mathcal{A}_{s_0}|^4 \right.$$
$$\left. \times \sum_{\alpha,\gamma} \sum_{s_\alpha, k_\gamma} |a_\alpha|^2 |a_\gamma|^2 \; |\mathcal{A}_{s_\alpha}|^2 \left|\mathcal{A}_{k_\gamma}\right|^2 e^{i\left[\Delta_0 \mathcal{S}_{s_0,s_\alpha} - \Delta_0 \mathcal{S}_{s_0,k_\gamma}\right]} \right\rangle \tag{5.21}$$

where

$$\Delta_0 \mathcal{S}_{s_0,s_\alpha} = \int_0^t \mathrm{d}\tau \; \nabla_0 \mathcal{U}_{01}[\mathbf{q}_{s_0}(\tau), \mathbf{q}_{s_\alpha}(\tau)] \cdot [\mathbf{q}_{k_0}(\tau) - \mathbf{q}_{s_0}(\tau)] \tag{5.22}$$

arises from the linearization of $\mathcal{U}_{01}$ on $k_0 \simeq s_0$ [7, 10], and $\mathbf{q}_{s_0}(\tau)$ lies on s_0 with $\mathbf{q}_{s_0}(0) = \mathbf{r}_0$ and $\mathbf{q}_{s_0}(t) = \mathbf{x}_0$. In Eq. (5.21) the integrations are restricted by $|\mathbf{y}_0 - \mathbf{x}_0| \leq \nu$ because of the finite resolution with which two paths can be equated.

Due to the non correlation of the environment'paths we obtain, $\langle \Delta_0 \mathcal{S}_{s_0,s_\alpha} \Delta_0 \mathcal{S}_{s_0,k_\gamma} \rangle = 0$. One may thus apply a separation of the phase and amplitude averages and use the CLT, this yields

$$\left\langle e^{i(\Delta_0 \mathcal{S}_{s_0,s_\alpha} - \Delta_0 \mathcal{S}_{s_0,k_\gamma})} \right\rangle = e^{-\left\langle [\Delta_0 \mathcal{S}_{s_0,s_\alpha}]^2 \right\rangle}.$$

$\langle \Delta_0 \mathcal{S}^2_{s_0,s_\alpha} \rangle$ can be expressed with the force correlator,

$$\langle \Delta_0^2 \mathcal{S}_{s_0,s_\alpha} \rangle = \int d\tau d\tau' \sum_{i,j=1}^{d_0} \langle \delta q_i(\tau) \delta q_j(\tau') \rangle \left\langle \frac{\partial \mathcal{U}_{01}[\mathbf{q}_{s_0}(\tau), \mathbf{q}_{s_\alpha}(\tau)]}{\partial q_{s_0,\,i}(\tau)} \frac{\partial \mathcal{U}_{01}[\mathbf{q}_{s_0}(\tau'), \mathbf{q}_{s_\alpha}(\tau')]}{\partial q_{s_0,\,j}(\tau')} \right\rangle,$$

with $\delta\mathbf{q}(\tau) = \mathbf{q}_{k_0}(\tau) - \mathbf{q}_{s_0}(\tau)$. We assume from now on a fast decay of the correlation,

$$\left\langle \frac{\partial \mathcal{U}_{01}[\mathbf{q}_{s_0}(\tau), \mathbf{q}_{s_\alpha}(\tau)]}{\partial q_{s_0,\,i}(\tau)} \frac{\partial \mathcal{U}_{01}[\mathbf{q}_{s_0}(\tau'), \mathbf{q}_{s_\alpha}(\tau')]}{\partial q_{s_0,\,j}(\tau')} \right\rangle \propto \frac{\gamma_0}{2}\,\delta_{ij}\,\delta(\tau-\tau'), \tag{5.23}$$

This particular shape for the correlator is taken here in order to simplify the discussion, however a more realistic exponential or power law time dependence can be considered with no qualitative changes in the following derivation. Since the distance between two initially close points increases exponentially with time for chaotic dynamics we have $|\delta\mathbf{q}(\tau)| = \exp[\lambda_0(\tau - t)]|\mathbf{y}_0 - \mathbf{x}_0|$ between the intermediate points of the trajectories [7]. The extra phase can now be evaluated and gives for the long time limit $\frac{\gamma_0}{\lambda_1}|\mathbf{y}_0 - \mathbf{x}_0|^2$. Performing now a change of coordinates $\int d\mathbf{x}_0 \sum C_{s_0} = \int d\mathbf{p}_0$ in Eq. (5.21), and using the asymptotic limit $C_{s_0} \propto e^{-\lambda_0 t}$ [6,19] valid for chaotic systems with Lyapunov exponent λ_0, one gets after performing all the integrations, and using the two sum rules of Eqs. (5.19),

$$\mathcal{P}_{\mathrm{sc}_2}(t) \;=\; \alpha_0(t)\exp[-\lambda_0 t], \tag{5.24}$$

This term is classical and decays with the system's Lyapunov exponents λ_0. It does not exist at short times $t < \tau_{\lambda_0}$, $\tau_{\lambda_0} = \lambda_0^{-1}\ln[\lambda_0/\nu^2\gamma_0]$ and has a prefactor $\alpha_0(t) = \alpha_0\, t^{-d}\Theta_{\tau_{\lambda_0}}(t)$ with $\alpha_0 = \mathcal{O}(1)$.

Classical contribution from the environment

The last time-dependent contribution corresponds to a full contraction of the environmental paths, i.e $s_\alpha \simeq k_\delta$ which requires $\mathbf{x}_1 \simeq \mathbf{y}_1$ and $\mathbf{r}_\alpha = \mathbf{r}_\delta$. It reads

$$\mathcal{P}_{\mathrm{sc}_3}(t) = \left\langle (4\pi\nu^2)^d \int \prod_{i=\{0,1\}} d\mathbf{x}_i d\mathbf{y}_i\, \delta_\nu\left(|\mathbf{x}_1 - \mathbf{y}_1|\right) \sum_{s_0,k_0} |\mathcal{A}_{s_0}|^2\, |\mathcal{A}_{k_0}|^2 \right.$$
$$\left. \times \sum_\alpha \sum_{s_\alpha} |a_\alpha|^4\, |\mathcal{A}_{s_\alpha}|^4\, e^{i\left[\Delta_1\mathcal{S}_{s_0,s_\alpha} - \Delta_1\mathcal{S}_{k_0,s_\alpha}\right]} \right\rangle \tag{5.25}$$

We note that on average $\langle |a_\alpha|^4\rangle \simeq \frac{1}{V_1^2}$, where V_1 is number of Gaussians considered in the initial state η_{env}. This number corresponds to the environment Hilbert space size for a complete continuous set of Gaussians. Following the same procedure used for the previous contribution we end up with,

$$\mathcal{P}_{\mathrm{sc}_3}(t) = \frac{\alpha_1(t)}{V_1}\exp[-\lambda_1 t] \tag{5.26}$$

The interpretation of Eq. (5.26) is straightforward, this is the classical contribution to the purity of the environment. Contrary to $\mathcal{P}_{\mathrm{sc}_2}(t)$, we have a prefactor V_1^{-1}. This is due to the indetermination of the environment's initial state. This contribution drops out for a a sufficiently large environment. Moreover this cancelation is enforced by taking $\lambda_1 \gg \lambda_0$, which is reasonable for an environment in which time scales must be shorter than the system's time scales.

Long time saturation contributions

The saturation of the purity is given by two terms. The first one is the system's saturation contribution and it corresponds to setting $s_0 = l_0$ and $k_0 = m_0$ in Eq. (5.14a) which requires $\mathbf{x}_0 \simeq \mathbf{y}_0$ and leads to an exact cancellation of all phases Φ_0, Φ_1, Φ_{01}. It reads,

$$\mathcal{P}_{\mathrm{sat}_1}(t) = \left\langle (4\pi\nu^2)^d \int \prod_{i=\{0,1\}} d\mathbf{x}_i d\mathbf{y}_i \, \delta_\nu \left(|\mathbf{x}_0 - \mathbf{y}_0|\right) \sum_{s_0,k_0} |\mathcal{A}_{s_0}|^2 \, |\mathcal{A}_{k_0}|^2 \right. \\ \left. \times \sum_{\alpha,\gamma} \sum_{s_\alpha,k_\gamma} |a_\alpha|^2 |a_\gamma|^2 \, |\mathcal{A}_{s_\alpha}|^2 \left|\mathcal{A}_{k_\gamma}\right|^2 \right\rangle \tag{5.27}$$

The integrations, again, have to be performed with $|\mathbf{x}_0 - \mathbf{r}_0| \leq \nu$. We incorporate this restriction into the calculation by making the ergodicity assumption, setting

$$\left\langle \int \prod_{i=\{0,1\}} \mathrm{d}\mathbf{x}_i \mathrm{d}\mathbf{y}_i \ldots \delta_\nu \left(|\mathbf{x}_0 - \mathbf{y}_0|\right) \right\rangle = \frac{1}{N_0} \left\langle \int \prod_{i=\{0,1\}} \mathrm{d}\mathbf{x}_i \mathrm{d}\mathbf{y}_i \ldots \right\rangle \Theta_{\tau_{\mathrm{E}}^{(0)}}(t), \tag{5.28}$$

which is valid for times larger than the Ehrenfest time $\tau_{\mathrm{E}}^{(0)} = \lambda_0^{-1} \ln[N_0]$ [20, 21], with N_0 the system's Hilbert space size. For shorter times, $t < \tau_E^{(0)}$, $\mathcal{P}_{\mathrm{sat}_1}(t)$ is included in $\mathcal{P}_{\mathrm{sc}_2}(t)$.

The use of the sum rule Eq. (5.19) gives

$$\mathcal{P}_{\mathrm{sat}_1}(t) = \frac{1}{N_0} \Theta_{\tau_E^{(0)}}(t). \tag{5.29}$$

Similarly the environmental saturation contribution corresponds to $s_\alpha = m_\delta$ and $k_\gamma = l_\beta$ which requires $\mathbf{x}_1 \simeq \mathbf{y}_1$ and $\mathbf{r}_\alpha = \mathbf{r}_\delta$, $\mathbf{r}_\beta = \mathbf{r}_\gamma$ and gives also a total cancelation of phases, thus

$$\mathcal{P}_{\mathrm{sat}_2}(t) = \frac{1}{N_1} \Theta_{\tau_E^{(1)}}(t). \tag{5.30}$$

Note that for $t < \tau_E^{(1)}$, this contribution does not exist by itself and is included in the $\mathcal{P}_{\mathrm{sc}_3}(t)$

Semiclassical results

According to our semiclassical derivation the purity is given to leading order by the sum of five terms of Eq. (5.20), (5.24), (5.26), (5.29) and (5.30),

$$\mathcal{P}_{sc}(t) = e^{-2\Gamma_{01}t} + \alpha_0(t) e^{-\lambda_0 t} + \frac{\alpha_1(t)}{V_1} e^{-\lambda_1 t} + \sum_{i=0}^{1} \frac{\Theta_{\tau_E^{(i)}}(t)}{N_i}, \tag{5.31}$$

The regime of validity of our semiclassical approach is given by $\delta_2 \leq \Gamma_{01} \leq B_2$, where B_2 and δ_2 are the two-particle bandwidth and level spacing respectively [8]. In this range, $\mathcal{U}_{01}$ are quantum-mechanically strong as individual levels are broadened beyond their average spacing, but classically weak, as B_2 is unaffected by $\mathcal{U}_{01}$ [7, 8].

We consider now the limit V_1, $N_1 \mapsto \infty$ and $\lambda_1 \gg \lambda_0$ of a large environment. Since Eq. (5.31) is a sum of exponentials, only the exponential with the minimal exponent survives. Eq. (5.31) distinguishes 2 regimes for the decay of the purity and the saturation :

1. The Golden rule exponential decay, $\mathcal{P}(t) \propto e^{-2\Gamma_{01}t}$, if $d_2 \leq \Gamma_{01} \leq \lambda_0$. It corresponds to a purely quantum regime generated by the coupling with the environment

2. The System's Lyapunov exponential decay, $\mathcal{P}(t) \propto e^{-\lambda_0 t}$, if $\lambda_0 \leq \Gamma_{01}$. It corresponds to a purely classical regime generated by the system's classical dynamics

3. The asymptotic saturation $\mathcal{P}(t) = N_0^{-1}$

5.2.3 Numerical simulation

We numerically check our results. We consider the Hamiltonian of Eq. (5.2) for two coupled kicked rotators

$$H_i = p_i^2/2 + K_i \cos(x_i) \sum_n \delta(t - nT), \tag{5.32a}$$

$$\mathcal{U}_{01} = \epsilon \sin(x_1 - x_2 - 0.33) \sum_n \delta(t - nT). \tag{5.32b}$$

The interaction potential $\mathcal{U}_{01}$ is long-ranged with a strength ϵ and acts at the same time as the kicks. Upon increasing K_i the classical dynamics of the i^{th} particle varies from fully integrable ($K_i = 0$) to fully chaotic [$K_i \geq 7$, with Lyapunov exponent $\lambda_i \approx \ln(K_i/2)$]. For $1 < K_i < 7$ the dynamics is mixed, i.e. stable and unstable motion coexist. We will vary $K_i \in [3, 12]$ to get a maximal variation of λ_i, while making sure that both ψ_1 and ψ_2 lie in the chaotic sea. We follow the usual quantization procedure on the torus $x_i, p_i \in [-\pi, \pi[$. The purity is computed for discrete time $t = n$ as,

$$\mathcal{P}(n) = \mathrm{Tr}_0 \left[\mathrm{Tr}_1^2 \left[\big(F\big)^n \eta(0) \big(F^*\big)^n \right] \right] \tag{5.33}$$

The Floquet operator F is an $M \times M$, ($M = N_0 N_1$, $\hbar_{\text{eff}} = 2\pi/\sqrt{N_0 N_1}$) unitary symmetric matrix. In angular momentum representation it has elements

$$F^{k_0' k_1'}_{k_0 k_1} = e^{-i\frac{\pi}{N_0}(k_0^2+k_0'^2)-i\frac{\pi}{N_1}(k_1^2+k_1'^2)}(UQU^\dagger)^{k_0' k_1'}_{k_0 k_1}, \tag{5.34a}$$

$$U^{k_0' k_1'}_{k_0 k_1} = N_0^{-1/2} e^{i\frac{2\pi}{N_0}k_0 k_0'} N_1^{-1/2} e^{i\frac{2\pi}{N_1}k_1 k_1'}, \tag{5.34b}$$

$$Q^{k_0' k_1'}_{k_0 k_1} = \delta_{k_0 k_0'} e^{-i\frac{N_0}{2\pi}K_0 \cos\left(\frac{2\pi}{N_0}k_0'\right)} \delta_{k_1 k_1'} e^{-i\frac{N_1}{2\pi}K_1 \cos\left(\frac{2\pi}{N_1}k_1'\right)} + e^{-i\frac{\epsilon}{\hbar_{\text{eff}}}\sin\left(\hbar_{\text{eff}}(k_1'-k_0')-0.33\right)}. \tag{5.34c}$$

Numerically the time evolved density matrix is computed by recursive calls to a fast Fourier transform routine [23]. Thanks to this algorithm only $\mathcal{O}(M \ln M)$ operations are required, which allowed us to reach system sizes up to $N_{0,1} = 2048$, more than one order of magnitude larger than any previously investigated case.

We first restrict ourselves to the chaotic case, where we consider the least reasonable model for the environment, roughly speaking two identical particles with a similar initial state. This is sufficient to confirm our main result Eq. (5.31). Setting $N_0 = N_1 = M$, $\hbar_{\text{eff}} = 2\pi/M$ the bandwidth and level spacing are given by $B_2 = 4\pi$ and $\delta_2 = 4\pi/M^2$.

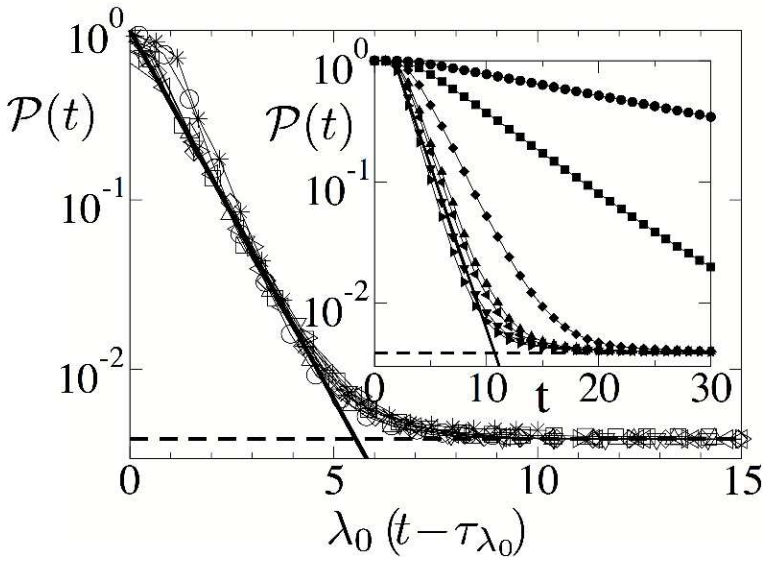

Figure 5.2: Main plot: Purity of the reduced density matrix for $N_0 = N_1 = 512$, $K_0 = K_1 \in [4, 12]$, and $\hbar_{\text{eff}}^{-1}\epsilon = 4$ giving $2\Gamma_{01} = 13.6 \gg \lambda_0 = \lambda_1$. Data have been calculated from 20 different initial states. The time axis has been shifted by the onset time τ_{λ_0} (see text) and rescaled with $\lambda_0 \in [0.5, 1.35]$. The full line indicates $\propto \exp[-\lambda_0 t]$, and the dashed line gives the asymptotic saturation $\mathcal{P}(\infty) = 2N_0^{-1}$. Inset: Purity for $K_0 = K_1 = 5.09$ for $\hbar_{\text{eff}}^{-1}\epsilon = 0.2$ (circles), 0.4 (squares), 0.8 (diamonds), 1.6, 2, 3 and 4 (triangles).

The behavior of $\mathcal{P}(t)$ is shown in Fig. 5.2. As ϵ increases, the rate of decoherence also increases, up to some value ϵ_c, after which it saturates. We have found that (i) prior to saturation, $\mathcal{P}(t)$ decays exponentially with a rate $\approx 0.85\epsilon^2\hbar_{\rm eff}^{-2}$, provided $\Gamma_{01} = 0.43\epsilon^2\hbar_{\rm eff}^{-2} > \delta_2$ is satisfied, and that (ii) ϵ_c behaves consistently with Eq.(5.31). Second, Fig. 5.2 shows that, for fixed $\epsilon > \epsilon_c$, the rescaling of the time axis $t \to \lambda_0 t$ allows to bring together six curves with $\lambda_0 = \lambda_1 \in [0.5, 1.35]$, varying by almost a factor three. This confirms the existence of the Lyapunov regime of purity decay.

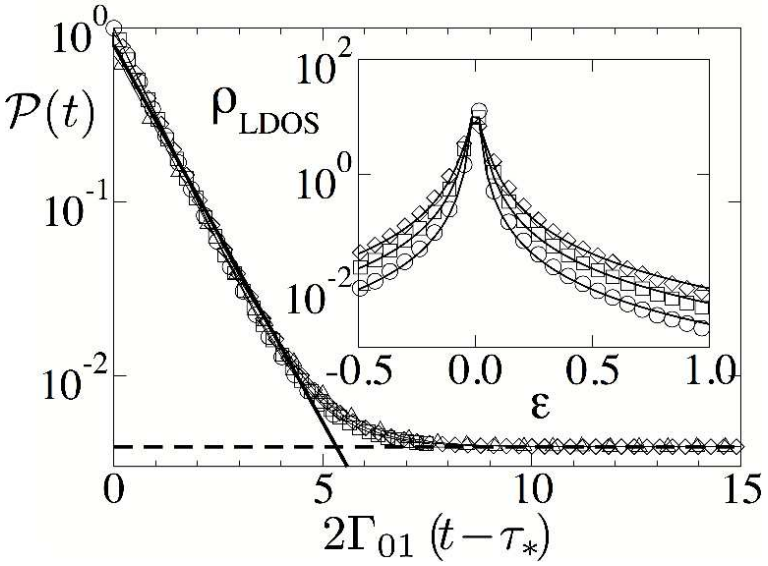

Figure 5.3: Main plot: Purity of the reduced density matrix for $N_0 = N_1 = 512$ in the the golden rule regime $\Gamma_{01} \gtrsim \lambda_i$ as a function of $\Gamma_{01} \approx 0.85\epsilon^2\hbar_{\rm eff}^{-2}$, for $K_0 = K_1 = 50.09$, with $\hbar_{\rm eff}^{-1}\epsilon = 0.06$ (circles), 0.3 (squares), 0.6 (diamonds) and 0.9 (triangles). Data have been calculated from 20 different initial states. The time axis has been shifted by the onset time τ_* and rescaled with $2\Gamma_{01} \in [5.\,10^{-2}, 8.\,10^{-1}]$. The full line indicate the decays$\propto \exp[2\Gamma_{01}t]$ with $\Gamma_{01} \simeq 0.43\ \epsilon^2\hbar_{\rm eff}^{-2}$. The dashed line gives the saturation $\mathcal{P}(\infty) = 2N_0^{-1}$. Inset: local spectral density of states $\rho_{LDOS}(\epsilon)$ of eigenstates of an uncoupled double kicked rotator with $K_0 = K_1 = 50.09$ over the eigenstates of an coupled double kicked rotator with the same kicks strength. System size is $N = 64$, with $\hbar_{\rm eff}^{-1}\epsilon = 0.1$ (circles), 0.2 (squares), 0.3 (diamonds). The solid lines are Lorentzian with widths $\Gamma_{01} \approx 0.07$, 0.016 and 0.042 in agreement with the formula $\Gamma_{01} = 0.43\ \epsilon^2\hbar_{\rm eff}^{-2}$.

Third we focus on the study of $\mathcal{P}(t)$ in the Fermi golden rule regime in Fig. 5.3. We show in the inset the behavior of the local spectral density

$$\rho_{LDOS}(\epsilon) \;=\; \sum_\alpha |\langle 0_\alpha, 1_\alpha|a\rangle|^2 \delta(\epsilon - E_a + \epsilon_\alpha^{(0)} + \epsilon_\alpha^{(1)}), \tag{5.35}$$

of eigenstates $\{|0_\alpha, 1_\alpha\rangle\}$ of $\sum_i H_i$ (with quasienergy eigenvalues $\sum_i \epsilon_\alpha^{(i)}$) over the eigenstates $\{|a\rangle\}$ of $\mathcal{H}$ (with quasienergy eigenvalues E_a). The local spectral

density $\rho_{LDOS}(\epsilon)$ has a Lorentzian shape with a width given by $\Gamma_{01} \approx 0.43\epsilon^2\hbar_{\text{eff}}^{-2}$. Having extracted the ϵ dependence of Γ_{01}, we next plot the purity $\mathcal{P}(t)$ in the main part of Fig. 5.3. The rescaling of the time axis $t \to 2\Gamma_{01}t$ with $2\Gamma_{01} \in [5.\,10^{-2},\, 8.\,10^{-1}]$ allows us to bring together four curves, varying by more than a factor ten. This confirms the existence of the Fermi Golden Rule regime of purity decay.

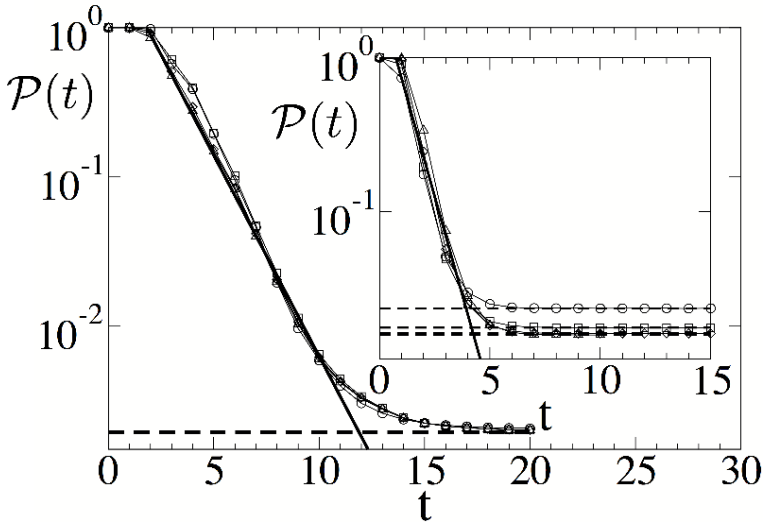

Figure 5.4: Main plot: Purity of the reduced density matrix for $N_0 = N_1 = 512$ in the the golden rule regime $\Gamma \ll \lambda_0$ as a function of t, for $K_0 = 5.09$, $N = 1024$ $\hbar_{\text{eff}}^{-1}\epsilon = 2$ with $K_1 = 5.09$, (circles), 10.09 (squares), 20.09 (diamonds), 50.09 (triangles). Data have been calculated from 20 different initial states. The full line indicates the decay $\propto \exp[-\lambda_0 t]$. The dashed line gives the saturation $\mathcal{P}(\infty) = 2N_0^{-1}$. Inset : Purity $\mathcal{P}(t)$ in the regime $\Gamma \ll \lambda_0$ as a function of t, for $K_0 = 10.09$, $K_1 = 50.09$, $N_0 = 64$ $\hbar_{\text{eff}}^{-1}\epsilon = 4$ with $N_1 = 128$ (circles), 512 (squares), 2048 (diamonds) 8192 (triangles). Data have been calculated from 20 different initial states. The full line indicates the decay $\propto \exp[-\lambda_0 t]$. The dashed lines give the saturation $\mathcal{P}(\infty) = N_0^{-1} + N_1^{-1}$.

Finally Fig. 5.4 is devoted to the confirmation of the environment's Lyapunov independence of the Purity. The main plot shows the behavior of the purity in the limit $\lambda_0 \ll \lambda_1$. With no rescaling and $\lambda_0 \simeq 0.97$, $\lambda_1 \in [0.97, 3.2]$ we show that four curves varying by almost a factor three have the same decay given by the system's Lyapunov exponent. In the inset we considere the limit $N_0 \ll N_1$, for $N_1 \in [64, 8192]$, all curve behave in accordance to our main result Eq. (5.31). Moreover we have a confirmation of the asymptotic value of the saturation $\mathcal{P}(\infty) = N_0^{-1} + N_1^{-1}$ obtained for a finite size of the environment. Also confirmed, in Fig. 5.2, Fig. 5.3 for the particular regime $N_0 = N_1$, is that $\mathcal{P}(t \to \infty) = 2N_0^{-1}$.

These numerical data thus confirm our analytical results.

5.2.4 Quantum-classical correspondance

The purity measures the weight of off-diagonal elements of $\eta_0(t)$, and hence the importance of coherent effects. In the regime $2\Gamma_{01} \gg \lambda_0$, $\mathcal{P}(t)$ reaches its minimal value at the Ehrenfest time $\tau_{\rm E}^{(0)} = \lambda_0^{-1} \ln N_0$, and thus, quantum effects that traditionally dominate the dynamics after the Ehrenfest time are killed before they have a chance to appear. In that regime, one thus expects the quantum-classical correspondence to become perfect in the semiclassical limit $N_{0,1} \to \infty$.

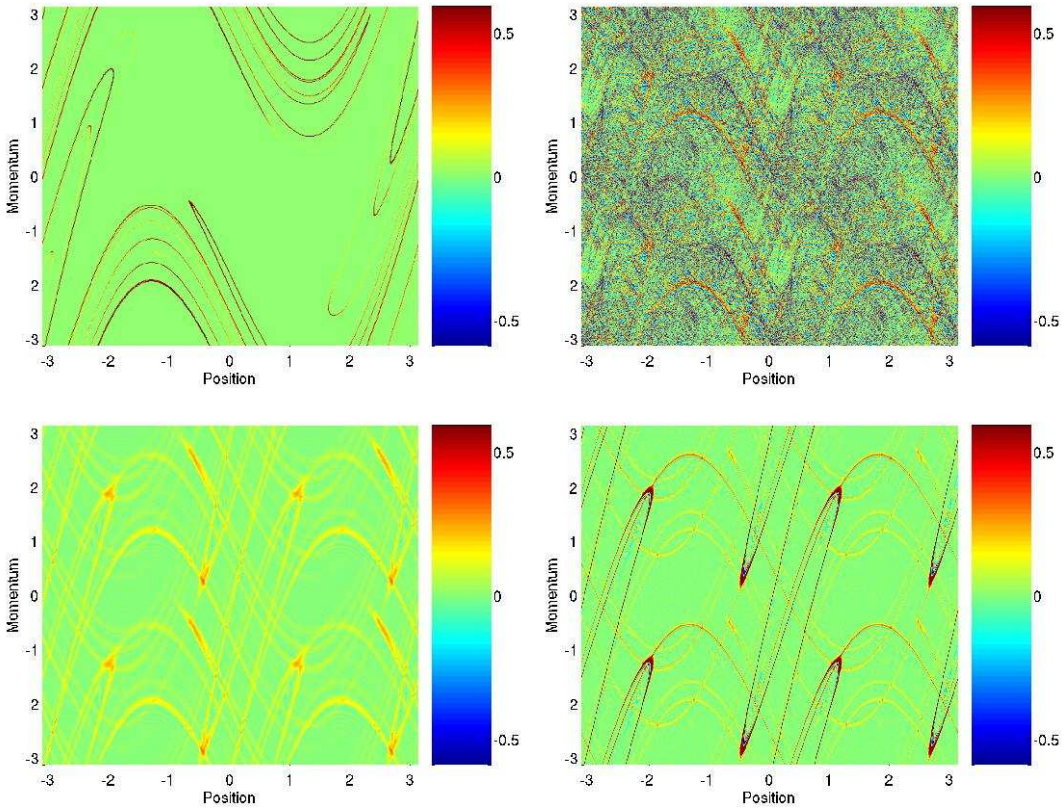

Figure 5.5: Phase-space plots for a classical distribution (top left), uncoupled (top right) and coupled (bottom left and right, $\hbar_{\rm eff}^{-1}\epsilon = 4$) quantum Wigner distributions, after five iterations of the coupled kicked rotator map with $K_1 = 3.09$ (fully chaotic regime, see text). The initial distributions are Gaussian centered in the chaotic sea at $(x, p) = (1, 2)$. In the bottom panels, the system is coupled to a second kicked rotator with $K_2 = 100$. One has $2\Gamma = 13.6 > \lambda_2 \gg \lambda_1$, and hence $\mathcal{P}(t) \simeq \exp[-\lambda_1 t]$. The left panel has $N_1 = N_2 = 512$ and the right panel has $N_1 = N_2 = 2048$.

This fact is numerically illustrated with the help of Wigner function's dynamics in phase space. Fig. 5.5 compares the time-evolution of a classical distribution (top left), with that of the Wigner function

$$W_0(\mathbf{p}, \mathbf{q}; t) = (2\pi\hbar)^{-d/2} \int \mathrm{d}\mathbf{x} \exp[i\mathbf{p}\mathbf{x}] \eta_0(\mathbf{q} + \mathbf{x}/2, \mathbf{q} - \mathbf{x}/2; t), \tag{5.36}$$

which are both quantum-mechanically evolved from a localized wavepacket with the same initial location and extension. Three quantum phase-space plots are shown: (i) (top right) for a free system, $\epsilon = 0$; (ii) and (iii) (bottom left and right) for a coupled system $\hbar^{-1}\epsilon = 4$, in the regime $\mathcal{P}(t) \simeq \exp[-\lambda_0 t]$. The bottom left panel has a system size $N_1 = N_2 = 512$ while the bottom right panel has $N_1 = N_2 = 2048$. All plots show phase-space distributions after 5 kicks. Quantizing the system on a torus results in the emergence of four-fold ghost images in the Wigner function, which have no physical content. They are artifacts of the phase-space boundary conditions, resulting from two reflections of the physical part of the distribution against the $x = 0$ and $p = 0$ axis [22]. Disregarding these four-fold ghost images, two things are clear from Fig. 5.5. First, a coupling is necessary and sufficient to achieve phase-space quantum-classical correspondence. Second, the correspondence becomes better as we move deeper in the semiclassical regime, This numerically confirms that in the regime of Lyapunov entanglement, there is complete quantum-classical correspondence in the semiclassical limit.

5.3 Multipartite model

5.3.1 Rescaling of the bipartite model

The knowledge gained from the investigations of decoherence in the bipartite study, can be applied to a more complex model; a system under the influence of N other dynamical interacting systems. Fundamentally we still consider a bipartite system, but add some complexity in the internal structure of the environment. Consequently in order to make a comparison with the initial model we need to introduce a rescaling of the strength of multipartite interaction. Since in the quantum regime both the influence functional and the purity are related to the Fermi Golden rule spreading, the physical picture requires a rescaling of the interaction by a factor $\frac{1}{\sqrt{N}}$ that is related to the number of direct links between the system and the environment.

We thus consider the following many-body Hamiltonian,

$$\mathcal{H}^{(N)} = \sum_{i=0}^{N} H_i \bigotimes_{j\neq i}^{N} \mathbb{I}_j + \sum_{i=0}^{N} \sum_{j>i} \frac{1}{\sqrt{N}} \mathcal{U}_{ij} \tag{5.37}$$

The one-particle hamiltonian H_i describes a chaotic dynamics. We stress that we use only bipartite interaction but the complete set of all possible interactions. Each interaction potential $\mathcal{U}_{ij}$ is smooth, varying over a distance much larger than the particle's de Broglie wavelength ν, and depends only on the distance between the particles i and j.

We consider an initial fully separable density matrix $\eta^{(N)}(0) = \bigotimes_{i=0}^{N} |\psi_i\rangle\langle\psi_i|$. In order to simplify the investigations, the initial state of each particle i is a

narrow Gaussian wave packet centered on $(\mathbf{r}_i,\ \mathbf{p}_i)$, i.e $\psi_i(\mathbf{q}) = (\pi\nu^2)^{-d_i/4}\exp[i\mathbf{p}_i\cdot(\mathbf{q}-\mathbf{r}_i) - |\mathbf{q}-\mathbf{r}_i|^2/2\nu^2]$.

5.3.2 Influence functional

The generalization of the two-particle semiclassical propagator Eq. (5.4) to the $N+1$ case is straightforward. The semiclassical multipartite propagator is expressed as sum over $N+1$ classical trajectories and can be written as,

$$\begin{aligned}&\left\langle \mathbf{x}_0,\cdots,\mathbf{x}_N\left|e^{-i\mathcal{H}t}\right|\mathbf{z}_0,\cdots,\mathbf{z}_N\right\rangle \\ &\quad=(-i)^{\frac{d}{2}}\sum_{s_0\cdots s_N}C^{1/2}_{s_0\cdots s_N}e^{i\left\{S_{s_0}(\mathbf{z}_0,\mathbf{x}_0;t)+\sum_{i=1}^N S_{s_i}(\mathbf{z}_i,\mathbf{x}_i;t)+\sum_{i=0}^N\sum_{j>i}\mathcal{S}_{s_i,s_j}(\mathbf{z}_i,\mathbf{x}_i;\mathbf{z}_j,\mathbf{x}_j;t)\right\}},\end{aligned} \tag{5.38}$$

where we let $d=\sum_{i=0}^N d_i$. As in the bipartite case we included the Maslov indices in the one-particle action integrals S_{s_i}, the two-particle action integrals are $\mathcal{S}_{s_i,s_j} = \int_0^t dt_1 \frac{1}{\sqrt{N}}\mathcal{U}_{kk'}\left(\mathbf{q}_{s_i}(t_1),\mathbf{q}_{s_j}(t_1)\right)$ and $C_{s_0\cdots s_N}$ is now the real positive determinant of the $(N+1)$ particle dynamics in the d-dimensional space [19].

We repeat the assumption as used in the bipartite study, that interaction do not change classical paths. Elements of the multipartite semiclassical reduced density matrix $\eta_0^{(N)} = \mathrm{Tr}_1\left[\cdots\left[\mathrm{Tr}_N\left[\eta^{(N)}\right]\right]\cdots\right]$ read as,

$$\eta_0^{(N)}(\mathbf{x}_0,\mathbf{y}_0;t) = \sum_{s_0,\,l_0}(4\pi\nu^2)^{\frac{d_0}{2}}\mathcal{A}_{s_0}\mathcal{A}^\dagger_{l_0}\mathcal{F}_{s_0,\,l_0}(t)\exp[i\varphi_0], \tag{5.39}$$

with,

$$\mathcal{F}_{s_0,l_0}(t) = (4\pi\nu^2)^{-\frac{d-d_0}{2}}\int\prod_{i=1}^N d\mathbf{x}_i\sum_{\substack{s_1\cdots s_N\\ l_1\cdots l_N}}\mathcal{A}_{s_1\cdots s_N}\mathcal{A}^\dagger_{l_1\cdots l_N}\exp\left[i\left(\varphi_i^{(N)}+\varphi_{ij}^{(N)}\right)\right] \tag{5.40}$$

and the phases

$$\varphi_0 = S_{s_0}(\mathbf{r}_0,\mathbf{x}_0;t) - S_{l_0}(\mathbf{r}_0,\mathbf{y}_0;t), \tag{5.41a}$$

$$\varphi_i^{(N)} = \sum_{i=1}^N\left(S_{s_i}(\mathbf{r}_i,\mathbf{x}_i;t) - S_{l_i}(\mathbf{r}_i,\mathbf{x}_i;t)\right), \tag{5.41b}$$

$$\varphi_{ij}^{(N)} = \sum_{i=1}^N\left(\mathcal{S}_{s_0,s_i}-\mathcal{S}_{l_0,l_i}\right)+\sum_{i=1}^N\sum_{j>i}\left(\mathcal{S}_{s_i,s_j}-\mathcal{S}_{l_i,l_j}\right). \tag{5.41c}$$

In Eq. (5.40) we let $\mathcal{A}_{s_1\cdots s_N} = \mathcal{A}_{s_1}\cdots\mathcal{A}_{s_N}$.

The functional $\mathcal{F}_{s_0,l_0}(t)$ in Eq. (5.40) is the semiclassical Feynman-Vernon influence functional [16]. As usual the semiclassical expression is obtained by a action phase minimization procedure. A stationary phase approximation on $\varphi_i^{(N)}$

corresponds to setting $s_i = l_i$ for all the environmental particles, this cancels the phase $\varphi_i^{(N)} = 0$, and the sum over the bipartite action phases reduces to $\varphi_{ij}^{(N)} = \sum_{i=1}^{N} \mathcal{S}_{s_0,s_i} - \mathcal{S}_{l_0,s_i}$. Eq. (5.40) becomes,

$$\mathcal{F}_{s_0,l_0}(t) = (4\pi\nu^2)^{-\frac{d-d_0}{2}} \prod_{i=1}^{N} \mathrm{d}\mathbf{x}_i \sum_{s_1 \cdots s_N} \left(\prod_{i=1}^{N} |\mathcal{A}_{s_i}|^2 e^{i(\mathcal{S}_{s_0,s_i} - \mathcal{S}_{l_0,s_i})} \right). \tag{5.42}$$

Since each pair of paths (s_i, l_i) is only related to the particle i and only bipartite interactions are involved in the calculation, there is no correlation between $\mathcal{S}_{s_0,s_i}$ and $\mathcal{S}_{s_0,s_j}$ if we consider different particles $i \neq j$. Thus,

$$\left\langle \prod_{i=1}^{N} e^{i(\mathcal{S}_{s_0,s_i} - \mathcal{S}_{l_0,s_i})} \right\rangle = \prod_{i=1}^{N} \left\langle e^{i(\mathcal{S}_{s_0,s_i} - \mathcal{S}_{l_0,s_i})} \right\rangle.$$

Moreover decoherence affect off-diagonal elements of the reduced density matrix, i.e $|\mathbf{y}_0 - \mathbf{x}_0| \gg \nu$ and $s_0 \neq l_0$. Due to the absence of correlation between $\mathcal{S}_{s_0,s_i}$ and $\mathcal{S}_{l_0,s_i}$, the separation of the phase and amplitude averages together with the CLT gives after performing all the integrations and using the sum rules Eq. (5.19),

$$\mathcal{F}_{s_0,l_0}(t) = \exp\left[-\sum_{i=1}^{N} \frac{1}{N} \Gamma_{0i} t \right]. \tag{5.43}$$

Where

$$\Gamma_{0i} = 2 \int_0^t \mathrm{d}\tau \left\langle \mathcal{U}_{0i}\left[\mathbf{q}_{s_0}(0), \mathbf{q}_{s_i}(0)\right] \mathcal{U}_{0i}\left[\mathbf{q}_{s_0}(\tau), \mathbf{q}_{s_i}(\tau)\right] \right\rangle \tag{5.44}$$

is the bipartite interaction correlator.

The analysis of Eq. (5.43) shows that the influence functional depends only on the coupling between the system and the environment. Consequently, environments with interacting particles and non-interacting particles lead to the same result. This result can be compared to the well established Caldeira-Legett approach [27, 28] where the environment is assumed to consist of non interacting oscillator. Here we show from a direct calculation that the non-interacting behavior is justified, and considering more complex interaction would not yields more information. We note that we have performed the maximal number of contractions and we do not have any system Lyapunov contribution. We will see that a system Lyapunov contribution exist for the purity.

The diagonal term of the reduced density matrix $s_0 = l_0$ cancels the influence phase and $\mathcal{F}_{s_0,s_0}(t) = 1$ as its should be. However a linearization around s_0 can be performed, if we consider terms close to the diagonal $\nu \ll |\mathbf{y}_0 - \mathbf{x}_0| \ll \xi$, where ξ is a typical length scale, which can be the range of the multipartite interaction potential or the scale over which it fluctuate. After the application of the CLT and the use of Eq. (5.23), we get for the long time limit,

$$\mathcal{F}_{s_0,l_0}(t) = \exp\left[\frac{1}{2} \frac{\gamma_0}{\lambda_0} |\mathbf{y}_0 - \mathbf{x}_0|^2 \right] \tag{5.45}$$

where $\langle \Delta_0 S_{s,l}^2 \rangle \propto \gamma_0$ and λ_0 is the system Lyapunov exponent. Close to the diagonal, elements have a gaussian decay in $\mathbf{y}_0 - \mathbf{x}_0$ and the decoherence is enhanced.

5.3.3 Multipartite purity

Before starting any derivation concerning the multipartite purity it is important to notice that we are still in the framework of a bipartite system.i.e. a system in interaction with a complex environment. This bipartite splitting is in fact essential. Indeed the concept of purity is related to the entanglement theory and the purity is a well defined measure of entanglement only for global bipartite pure states. We warn that investigating multipartite entanglement is a very difficult task. More subtle objects like the generalized I-concurence [24] must be invoked. We refer the interested reader to the report on multiparticle entanglement by Mintert and coworkers [25].

From the previous development we can express the multlipartite purity as,

$$\mathcal{P}^{(N)}(t) = (4\pi\nu^2)^d \int \prod_{i=0}^{N} d\mathbf{x}_i d\mathbf{y}_i \sum_{s_0,l_0,k_0,m_0} \mathcal{A}_{s_0}\mathcal{A}_{s_0}^{\dagger}\mathcal{A}_{k_0}\mathcal{A}_{m_0}^{\dagger} e^{i\Phi_0} \times \sum_{\substack{s_1\cdots s_N \\ l_1\cdots l_N}} \sum_{\substack{k_1\cdots k_N \\ m_1\cdots m_N}} \mathcal{A}_{s_1\cdots s_N}\mathcal{A}_{s_1\cdots s_N}^{\dagger}\mathcal{A}_{k_1\cdots s_N}\mathcal{A}_{m_1\cdots m_N}^{\dagger} e^{i\left(\Phi_i^{(N)}+\Phi_{ij}^{(N)}\right)}, \quad (5.46)$$

with the phases

$$\begin{aligned}
\Phi_0 &= S_{s_0}(\mathbf{r}_0,\mathbf{x}_0;t) - S_{l_0}(\mathbf{r}_0,\mathbf{y}_0;t) + S_{k_0}(\mathbf{r}_0,\mathbf{y}_0;t) - S_{m_0}(\mathbf{r}_0,\mathbf{x}_0;t), & (5.47a)\\
\Phi_i^{(N)} &= \sum_{i=1}^{N} S_{s_i}(\mathbf{r}_i,\mathbf{x}_i;t) - S_{l_i}(\mathbf{r}_i,\mathbf{y}_i;t) + S_{k_i}(\mathbf{r}_i,\mathbf{y}_i;t) - S_{m_i}(\mathbf{r}_i,\mathbf{x}_i;t), & (5.47b)\\
\Phi_{ij}^{(N)} &= \sum_{i=1}^{N} \left(\mathcal{S}_{s_0,s_i} - \mathcal{S}_{l_0,l_i} + \mathcal{S}_{k_0,k_i} - \mathcal{S}_{m_0,m_i}\right) \\
&+ \sum_{i=1}^{N}\sum_{j>i} \left(\mathcal{S}_{s_i,s_j} - \mathcal{S}_{l_i,l_j} + \mathcal{S}_{k_i,k_j} - \mathcal{S}_{m_i,m_j}\right). & (5.47c)
\end{aligned}$$

Eq. 5.46 is depicted in Fig. (5.6), with the same rules as defined in the bipartite case.

We will limit the study to only the dominant semiclassical time dependent contributions. These ones are obtained by $N+1$ successive stationary phase approximations. A stationary phase approximation over Φ_0 will cancel the phase by setting $s_0 = m_0$ and $k_0 = l_0$. Similarly stationary phase approximations over $\Phi_i^{(N)}$ correspond to setting $s_i = l_i$ and $k_i = m_i$ for each particle i. Thus the multipartite purity can be expressed over a set of $2\,(N+1)$ classical trajectories,

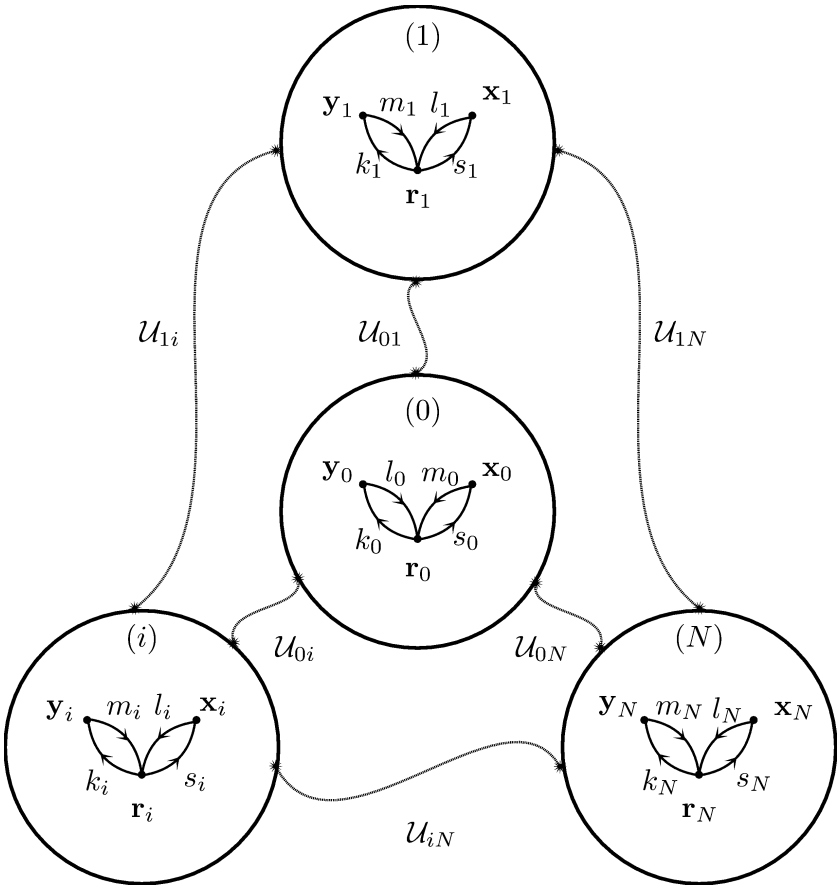

Figure 5.6: Diagrammatic representation of the multipartite purity.

$\{s_0, k_0\,;\, s_1,\, k_1;\, \cdots;\, s_N\,, k_N\}$. The phase $\Phi_{ij}^{(N)}$ reduces to

$$\delta\Phi_{ij}^{(N)} = \Phi_{0i}^{(N)} = \sum_{i=1}^{N} \mathcal{S}_{s_0,s_i} - \mathcal{S}_{k_0,s_i} + \mathcal{S}_{k_0,k_i} - \mathcal{S}_{s_0,k_i} \tag{5.48}$$

and the multipartite parity is given by

$$\mathcal{P}_{sc}^{(N)}(t) = \left\langle (4\pi\nu^2)^{-d} \int \prod_{i=0}^{N} \mathrm{d}\mathbf{x}_i \mathrm{d}\mathbf{y}_i \sum_{\substack{s_0\cdots s_N \\ k_0\cdots k_N}} |\mathcal{A}_{s_0}|^2 |\mathcal{A}_{k_0}|^2 |\mathcal{A}_{s_1\cdots s_N}|^2 |\mathcal{A}_{k_1\cdots s_N}|^2 e^{i\Phi_{0i}^{(N)}} \right\rangle \tag{5.49}$$

From the Eq. (5.49) we can derive all the dominant time dependent contributions. We have learned from the bipartite derivation, that these terms are related to the presence or absence of correlations between different semiclassical paths of the same particle. From the diagrammatic this corresponds to contracting two paths together. As we have $N + 1$ particles and each particle possesses 2 sets of paths, we can have $(N + 1)!$ diagrams depending on which combination of particles we choose for the contraction. We will present only the four dominant

contributions, which are the *non diagonal contribution* , the *system diagonal contribution* , the *Fully Diagonal Environmental contribution* , and the first *mixed contributions*.

Non diagonal contribution

The non diagonal contribution corresponds to a complete absence of correlations between all paths. The application of the CLT and the sum rules Eq. (5.19) leads to

$$\mathcal{P}_{\mathrm{sc}_1}^{(N)}(t) \;=\; \exp\left[-2\sum_{i=1}^{N}\frac{1}{N}\Gamma_{0i}t\right] \tag{5.50}$$

with Γ_{0i} given by Eq. (5.44). This is the Fermi Golden rule regime. The semi-classical multipartite purity cannot distinguish between an interacting and a non-interacting environment. The interacting isotropic case $\Gamma_{ij} = \Gamma$, or the non-interacting isotropic case $\Gamma_{ij} = \Gamma\delta_{i0}$, delivers the same result $\mathcal{P}^{(N)}(t) = \exp\left[-2\Gamma t\right]$, which is independent of N.

System diagonal contribution

The System diagonal contribution corresponds to a contraction of path $s_0 \simeq k_0$, which requires $\mathbf{x_0} \simeq \mathbf{y_0}$. Since all paths of the environment particles are uncorrelated, the linearization of k_0 over s_0 and the application of the CLT give for the phase,

$$\left\langle e^{i\Phi_{0i}^{(N)}}\right\rangle = \left\langle e^{i(\Delta_0\mathcal{S}_{s_0,s_i}-\Delta_0\mathcal{S}_{s_0,k_i})}\right\rangle^N = e^{-N\left\langle\Delta_0^2\mathcal{S}_{s_0,s_i}\right\rangle} \tag{5.51}$$

Assuming the same fast decay for the force correlator as in Eq. (5.23) delivers $\langle\Delta^2\mathcal{S}_{s_0,s_i}\rangle \propto \frac{\gamma_0}{N}$. One finally obtains, with the same reasoning used for the derivation of $\mathcal{P}_{sc_2}(t)$,

$$\mathcal{P}_{\mathrm{sc}_2}^{(N)}(t) = \alpha_0(t)\exp[-\lambda_0 t] \tag{5.52}$$

This is term is the System‘s Lyapunov contribution.

Fully Diagonal Environmental contribution

The Fully Diagonal Environmental contribution, corresponds to the contraction of paths $s_i \simeq k_i$ for the complete set of environmental particles. From the diagrammatics it is easy to see that each contraction will give a contribution of the form of Eq. (5.52), namely

$$\left\langle e^{i\Phi_{0i}^{(N)}}\right\rangle = \prod_{i=1}^{N}\left\langle e^{i(\Delta_i\mathcal{S}_{s_0,s_i}-\Delta_i\mathcal{S}_{k_0,s_i})}\right\rangle = \prod_{i=1}^{N} e^{-\left\langle\Delta_i^2\mathcal{S}_{s_0,s_i}\right\rangle} \tag{5.53}$$

and $\langle \Delta_i^2 \mathcal{S}_{s_0,s_i} \rangle \propto \frac{\gamma_i}{N}$, this will gives a factor $N^{\frac{d-d_0}{2}}$ after the gaussian integration and we obtain,

$$\mathcal{P}_{\mathrm{sc}_3}^{(N)}(t) = N^{\frac{d-d_0}{2}} \left(\prod_{i=1}^{N} \alpha_i(t) \right) \exp \left[- \sum_{i}^{N} \lambda_i t \right]. \tag{5.54}$$

For sufficiently strong λ_i or enough environment particles this term vanishes.

Mixed contributions

From the diagrammatics we can easily find that if we consider only a restricted number of contractions, we can obtain mixed terms i.e terms with some Lyapunov contributions and some Fermi Golden rule contributions.

A general formula for an arbitrary number of contractions can be derived, but for a suitable set of parameters these contributions can be neglected. That is why we present only the case, where one and only one environmental particle labelled k is contracted. For this situation, the phase $\Phi_{0i}^{(N)}$ becomes,

$$\begin{aligned} \left\langle e^{i\Phi_{0i}^{(N)}} \right\rangle &= \left\langle e^{i(\mathcal{S}_{s_0,s_k} - \mathcal{S}_{s_0,k_k} + \mathcal{S}_{k_0,k_k} - \mathcal{S}_{k_o,s_k})} \right\rangle \left\langle e^{i\sum_{i=1,\neq k}^{N} \mathcal{S}_{s_0,s_i} - \mathcal{S}_{s_0,k_i} + \mathcal{S}_{k_0,k_i} - \mathcal{S}_{k_o,s_i}} \right\rangle \\ &= e^{-\left\langle \Delta_k^2 \mathcal{S}_{s_0,s_k} \right\rangle} e^{-\sum_{i=1,\neq k}^{N} \left\langle \mathcal{S}_{s_0,s_i}^2 \right\rangle} \end{aligned} \tag{5.55}$$

thus we obtain, directly,

$$\mathcal{P}_{\mathrm{sc}_4}^{(N)}(t) = N^{\frac{d_k}{2}} \alpha_k(t) e^{-\lambda_k t} e^{-2\sum_{i=1,\neq k}^{N} \frac{1}{N} \Gamma_{0i} t}. \tag{5.56}$$

Semiclassical results

Our semiclassical derivation of the multipartite purity, shows that to the leading order the decay is given by the sum of tree terms, Eqs. (5.50), (5.52), (5.54), thus for chaotic systems we get,

$$\mathcal{P}_{\mathrm{sc}}(t) = e^{-2\sum_{i=1}^{N} \frac{1}{N} \Gamma_{0i} t} + a_0(t) e^{-\lambda_0 t} + N^{\frac{d-d_0}{2}} \left(\prod_{i=1}^{N} a_i(t) \right) e^{-\sum_i^N \lambda_i t} \tag{5.57}$$

We finally note that in the limit of $N \mapsto \infty$ the long time saturation $\mathcal{P}_{sc}^{(N)}(\infty) = N_0^{-1}$ is obtained from Eq. (5.46) with the contraction $s_0 = l_0$ and $k_0 = m_0$.

5.3.4 RMT approach versus semiclassical description

This part is devoted to a random matrix calculation of the multipartite purity $\mathcal{P}^{(N)}(t)$. First we denote the set of eigenstates of the free hamiltonians H_j by $\{|j_\alpha\rangle\}$ (with the energy eigenvalues $\epsilon_\alpha^{(j)}$) and the eigenstates of the interacting

hamiltonian $\mathcal{H}$ by $\{|a\rangle\}$ (with quasienergy eigenvalues E_a). In order to simplify the notation we define the eigenstates $|\mathbf{j}_\alpha\rangle = \bigotimes_{j=1}^{N} |j_\alpha\rangle$ and $|\mathbf{X}_\mathbf{j}\rangle = \bigotimes_{j=1}^{N} |\mathbf{x}_j\rangle$. We let $N_\mathrm{E} = \prod_{j=1}^{N} N_i$ be the total size of the environmental Hilbert space and we let $\Omega_\mathrm{E} = \prod_{j=1}^{N} \Omega_i$ be its spacial volume.

With these notations the multipartite purity is given by

$$\begin{aligned}\mathcal{P}^{(N)}_{\mathrm{RMT}}(t) = \int \prod_{i=0}^{N} \mathrm{d}\mathbf{x}_i \mathrm{d}\mathbf{y}_i \sum_{\text{indices}} & \overline{\langle 0_\delta, \mathbf{j}_\delta | \eta(0) | 0_\beta, \mathbf{j}_\beta \rangle \langle 0_{\delta'}, \mathbf{j}_{\delta'} | \eta(0) | 0_{\beta'}, \mathbf{j}_{\beta'} \rangle} \\ \times & \overline{\langle 0_\beta, \mathbf{j}_\beta | e^{-i\mathcal{H}t} | 0_\alpha, \mathbf{j}_\alpha \rangle \langle 0_\gamma, \mathbf{j}_\gamma | e^{i\mathcal{H}t} | 0_\delta, \mathbf{j}_\delta \rangle \langle 0_{\beta'}, \mathbf{j}_{\beta'} | e^{-i\mathcal{H}t} | 0_{\alpha'}, \mathbf{j}_{\alpha'} \rangle \langle 0_{\gamma'}, \mathbf{j}_{\gamma'} | e^{i\mathcal{H}t} | 0_{\delta'}, \mathbf{j}_{\delta'} \rangle} \\ \times & \overline{\langle 0_\alpha, \mathbf{j}_\alpha | \mathbf{x}_0, \mathbf{X}_\mathbf{j} \rangle \langle \mathbf{x}_0, \mathbf{Y}_\mathbf{j} | 0_\gamma, \mathbf{j}_\gamma \rangle \langle 0_{\alpha'}, \mathbf{j}_{\alpha'} | \mathbf{y}_0, \mathbf{Y}_\mathbf{j} \rangle \langle \mathbf{y}_0, \mathbf{X}_\mathbf{j} | 0_{\gamma'}, \mathbf{j}_{\gamma'} \rangle} \end{aligned} \tag{5.58}$$

RMT states that both sets of eigenstates are rotationally invariant [26]. This implies that the averages are independent of the initial states and yields,

$$\begin{aligned}\overline{\langle 0_\delta, \mathbf{j}_\delta | \eta(0) | 0_\beta, \mathbf{j}_\beta \rangle \langle 0_{\delta'}, \mathbf{j}_{\delta'} | \eta(0) | 0_{\beta'}, \mathbf{j}_{\beta'} \rangle} = \frac{1}{N_0^2 N_\mathrm{E}^2} \prod_{j=1}^{N} \Big(& \delta_{0_\beta 0_\delta} \delta_{0_{\beta'} 0_{\delta'}} \delta_{j_\beta j_\delta} \delta_{j_{\beta'} j_{\delta'}} \\ & + \delta_{0_\beta 0_{\delta'}} \delta_{0_{\beta'} 0_\delta} \delta_{j_\beta j_{\delta'}} \delta_{j_{\beta'} j_\delta} \\ & + \delta_{0_\beta 0_{\delta'}} \delta_{0_{\beta'} 0_\delta} \delta_{j_\beta j_\delta} \delta_{j_{\beta'} j_{\delta'}} \\ & + \delta_{0_\beta 0_\delta} \delta_{0_{\beta'} 0_{\delta'}} \delta_{j_\beta j_{\delta'}} \delta_{j_{\beta'} j_\delta} \Big) \end{aligned} \tag{5.59}$$

and

$$\begin{aligned} & \overline{\langle 0_\alpha, \mathbf{j}_\alpha | \mathbf{x}_0, \mathbf{X}_\mathbf{j} \rangle \langle \mathbf{x}_0, \mathbf{Y}_\mathbf{j} | 0_\gamma, \mathbf{j}_\gamma \rangle \langle 0_{\alpha'}, \mathbf{j}_{\alpha'} | \mathbf{y}_0, \mathbf{Y}_\mathbf{j} \rangle \langle \mathbf{y}_0, \mathbf{X}_\mathbf{j} | 0_{\gamma'}, \mathbf{j}_{\gamma'} \rangle} \\ = & \quad \frac{1}{\Omega_0^2 \Omega_\mathrm{E}^2} \delta_{0_\alpha 0_\gamma} \delta_{0_{\alpha'} 0_{\gamma'}} \prod_{j=1}^{N} \delta_{j_\alpha j_{\gamma'}} \delta_{j_{\alpha'} j_\gamma} \end{aligned} \tag{5.60}$$

If we introduce the eigenbasis of $\mathcal{H}$ in the propagator terms, it follows that the purity reduces to,

$$\begin{aligned} \mathcal{P}^{(N)}_{\mathrm{RMT}}(t) = & \quad \frac{1}{N_0} + \frac{1}{N_\mathrm{E}} \\ & + \frac{1}{N_0^2 N_\mathrm{E}^2} \Bigg(\sum_{\text{indices}} \overline{\langle 0_\beta, \mathbf{j}_\beta | a \rangle \langle a | 0_\alpha, \mathbf{j}_\alpha \rangle \langle 0_\alpha, \mathbf{j}_{\alpha'} | b \rangle \langle b | 0_\beta, \mathbf{j}_{\beta'} \rangle} \\ & \qquad \overline{\langle 0_{\beta'}, \mathbf{j}_{\beta'} | c \rangle \langle c | 0_{\alpha'}, \mathbf{j}_{\alpha'} \rangle \langle 0_{\alpha'}, \mathbf{j}_\alpha | d \rangle \langle d | 0_{\beta'}, \mathbf{j}_\beta \rangle} e^{-it(E_a - E_b + E_c - E_d)} \Bigg) \\ & + \frac{1}{N_0^2 N_\mathrm{E}^2} \Bigg(\sum_{\text{indices}} \overline{\langle 0_\beta, \mathbf{j}_\beta | a \rangle \langle a | 0_\alpha, \mathbf{j}_\alpha \rangle \langle 0_\alpha, \mathbf{j}_{\alpha'} | b \rangle \langle b | 0_{\beta'}, \mathbf{j}_\beta \rangle} \\ & \qquad \overline{\langle 0_{\beta'}, \mathbf{j}_{\beta'} | c \rangle \langle c | 0_{\alpha'}, \mathbf{j}_{\alpha'} \rangle \langle 0_{\alpha'}, \mathbf{j}_\alpha | d \rangle \langle d | 0_\beta, \mathbf{j}_{\beta'} \rangle} e^{-it(E_a - E_b + E_c - E_d)} \Bigg). \end{aligned} \tag{5.61}$$

Now we note that the Local Density Of State of an isolated system of interacting particles can be approximated [29] in the weak coupling limit by,

$$\left|\left\langle 0_\alpha, \mathbf{j}_\alpha \middle| a \right\rangle\right|^2 \rho^{-1}(E_a) = \frac{1}{2\pi} \frac{\tilde{\Gamma}}{\left(E_a - \sum_{j=0}^{N} \epsilon_\alpha^{(j)}\right)^2 + \frac{1}{4}\tilde{\Gamma}^2}, \tag{5.62}$$

where $\rho(E_a)$ denotes the density of state of the many-body problem and $\tilde{\Gamma}$ is the many-body Fermi Golden rule spreading, which reads

$$\tilde{\Gamma} = 2\pi \overline{\left|\left\langle 0_\alpha, \mathbf{j}_\alpha \middle| \mathcal{U} \middle| 0_\varphi, \mathbf{j}_\varphi \right\rangle\right|^2} \Delta^{-1}, \tag{5.63}$$

where Δ^{-1} is the typical mean interval between the final basis state $|0_\varphi, \mathbf{j}_\varphi\rangle$ which can be connected with the particular basis state $|0_\alpha, \mathbf{j}_\alpha\rangle$ by the interaction $\mathcal{U}$. We note that the latter can be related to the bipartite Fermi Golden rule spreading, $\Gamma_{ij} = 2\pi \overline{\left|\left\langle i_\alpha, j_\alpha \middle| \mathcal{U}_{ij} \middle| i_\varphi, j_\varphi \right\rangle\right|^2} \Delta^{-1}$ as

$$\tilde{\Gamma} = \sum_{j=0}^{N} \sum_{l \geq j}^{N} \Gamma_{jl} \frac{1}{N}. \tag{5.64}$$

We perform the transformation from the eigenbasis summation to the energy representation $\sum_a \to \int \mathrm{d}E_a \rho^{-1}(E_a)$ in Eq. (5.61). This yields, after computing the Fourrier transform of the local density of state, to

$$\mathcal{P}_{\mathrm{RMT}}^{(N)}(t) = \frac{1}{N_0} + \frac{1}{N_{\mathrm{E}}} + e^{-t \sum_{i=0}^{N} \sum_{j \geq i} \Gamma_{ij} \frac{1}{N}} + \frac{\mathrm{e}^{-t \sum_{i=0}^{N} \sum_{j \geq i} \Gamma_{ij} \frac{1}{N}}}{N_0 N_{\mathrm{E}}}. \tag{5.65}$$

This result confirms the long time saturation of the multipartite purity. In the particular case of the bipartite configuration, semiclassical and RMT derivations are in agreement with each other. Otherwise in all other situations the RMT and the semiclassical approach lead to different results. As an illustration we consider an interacting isotropic environment $\Gamma_{ij} = \Gamma \ , \ \forall\, (i,j)$. RMT predicts a decay $\propto \exp[-2N\Gamma t]$ in contrast to the semiclassical one $\propto \exp[-2\Gamma t]$. Why do the two methods differ ? This question is still open, however it seems that our semiclassical approach is too naive. Our semiclassical approach neglects the change of the classical trajectories due to the interaction, this approximation is quite well justified in the bipartite case by the structural stability and the shadowing theorem. However an extension to more particles is at the very least not completely obvious.

The only way to obtains N^2 interactions, in the semiclassical approach, is if a particle 1 modifies the trajectory of a particle 2 in interaction with a third one 3. Indeed during the interaction we have an accumulation of phase Φ_{23} , this latter will be affected by the particle 1. Future work will be devoted to the inclusion of this classical path modification effect.

5.4 Conclusion

In this chapter we investigated the effect of decoherence in interacting dynamical systems. At first for a bipartite model; to leading order in $\hbar_{\text{eff}}$, our semiclassical calculation gives the time-evolution of the purity as

$$\mathcal{P}(t) \simeq \exp[-\min(\lambda_0, \lambda_1, 2\Gamma_{01})t] + N_0^{-1} + N_1^{-1}. \tag{5.66}$$

Eq. (5.66) reconciles the numerical results of Refs. [13] and [14]. Its regime of validity, $\delta_2 \leq \Gamma_{01} \leq B_2$, is parametrically large in the semiclassical limit $N_i \to \infty$. We note that the same approach can also be applied to regular systems, in which case the exponentially decaying Lyapunov terms are replaced by power-law decaying terms [11, 15]. We stress one important advantage of our approach, namely that $\mathcal{P}(t)$ can be directly calculated, without the step of numerically integrating a differential equation for $\eta_0(t)$. Secondly, based on a Wigner function dynamics simulation we clearly illustrate the quantum-classical correspondence in the Lyapunov regime.

Finally the investigations on a multiparticle model reveal, that the RMT treatment and the semiclassical treatment lead to different results in this case. More investigations are necessary to understand this discrepancy.

Bibliography

[1] E. Joos, H.D. Zeh, C. Kiefer, D. Giulini, J. Kupsch, I.-O. Stamatescu, *Decoherence and the Appearance of a Classical World in Quantum Theory*, 2nd Ed. (Springer, Berlin 2003).

[2] W.H. Zurek, Rev. Mod. Phys. **75**, 715 (2003).

[3] S. Habib, K. Shizume, and W.H. Zurek, Phys. Rev. Lett. **80**, 4361 (1998).

[4] F. Toscano, R.L. de Matos Filho, and L. Davidovich, Phys. Rev. A **71**, 010101(R) (2005).

[5] A.K. Pattanayak, Phys. Rev. Lett. **83**, 4526 (1999); D. Monteoliva and J.P. Paz, Phys. Rev. Lett. **85**, 3373 (2000).

[6] Refs. [5] show entropy production rates for a single λ.

[7] R.A. Jalabert and H.M. Pastawski, Phys. Rev. Lett. **86**, 2490 (2001).

[8] Ph. Jacquod, P.G. Silvestrov, and C.W.J. Beenakker, Phys. Rev. E **64**, 055203(R) (2001).

[9] F.M. Cucchietti, D.A.R. Dalvit, J.P. Paz, and W.H. Zurek, Phys. Rev. Lett. **91**, 210403 (2003).

[10] J. Vanicek and E.J. Heller, Phys. Rev. E **68**, 056208 (2003).

[11] Ph. Jacquod, Phys. Rev.Lett. **92**, 150403 (2004).

[12] K. Furuya, M.C. Nemes, and G.Q. Pellegrino, Phys. Rev. Lett. **80**, 5524 (1998); J.N. Bandyopadhyay and A. Lakshminarayan, Phys. Rev. Lett **89**, 060402 (2002); M. Žnidarič and T. Prosen, J. Phys. A **36**, 2463 (2003); R.M. Angelo and K. Furuya, Phys. Rev. A **71**, 042321 (2005); M.Lombardi and A. Matzkin, quant-ph/0506188.

[13] P.A. Miller and S. Sarkar, Phys. Rev. E **60**, 1542 (1999).

[14] A. Tanaka, H. Fujisaki, and T. Miyadera, Phys. Rev. E **66**, 045201(R) (2002).

[15] M. Žnidarič and T. Prosen, Phys. Rev. A **71**, 032103 (2005).

[16] R.P. Feynman and F.L. Vernon, Ann. Phys. **24** 118 (1963).

[17] K. Möhring and U. Smilansky, Nucl. Phys. **A338** 227 (1980).

[18] P. Collet and J.-P. Eckmann J. Stat. Phys. **115**, 217 (2004).

[19] P. Cvitanović, R. Artuso, R. Mainieri, G. Tanner, and G. Vattay, *Chaos: Classical and Quantum*, `ChaosBook.org` (Niels Bohr Institute, Copenhagen 2003).

[20] G.P. Berman and G.M. Zaslavsky, Physica A **91**, 450 (1978).

[21] M.V. Berry and N.L. Balasz, J. Phys. A **12**, 625 (1979).

[22] A. Arguelles and T. Dittrich, Physica A **356**, 72 (2005).

[23] F.M. Izrailev, Phys. Rep. **196**, 299 (1990).

[24] A.R.R Carvalho, F.Minter and A. Buchleitner, Phys. Rev. Lett.**93** , 230501 (2004)

[25] F.Minter, A.R.R Carvalho, M. Kus and A. Buchleitner, Phys. Rep. **415** , 207 (2005)

[26] M.L. Mehta, *Random Matrices* (Academic, New York, 1991).

[27] A.O. Calderira and A.J. Leggett, Ann. Phys. (N.Y.) **149**, 375 (1983).

[28] A.O. Calderira and A.J. Leggett, Phys. Rev. A **31**, 1059 (1985).

[29] V.V. Flambaum and F.M. Izrailev, PRE **61**, 2539 (2000)

Part IV

Dephasing and Ballistic Transport : A Semiclassical Approach

CHAPTER 6

Decoherence in quantum chaotic transport : a semiclassical approach

6.1 Introduction

6.1.1 Dephasing and quantum transport

In mesoscopic systems, quantum coherence depends on the physical properties investigated, and in this sense is not characterized by a unique parameter. For example the conductance through such systems is affected by quantum interference effect up to a length scale that depends on the temperature and the applied voltage. Quantum coherent effects in mesoscopic transport are numerous, weak localization, universal conductance fluctuations and Aharonov-Bohm effects [1–3] are certainly the most important ones. Due to their typical intermediate size, mesoscopic systems are the ideal framework to investigate the quantum-to-classical transition from a microscopic coherent world, where quantum interference effects prevail, to a macroscopic classical world [4]. Indeed, the disappearance of quantum coherence due to dephasing processes has raised lot of theoretical [5, 7–14] and experimental [15–19] interest. At sufficiently low temperature, it is now well established, that the dominant processes of dephasing are electronic interactions. For a disordered quantum dot, the electronic interactions can be well modeled by a classical noise potential [5, 6], which yields an algebraic suppression of the weak-localization contribution to conductance through

$$g^{\mathrm{wl}} = \frac{g_0^{\mathrm{wl}}}{1 + \tau_{\mathrm{D}}/\tau_\phi}, \tag{6.1}$$

where g_0^{wl} is the contribution (in units of $2e^2/h$) in the absence of dephasing. The dephasing time τ_ϕ is given by the noise power, and the dwell time $\tau_{\mathrm{D}} = \tau_0 L/(W_{\mathrm{L}} + W_{\mathrm{R}})$ for a system of size L with time of flight τ_0 connected to two external, L (left) and R (right) leads of widths $W_{\mathrm{L}}, W_{\mathrm{R}}$. The robustness of Eq. 6.1 is quite remarkable, indeed it is insensitive to most noise-spectrum details, and holds for various sources of noise such as electron-electron and electron-phonon interactions, or external microwave fields.

There exist other, mostly phenomenological models, to investigate the disappearance of quantum effect on conductance in ballistic systems [8–13]. Voltage [8] and dephasing probe [9] models are certainly the most popular ones. In these two models, a third lead of width W_3 is connected to the system via a point contact of transparency ρ. A voltage is applied to the third lead to ensure that no current flows through it. Voltage and dephasing probes are used to introduce respectively inelastic and elastic incoherent scattering, into a fully quantum coherent system. This is clearly, the origin of the success, of this approach. Indeed one can directly use the formalism, developed in the purely coherent limit. Nevertheless, the mechanisms used here differ from the real microscopic processes involved such as electron-electron and electron-phonon interactions, or external microwave fields. These two models tend only to mimic such process. This it is obvious for the conceptual dephasing probe, but it's important to note that the phenomenological character still holds for the the voltage probe even if it is a real physical component widely used in mesoscopic experiments [20–23].

It has been shown that the equivalence between these two models, is exact only in the one channel limit [24]. However, if we limit the investigation to the current at low frequency and zeros temperature, result will not differ. A random matrix theory (RMT) treatment of the dephasing lead model leads to Eq. (6.1) with $\tau_\phi = \tau_0 L/(\rho W_3)$ [28,29], where ρ is the transmission probability of its tunnel-barrier. Thus it is commonly assumed that dephasing is system-independent for noise with a broad enough spectrum.

6.1.2 Dephasing in ballistic transport

Our purpose in this chapter is to revisit dephasing in open chaotic ballistic systems. According to the Bohigas Giannoni Schmit surmise [25], the Hamiltonian matrix of a closed chaotic system exhibits the universality of random matrix theory. Opening up the system, transport properties derive from the corresponding scattering matrix, which is determined by both the Hamiltonian of the closed system and its coupling to external leads [26]. It has been shown that for not too strong coupling, and when the Hamiltonian matrix is an element of one of the Gaussian ensembles of random hermition matrices, the corresponding scattering matrix is an element of one of the circular ensembles of unitary random matrices [27]. Accordingly transport properties of such ballistic systems are well described by the random matrix theory of transport [28–31].

However, one problem with the random matrix approach is its deficiency to deliver information about the crossover to the classical limit. That is why semiclassical methods have been involved in this field [32–46]. In the context of quantum ballistic transport, it is important to realize that whereas the dephasing time τ_ϕ is the long time cut-off for quantum interference, there is, as firstly noticed by Aleiner and Larkin [47], a new time scale that controls the appearance of such interference. This is the so called Ehrenfest time $\tau_{\rm E}$. This time scale corresponds to the time during which a well localized wavepacket spreads to a macroscopical length scale. Typically in open chaotic systems, two classical lengths are relevant, the system size L and the lead width W. We can thus define an Ehrenfest time associated to each one [48,49], the closed cavity Ehrenfest time $\tau_{\rm E}^{\rm cl} = \lambda^{-1}\ln[L/\lambda_{\rm F}]$ and the open cavity Ehrenfest time $\tau_{\rm E}^{\rm op} = \lambda^{-1}\ln[W^2/\lambda_{\rm F}L]$, where λ is the classical Lyapunov exponent of the cavity.

In the semiclassical limit of large ratio $L/\lambda_{\rm F}$ of the system size to Fermi wavelength, influence of a finite Eherenfest time has been now widely analytically analyzed, in various contexts, like weak localization correction [34–38], shot noise [39, 40], universal conductance fluctuation [41] or even quantum pumping [42].

Except for the analytical work of Ref. [47] and a numerical investigation [53], the investigation on the competition between the Ehrenfest time and the dephasing time was not so developed until recently [50, 51]. This is surprising, because such a study conduct to address the fundamental question of the system dependence of dephasing in the deep semiclassical limit. This question will be the focus of this chapter. These investigations are experimentally relvant. More precisely, Yevtushenko and collaborators investigated weak localization in a two-dimensional collection of randomly placed anti-dots. They observed an exponential suppression of weak localization with increasing temperature T. They interpreted this observation as arising from the competition between $\tau_{\rm E}$ and τ_ϕ [52]. From a theoretical point of view, it was shown in [47] that classical noise lead to an exponential suppression of weak localization, $\propto \exp[-\tau_{\rm E}^{\rm cl}/\tau_\phi]/(1+\tau_{\rm D}/\tau_\phi)$. This was numerically confirmed by simulations of the dephasing lead model [53].

Here we analytically investigate two different models of dephasing, and show that the suppression of weak localization corrections to the conductance is strongly model-dependent. First, we consider an external environment modeled by a capacitively coupled, single-electron closed quantum dot. We restrict ourselves to the regime of pure dephasing, where the environment does not alter the classical dynamics of the system. Secondly, following the work of Whitney [54] we provide a semiclassical treatment of transport in the dephasing lead model. We show that in both cases, the weak localization correction to conductance is given by

$$g^{\rm wl} = \frac{g_0^{\rm wl}}{1+\tau_{\rm D}/\tau_\phi}\,\exp[-\tilde{\tau}/\tau_\phi], \tag{6.2}$$

with a system-dependent time scale $\tilde{\tau}$. For the dephasing lead model, $\tilde{\tau} = \tau_{\rm E}^{\rm cl} + (1-\rho)\tau_{\rm E}^{\rm op}$ in terms of the transparency ρ of the contacts to the leads, and the

open system Ehrenfest time. Up to logarithmic corrections, this agrees with the prediction of Ref. [47] and sheds analytical light on the numerics of Ref. [53]. For the two-cavity model, however, $\tilde{\tau} = \lambda^{-1} \ln[(L/\xi)^2]$ depends on the correlation length ξ of the coupling potential between the two dots, and we thus conclude that dephasing in the semiclassical limit is strongly system dependent.

6.1.3 Outline of this chapter

The outline of this chapter goes as the follows. Section 6.2 is devoted to the treatment of the system-environment model. In particular, we present the new scattering formalism perviously used in [51]. The latter permits us to incorporate the coupling to external degrees of freedom. We then applied this formalism to determine, from a semiclassical point view, the Drude conductance and the weak localization correction to the transport. In particular we present a semiclassical calculation of the coherent-backscattering that shows the current conserving behavior of the method.

In Section 6.3 we present the first trajectory based derivation of the dephasing model, firstly in it is simpler formulation for a fully transparent barrier and then for the opaque case. We also comment on the multiprobe dephasing model.

Finally in section 6.4, we present for the system-environment model, a numerical simulation of the magnetoconductance.

Summary and conclusions are presented in Section 6.5. Technical details are presented in appendix.

6.2 Transport theory for a system-environement

The well known scattering approach is characterized by its ability to provide a clear and simple physical understanding of various transport phenomena, however in this standard approach all dissipative processes occur in the leads. Thus apart from this lead connection, the system is isolated and this formalism cannot directly describe the effects due to the coupling with an external environment. This coupling can induce decoherence and dissipation. In this chapter we will avoid the latter and focus on a pure dephasing picture. In the conceptual theory of decoherence, the starting point is the total density matrix $\eta_{\rm tot}$ that include both system and environmental degrees of freedom [4]. The observed properties of the system alone are given by the reduced density matrix $\eta_{\rm sys}$, obtained from $\eta_{\rm tot}$ by tracing over the environmental degrees of freedom. This procedure is probability conserving, $\mathrm{Tr}\left[\eta_{\rm sys}\right] = 1$, but it renders the time-evolution of $\eta_{\rm sys}$ non-unitary. The decoherence time is inferred from the decay rate of the off-diagonal matrix elements, which can be measured by a basis independent quantity, the purity [55]; $0 \leq \mathrm{Tr}\left[\eta_{\rm sys}^2\right] \leq 1$. We generalize this standard approach to the transport problem.

6.2.1 The scattering formalism in the presence of an environment

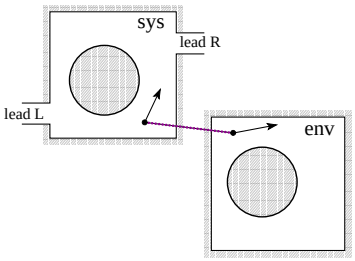

Figure 6.1: Schematic of the environment model. The system is an open quantum dot that is coupled to an environment in the shape of a second, closed quantum dot.

In order to include the coupling to an environment in the scattering approach, we consider two coupled interacting chaotic cavities as sketched in Fig. 6.1. One of them, the system "sys", is an open, two-dimensional quantum dot, ideally connected to two external leads. The second one is a closed quantum dot and plays the role of the environment "env". The two dots are capacitively coupled, and in particular, they do not exchange particles. We require that the size of the opening of the system's contacts to the leads is much smaller than the perimeter of the system cavity but is still semiclassically large, so that the number of transport channels satisfies $1 \ll N_{\mathrm{L,R}} \ll L/\lambda_F$. This ensures that the chaotic dynamics inside the dot has enough time to develop, $\lambda\tau_{\mathrm{D}} \gg 1$. Electrons in the leads do not interact with the second dot and as we are concerned only by pure dephasing, the second order electron-electron interactions mediated by the coupling are neglected. We emphasize that few-electron double-dot systems such as the one considered here have recently been the focus of intense experimental efforts [56].

The total system is describes by the Hamiltonian (we set $\hbar = 1$),

$$\mathcal{H} = H_{\mathrm{sys}} + H_{\mathrm{env}} + \mathcal{U}. \tag{6.3}$$

Inside each cavity the chaotic dynamics is generated by the corresponding one-particle Hamiltonian $H_{\mathrm{sys,\,env}}$. We only specify that the capacitive coupling potential $\mathcal{U}$ is a smooth function of the distance between the particles. It is characterized by its magnitude U and its correlation length ξ such that its typical gradient is U/ξ. From an experimental point of view, most systems are constructed in semiconductor heterostructures, where dots and transport channels are defined by means of external gates. The presences of theses gates will determine the screening length and the strength of the interaction between electrons in different dots. Consequently these parameters can be tuned, for example by imposing variation on the electrostatic potential on the gates or by considering different samples. This illustrates thus the experimental relevance of our parameter U,

which can be define as the typical change in the interaction as both particle move under their respective single particle Hamiltonian. Similarly our parameter ξ can be defines as the typical length scale over which this change occurs.

We just recall here that in the standard scattering approach, i.e without environment, the transport properties of the system derive from its scattering matrix [8]

$$\hat{\mathbf{S}} = \begin{pmatrix} \mathbf{s}_{\mathrm{LL}} & \mathbf{s}_{\mathrm{RL}} \\ \mathbf{s}_{\mathrm{LR}} & \mathbf{s}_{\mathrm{RR}} \end{pmatrix}, \tag{6.4}$$

which we write in terms of $N_{\mathrm{L}} \times N_{\mathrm{R}}$ transmission ($\mathbf{t} = \mathbf{s}_{\mathrm{LR}}$) and reflection ($\mathbf{s}_{\alpha,\alpha}$, $\alpha \in \{\mathrm{L}, \mathrm{R}\}$) matrices. From $\hat{\mathbf{S}}$, the system's conductance is given by

$$g = \mathrm{Tr}(\mathbf{t}^{\dagger}\mathbf{t}). \tag{6.5}$$

The environment coupling can be included in the standard scattering approach. We need only to define an extended scattering matrix $\mathbb{S}$ that includes the external non-current carrying degrees of freedom in a time-resolved manner.

To construct $\mathbb{S}$ we use the evolution operator $\mathbb{U}_{\mathrm{tot}} = \exp[i\mathcal{H}]$ that propagates the total system. We let M_{sys} and M_{env} be respectively the size of the Hilbert space of the system and environment cavity. Firstly we couple the system cavity to the left (L) and right (R) leads by introducing a $(N_{\mathrm{L}} + N_{\mathrm{R}}) \times (M_{\mathrm{sys}}M_{\mathrm{env}})$ projection matrix $\mathbb{P}_{\mathrm{tot}} = P^{(\mathrm{L})} \otimes \mathbb{I}_{\mathrm{env}} + P^{(\mathrm{R})} \otimes \mathbb{I}_{\mathrm{env}}$. Expressed in the basis of channel modes, the projection matrices, which act only on the system, read $P^{(\mathrm{L,R})}_{nm} = 1$ if $m = n \in \{m_i^{(\mathrm{L,R})}\}$ and $P^{(\mathrm{L,R})}_{nm} = 0$ otherwise. The sets $\{m_i^{(\mathrm{L,R})}\}$ are the $N_{\mathrm{L,R}}$ components of $\mathbb{U}^{\mathrm{tot}}$ ideally connected to the modes of the L or R lead respectively. Now following the techniques developed in the particular case of a chaotic map [57], the scattering matrix $\mathbb{S}$ can be express in terms of the time resolved scattering matrix $\mathbb{S}(\tau)$ as

$$\begin{aligned} \mathbb{S} &= \sum_{\tau=0}^{\infty} \mathbb{S}(\tau), \qquad (6.6a) \\ \mathbb{S}(\tau) &= \mathbb{P}_{\mathrm{tot}}[\mathbb{U}_{\mathrm{tot}}(\mathbb{I}_{\mathrm{tot}} - \mathbb{P}^{\dagger}_{\mathrm{tot}}\mathbb{P}_{\mathrm{tot}})]^{\tau}\mathbb{U}_{\mathrm{tot}}\mathbb{P}^{\dagger}_{\mathrm{tot}}. \end{aligned}$$

Each τ^{th} term in the above Taylor expansion corresponds to the time-evolution of a particle, coupled to the environment, colliding exactly τ times at the boundary of the system cavity before exiting. We note that the use of a discrete description of time is clearly justified in the particular case of a map. In the limit of a large dwell time over time of flight ratio, the discrete summation can be easily replaced by a continuous time integration $\sum_{\tau=0}^{\infty} \mapsto \int_0^{\infty} \mathrm{d}t$.

Under the assumption of non interacting lead, when a particle enters into the system, the total system state η_{tot} is in a product state. The initial density matrix can be written as $\eta_{\mathrm{tot}} = \eta^{(n)}_{\mathrm{sys}} \otimes \eta_{\mathrm{env}}$, with $\eta^{(n)}_{\mathrm{sys}} = |n\rangle\langle n|$ ($n \in \{1, \cdots, N_{\mathrm{L}}\}$) and η_{env} a random matrix as the environment is large and chaotic. We note that

our approach is not restricted to that particular choice of $\eta_{\rm env}$. We define the conductance matrix as the trace over the environment degrees of freedom,

$$g_{mn}^{(r)} = \left\langle m \left| \mathrm{Tr}_{\rm E} \left[\mathbb{S} \left[\eta_{\rm sys}^{(n)} \otimes \eta_{\rm env} \right] \mathbb{S}^{\dagger} \right] \right| m \right\rangle \tag{6.7}$$

A more formal derivation of this conductance matrix is presented in the appendix 6.6. The conductance g is given by,

$$g = \sum_{m=0}^{N_{\rm R}} \sum_{n=0}^{N_{\rm L}} g_{mn}^{(r)} \tag{6.8}$$

We emphasize that our approach is a current conserving procedure, indeed the particle flux conservation of this construction is similar to the probability conservation in the standard decoherence approach. However the environment-coupling generate decoherence and the suppression of the coherent contribution to transport. We caution the reader that this conductance will depends on the initial choice of the environment (see Eq. (6.7)), thus fluctuation of the decoherence time can be expected. Alternatively we can focus on the average conductance over various cavity environment $\eta_{\rm env}$, this is the choice follow here.

Eqs. (6.7,6.8) are the extension of the Laudauer-Buttikker formula in the presence of an external environment. They will constitute the backbone of our trajectory-based semiclassical theory of dephasing. We will now derive the classical Drude conductance and successively the quantum correction to the transmission and the reflection.

6.2.2 Drude conductance

The semiclassical derivation of the one particle scattering matrix has become standard [59–63]. Once we introduce the environment we deal with a bipartite problem, here we use the two-particle semiclassical propagator developed in the entanglement and decoherence framework [69, 70]. The extended scattering matrix element can be written as,

$$\begin{aligned} \mathbb{S}_{\rm mn}(\mathbf{q}_0, \mathbf{q}) &= (2\pi)^{-1} \int_0^{\infty} \mathrm{d}t \int_{\rm L} \mathrm{d}\mathbf{y}_0 \int_{\rm R} \mathrm{d}\mathbf{y} \ \langle m|\mathbf{y}\rangle \langle \mathbf{y}_0|n\rangle \\ &\times \sum_{\gamma,\Gamma} (C_\gamma \, C_\Gamma)^{\frac{1}{2}} \exp[i \{S_\gamma + S_\Gamma + \mathcal{S}_{\gamma,\Gamma}\}]. \end{aligned} \tag{6.9}$$

At this point, $\mathbb{S}$ depends on the coordinates of the environment and is given by a sum over pairs of classical trajectories, labeled γ for the system and Γ for the environment. In the regime of pure dephasing, the classical path γ (Γ) connecting $\mathbf{y_0}$ ($\mathbf{q_0}$) to $\mathbf{y}$ ($\mathbf{q}$) in the time t is solely determined by $H_{\rm sys}$ ($H_{\rm env}$). Each pair of paths gives a contribution weighted by the square root of the inverse determinant $C_\gamma C_\Gamma$ of the stability matrix [64–66], and oscillating with one-particle (S_γ and S_Γ, where Maslov indices are included inside) and two-particle ($\mathcal{S}_{\gamma,\Gamma} = \int_0^t \mathrm{d}\tau \mathcal{U}[\mathbf{y}_\gamma(\tau), \mathbf{q}_\Gamma(\tau)]$) action integrals accumulated along γ and Γ.

We insert Eq. 6.9 in Eq. (6.7), perform the sum over channel indices with the semiclassical approximation [67], $\sum_n^{N_\mathrm{L}} \langle \mathbf{y}_0|n\rangle\langle n|\mathbf{y}_0'\rangle \approx \delta(\mathbf{y}_0' - \mathbf{y}_0)$ and use the random matrix result [68] $\overline{\langle \mathbf{q}_0|\eta_\mathrm{env}|\mathbf{q}_0'\rangle} \approx \Omega_\mathrm{env}^{-1}\delta(\mathbf{q}_0' - \mathbf{q}_0)$ (Ω_env is the environment volume).

The conductance then reads,

$$\begin{aligned} g &= \left(4\pi^2\,\Omega_\mathrm{env}\right)^{-1} \int_0^\infty \mathrm{d}t\mathrm{d}t' \int_{\Omega_\mathrm{E}} \mathrm{d}\mathbf{q}_0\mathrm{d}\mathbf{q} \int_\mathrm{L} \mathrm{d}\mathbf{y}_0 \int_\mathrm{R} \mathrm{d}\mathbf{y} \\ &\times \sum_{\gamma,\Gamma;\gamma',\Gamma'} \left(C_\gamma\, C_\Gamma\, C_{\gamma'}\, C_{\Gamma'}\right)^{\frac{1}{2}}\ e^{i(\Phi_\mathrm{sys}+\Phi_\mathrm{env}+\Phi_\mathcal{U})}, \end{aligned} \tag{6.10}$$

This is a quadruple sum over classical paths of the system (γ and γ', going from $\mathbf{y}_0$ to $\mathbf{y}$) and the environment (Γ and Γ', going from $\mathbf{q}_0$ to $\mathbf{q}$) with action phases,

$$\Phi_\mathrm{sys} = S_\gamma\left(\mathbf{y}_0, \mathbf{y}; t\right) - S_{\gamma'}\left(\mathbf{y}_0, \mathbf{y}; t'\right), \tag{6.11a}$$

$$\Phi_\mathrm{env} = S_\Gamma\left(\mathbf{q}_0, \mathbf{q}; t\right) - S_{\Gamma'}\left(\mathbf{q}_0, \mathbf{q}; t'\right), \tag{6.11b}$$

$$\Phi_\mathcal{U} = \mathcal{S}_{\gamma,\Gamma}(\mathbf{y}_0, \mathbf{y}; \mathbf{q}_0, \mathbf{q}; t) - \mathcal{S}_{\gamma',\Gamma'}(\mathbf{y}_0, \mathbf{y}; \mathbf{q}_0, \mathbf{q}; t'). \tag{6.11c}$$

We are interested in quantities averaged over variations in the energy or the cavity shapes. For most set of paths the phase of a given contribution will oscillate wildly with these variations, so the contribution averages to zero. In the semiclassical limit Eq. (6.10) is thus dominated by terms which satisfy a Stationary Phase Condition (SPA), i.e. where the variation Φ_sys, Φ_env and $\Phi_\mathcal{U}$ has to be minimized. The most obvious contributions that survive averaging are the diagonal ones. These contributions give the Drude conductance. Indeed the stationary phase approximation over Φ_sys delivers $\gamma = \gamma'$ and the one over Φ_env delivers $\Gamma = \Gamma'$. These two SPA require $t = t'$ and lead to an exact cancellation of all the phases $\Phi_\mathrm{sys} = \Phi_\mathrm{env} = \Phi_\mathcal{U} = 0$. The Drude conductance is given by,

$$\begin{aligned} g^\mathrm{D} &= \int_0^\infty \mathrm{d}t \left(2\pi\,\Omega_\mathrm{env}\right)^{-1} \int_{\Omega_\mathrm{env}} \mathrm{d}\mathbf{q}_0\mathrm{d}\mathbf{q} \sum_\Gamma C_\Gamma \\ &\times \left(2\pi\right)^{-1} \int_\mathrm{L} \mathrm{d}\mathbf{y}_0 \int_\mathrm{R} \mathrm{d}\mathbf{y} \sum_\gamma C_\gamma \end{aligned} \tag{6.12}$$

Now the calculation proceeds along the lines of Ref. [37], and here we only sketch it. The main idea is to relate semiclassical amplitudes with classical probabilities. This is done by the introduction of two sum rules, that express the ergodic properties of open cavities Eq. (6.13a) and of closed ones Eq. (6.13b).

$$\sum_\gamma C_\gamma \left[\cdots\right]_\gamma = \int_{-\frac{\pi}{2}}^{\frac{\pi}{2}} \mathrm{d}\theta_0\mathrm{d}\theta\, P_\mathrm{sys}(\mathbf{Y}_0; \mathbf{Y}; t) \left[\cdots\right]_\gamma \tag{6.13a}$$

$$\sum_\Gamma C_\Gamma \left[\cdots\right]_\Gamma = \int_{-\pi}^{\pi} \mathrm{d}\phi_0\mathrm{d}\phi\, \tilde{P}_\mathrm{env}(\mathbf{Q}_0; \mathbf{Q}; t) \left[\cdots\right]_\Gamma \tag{6.13b}$$

We define $P_{\rm sys}(\mathbf{Y}_0;\mathbf{Y};t) = p_{\rm F}\cos\theta_0 \times \tilde{P}_{\rm sys}(\mathbf{Y}_0;\mathbf{Y};t)$, where $p_{\rm F}\cos\theta_0$ is the initial system momentum along the injection lead. $\tilde{P}_{\rm sys}(\mathbf{Y}_0;\mathbf{Y};t)$ and $\tilde{P}_{\rm env}(\mathbf{Q}_0;\mathbf{Q};t)$ are the classical probability densities. Note that the phase points $\mathbf{Y}_0 = (\mathbf{y}_0,\theta_0)$ and $\mathbf{Y} = (\mathbf{y},\theta)$ are in the leads, contrary to $\mathbf{Q}_0 = (\mathbf{q}_0,\phi_0)$ and $\mathbf{Q} = (\mathbf{q},\phi)$ which are inside the closed environment cavity.

As long as no restriction is imposed on the trajectories inside the system cavity, the average of $P_{\rm sys}$ over an ensemble system or over energy gives a smooth function. We obtain,

$$\left\langle \tilde{P}_{\rm sys}(\mathbf{Y}_0;\mathbf{Y};t)\right\rangle = \frac{\cos\theta}{2\left(W_{\rm L}+W_{\rm R}\right)\tau_{\rm D}} e^{-\frac{t}{\tau_{\rm D}}} \tag{6.14a}$$

and on the basis of ergodic assumption on the average of $\tilde{P}_{\rm env}$ we finally get,

$$\left\langle \tilde{P}_{\rm env}(\mathbf{Q}_0;\mathbf{Q};t')\right\rangle = \frac{1}{2\pi\Omega_{\rm env}} \tag{6.14b}$$

Using Eq. (6.14a, 6.14b), performing all the integration starting with time then the environmental and system variables and using $N_{\rm L,R} = W_{\rm L,R}/(\pi\lambda_{\rm F})$, we recover the classical Drude conductance,

$$g^{\rm D} = \frac{N_{\rm L}N_{\rm R}}{N_{\rm L}+N_{\rm R}} \tag{6.15}$$

6.2.3 Weak localization for transmission

Suppression of the weak localization correction due to finite Ehrenfest time was first derived by Aleiner and Larkin [47]. However the trajectory based approach was initiated by the work of Richter and Sieber [32, 33]. They point out the existence of system's trajectories paired almost everywhere except in the vicinity of an encounter (see Fig. 6.2). One of the trajectories, say γ, intersects itself, while the other one, say $\gamma' = \gamma_{\rm wl}$, avoids the crossing. Thus, they travel along the loop they form in opposite direction. For shorter time two trajectories leaving an encounter remain close enough to each other that the probability of forming a loops cancel, thus a minimal duration of the loop $T_{\rm L}$ must be introduced [33]. If we let ϵ be the small crossing angle of the encounter, the hyperbolic dynamics gives [71],

$$T_{\rm L}(\epsilon) \approx \lambda^{-1}\ln[\epsilon^{-2}]. \tag{6.16}$$

From these investigations, Richter and Sieber [33] obtained the quantum universal result, predicted by random matrix theory. The first attempt to introduce the finite Ehrenfest time in this framework was done by Adagideli [34]. However a subtle mechanism was missed, as firstly noticed by Rahav and Brouwer [36] the presence of correlated and uncorrelated escape, plays a crucial role. As in a transmission process only uncorrelated contributions are involved, the existence of theses correlations introduces a minimal time,

$$T_{\rm W} \approx \lambda^{-1}\ln[\epsilon^{-2}(W/L)^2], \tag{6.17}$$

before which the encounter is allowed to appear [37].

The presence of an environment, will not change this physical picture, nevertheless when the paths are more than the correlation length ξ apart, they feel the same environment and no dephasing can occur. We can thus define of new cut off time T_ξ as twice the time between the encounter and the start of the dephasing,

$$T_\xi \approx \lambda^{-1} \ln[\epsilon^{-2}(\xi/L)^2]. \tag{6.18}$$

We recall that a typical weak localization path is divided iton one loop and two legs. This typical division can be interpreted in the language of the disorder formalism, as a cooperon contribution and two diffuson contributions. We note that the dephasing occurs mostly in the loop part (see Fig. 6.2), however if $\xi < \epsilon L$, dephasing starts before the paths reach the encounter, $T_\xi < 0$. This means that dephasing affects also the diffuson part of the transport. This point will be discussed in more detail in paragraph 6.2.5.

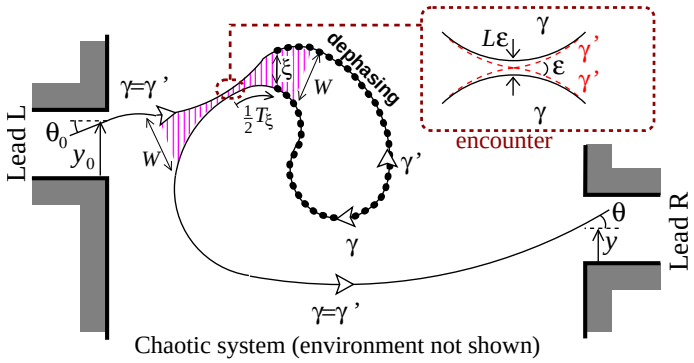

Figure 6.2: A semiclassical contribution to weak localization for the system-environment model. The paths are paired everywhere except at the encounter. There one crosses itself at angle ϵ, while the other does not (going the opposite way around the loop). Here we show $\xi > \epsilon L$, so the dephasing (dotted path segment) starts in the loop ($T_\xi > 0$).

In the absence of dephasing each weak localization contribution accumulates a phase difference $\delta\Phi_{\rm sys}$ [33, 36–38]. The determination of this phase is straightforward [72] and yields $\delta\Phi_{\rm syst} = E_{\rm F}\epsilon^2/\lambda$. In the presence of a coupling with an environment, each weak localization pair of paths accumulates an additional action phase difference $\delta\Phi_{\mathcal{U}}$. The derivation then proceeds as for $\mathcal{U} = 0$ [37]. We note that the system's probability $P_{\rm sys}$ introduced above can be written as,

$$\begin{aligned} P_{\rm sys}(\mathbf{Y}_0, \mathbf{Y}; t) &= p_{\rm F} \cos\theta_0 \int_C {\rm d}\mathbf{R}_2 {\rm d}\mathbf{R}_1 \tilde{P}_{\rm sys}(\mathbf{R}_2, \mathbf{Y}; t - t_2) \\ &\times \tilde{P}_{\rm sys}(\mathbf{R}_1, \mathbf{R}_2; t_2 - t_1) \tilde{P}_{\rm sys}(\mathbf{Y}_0, \mathbf{R}_1; t_1)\,, \end{aligned} \tag{6.19}$$

where $\tilde{P}_{\rm sys}(\mathbf{R}_1, \mathbf{R}_2; t)$ is the probability density to go from a point inside the system $\mathbf{R}_1 = (\mathbf{r_1}, \phi_1)$ to $\mathbf{R}_2 = (\mathbf{r_2}, \phi_2)$ in time t. We then restrict the probabilities

inside the integral to trajectories which cross themselves at phase-space positions $\mathbf{R}_{1,2}$ with the first (second) visit to the crossing occurring at time t_1 (t_2). We can write [37] $\mathrm{d}\mathbf{R}_2 = v_\mathrm{F}^2 \sin\epsilon \mathrm{d}t_1 \mathrm{d}t_2 \mathrm{d}\epsilon$ and set $\mathbf{R}_2 = (\mathbf{r}_\mathbf{1}, \phi_1 \pm \epsilon)$. One can now apply a separation of the phase and amplitude average in Eq. (6.10) and computes the residual coupling phase $\delta\Phi_\mathcal{U}$. As only a part of the system's trajectories, the separation of which is larger than ξ are involved, the coupling phase action integral must be limited to times $\tau \in [t_1 + T_\xi/2, t_2 - T_\xi/2]$.

$$\delta\Phi_\mathcal{U} = \int_{t_1+T_\xi/2}^{t_2-T_\xi/2} \mathrm{d}\tau \left[\mathcal{U}\big(\mathbf{r}_\gamma(\tau), \mathbf{q}_\Gamma(\tau)\big) - \mathcal{U}\big(\mathbf{r}_{\gamma'}(\tau), \mathbf{q}_\Gamma(\tau)\big)\right], \tag{6.20}$$

We notice that the square average of the residual phase $\delta\Phi_\mathcal{U}$ can be expressed in terms of the interaction correlator,

$$\begin{aligned}\left\langle \delta\Phi_\mathcal{U}^2 \right\rangle &= 2\int_{t_1+T_\xi/2}^{t_2-T_\xi/2} \mathrm{d}\tau\mathrm{d}\tau' \left\langle \mathcal{U}\big(\mathbf{r}_\gamma(\tau), \mathbf{q}_\Gamma(\tau)\big)\, \mathcal{U}\big(\mathbf{r}_\gamma(\tau'), \mathbf{q}_\Gamma(\tau')\big)\right\rangle \\ &- 2\int_{t_1+T_\xi/2}^{t_2-T_\xi/2} \mathrm{d}\tau\tau\mathrm{d}\tau' \left\langle \mathcal{U}\big(\mathbf{r}_\gamma(\tau), \mathbf{q}_\Gamma(\tau)\big)\, \mathcal{U}\big(\mathbf{r}_{\gamma'}(\tau'), \mathbf{q}_\Gamma(\tau')\big)\right\rangle \end{aligned} \tag{6.21}$$

We assume now a fast decaying interaction correlator,

$$\begin{aligned}&\left\langle \mathcal{U}\big(\mathbf{r}_\gamma(\tau), \mathbf{q}_\Gamma(\tau)\big)\, \mathcal{U}\big(\mathbf{r}_{\gamma'}(\tau'), \mathbf{q}_\Gamma(\tau')\big)\right\rangle \\ &= \left\langle \mathcal{U}^2\big(\mathbf{r}_\gamma(\tau), \mathbf{q}_\Gamma(\tau)\big)\right\rangle f\left(\frac{|\mathbf{r}_\gamma(\tau) - \mathbf{r}_{\gamma'}(\tau)|}{\xi}\right) g\left(\lambda_\mathrm{env}|\tau - \tau|\right), \end{aligned} \tag{6.22}$$

where $f(x), g(x)$ are fast decaying functions of x. These decaying correlation functions define ξ. The spatial correlation function decays even when $\mathcal{U}\big(\mathbf{r}, \mathbf{q}\big)$ is an oscillating function, because the averaging over many initial conditions of the environment is like averaging over $\mathbf{q}$. The exact nature of the decay, i.e. the form of $f(x)$, will depend on system details which are of little interest here. We note that we assumed that the temporal correlation function, decays on the same time scale as $\langle q(t)q(0)\rangle$ and thus the time scale is of order $\lambda_\mathrm{env}^{-1}$, where λ_env is the environment Lyapunov exponent. Assuming that the environment is sufficiently chaotic that we can approximate the temporal correlations by white noise, we let $g(x) \simeq \delta(x)$. This approximation is justified in the limit $\lambda_\mathrm{env} \ll \tau_\mathrm{D}^{-1}, \tau_\mathrm{E}^{-1}$. If we use the fact that $|\mathbf{r}_\gamma(\tau) - \mathbf{r}_{\gamma'}(\tau)|$ exponentially vanishes in the legs (for times $\tau < t_1 + T_\xi/2$ and $\tau > t_2 - T_\xi/2$) we get,

$$\begin{aligned}&\left\langle \mathcal{U}\big(\mathbf{r}_\gamma(\tau), \mathbf{q}_\Gamma(\tau)\big)\, \mathcal{U}\big(\mathbf{r}_{\gamma'}(\tau'), \mathbf{q}_\Gamma(\tau')\big)\right\rangle \\ &\sim \begin{cases} \left\langle \mathcal{U}^2\big(\mathbf{r}_\gamma(\tau), \mathbf{q}_\Gamma(\tau)\big)\right\rangle \lambda_\mathrm{env}^{-1}\delta(\tau' - \tau) & \text{in legs} \\ \delta_{\gamma\gamma'} \left\langle \mathcal{U}^2\big(\mathbf{r}_\gamma(\tau), \mathbf{q}_\Gamma(\tau)\big)\right\rangle \lambda_\mathrm{env}^{-1}\delta(\tau' - \tau) & \text{in loop} \end{cases} \end{aligned} \tag{6.23}$$

Finally using the Central limit Theorem, the average phase due to $\mathcal{U}$ reads

$$\left\langle e^{i\delta\Phi_\mathcal{U}} \right\rangle = e^{-\frac{1}{2}\langle\delta\Phi_\mathcal{U}^2\rangle} = \exp\left[-(t_2 - t_1 - T_\xi)/\tau_\phi\right], \tag{6.24}$$

where

$$\tau_\phi^{-1} \propto \lambda_{\rm env}^{-1} \left\langle \mathcal{U}^2(\mathbf{r},\mathbf{q}) \right\rangle \tag{6.25}$$

As both residual phases are in average independent of any spacial variables, the integration over environment variables can be computed independently and gives one. The weak localization correction can be expressed as,

$$g^{\rm wl} = \int_{\rm L} {\rm d}\mathbf{Y}_0 \int {\rm d}\epsilon \, {\rm Re}\big[e^{i\delta\Phi_{\rm sys}}\big] \big\langle F(\mathbf{Y}_0,\epsilon)\big\rangle, \tag{6.26a}$$

with,

$$\begin{aligned} F(\mathbf{Y}_0,\epsilon) &= \frac{2v_{\rm F}^2 \sin\epsilon}{\pi} \int_{T_{\rm L}+T_{\rm W}}^{\infty} {\rm d}t \int_{T_{\rm L}+\frac{T_{\rm W}}{2}}^{t-\frac{T_{\rm W}}{2}} {\rm d}t_2 \int_{\frac{T_{\rm W}}{2}}^{t_2-T_L} {\rm d}t_1 \\ &\times \int_{\rm R} {\rm d}\mathbf{Y} \int_C {\rm d}\mathbf{R}_1 e^{-\frac{1}{2}\langle \delta\Phi_{\mathcal{U}}^2\rangle} \tilde{P}_{\rm S}(\mathbf{R}_2,\mathbf{Y};t-t_2) \\ &\times \tilde{P}_{\rm S}(\mathbf{R}_1,\mathbf{R}_2;t_2-t_1) P_{\rm S}(\mathbf{Y}_0,\mathbf{R}_1;t_1), \end{aligned} \tag{6.26b}$$

We note that in absence of coupling $\delta\Phi_{\mathcal{U}} = 0$, we recover the weak localization correction (Cf. Eq. (35) of Ref. [37]) of an isolated system as it should be. Assuming a uniform phase space probability for the system we gets

$$\langle \tilde{P}_{\rm sys}(\mathbf{Y}_0,\mathbf{R}_1,;t_1)\rangle = \frac{1}{2\pi\Omega_{\rm sys}} \exp[-t_1/\tau_{\rm D}]$$

and the loop formation probability density is

$$\langle \tilde{P}_{\rm sys}(\mathbf{R}_1,\mathbf{R}_2;t_2-t_1)\rangle = \frac{1}{2\pi\Omega_{\rm sys}} \exp[-\{t_2-t_1-T_{\rm W}/2\}/\tau_{\rm D}],$$

with $\Omega_{\rm sys}$ the real space area of the system cavity. Finally the conditional probability density for the final leg is

$$\langle \tilde{P}_{\rm sys}(\mathbf{R}_2,\mathbf{Y};t-t_2)\rangle = \frac{1}{2(W_L+W_R)\tau_{\rm D}} \cos\theta \exp[-\{t-t_2-T_{\rm W}/2\}/\tau_{\rm D}].$$

Inserting Eq. (6.24) in Eq. (6.26b), and performing all the integrations we get

$$\langle F(\mathbf{Y}_0,\epsilon)\rangle \propto \exp[-T_{\rm L}/\tau_{\rm D}] \frac{\exp\left[-\tau_\xi/\tau_\phi\right]}{1+\tau_{\rm D}/\tau_\phi}, \tag{6.27}$$

where $\tau_\xi = \lambda^{-1}\ln[(L/\xi)^2]$. In fact this result is similar to the one obtain without dephasing, except that during the time $(t_2-t_1-T_\xi)$, the dwell time is effectively renormalized by the dephasing, so the (t_2-t_1)-integral generates the extra prefactor $\exp\left[-\tau_\xi/\tau_\phi\right]/(1+\tau_{\rm D}/\tau_\phi)$

Thus the weak localization correction is given by,

$$g^{\rm wl} = \frac{g_0^{\rm wl}}{1+\tau_{\rm D}/\tau_\phi} \exp[-\tau_\xi/\tau_\phi], \tag{6.28}$$

where $g_0^{\rm wl}$ is the finite-$\tau_{\rm E}^{\rm cl}$ correction in the absence of dephasing [33, 34, 37, 38], and hence

$$g_0^{\rm wl} = -\exp[-\tau_{\rm E}^{\rm cl}/\tau_{\rm D}] \; N_{\rm L}N_{\rm R}/(N_{\rm L}+N_{\rm R})^2. \tag{6.29}$$

6.2.4 Weak localization for reflection and coherent backscattering

The purpose of this section is to show explicitly that our semiclassical method preserves the probability i.e. conserves the current. Quantum corrections to reflection are given by two leading-order off-diagonal corrections, the first one reduces the probability of reflection to arbitrary momentum (Weak localization for reflection) and the second one is the coherent-backscattering which enhances the probability of reflection to the time reversed injection state. The distinction between these two contributions is related to the correlation between the escaped system pair of path. Coherent-backscattering have a correlated escape (see Fig. 6.3) contrary to the former.

The derivation of the weak localization for reflection $r^{\rm wl}$ in the presence of a coupling is straightforward and derived in the same manner as the $g^{\rm wl}$, replacing the factor $N_{\rm R}/(N_{\rm R}+N_{\rm L})$ by $N_{\rm L}/(N_{\rm R}+N_{\rm L})$. We finally get,

$$r^{\rm wl} = \frac{r_0^{\rm wl}}{1+\tau_{\rm D}/\tau_\phi}\ \exp[-\tau_\xi/\tau_\phi], \tag{6.30}$$

where $r_0^{\rm wl} = -\exp[-\tau_{\rm E}^{\rm cl}/\tau_{\rm D}]\ N_{\rm L}^2/(N_{\rm L}+N_{\rm R})^2$ is the finite-$\tau_{\rm E}^{\rm cl}$ correction in absence of dephasing [37].

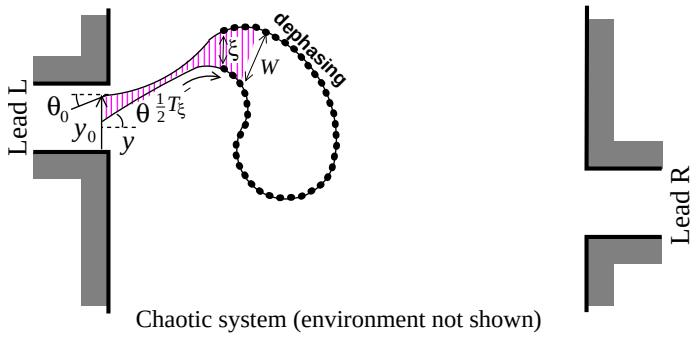

Figure 6.3: A semiclassical contribution to coherent backscattering for the system-environment model. It involves paths which return close but anti-parallel to themselves at lead L. The cross-hatched region is when the two solid paths are paired (within W of each other). Here we show $\xi > \epsilon L$, so the dephasing (dotted path segment) starts in the loop ($T_\xi > 0$). In the basis parallel and perpendicular to γ at injection the initial position and momentum of path γ at exit are $r_{0\perp} = (y_0 - y)\cos\theta_0$, $r_{0\|} = (y_0 - y)\sin\theta_0$ and $p_{0\perp} = p_{\rm F}(\theta - \theta_0)$.

A typical contribution of coherent-backscattering with dephasing is shown in Fig. 6.3. As the environment is again treated in the diagonal approximation the effect of the latter will be similar as before. The specificity of coherent-backscattering contribution is due to the correlation between system injection and exit positions and momenta, this induces an action difference $\delta\Phi_{\rm sys} = \delta S_{cbs}$

not given by the Richter-Sieber expression. From a fundamental point of view coherent-backscattering corresponds to term snot included in Eq. 6.30, i.e. trajectory where legs escape within $T_{\rm W}/2$. However is technically more convenient [37] to calculate the residual phase in terms of the injection variables $r_{0\perp} = (y_0 - y)\cos\theta_0$ and $p_{0\perp} = p_{\rm F}(\theta - \theta_0)$ (see Fig. 6.3). This delivers a system action difference of $\delta S_{cbs} = -\tilde{p}_{0\perp} r_{0\perp}$ with $\tilde{p}_0 = (p_{0\perp} + m\lambda r_{0\perp})$.

Similarly to the previous investigations we can express three cut off times $T'_{\rm L}$, $T'_{\rm W}$, T'_{ξ} that we estimate as $T'_{\ell}(r_{0\perp}, p_{0\perp}) \simeq \lambda^{-1}\ln[(\lambda\ell)^2/|v_{0\perp} + \lambda r_{0\perp}|^2]$, with $\ell = \{{\rm L}, {\rm W}, \xi\}$.

The coherent-backscattering contribution can be read as

$$r^{\rm cbs} \;=\; \int_{\rm L} {\rm d}\mathbf{Y}_0 {\rm Re}\big[e^{i\delta S_{\rm cbs}}\big]\big\langle F^{\rm cbs}(\mathbf{Y}_0, r_{0\perp}, p_{0\perp})\big\rangle, \tag{6.31a}$$

with,

$$\begin{aligned} F^{\rm cbs}(\mathbf{Y}_0, r_{0\perp}p_{0\perp}) &= \int_{\rm L} {\rm d}\mathbf{Y} \int_{T'_{\rm L}}^{\infty} \langle P_{\rm sys}(\mathbf{Y}_0, \mathbf{Y}, t)\rangle \\ &= \frac{p_{\rm F}\sin\theta_0}{\pi}\frac{N_{\rm L}}{N_{\rm R}+N_{\rm L}}\exp[-(T'_{\rm L} - T'_{\rm W}/2)/\tau_{\rm D}] \\ &\times \frac{\exp[-\tau_\xi/\tau_\phi]}{1+\tau_{\rm D}/\tau_\phi}, \end{aligned} \tag{6.31b}$$

noticing that $p_{\rm F}\sin\theta_0 {\rm d}\mathbf{Y}_0 = {\rm d}p_{0\perp}{\rm d}r_{0\perp}$, [61, 62]. Extending the momentum integral to infinity, and evaluating the $r_{0\perp}-$integral over the range $W_{\rm L}$with the help of an Euler Γ-function we obtain,

$$r^{\rm cbs} = \frac{r_0^{\rm cbs}}{1+\tau_{\rm D}/\tau_\phi}\;\exp[-\tau_\xi/\tau_\phi], \tag{6.32}$$

where $r_0^{\rm cbs} = \exp[-\tau_{\rm E}^{\rm cl}/\tau_{\rm D}]\; N_{\rm L}/N_{\rm L}+N_{\rm R}$ is the finite-$\tau_{\rm E}^{\rm cl}$ correction in the absence of dephasing [37, 38]. Hence $r^{\rm cbs} + r^{\rm wl} = -g^{\rm wl}$ and the unitarity is preserved. As a final remark, a careful reader may have noticed that we only considered cases where, either both systems are treated in the diagonal approximation, or the system dot has a weak localization kind of contribution and the environmental dot is treated in the diagonal approximation. Thus one could argue that there exist also configurations where the system is treated in the diagonal approximation and the environment has a weak localization or coherent-backscattering contribution. This is indeed the case, however these contributions cancel. This cancellation is an effect due to the integration over all final positions of the environment. Indeed if we consider an isolated environment the sum over environment weak localization and coherent-backscattering will be zero due to unitarity. Next if we let the environment interact with the system the diagonal approximation, then these contributions will decohere in the same way and will again sum to zero. In addition we note that this contribution can be explicitly calculated. Using the same technique developed previously we obtain

$r_{\rm env}^{\rm cbs} = -g_{\rm env}^{\rm wl} = \left(\frac{\Omega_{\rm sys}}{\Omega_{\rm env}}\right) \frac{N_{\rm L}N_{\rm R}}{(N_{\rm L}+N_{\rm R})^2} \exp[-\tau_{\rm E}^{\rm cl,\,env}/\tau_{\rm D}] \exp[-\tau_\xi^{\rm env}/\tau_\phi] (1+\frac{\tau_{\rm D}}{\tau_\phi})^{-1}$, with $\tau_\xi^{\rm env} = \lambda_{\rm env}^{-1} \ln[(L_{\rm env}/\xi)^2]$ and $\tau_{\rm E}^{\rm cl,\,env}$ the Ehrenfest time of the environment. Finally our approach is still probability- and thus current-conserving.

6.2.5 Discussion and limit of the environment-model

Technical details apart, the central result of this chapter is that in the semiclassical limit, the behavior of coherent corrections to transport no longer depend solely on the ratio of the dephasing time τ_Φ to the dwell time $\tau_{\rm D}$, but acquire a new exponential dependence with a new time scale τ_ξ. In contrast to Ref. [47], thos additional exponential damping depends on ξ, but not on the Fermi wavelength $\lambda_{\rm F}$. Ref. [47] mentions that they do not expect their result to hold when ξ is a classical scale. Care should be taken in extrapolating our results to the limit $\xi \to 0$, since this limit generates more and more diffraction effects and with them the breakdown of our semiclassical approach. We also ignore the fact that the noise will modify the classical paths. What exactly is the limit of our method ? More precisely we must answer the question if our method is legitimate for correlation lengths smaller than the encounter size $[\lambda_{\rm F} L]^{1/2}$.

To see significant dephasing we need $\tau_\phi \sim \tau_D$, thus we cannot take the interaction strength to zero. However we notice that a typical classical noise force on a particle goes like the gradient of the interaction U/ξ. To see if this noisy force significantly modifies the paths close to the encounter, we compare it with the relative force of the chaotic system Hamiltonian on the chaotic particle at the encounter. The ratio (noisy force)/(system force) is $[(L\lambda_F)/(\xi^2\lambda\tau_D)]^{-1/2}$. Thus one can ignore the modifications of the classical paths due to the coupling to the environment, as long as $\xi \gg [\lambda_{\rm F} L/\lambda\tau_D]^{1/2}$. Thus our method is applicable for ξ smaller (as well as larger) than the encounter size, but *not* for $\xi \sim \lambda_{\rm F}$.

6.3 Dephasing lead model

In its simplest formulation the dephasing lead model consist of adding a fictitious lead 3 to the cavity as illustrated in Fig. 6.4. Contrary to the two real leads L,R, the potential voltage on lead 3 is tuned such that the net current through it is zero. Thus every electron that leaves through lead 3 is replaced by one with an unrelated phase, leading to a loss of phase information without loss of particles.

In this situation the conductance from L to R is given by [8]

$$g = T_{\rm RL} + \frac{T_{\rm R3}\, T_{\rm 3L}}{T_{\rm 3L} + T_{\rm 3R}}, \tag{6.33}$$

where T_{nm} is the conductance from lead m to lead n in the absence of a voltage on lead 3. We next note that we can separate the Drude and weak-localization

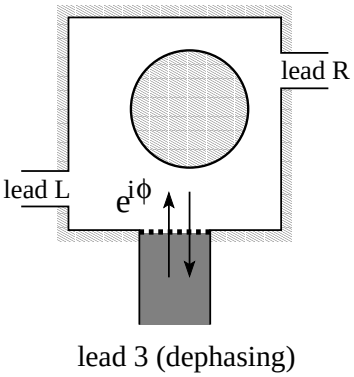

Figure 6.4: Schematic of the dephasing lead model. The system is an open quantum dot that is coupled to an dephasing probe.

parts of T_{mn}, writing it as

$$T_{nm} = T^{\mathrm{D}}_{nm} + \delta T_{nm} + \mathcal{O}[N^{-1}], \tag{6.34}$$

where the Drude contribution, T^{D}_{nm}, is $\mathcal{O}[N]$ and the weak-localization contribution, δT_{nm}, is $\mathcal{O}[N^0]$ and $N = N_{\mathrm{L}}+N_{\mathrm{R}}+N_3$ is the total number of channels of this three lead geometry. If we now expand g for large N and collect all $\mathcal{O}[N]$-terms (Drude contributions)and all $\mathcal{O}[N^0]$-terms (weak-localization contributions) we get $g = g^{\mathrm{D}} + g^{\mathrm{wl}}$, with

$$g^{\mathrm{D}} = T^{\mathrm{D}}_{\mathrm{RL}} + \frac{T^{\mathrm{D}}_{\mathrm{R3}} T^{\mathrm{D}}_{\mathrm{3L}}}{T^{\mathrm{D}}_{\mathrm{3L}} + T^{\mathrm{D}}_{\mathrm{3R}}} \tag{6.35a}$$

$$g^{\mathrm{wl}} = \delta T_{\mathrm{RL}} + \frac{(T^{\mathrm{D}}_{\mathrm{R3}})^2 \delta T_{\mathrm{3L}} + (T^{\mathrm{D}}_{\mathrm{3L}})^2 \delta T_{\mathrm{3R}}}{(T^{\mathrm{D}}_{\mathrm{3R}} + T^{\mathrm{D}}_{\mathrm{3L}})^2} \tag{6.35b}$$

To get the second result we used $T^{\mathrm{D}}_{ij} = T^{\mathrm{D}}_{ji}$ and $\delta T_{ij} = \delta T_{ji}$. These equations form the basis of our semiclassical derivation of the effect of a dephasing leads. We first consider the case of a dephasing lead coupled directly to the cavity (no tunnel barrier). We then move on to consider a dephasing lead with a tunnel barrier of transparency, ρ, and finally discuss multiple dephasing leads.

6.3.1 Dephasing lead without tunnel-barrier

If we consider a model with no tunnel-barriers on any lead (L,R,3), then the derivation is straightforward. The Drude conductance and weak-localization correction (at finite Ehrenfest time but without dephasing) from lead n to lead m a three-lead cavity is

$$T^{\mathrm{D}}_{nm} = \frac{N_n N_m}{N}, \tag{6.36}$$

$$\delta T_{nm} = -\frac{N_n N_m}{N^2} \exp[-\tau^{\mathrm{cl}}_{\mathrm{E}}/\tilde{\tau}_{\mathrm{D}}] \tag{6.37}$$

where $\tilde{\tau}_{\rm D}^{-1} = (\tau_0 L)^{-1}(W_{\rm L}+W_{\rm R}+W_3)$. We substitute these results into Eq. (6.35a) and Eq. (6.35b), and then write the answer in terms of the dwell time in the two leads (L and R) geometry, $\tau_{\rm D}$, and the dephasing rate, τ_ϕ^{-1}, which we define as the decay rate to lead 3. Thus

$$\tau_{\rm D}^{-1} = (\tau_0 L)^{-1}(W_{\rm L}+W_{\rm R}), \tag{6.38}$$
$$\tau_\phi^{-1} = (\tau_0 L)^{-1} W_3, \tag{6.39}$$

hence $\tilde{\tau}_{\rm D}^{-1} = \tau_{\rm D}^{-1} + \tau_\phi^{-1}$. From this we find that the Drude conductance and weak localization correction are given by

$$g^{\rm D} = g_0^{\rm D} \tag{6.40}$$
$$g^{\rm wl} = \frac{g_0^{\rm wl}}{1+\tau_{\rm D}/\tau_\phi}\exp[-\tau_{\rm E}^{\rm cl}/\tau_\phi] \tag{6.41}$$

where $g_0^{\rm D}$ and $g_0^{\rm wl}$ are the results for a two lead cavity in the absence of dephasing, given in Eqs. (6.15,6.29). We note that that the $\exp[-\tau_{\rm E}^{\rm cl}/\tau_{\rm D}]$ is included in $g_0^{\rm wl}$. Consequently the weak localization correction with a dephasing lead has a similar structure to that with a real environment. However here the time scale involved in the additional exponential suppression contains no independent parameter analoguous to ξ. We had initially expected that the width of the dephasing lead would play a role similar to ξ. However this turns out not to be the case, instead the Fermi wavelength appears in place of ξ, so the time scale in the additional exponential suppression is the Ehrenfest time, $\tau_{\rm E}^{\rm cl}$.

6.3.2 Dephasing lead with tunnel-barrier

We now consider a model in which there is a tunnel-barrier on the dephasing lead (lead 3). This model is attractive because one can avoid the local character of the dephasing probe model by considering a wide third lead with an almost opaque barrier [12]. This is also the model studied numerically in Ref. [53] in the context of conductance fluctuations.

We follow the trajectory-based calculation of weak localization with tunnel-barriers in Ref. [54]. There it was shown that introducing tunnel-barriers on the leads (with transparency ρ_n for lead n) requires the following three changes to the theory of weak-localization discussed in Ref. [37].

(i) The dwell time (single path survival time) becomes

$$\tau_{\rm D1}^{-1} = (\tau_0 L)^{-1}\sum_n \rho_n W_n, \tag{6.42}$$

because a typical path may hit a lead but be reflected off the tunnel-barrier (remaining in the cavity) numerous times before escaping.

(ii) The paired paths survival time for paths closer than the lead width is no longer equal to the dwell time, instead it is given by

$$\tau_{\mathrm{D}2}^{-1} = (\tau_0 L)^{-1} \sum_n \rho_n (2 - \rho_n) W_n. \tag{6.43}$$

This is because a second path following a path which has not escaped will hit the same tunnel-barriers, and thus may escape even though the first path did not. Compare this with a system without tunnel barriers, there if a path has not escaped it is because it has not touched the leads, thus a second path following the first has no probability to escape.

(iii) The coherent-backscattering peak contributes to transmission as well as reflection. This positive contribution to transmission partially cancels the usual (negative) weak localization contribution. This will be discussed in detail below.

When we calculate the Drude conductance, only change (i) above is required, giving us

$$T_{nm}^{\mathrm{D}} = \rho_n \rho_m \frac{N_n N_m}{\mathcal{N}} \tag{6.44}$$

where $\mathcal{N} = \sum_k \rho_k N_k$.

When calculating the conventional weak-localization contribution we need changes (i) and (ii) above. The contribution's classical path stays close to itself (within W, marked by the dashed region of Fig. 6.2) for a time $T_W(\epsilon)/2$ on either side of the encounter, thus we must use the paired-paths survival time, $\tau_{\mathrm{D}2}$, for these parts of the path. Elsewhere the escape time is given by the single path survival time (dwell time), $\tau_{\mathrm{D}1}$. With these new ingredients we find that the conventional weak-localization contribution becomes [54]

$$\delta T_{nm}^{\mathrm{wl}} = -\frac{\rho_n \rho_m \tau_{\mathrm{D}1} N_n N_m}{\tau_{\mathrm{D}2} \mathcal{N}^2} \exp\left[-\frac{\tau_{\mathrm{E}}^{\mathrm{op}}}{\tau_{\mathrm{D}_2}} - \frac{\tau_{\mathrm{E}}^{\mathrm{cl}} - \tau_{\mathrm{E}}^{\mathrm{op}}}{\tau_{\mathrm{D}_1}} \right] \tag{6.45}$$

where $\tau_{\mathrm{E}}^{\mathrm{op}} = \lambda^{-1} \ln[(L/\lambda_{\mathrm{F}})(W/L)^2]$ is the open cavity Ehrenfest time [48, 49]. The exponential is simply the probability that the path segments survive an time $\tau_{\mathrm{E}}^{\mathrm{op}}$ as a pair ($\tau_{\mathrm{E}}^{\mathrm{op}}/2$ either side of the crossing) and survive an additional time ($\tau_{\mathrm{E}}^{\mathrm{cl}} - \tau_{\mathrm{E}}^{\mathrm{op}}$) unpaired (to complete a loop of length $\tau_{\mathrm{E}}^{\mathrm{cl}}$).

However this is *not* the total weak-localization contribution to conductance, because coherent-backscattering can also contribute to conductance (this is the third change from a system without tunnel barriers). We call this the *failed coherent-backscattering*, it involves a path which returns to close but anti-parallel to itself at the moment it was injected from lead n, but then reflects off the tunnel-barrier on lead n, remaining in the cavity until it eventually escapes through a lead m. One can calculate the backscattering amplitude as in Ref. [37] (see also Ref. [38]), but using the paired-path survival time, $\tau_{\mathrm{D}2}$, when the paths are within W of each other (dashed area of Fig. 6.5) and the single path survival

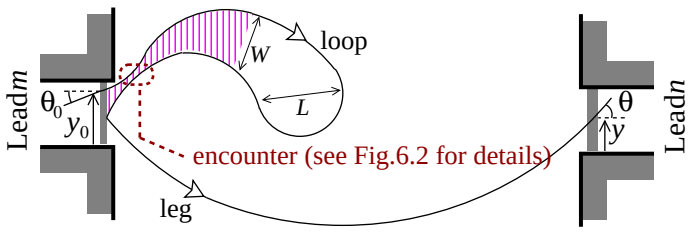

Figure 6.5: An failed coherent-backscattering contribution to conductance, $\delta T^{\rm cbs}_{nm}$. It involves paths which return close but anti-parallel to themselves at lead m, but reflect off the tunnel-barrier, remaining in the cavity to finally escape via lead n. The cross-hatched region is where the two solid paths are paired (within W of each other).

time,$\tau_{\rm D1}$, elsewhere. This result is then multiplied by the probability that the path reflects off lead n and then escapes through lead m. This gives a contribution to conductance of the form

$$\delta T^{\rm cbs}_{nm} = -\frac{\rho_m(1-\rho_m)\rho_n N_m N_n}{\mathcal{N}^2}\exp\left[-\frac{\tau_{\rm E}^{\rm op}}{\tau_{\rm D_2}}+\frac{\tau_{\rm E}^{\rm cl}-\tau_{\rm E}^{\rm op}}{\tau_{\rm D_1}}\right] \tag{6.46}$$

assuming $n \neq m$. There is a second coherent-backscattering contribution which is the same with $n \leftrightarrow m$ throughout. Summing these two coherent-backscattering contributions and the conventional weak localization one in Eq. (6.45) one gets for $n \neq m$,

$$\begin{aligned}\delta T_{nm} &= \rho_n\rho_m\frac{N_n N_m}{\mathcal{N}^2}\left(\rho_n+\rho_m-\frac{\tilde{\mathcal{N}}}{\mathcal{N}}\right)\\ &\quad\times\exp\left[-\tau_{\rm E}^{\rm op}/\tau_{\rm D_2}-(\tau_{\rm E}^{\rm cl}-\tau_{\rm E}^{\rm op})/\tau_{\rm D_1}\right],\end{aligned} \tag{6.47}$$

where $\tilde{\mathcal{N}} = \sum_k \rho_k^2 N_k$.

Now we assume that $\rho_L = \rho_R = 1$ so only the dephasing lead has a tunnel barrier, then substituting the Drude and weak-localization contributions into Eq. (6.35b) we find that,

$$g^{\rm wl} = \frac{g_0^{\rm wl}}{1+\tau_{\rm D1}/\tau_\phi}\exp\left[-(1-\rho)\tau_{\rm E}^{\rm op}/\tau_\phi-\tau_{\rm E}^{\rm cl}/\tau_\phi\right]. \tag{6.48}$$

Note that the exponent is simply the probability that a path survives throughout the paired-region ($\tau_{\rm E}^{\rm op}/2$ one either side of encounter) without escaping into lead 3, multiplied by the probability to survive the extra time ($\tau_{\rm E}^{\rm cl}-\tau_{\rm E}^{\rm op}$) unpaired without escaping into lead 3 (to close a loop of length $\tau_{\rm E}^{\rm cl}$). The first probability is $\exp[-(2-\rho)\tau_{\rm E}^{\rm op}/\tau_\phi]$ while the second is $\exp[-(\tau_{\rm E}^{\rm cl}-\tau_{\rm E}^{\rm op})/\tau_\phi]$.

We finally note that if we consider a nearly opaque barrier, the relevant time scale involved in the exponent is $\tau_{\rm E}^{\rm cl}+\tau_{\rm E}^{\rm op} \simeq 2\tau_{\rm E}^{\rm cl}$. Thus by tuning the opacity of the barrier, we can vary the exponential contribution to dephasing from $\exp[-\tau_{\rm E}^{\rm cl}/\tau_\phi]$ to $\exp[-2\tau_{\rm E}^{\rm cl}/\tau_\phi]$, but we cannot remove the exponent. Thus we cannot mimic dephasing due to a real environment with $\xi \sim L$, since that has only powerlaw dephasing.

6.3.3 Multiple dephasing leads

The n probe dephasing model consists of adding n fictitious leads to the cavity (labelled $\{3, \cdots, n+2\}$) in addition to lead L, R. The voltage on each supplementary lead is tuned so that the current it carries is zero. Without loss of generality we define $V_{\rm R} = 0$, then we get the set of equations

$$I_{\rm R} = T_{\rm RL} V_{\rm L} + \mathbf{T}_{\rm R}^T \mathbf{V} \tag{6.49a}$$

$$0 = \mathbf{I} = -\mathbf{T}_{\rm sub} \mathbf{V} + \mathbf{T}_{\rm L} V_L \tag{6.49b}$$

where the superscript-T indicates the transpose. The column-vectors $\mathbf{I}$, $\mathbf{V}$ have an ith element giving the current or voltage (respectively) for the dephasing lead $i \in \{3, n+2\}$. The column-vectors $\mathbf{T}_{\rm L}$ and $\mathbf{T}_{\rm R}$ have an ith element given by T_{Li} and T_{Ri}, respectively. Finally the matrix $\mathbf{T}_{\rm sub}]$ has an i,jth element given by

$$[\mathbf{T}_{\rm sub}]_{ij} = N_i \delta_{ij} - T_{ij} \tag{6.50}$$

$$= \left[\sum_{k \neq j} T_{kj}\right] \delta_{ij} - T_{ij}(1 - \delta_{ij}) \tag{6.51}$$

where again $i, j \in \{3, n+2\}$. Substituting $\mathbf{V}$ from Eq. (6.49b) into Eq. (6.49a) and using $I_{\rm R} = g V_{\rm L}$ gives us the conductance from L to R as,

$$g = T_{\rm LR} + \mathbf{T}_{\rm L}^T \mathbf{T}_{\rm sub}^{-1} \mathbf{T}_{\rm R} \tag{6.52}$$

Thus finding g requires the inversion of the matrix $\mathbf{T}_{\rm sub}$. This is cumbersome, so instead here we present a simple argument to extract only the information we are interested in (the nature of the exponential in the dephasing).

We argue that whatever the formula for conductance for n dephasing leads is, we can expand it in powers of N and collect the $\mathcal{O}[N^0]$-terms to get a formula for weak-localization of the form

$$g^{wl} = \delta T_{\rm LR} + \sum_{j=3}^{n+2} A_j \delta T_{{\rm L}j} + B_j \delta T_{j{\rm R}} + \sum_{i,j=3}^{n+2} C_{ij} \delta T_{ij} \tag{6.53}$$

where the sum is over all dephasing leads. To get the prefactors A_j, B_j, C_{ij} we would have to solve the full problem by inverting $\mathbf{T}_{\rm sub}$, however we can already see that they will be combinations of Drude conductances and thus independent of the Ehrenfest time. In contrast all the weak-localization contributions contain an exponential of the same form, that form being

$$\exp[-\tau_{\rm E}^{\rm op}/\tau_{\rm D_2} + (\tau_{\rm E}^{\rm cl} - \tau_{\rm E}^{\rm op})/\tau_{\rm D_1}] \tag{6.54}$$

Thus defining τ_ϕ^{-1} as the rate of escape into any of the dephasing leads, so $\tau_\phi^{-1} = (\tau_0 L)^{-1} \sum_{j=3}^{n} \rho_j W_j$, we see that $g^{\rm wl}$ decays with an exponential

$$\exp[-(1-\tilde{\rho})\tau_{\rm E}^{\rm op}/\tau_\phi + \tau_{\rm E}^{\rm cl}/\tau_\phi] \tag{6.55}$$

where we define $\tilde{\rho}$ such that $\tilde{\rho}\tau_\phi^{-1} = (\tau_0 L)^{-1} \sum_j \rho_j^2 W_j$. Hence we have shown that multiple dephasing leads cause an exponential suppression of the weak localization which is qualiatively similar to that caused by a single dephasing lead. The exponent is proportional to the Ehrenfest time, and contains no independent parameter analoguous to ξ.

6.4 Numerical simulations

We finally check our semiclassical theory for weak localization for the system-environment model. Like in most experiments, the numerics will be based on the magnetoconductance. A weak magnetic field has little effect on the classical dynamics but it generates a phase difference between two trajectories that go in opposite ways around a weak localization closed loop. This phase difference is $\Omega_{\rm loop}\Phi$ where $\Omega_{\rm loop}$ is the directed area enclosed by the loop, and Φ is the flux in units of the flux quantum. To incorporate this into the previous semiclassical treatment we must introduce a factor of $\exp[i\Omega_{\rm loop}\Phi]$ into Eq. (6.26b). A direct transcription of the calculation presented in Ref. [37], gives for finite flux and large coupling length a Lorentzian shape to the quantum corrections to the average conductance

$$g^{\rm wl}(\Phi) = g_0^{\rm wl}\frac{\exp[-\tau_\xi/\tau_\phi]}{1+\tau_{\rm D}/\tau_\phi+\alpha\Omega_{\rm S}^2\,(\tau_{\rm D}/\tau_0)\,\Phi^2}, \tag{6.56}$$

α is a system cavity-dependent parameter of order unity, and we recall that τ_0 is the time of flight between two consecutive bounces at the system cavity's wall.

We consider the Hamiltonian of Eq. (6.3) for two coupled kicked rotators (with $i \in \{\text{sys, env}\}$)

$$\begin{aligned} H_i &= \frac{(p_i-p_0)^2}{2} + K_i\cos(x_i-x_0)\sum_n \delta(t-n\tau_0), \\ \mathcal{U} &= \varepsilon\ \sin\left(\frac{x_{\rm sys}-x_{\rm env}-0.33}{\xi}\right)\sum_n \delta(t-n\tau_0). \end{aligned} \tag{6.57}$$

The interaction potential $\mathcal{U}$ is ξ-ranged with a strength ε and acts at the same time as the kicks. Upon increasing K_i the classical dynamics of the corresponding system varies from fully integrable ($K_i = 0$) to fully chaotic [$K_i \gtrsim 7$, with Lyapunov exponent $\lambda_i \approx \ln(K_i/2)$]. For $1 < K_i < 7$ the dynamics is mixed, i.e. stable and unstable motion coexist. We fix $K_i = 34.08$ to get a fully developed chaotic sea. The parameters p_0 and x_0 are introduced to break the Hamiltonian's two symmetries [73]. Only when these two symmetries are broken does one witness a crossover from the GOE to the GUE universality class [68], corresponding to breaking the time reversal symmetry [73]. In oder to reach a nice Lorentzian response of the magetocondutance we follow the procedure of Ref. [74], that consists of varing x_0 and keeping p_0 constant. We follow the usual quantization procedure on the torus x_i, $p_i \in [-\pi, \pi]$. The contacts of the system cavity are defined via two absorbing phase-space strips $[x_L-\delta x, x_L+\delta x]$ and $[x_R-\delta x, x_R+\delta x]$, each of them with a width $2\delta x = \pi/\tau_{\rm D}$. We restrict ourselves to the symmetric situation with $N_{\rm R,L} = N$. The extended scattering matrix can be constructed from a quantum representation of the Hamiltonian Eq. (6.57 provided by the unitary $(M_{\rm sys}\,M_{\rm env}) \times (M_{\rm sys}\,M_{\rm env})$ Floquet operator, which gives the time evolution for one iteration of the double coupled standard map. The average is provided by a

variation of the lead position and the consideration of different sets of quasienergies. We calculate the reduced magetoconductance from the scattering matrix, which we numerically construct via an iterative procedure as in Refs. [53,75]. On the basis of the result found by Bardarson and collaborators [74], the magnetic field parameter x_0 is express in unit of $x_c = 4\pi\sqrt{N}/(K_{\rm sys}M_{\rm sys}^{3/2})$.

Fig. 6.6 show the magnetoconductance $\Delta g(x_0)$ as function of the magnetic field

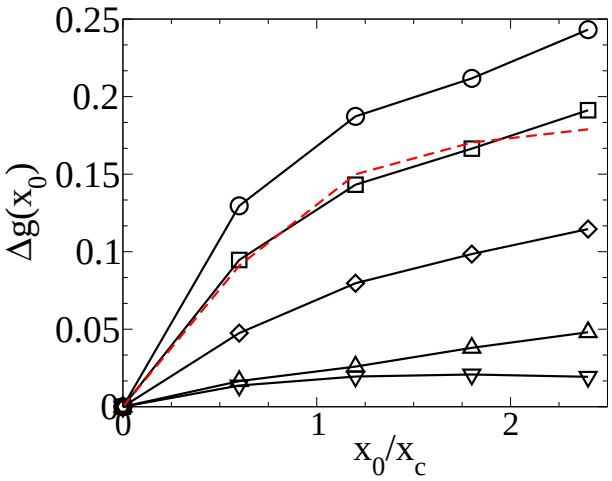

Figure 6.6: Magnetoconductance curves $\Delta g(x_0) = g(x_0) - g(0)$ for the open-close double kicked rotator model (defined in the text) at fixed classical configuration $K = K_{\rm sys} = K_{\rm env} = 34,08$ ($\lambda \approx 2.8$), $\tau_{\rm D}/\tau_0 = 8$, and fixed Hilbert space sizes, $M_{\rm sys} = 256$, $M_{\rm env} = 16$ for $\xi/L = 1$ and different coupling strength. $\hbar_{\rm eff}^{-1}\varepsilon = 0$ (circles), $\simeq 0.25$ (squares), $\simeq 0.5$ (diamonds), $\simeq 1$ (upward triangles), $\simeq 2$ (downward triangles). Data have been obtained after averaging over 6250 different samples (25 classically different system cavities, each with 25 different quasienergies and 10 different initials conditions for the environment). The red dashed line gives the best Lorentzian fit for the $\hbar_{\rm eff}^{-1}\varepsilon \simeq 0.25$ curve $\Delta g(x_0) = 0.19 - 0.19/(1 + 2.5(x_0/x)^2)$

parameter for different coupling strengths ϵ and a fixed correlation length $\xi = L$. The data clearly confirms the Lorentzian shape and the reduction of the weak localization correction. We can also affirm that we can see that there is no exponential suppression. Indeed we numerically estimated from an independent study based on a bipartite closed system $\tau_\Phi^{-1} \propto 0.425\varepsilon^2\hbar_{\rm eff}^{-2}$. Consquently, if there was exponential suppression of the form $\exp[-\tau_{\rm E}/\tau_\Phi]$, then the diamonds (third curve from top) would only go up to 0.02, instead of 0.125.

6.5 Conclusions

In this chapter we investigated the dephasing properties of open quantum chaotic system in the deep semiclassical limit. Two models has been examined for which we find that weak localization suppression are remarkably different. Firstly we

showed using a new scattering formalism that our system-environment model presents a supplementary exponential suppression controled by a macroscopic time scale $\tilde{\tau} = \tau_\xi$, secondly we showed that the popular dephasing-lead model has no independent parameter ξ. To our surprise it is the Fermi wavelength, not the dephasing-lead's width, which plays a role similar to ξ. This inequivalence between the dephasing lead model and a real environment can be most clearly seen in a situation where the interaction with a real environment has $\xi \simeq L$ at finite $\tau_{\mathrm{E}}^{\mathrm{cl}}$. Then the environment induces only powerlaw dephasing, which is impossible to mimic with a dephasing lead. We emphasize that a similar result has been obtained for universal fluctuation conductance by A. Altland and collaborators [50]. Their conclusions show clearly a distinction between an external source of dephasing which lead to result similar to our environment model and an internal source of dephasing which delivers results closer to the result in Ref. [47].

As a final conclusion we note that these investigations on the dephasing have open a certain number of questions. The first one is the intriguing similarity between our result for the dephasing lead model and the one obtained in Ref. [47]. Further work will be devoted to fix the origins of this similarity, accordingly we plan to investigate the link between the destruction of classical determinism by the dephasing process and the appearance of the Ehrenfest time scale. Another issue is related to the phenomenological nature of the dephasing lead model. In principle more subtle arrangement scan be designed. The purpose would be to introduce an additional independent parameter. This could be done, in principle, by considering the effect of two correlated tips on our open quantum dot. However this leads us to derive semiclassically a full hierarchy of density of state (injectivities, emissivities,... see [78]) that seems not trivial at all.

Finally, it would be nice to complement this theory with a calculation showing that dephasing does not affect shot-noise and extended the investigation to the universal conductance fluctucatuation.

6.6 Appendix A : Scattering approach to transport in the presence of an environment

We here extend the scattering approach to transport to account for coupled environmental degrees of freedom. We follow the lines of the derivation of the expression for noise presented in Ref. [77], focusing on the two-terminal configuration.

In the presence of an environment, the current operator at time t on a cross-

section of lead $\alpha = L, R$ reads

$$\begin{aligned}&\hat{I}_\alpha(\mathbf{q}, \mathbf{q}', t)\\ &= \frac{e}{h}\int \mathrm{d}E\mathrm{d}E' e^{i(E-E')t} \sum_n \Big[\hat{a}^\dagger_{\alpha n}(E')\hat{a}_{\alpha n}(E)\hat{\Phi}^\dagger(\mathbf{q}')\hat{\Phi}(\mathbf{q}) - \hat{b}^\dagger_{\alpha n}(E')\hat{b}_{\alpha n}(E)\hat{\Phi}^\dagger(\mathbf{q}')\hat{\Phi}(\mathbf{q})\Big].\end{aligned} \tag{6.58}$$

Here the coupling to external degrees of freedom has been introduced by means of environmental field operators $\hat{\Phi}(\mathbf{q})$, and accordingly, the current operator depends on the environmental spatial coordinates $\mathbf{q}$. The second quantized operators $\hat{a}^{(\dagger)}$ and $\hat{b}^{(\dagger)}$ create and destroy incoming and outgoing particles respectively, and the index n labels the different channels in lead α. Because of the coupling to the environment, the S-matrix linearly relating $\hat{a}-$operators to $\hat{b}$-operators now depends on the coordinates of the environment,

$$\hat{b}_{\alpha n}(E)\hat{\Phi}(\mathbf{q}) = \sum_{\beta;j}\int \mathrm{d}\mathbf{q}'\, \mathbb{S}_{\alpha\beta;nj}(\mathbf{q}, \mathbf{q}')\, \hat{a}_{\beta j}(E)\, \hat{\Phi}(\mathbf{q}'). \tag{6.59}$$

Here, $\mathbb{S}_{\alpha\beta;nj}(\mathbf{q}, \mathbf{q}')$ gives the transmission amplitude from channel j in lead β to channel n in lead α with the environment evolving from $\mathbf{q}'$ to $\mathbf{q}$ during the transmission. Using (6.59) we rewrite the current operator as

$$\begin{aligned}&\hat{I}_\alpha(\mathbf{q}, \mathbf{q}', t) = \frac{e}{h}\int \mathrm{d}E\; \mathrm{d}E' e^{i(E-E')t}\\ &\times \sum_{\beta,\gamma}\sum_{m,n}\Big[\delta_{mn}\delta_{\alpha\beta}\delta_{\alpha\gamma}\; \hat{a}^\dagger_{\alpha n}(E')\; \hat{a}_{\alpha n}(E)\; \hat{\Phi}^\dagger(\mathbf{q}')\; \hat{\Phi}(\mathbf{q})\\ &\qquad - \int \mathrm{d}\mathbf{q}_1\; \mathrm{d}\mathbf{q}_1' \sum_k \Big(\mathbb{S}_{\alpha\beta;mn}(\mathbf{q}_1', \mathbf{q}')\Big)^*\; \mathbb{S}_{\alpha\gamma;nk}(\mathbf{q}, \mathbf{q}_1)\; \hat{a}^\dagger_{\beta m}(E')\; \hat{a}_{\gamma k}(E)\; \hat{\Phi}^\dagger(\mathbf{q}_1')\; \hat{\Phi}(\mathbf{q}_1)\Big].\end{aligned} \tag{6.60}$$

The current is obtained by taking the expectation value of the current operator over both system and environmental degrees of freedom. One uses

$$\langle \hat{a}^\dagger_{\alpha m}(E')\; \hat{a}_{\beta n}(E)\rangle = \delta_{\alpha\beta}\; \delta_{mn}\; \delta(E - E')\; f_\alpha(E) \tag{6.61a}$$

$$\langle \hat{\Phi}^\dagger(\mathbf{q})\hat{\Phi}(\mathbf{q}')\rangle = F(\mathbf{q})\; \delta(\mathbf{q} - \mathbf{q}'). \tag{6.61b}$$

Here, f_α is the Fermi function, and F gives the spatial distribution of the environment. For the sake of simplicity, we will take $F(\mathbf{q}) \equiv 1$. Together with the unitarity of the scattering matrix, which we write as

$$\int \mathrm{d}\mathbf{q}_1 \sum_{\beta k}\Big(\mathbb{S}_{\alpha\beta;nk}(\mathbf{q}_1, \mathbf{q}')\Big)^*\; \mathbb{S}_{\alpha\beta;kn}(\mathbf{q}, \mathbf{q}_1) = \delta(\mathbf{q} - \mathbf{q}'). \tag{6.62}$$

Together with (6.60) and (6.61), this gives the current in the left lead as

$$\langle\langle I_L\rangle\rangle = \frac{e}{h}\sum_{n,k}\int \mathrm{d}\mathbf{q}_1\mathrm{d}\mathbf{q}\int \mathrm{d}E\Big(\mathbb{S}_{LR;nk}(\mathbf{q}_1, \mathbf{q})\Big)^*\; \mathbb{S}_{LR;kn}(\mathbf{q}, \mathbf{q}_1)\Big[f_L(E) - f_R(E)\Big]. \tag{6.63}$$

From this formula we see that the current (and hence the conductance) is obtained by tracing over the environmental degrees of freedom of the product of two scattering matrices. Besides this prescription, Eq. (6.63) is similar to the current in the standard scattering approach to transport.

Bibliography

[1] Y. Imry, *Introduction to Mesoscopic Physics*, Oxford University Press (New York, 1997).

[2] A.D. Stone in *Physics of Nanostructures*, J.H. Davies and A.R. Long Eds., Institute of Physics and Physical Society (London, 1992).

[3] A. Stern, Y. Aharonov, and Y. Imry, Phys. Rev. A **40**, 3436 (1990).

[4] E. Joos, H.D. Zeh, C. Kiefer, D. Giulini, J. Kupsch, I.-O. Stamatescu, *Decoherence and the Appearance of a Classical World in Quantum Theory* (Springer, Berlin 2003).

[5] B.L. Altshuler, A.G. Aronov, and D. Khmelnitsky, J. Phys. C **15**, 7367 (1982);

[6] S. Chakravarty and A. Schmid, Phys. Rep. **140**, 195 (1986);

[7] I.L. Aleiner, B.L. Altshuler, and M.E. Gershenson, Waves in Random Media **9**, 201 (1999).

[8] M. Büttiker, Phys. Rev. B **33**, 3020 (1986).

[9] M. J. M de Jong and C. W. J. Beenakker Physica A **230**, 219 (1996)

[10] M.G. Vavilov and I.L. Aleiner, Phys. Rev. B **60**, R16311 (1999).

[11] G. Seelig and M. Büttiker, Phys. Rev. B **64**, 245313 (2001).

[12] P. W. Brouwer and C. W. J. Beenakker Phys. Rev. B **55**, 4695 (1997)

[13] M.L. Polianski and P.W. Brouwer,J. Phys. A: Math Gen. **36**, 3215 (2003).

[14] C. Texier and G. Montambaux, Phys. Rev. B **72**, 115327 (2005).

[15] C.M. Marcus et al., Chaos, Solitons and Fractals **8**, 1261 (1997).

[16] A.G. Huibers, M. Switkes, C.M. Marcus K. Campman, and A.C. Gossard, Phys. Rev. Lett. **81**, 200 (1998).

[17] A.E. Hansen, A. Kristensen, S. Pedersen, C.B. Sørensen, and P.E. Lindelof, Phys. Rev. B **64**, 045327 (2001).

[18] K. Kobayashi, H. Aikawa, S. Katsumoto, and Y. Iye, J. Phys. Soc. Jpn. **71**, 2094 (2002).

[19] F. Pierre, A.B. Gougam, A. Anthore, H. Pothier, D. Esteve, and N.O. Birge, Phys. Rev. B **68**, 085413 (2003).

[20] A. D. Benoit, S. Washburn, C. P. Umbach, R. B. Laibowitz, and R. A. Webb, Phys. Rev. Lett. **57**, 1765 (1986).

[21] K. L. Shepard, M. L. Roukes, and B. P. Van der Gaag, Phys. Rev. Lett. **68**, 2660 (1992); Phys. Rev. B **46**, 9648 (1992).

[22] R. de Picciotto, H. L. Stormer, L. N. Pfeiffer, K. W. Baldwin, and K. W. West, Nature **411**, 51 (2001).

[23] B. Gao, Y. F. Chen, M. S. Fuhrer, D. C. Glattli, and A. Bachtold, Phys. Rev. Lett. **95**, 196802 (2005).

[24] H. Forster, P. Samuelsson, S. Pilgram, M. Buttiker,Phys. Rev. B **75**, 035340 (2007).

[25] O. Bohigas, M. J. Giannoni, and C. Schmit. Phys. Rev. Lett. **52**, 1 (1984).

[26] Z. Pluhar, H.A. Weidenmüller, J A. Zuk, and . H.Lewenkopf, Phys. Rev. Lett. **73**, 2115 (1994).

[27] C.H. Lewenkopf and H. A. Weidenmüller, Ann. Phys. **212**, 53 (1991); P.W. Brouwer, Phys. Rev. B **51**, 16878 (1995).

[28] C.W.J. Beenakker, Rev. Mod. Phys. **69**, 731 (1997).

[29] H.U. Baranger and P.A. Mello, Waves in Random Media **9**, 105 (1999).

[30] P. W. Brouwer and C. W. J. Beenakker, J. Math. Phys. **37**, 4904 (1996)

[31] S. Iida, H. A. Weidenmüller, and J. A. Zuk, Phys. Rev. Lett. **64**, 583 (1990); Annals of Physics, **200**, 219 (1990)

[32] M. Sieber and K. Richter, Phys. Scr. **T90**, 128 (2001); M. Sieber, J. Phys. A: Math. Gen. **35**, L613 (2002).

[33] K. Richter and M. Sieber, Phys. Rev. Lett. **89**, 206801 (2002).

[34] İ. Adagideli, Phys. Rev. B **68**, 233308 (2003).

[35] R.S. Whitney and Ph. Jacquod, Phys. Rev. Lett. **94**, 116801 (2005)

[36] S. Rahav and P.W. Brouwer, Phys. Rev. Lett. **95**, 056806 (2005); Phys. Rev. B, **73**, 035324 (2006).

[37] Ph. Jacquod and R.S. Whitney, Phys. Rev. B **73**, 195115 (2006).

[38] S. Rahav and P.W. Brouwer, Phys. Rev. Lett. **96**, 196804 (2006).

[39] O. Agam, I. Aleiner and A. Larkin, Phys. Rev. Lett.**85**, 3153 (2000).

[40] R.S. Whitney and Ph. Jacquod, Phys. Rev. Lett. **96**, 206804 (2006).

[41] P.W. Brouwer and S. Rahav, Phys. Rev. B **74**, 075322 (2006)

[42] P.W. Brouwer, and S. Rahav,Phys. Rev. B, **74**, 205327 (2006).

[43] S. Heusler, S. Müller, P. Braun, and F. Haake, Phys. Rev. Lett. **96**, 066804 (2006)

[44] H. Schanz, M. Puhlmann and T. Geisel,Phys. Rev. Lett. **91**, 134101 (2003).

[45] P. Braun, S. Heusler, S. Müller, and F. Haake, J. Phys. A: Math. Gen. **39**, L159 (2006).

[46] S. Müller, S. Heusler, P. Braun, F. Haake, New J. Phys. **9**, 12, (2007).

[47] I.L. Aleiner and A.I. Larkin, Phys. Rev. B **54**, 14423 (1996); Phys. Rev. E **55**, R1243 (1997).

[48] M.G. Vavilov and A.I. Larkin, Phys. Rev. B **67**, 115335 (2003).

[49] H. Schomerus and Ph. Jacquod, J. Phys. A. **38**, 10663 (2005).

[50] A. Altland, C. Tian and P.W. Brouwer, eprint: cond-mat/0605051.

[51] C. Petitjean, P. Jacquod and R. Whitney, eprint: cond-mat/0612118.

[52] O. Yevtushenko, G. Lütjering, D. Weiss and K. Richter, Phys. Rev. Lett. **84**, 542 (2000).

[53] J. Tworzydlo, A. Tajic, H. Schomerus, P.W. Brouwer, and C.W.J. Beenakker, Phys. Rev. Lett. **93**, 186806 (2004).

[54] R.S. Whitney, Phys. Rev. B 75, 235404 (2007).

[55] W. H. Zurek, Rev. Mod. Phys. **75**, 715 (2003).

[56] W.G. van der Wiel, S. De Franceschi, J.M. Elzerman, T. Fujisawa, S. Tarucha, and L.P. Kouwenhoven, Rev. Mod. Phys. **75**, 1 (2003).

[57] Y.V. Fyodorov and H.-J. Sommers, JETP Letters **72**, 422(2000).

[58] M.V. Berry, Proc. R. Soc. Lond. A, **400**, 229 (1985).

[59] D.S. Fisher and P.A. Lee, Phys. Rev. B **23**, R6851 (1981).

[60] H.U. Baranger, D.P. DiVincenzo, R.A. Jalabert, and A.D. Stone Phys. Rev. B **44**, 10637 (1991).

[61] H.U. Baranger, R.A. Jalabert, and A.D. Stone, Phys. Rev. Lett. **70**, 3876 (1993);

[62] H.U. Baranger, R.A. Jalabert, and A.D. Stone, Chaos **3**, 665 (1993).

[63] K. Richter, *Semiclassical Theory of Mesoscopic Quantum Systems*, Springer Tracts in Modern Physics **161**, Berlin (2000).

[64] M. Gutzwiller, *Chaos in Classical and Quantum Mechanics*, Springer (New York, 1991).

[65] F. Haake, *Quantum Signatures of Chaos*, 2^{nd} Edition, Springer, (Berlin, 2001).

[66] P. Cvitanović, R. Artuso, R. Mainieri, G. Tanner, and G. Vattay, *Chaos: Classical and Quantum*, `ChaosBook.org` (Niels Bohr Institute, Copenhagen 2003).

[67] The semiclassical approximation of the sum over lead modes has been introduced in Ref. [37] and clearly explained in Ref. [54]. The crucial point for this derivation is that the sum over the fast oscillating term in $(\mathbf{y}_0 - \mathbf{y}'_0)$ acts like a Dirac $\delta-$function, when it is multiplied by a function which varies slowly on the scale of $\lambda_{\rm F}$.

[68] M. L. Mehta, *Random Matrices* (acadamic, New York, 1991).

[69] Ph. Jacquod, Phys. Rev. Lett. **92**, 150403 (2004).

[70] C. Petitjean and Ph. Jacquod, Phys. Rev. Lett. **97**, 194103 (2006).

[71] More precisely the presence of the encounter introduce a typical length scale $d_\perp$, that correspond to the typical separation between the two paired path at the vicinity of the encounter. According to the hyperbolic dynamics, we get $d_\perp = \frac{v_{\rm F}\epsilon}{2\lambda}$, and the exact definition of a typical cut of time is given by $T_\ell(\epsilon) = \lambda^{-1}\ln[(\ell/d_\perp)^2]$, with $\ell = \{\mathrm{L}, \mathrm{W}, \xi\}$.

[72] Classical action in time representation should be denominated Hamilton principle function but as no confusion is possible we named it classical action in the main text (see H. Goldstein, *Classical Mechanics*, Addison-Wesley Publishing Company, Inc., Reading, Massachusetts, 1956). Hamilton principle function are related to classical action in energy representation by a Legendre transformation, and as the energy surface in always equated to Fermi energy $E_{\rm F}$ we recover the action difference of Richter-Sieber [33].

[73] F. M. Izrailev, Phys. Rep. **196**, 299 (1990).

[74] J.H. Bardarson, J. Tworzydlo, and C.W.J. Beenakker, Phys. Rev. B **72**, 235305 (2005).

[75] Ph. Jacquod, and E.V. Sukhorukov, Phys. Rev Lett. **92** 116801 (2004).

[76] M. Büttiker, Phys. Rev. B **46**, 12485 (1992).

[77] Ya.M. Blanter and M. Büttiker, Phys. Rep. **336**, 1, (2000).

[78] M. Büttiker, Pramana-J. Phys. **58**, 241 (2002).

Part V

Outlooks

CHAPTER 7

Outlooks

In the course of these various investigations on quantum reversibility, entanglement, decoherence and quantum transport, we have been confronted to some interesting difficulties. Indeed we have pointed out that the semiclassical method suffers from two weaknesses. The first one is the difficulty to introduce *Dissipation* on an equal footing with *Decoherence*. The second one is related to the difficult treatment of the problem of interaction between our dynamical systems. Overcoming these two weaknesses will be essential if we want to tackle, from a semiclassical point of view the behavior of *dissipative interacting dynamical systems*.

We note that a careful treatment of dissipation and interaction, is by itself of fundamental interest, but we emphasize that the knowledge, that could be gained, will also be experimentally relevant. Indeed in a real experimental setup, the outcomes are strongly affected by dissipation and/or interactions. Fairly we can hope that the semiclassical treatment of such notions can deliver a more intuitive physical pictures of these effects.

From a purely quantum point of view, the most versatile treatment of out-of-equilibrium many body systems, is the so called *Keldysh formalism* [1]. There exist a number of pedagogical presentations [2, 3], of these methods. We noted that, although the Keldysh formulation of the many body theory is primarily useful for systems that are not in thermal equilibrium, this approach is also useful for equilibrium systems when traditional techniques (Matsubara technique) become cumbersome. We emphasize also that classical counterparts of these techniques are extremely powerful in the framework of classical stochastic systems (see for example the *Martin-Siggia-Rose technique* [4] or the *stochastic path integral approach* [5]).

However it is important to built a truly semiclassical approach, especially if we want to investigate the entanglement properties of such out-of-equilibrium

dynamical systems. This is clearly a difficult task that can not be solved quickly. Nevertheless we can try to initiate the project. We first split the difficulty into two simpler projects The first one will focus one the inclusion of *dissipative effects* in our previous work and will be detailed in paragraph 7.1. In the second, presented in paragraph 7.2, our efforts will be restricted to the treatment of the *interaction*.

7.1 Dissipation and semiclassical methods

The relation between chaos and quantum dissipation has attracted a lot of interest for a long time. Most works use environments with many degrees of freedom, as in the Caldeira-Leggett model [6]. However there are some important aspects in previous studies of quantum dissipation which are not easily described by the traditional semiclassical methods. As an example, the Caldeira-Leggett model admits a perturbative treatment at short times and small friction coefficients which describes both the classical and the quantum properties on the same footing. This equal footing treatment is more difficult to implement semiclassically, indeed an environment which induces friction also changes simultaneously, the classical trajectories and the quantum coherence features. The difficulty is related to the introduction of a self consistent change of the classical trajectories.

Nevertheless, recently Bonanca and Aguiar [7] have studied the effect of dissipation and decoherence on a harmonic oscillator induced by the coupling with a chaotic environment. This investigation has been based on a semiclassical treatment of the chaotic system and a Feynman-Vernon approach [8]. They showed that in this particular case the dissipation and decoherence come directly from a purely dynamical function. I plan to combine this treatment with our previous study of entanglement, giving us a better understanding of the semiclassical treatment of dissipation.

Apart from the above mentioned technical aspect of the motivation we intend to give to this project a more physical impact by focusing on entanglement experiments. Indeed most experiments, due to unavoidable environment coupling, do not allow one to prepare an ideal pure state and end up finally with a mixed state. One possible entanglement measure of mixed states is based on the minimal average of the generalized concurrence [9] over all possible ensembles that describe the particular mixed state. This calculation rather quickly becomes cumbersome, nevertheless it was shown by Mintert and Buchleitner [10] that this generalized concurrence admits a lower bound that can be related quite easily to the *Purity*.

Consequently our first project would be to study the dissipation and decoherence of a dynamically entangled bipartite system prepared in a mixed state under the influence of a chaotic environment. The key to solving this problem will be to design a scheme that permits one to control the self consistent change of the classical paths. The true advantage of this particular formulation of the problem, is the initial separation between the dissipative effects due to the surrounding environment and the entanglement part intrinsic of the bipartite system. We could address dissipation and entanglement in the same approach. We will firstly derive

a master equation, in which the dissipative part will be included via a semiclassical dissipative superoperator, and simultaneously treat exactly the entanglement process in the bipartite system.

The goal of this research would be to shed light on the entanglement destruction, that is of crucial importance in a currently not intensively investigated regime of dynamical systems.

7.2 Interaction and semiclassical methods

Interaction effects become important as soon we consider reduced dimension or nearly closed systems. In mesoscopic physics this happens when we consider closed quantum dots, which are in fact weakly coupled to leads via tunneling barriers. Indeed in almost-closed dots, conductance occurs by tunneling, the charge on the dot is quantized, and electron-electron interactions play an important role. At low temperatures transport is dominated by Coulomb blockade [11], which leads to the conductance peaks observed experimentally. From a theoretical point of view substantial work has been done in order to incorporate interaction. Most of these works are based on random matrix considerations [12]. At the semiclassical level statistical properties of ballistic quantum cavities have also been investigated [13], and more recently an hybrid method based on a random wave model and a semiclassical approach [14] has been proved to be very promising and powerful.

Now although Coulomb blockade is reasonably well understood for an almost isolated system, fundamental questions appear as soon we include the Coulomb blockade system in an electrical circuit. Indeed the Coulomb blockade can be lifted when the conductance of the contact is larger than the quantum conductance. This regime is usually referred to as *weak Coulomb blockade*. This problem has been addressed previously in the literature [15–17]. At the moment the most developed work by Brouwer et al. [18] is technically demanding (Bosonized description) and based on an expansion in the inverse number of channels.

In this second project we want to investigated this problem from a semiclassical point of view. The system that we consider will be a quantum dot coupled to two perfect point contacts. Electrons inside the contacts are non interacting. The dot itself will be treated as a chaotic cavity, the goal will be to determine semiclassically the current of such a system. We focus on the fact that this problem is not trivial, indeed as it was shown in the particular case of the trace formula [19], exact inclusion of interaction in the semiclassical formalism can be quite sophisticated.

The method we plan to used is based a the scattering matrix approach. Indeed, as already mentioned the scattering approach is one of the most powerful formalisms in the theory of quantum transport. The interest of this choice is double. Firstly in the most general case, outgoing and incoming field operators are related by a two time scattering matrix [20]. Secondly it has been recently shown that, in the particular case of periodically driven systems and for non

interacting electrons, an energy representation of the scattering matrix and the Keldysh Green's function formalism lead to the same conclusions [21]. Consequently the first step would be to derive a semiclassical analogue of the two time scattering matrix for the non interacting case, then include the interaction in a perturbative way. We note that the reduction to a weakly interacting problem, is a strong limitation. However this is the first step that we need to take if we want to carry out a semiclassical Keldysh treatment and ultimately go beyond.

We emphasis that from a practical point of view, the understanding of weak Coulomb blockad is crucial. Indeed almost all relevant engineering applications of coulomb blockade will take place in the open regime. Consequently the physical picture we could obtain from our semiclassical description would be extremely valuable.

Bibliography

[1] L.V. Keydysh, Zh. Eksp. Theor. Fiz. **47** , 1515 (1964); L.V. Keydysh, Sov. Phys. JETP **20**,1018 (1965).

[2] G.D. Mahan, *Many-particle physics*, (Plenum Press, N.Y. 1990).

[3] A. Kamenev, *Many-body theory of non-equilibrium systems*, Les Houches Summer School on "Nanoscopic Quantum Transport", eprint: cond-mat/0412296.

[4] P. C.Martin, E. D. Siggia, and H. A. Rose, Phys. Rev. A **8**, 423 (1973).

[5] A.N. Jordan, E.V. Sukhorukov, S. Pilgram, J. Math. Phys. 45, 4386 (2004)

[6] A. O. Caldeira and A. J. Leggett, Physica **A 121**, 587 (1983).

[7] M.V.S. Bonanca and M.A.M de Aguira, Phys. Rev. A **74**, 012105 (2006).

[8] R. P. Feynman and F. L. Vernon, Ann. Phys. **24**, 118 (1963).

[9] F. Mintert, A.R.R. Carvalho, M.Kus and A. Buchleitner, Phys. Rep, **415**, 207 (2005).

[10] F. Mintert and A. Buchleitner, Phys. Rev. Lett. **98**, 140505 (2007).

[11] Y. Alhassid Rev. Mod. Phys. **72**, 895 - 968 (2000).

[12] R. A. Jalabert, A. D. Stone, and Y. Alhassid, Phys. Rev. Lett. **68**, 3468(1992).

[13] E.E. Narimanov, H.U. Baranger, N. R. Cerruti, and S. Tomsovic, Phys. Rev. B **64**, 235329 (2001).

[14] J. D. Urbina, K. Richter, Phys. Rev. Lett. 97, 214101 (2006).

[15] P. W. Brouwer and I. L. Aleiner, Phys. Rev. Lett. **82** , 390 (1999).

[16] I. L. Aleiner, P. W. Brouwer, and L. I. Glazman, Phys. Rep. **358** ,309 (2002).

[17] D. S. Golubev and A. D. Zaikin, Phys. Rev. B **69**, 075318 (2004) .

[18] P.W. Brouwer, A. Lamacraft and K. Flensberg, Phys. Rev B **72**, 075316 (2005).

[19] J. Sakhr, R.S. Dumont and N.D. Whelan, Phys. Rev A **74**, 052104 (2006).

[20] M.L. Polianski and P.W. Brouwer, J. Phys. A **36**, 3215 (2003).

[21] L. Arrachea and M. Moskalets, Phys. Rev B **74**, 245322 (2006).

Curriculum Vitae

Cyril PETITJEAN

Department of Theoretical Physics
University of Geneva
24, Quai Ernest Ansermet
CH-1211 Geneva 4
Switzerland
☏+41 22 379 6379
Cyril.Petitjean@physics.unige.ch
http://theory.physics.unige.ch/~petitj/

27 years old
Married, one child
French citizen

EDUCATION

Since 2003 :	Ph.D. student in theoretical physics, University of Geneva (Switzerland)
June 2003 :	« DEA de la matière condensée », Université Louis Pasteur (France)
June 2002 :	« Maitrise de Physique, » Université Louis Pasteur
June 2001 :	« Licence de Physique, » Université Louis Pasteur
June 2000 :	« DEUG de Physique, » Université Louis Pasteur

SCIENTICFIC INTEREST

Quantum chaos :	Decoherence, Irreversibility and Echo in Dynamical Systems
Entanglement :	Entanglement in Multipartite Dynamical Systems.
Mesoscopic physic :	Dephasing and Semiclassical Transport in Ballistic Systems

WORK EXPERIENCES

- ***TEACHING at the University of Geneva***

Since 2004 :	Exercise of the course « Mathematical methods for physicist » (Prof. P. Wittwer)
2003 -2004:	Laboratory of physics for students in biology and medecine (Prof. M. Decroux)

- ***RESEARCH TRAINEE***

February 2003 :	Mesoscopic fluctuations in ultrasmall supraconducting grains (Prof. X. Waintal, CEA Saclay, France)
February 2002 :	Lie Algebra : Elementary particle applications (Prof. M. Rausch de Traubenberg, DPT Strasbourg, France)
September 2001:	Linear stability of Poiseuille flow in cylindral geometry (Prof. J. Dusek , IMF Strasbourg, France)
July 2001 :	Spin-Orbit interaction in magnetic pevroskites (Prof. M. Alouani, IPCMS Strasbourg France)
April 2001 :	Coherent State and Semiclassical limit (Prof. J. Polonyi, DPT Strasbourg, France)
September 2000 :	β decay interest for exotic nuclei study and a Ge-Si TAgS detector study (Prof. P. Dessagne, IReS Strasbourg, France)

- ***SUMMER JOB***

2000 :	Alstom Magnets and Supraconductors (Belfort, France)

COMPUTER SCIENCE SKILLS

Programming :	Fortran, C++
Symbolic Manipulation :	Matlab, Mapple, Mathematica
OS :	UNIX, LINUX , Mac OS X , WINDOWS

LANGUAGES SPOKEN

French, English, German (notions)

TALKS

« Dephasing and quatum transport through chaotic systems. (a semiclassical approach) »
January 2007 : Regensburg University, Regensbourg (Germany)

« Boltzmann Echoes (Quantum Reversibility in Interacting Systems) »
January 2007 : Université Louis Pasteur, Strasbourg (France)
November 2006 : Harvard University, Cambridge (USA)
October 2006 : Institue Laue Langevin, Grenoble (France)

« Dynamically induced entanglement and decoherence The Quantum to classical crossover. »
January 2006 : University of Arizona, Tucson (USA)
November 2005 : University of Geneva, Geneva (Switzerland)
September 2005 : Max Planck Institute for the Physics of Complex Systems, Dresden (Germany)

« Mesoscopic Fluctuation of the Loshmidt echoe »
Mars 2005 : Transalpin seminar, Dolomieu (France)

« Mesoscopic fluctuation in Ultrasmall Superconducting Grains : Introduction to Richardson Solution. »
June 2003 : University of Geneva, Geneva (Switzerland)

CONFERENCES AND SCHOOLS

October 2006 :	GDR Physique Quantique Mesoscopique. (La Grande Motte, France)
May 2006 :	Quantum Coherence, Noise and Decoherence in Nanostructure. (Dresden, Germany)
February 2006 :	SPS Meeting (Lausanne, Switzerland)
January 2006 :	International Conference Nanoelectonics 2006 and School on Counting Statistics. (Lancaster, United Kingdom)
August-October 2005 :	Summer School on Quantum Information. (Dresden, Germany)
Mars 2005 :	Séminaire Transalpin : From Micro to Nano-photonics. (Dolomieu, France)
November 2004 :	School and Workshop on Quantum Entanglement, Decoherence, Information and Geometrical Phase in Complex Systems .(Trieste, Italy)

LIST OF PUBLICATIONS

- «Dephasing in the semiclassical limit is system-dependent»
C. Petitjean, Ph. Jacquod and R.S. Whitney, cond-mat/0612118 ; submitted to Phys. Rev. Lett.

- « Displacement Echoes: Classical Decay and Quantum Freeze »
C. Petitjean, D.V. Bevilaqua, E.J. Heller and Ph. Jacquod, Phys. Rev. Lett. **98**, 164101 (2007).

- « Lyapunov Generation of Entanglement and the Correspondence Principle »
C. Petitjean and Ph. Jacquod, Phys. Rev. Lett. **97**, 194103 (2006).

- « Quantum Reversibility and Echoes in Interacting Systems »
C. Petitjean and Ph. Jacquod, Phys. Rev. Lett. **97**, 124103 (2006)

- « Mesoscopic Fluctuations of the Loschmidt Echo »
C. Petitjean and Ph. Jacquod, Phys. Rev. **E 71**, 036223 (2005)

OTHERS ACTIVITIES

Member of S.F.P., Aïkido, Dance, Swimming.